



UNIL | Université de Lausanne

Unicentre

CH-1015 Lausanne

<http://serval.unil.ch>

Year : 2018

REACTIVITY OF MNO₂ IN BACTERIA-MINERAL

Gonzalez Holguera Julia

Gonzalez Holguera Julia, 2018, REACTIVITY OF MNO₂ IN BACTERIA-MINERAL

Originally published at : Thesis, University of Lausanne

Posted at the University of Lausanne Open Archive <http://serval.unil.ch>

Document URN : urn:nbn:ch:serval-BIB_BD66C7F56CF33

Droits d'auteur

L'Université de Lausanne attire expressément l'attention des utilisateurs sur le fait que tous les documents publiés dans l'Archive SERVAL sont protégés par le droit d'auteur, conformément à la loi fédérale sur le droit d'auteur et les droits voisins (LDA). A ce titre, il est indispensable d'obtenir le consentement préalable de l'auteur et/ou de l'éditeur avant toute utilisation d'une oeuvre ou d'une partie d'une oeuvre ne relevant pas d'une utilisation à des fins personnelles au sens de la LDA (art. 19, al. 1 lettre a). A défaut, tout contrevenant s'expose aux sanctions prévues par cette loi. Nous déclinons toute responsabilité en la matière.

Copyright

The University of Lausanne expressly draws the attention of users to the fact that all documents published in the SERVAL Archive are protected by copyright in accordance with federal law on copyright and similar rights (LDA). Accordingly it is indispensable to obtain prior consent from the author and/or publisher before any use of a work or part of a work for purposes other than personal use within the meaning of LDA (art. 19, para. 1 letter a). Failure to do so will expose offenders to the sanctions laid down by this law. We accept no liability in this respect.



UNIL | Université de Lausanne

Faculté des géosciences et de l'environnement
Institut des dynamiques de la surface terrestre

**REACTIVITY OF MNO_2 IN
BACTERIA-MINERAL ASSEMBLAGES**

Thèse de Doctorat

à l'Institut des dynamiques de la surface terrestre

en géosciences et environnement mention "Sciences de l'environnement"

Présentée à la Faculté des géosciences et de l'environnement de

l'Université de Lausanne par

Julia González Holguera

Titulaire d'un *MSci in Chemistry* délivré par

Imperial College London

Jury :

Prof. Jasquelin Peña, Université de Lausanne (Suisse); directrice de thèse

Prof. Pilar Junier, Université de Neuchâtel (Suisse); experte externe

Prof. Owen Duckworth, University of North Carolina (Etats-Unis); expert externe

Prof. Torsten Vennemann, Université de Lausanne (Suisse); expert interne

Dr. Stéphanie Grand, Université de Lausanne (Suisse); experte interne

Sous la présidence de Prof. Michel Jaboyedoff, Université de Lausanne (Suisse)

Lausanne, 2018

IMPRIMATUR

Vu le rapport présenté par le jury d'examen, composé de

Président de la séance publique :	M. le Professeur Michel Jaboyedoff
Président du colloque :	M. le Professeur Michel Jaboyedoff
Directrice de thèse :	Mme la Professeure Jasquelin Peña
Expert interne :	M. le Professeur Torsten Vennemann
Experte interne :	Mme la Docteure Stéphanie Grand
Experte externe :	Mme la Professeure Pilar Junier
Expert externe :	M. le Professeur Owen Duckworth

Le Doyen de la Faculté des géosciences et de l'environnement autorise l'impression de la thèse de

Madame Julia GONZALEZ-HOLGUERA

Titulaire d'un
Master en Chimie
de l'Imperial College London

intitulée

Reactivity of MNO_2 in bacteria-mineral assemblages

Lausanne, le 6 juillet 2018

Pour le Doyen de la Faculté des géosciences et de
l'environnement


Professeur Michel Jaboyedoff

Abstract

Layer-type manganese oxides (MnO_2) are secondary phase nanoparticulate minerals ubiquitous in soils, sediments and water bodies. Because their high surface area and negative surface charges promote metal sequestration on their surfaces, MnO_2 are recognized to affect the mobility and bioavailability of contaminants in both natural and engineered systems. In addition, high valent Mn species are among the strongest oxidants in natural systems. Naturally-occurring MnO_2 are precipitated by microorganisms and therefore often occur admixed with organic molecules and intact bacterial cells. The association of mineral phases with organic and biological components can significantly affect the mineral's reactivity through passive organo-mineral interactions that may lead to partial reduction of the oxide, the redox recycling of oxidized Mn [Mn(III) and Mn(IV)] and by exposing the mineral to the cells metabolic activity.

The objective of this thesis was therefore to study the reactivity of MnO_2 , both its affinity towards metals and towards organic reductants, in bio-mineral assemblages. We used suspensions of biogenic MnO_2 , precipitated by the Mn(II)-oxidizing model *Pseudomonas putida* GB-1, and of the abiotic δ - MnO_2 . By combining sorption isotherms and EXAFS spectroscopy, we showed that the loading of cations on MnO_2 depends largely on their capacity to displace Mn(III) already present on the mineral. We then evaluated the effect of pH on Mn(III, IV) reduction in δ - MnO_2 and biogenic MnO_2 suspensions. We finally conducted a literature review to identify the knowledge gaps regarding the coupled interactions between Mn and C in natural systems.

The results from this thesis provide a better understanding of the impact of the biological matrix on the reactivity of biogenic MnO_2 . We showed that the scavenging properties of the mineral are strongly affected by the bacteria's presence, both because a Mn(III)-enrichment of the oxide can influence the capacity of the mineral to adsorb cations and because the microbial metabolic activity can undermine the stability of the mineral. Similarly, the role Mn species can play as oxidants is strongly affected by local pH changes that the metabolic activity can establish. Furthermore, the presence of Mn(II)-oxidizers in biogenic MnO_2 provides the system with the capacity to regenerate high valent Mn species, a necessary condition to overcome the imbalance between the electron reducing equivalent of soil C residues and the electron accepting capacity of high valent Mn. These findings are necessary to the comprehension of the reactivity of MnO_2 in natural systems.

Résumé

L'oxyde de manganèse (MnO_2) est un minéral secondaire extrêmement réactif et omniprésent dans les sols, les sédiments et les systèmes aquatiques. Sa grande surface spécifique ainsi que sa charge négative favorisent l'adsorption de cations métalliques à sa surface, ce qui en fait un acteur majeur de la distribution et biodisponibilité des contaminants inorganiques des sols. De plus, MnO_2 est une des espèces naturelles les plus oxydantes, capable d'oxyder de nombreux agents inorganiques et organiques. Dans l'environnement, la précipitation du MnO_2 est le résultat de l'oxydation microbienne de Mn(II) en Mn(IV). Ce minéral est donc souvent incrusté dans un assemblage de biomasse microbienne qui influence la réactivité du minéral à travers des interactions organo-minérales, le recyclage des états oxydés du Mn [Mn(III) et Mn(IV)], ainsi qu'en exposant le minéral à l'activité métabolique des microorganismes.

L'objectif a été d'étudier la réactivité de MnO_2 , aussi bien son affinité envers les cations que sa réactivité oxydante, dans un assemblage biominéral. Nous avons utilisé des suspensions biogéniques de MnO_2 précipitées par *Pseudomonas putida* GB-1, ainsi que des suspensions abiotiques de $\delta\text{-MnO}_2$. En combinant des isothermes d'adsorption à des mesures spectroscopiques EXAFS, nous montrons que l'adsorption de cations sur MnO_2 dépend de leurs capacités à déplacer le Mn(III) présent sur le minéral. Nous évaluons ensuite l'effet du pH sur la réduction du Mn(III, IV) dans des suspensions de $\delta\text{-MnO}_2$ ainsi que des suspensions biogéniques. Finalement, à travers une revue de la littérature, nous identifions les lacunes dans la compréhension de la réactivité du Mn qui nécessitent d'être comblées pour comprendre les interactions entre les cycles du Mn et du C dans les sols.

Les résultats de cette thèse apportent une meilleure compréhension de l'influence de la matrice biologique sur la réactivité de MnO_2 . Nous montrons que les propriétés d'adsorption du minéral sont dépendantes de la présence des bactéries, à travers un enrichissement de l'oxyde en Mn(III) et parce que l'activité microbienne peut déstabiliser le minéral. De même, le rôle du Mn comme oxydant est dépendant des conditions de pH qui peuvent être modifiées par l'activité métabolique. La présence de biomasse microbienne apporte également au système la capacité de régénérer du Mn(III) et Mn(IV), une condition essentielle pour surmonter le déséquilibre entre les concentrations de réducteurs et celles de Mn. Ces résultats sont nécessaires à la compréhension de la réactivité du MnO_2 dans les systèmes naturels.

Table of Contents

CHAPTER 1	9
GENERAL INTRODUCTION	9
<i>The soil ecosystem: organo-mineral-microbial interfaces</i>	9
<i>Manganese in the environment</i>	10
<i>Structure and composition of MnO₂</i>	11
<i>Reactivity of MnO₂: state of the art</i>	12
<i>Formation of biogenic Mn oxides</i>	13
<i>Reactivity of biogenic MnO₂: state of the art on the impact of bacterial cells and organic molecules on the mineral reactivity</i>	15
<i>Research objective and dissertation organization</i>	17
CHAPTER 2	25
PB, ZN AND MN SORPTION ON BIOGENIC MNO₂: CONTAMINANT LOADING AND COMPETITIVE ACCESS TO VACANCY SITES	25
ABSTRACT	25
INTRODUCTION	26
MATERIAL AND METHODS	28
<i>Preparation of sorbent suspensions</i>	28
<i>Zn(II) and Pb(II) sorption by biomass-only and biogenic MnO₂ sorbents</i>	29
<i>Zn K-edge and Pb L₃-edge X-ray absorption spectroscopy</i>	30
RESULTS	32
<i>Sorption of Pb(II) and Zn(II) by P. putida biomass and biogenic MnO₂</i>	32
<i>Release of Mn to solution upon Zn(II) and Pb(II) sorption</i>	34
<i>Coordination environment of Zn(II) on biogenic MnO₂</i>	35
<i>Coordination environment of Pb(II) on biogenic MnO₂</i>	37
DISCUSSION	39
<i>Cation exchange at interlayer vacancies and selectivity sequence</i>	39
<i>Contribution of secondary sites, edge and biomass, for Zn(II) and Pb(II) sorption</i>	40
<i>Pb(II) sorption on biogenic MnO₂ and displacement of interlayer Mn(III)</i>	43
<i>Environmental implications</i>	45
ACKNOWLEDGMENTS	46
REFERENCES	46
CHAPTER 3	51
ABIOTIC OXIDATION OF GLUCOSE AND GLUCONATE BY MNO₂	51
ABSTRACT	51

INTRODUCTION	52
MATERIAL AND METHODS	54
<i>Dissolution experiments</i>	55
<i>Glucose consumption in glucose solutions reacted with δ-MnO₂ as a function of pH</i> ..	56
<i>Reaction of δ-MnO₂ with glucose and gluconate monitored by ATR-FTIR</i>	57
RESULTS	57
<i>Reductive dissolution of MnO₂</i>	57
<i>Glucose consumption upon reaction with δ-MnO₂</i>	59
<i>Reaction of glucose with δ-MnO₂ monitored by ATR-FTIR</i>	60
DISCUSSION	62
<i>Reductive dissolution of δ-MnO₂</i>	62
<i>Electron transfer to MnO₂: aqueous and surface-bound Mn</i>	66
<i>Oxidation of the organic substrates</i>	68
REFERENCES	72
CHAPTER 4	75
GLUCOSE METABOLISM IN <i>PSEUDOMONAS PUTIDA</i> GB-1 INDUCES THE DISSOLUTION OF MNO₂	75
ABSTRACT.....	75
INTRODUCTION	76
MATERIAL AND METHODS	78
<i>Preparation of bacterial suspensions</i>	79
<i>Preparation of bacteria-MnO₂ suspensions</i>	80
<i>Glucose, gluconate and 2-keto-gluconate consumption and production</i>	81
<i>Glucose-induced changes in dissolved oxygen and pH</i>	82
<i>Calculation of changes in dissolved oxygen and pH</i>	84
<i>Glucose-induced reductive dissolution of MnO₂</i>	86
RESULTS	89
<i>Glucose consumption and changes in solution pH and dissolved oxygen</i>	89
<i>Extracellular acidification of biomass suspended in defined electrolytes</i>	91
<i>Modelling the acidification induced by glucose metabolism</i>	93
<i>Impact of glucose metabolism on MnO₂ stability</i>	95
DISCUSSION	97
<i>Glucose metabolism results in extracellular acidification</i>	97
<i>Reductive dissolution of MnO₂ upon metabolic transformation of glucose</i>	99
<i>Differences observed in the synthetic biomineral and biogenic MnO₂ suspensions</i>	100
<i>Implications for the redox cycling of MnO₂ in natural systems</i>	101
REFERENCES	103

CHAPTER 5.....	107
COUPLED C AND MN DYNAMICS IN SOIL SYSTEMS	107
ABSTRACT	107
1. INTRODUCTION	108
1.1 <i>Cycling of soil organic C</i>	108
1.2 <i>Manganese and soil organic C</i>	110
1.3 <i>Objective of the review</i>	112
2. STABILISATION OF ORGANIC MOLECULES BY MnO_2	116
2.1 <i>Adsorption of organic C on MnO_2</i>	116
2.2 <i>Oxidative polymerization</i>	119
2.3 <i>Synergy between OM sorption and oxidative polymerization</i>	121
3. DEGRADATION OF ORGANIC MOLECULES BY $Mn(III)$ AND $Mn(IV)$	122
3.1 <i>Abiotic oxidation of organic C</i>	123
3.2 <i>MnO_2-catalyzed hydrolysis</i>	126
3.3 <i>Organic C oxidation by Mn-reducing organisms</i>	128
4. RELEVANCE OF $Mn(III)$ AND $Mn(IV)$ SPECIES IN SOIL SYSTEMS.....	128
4.2 <i>Occurrence of $Mn(IV)$ oxides</i>	129
4.2 <i>Occurrence of $Mn(III)$ complexes</i>	130
4.3 <i>Relative importance of $Mn(III)$ and $Mn(IV)$ species</i>	130
5. OPPORTUNITY FOR COUPLED Mn AND C CYCLES IN SOILS	132
5.1 <i>Stabilization interactions</i>	132
5.2 <i>Degradation interactions</i>	133
5.3 <i>Recommendations for future studies</i>	135
REFERENCES	137
CHAPTER 6.....	147
GENERAL CONCLUSION.....	147
SUMMARY.....	147
REACTIVITY OF BIOGENIC MnO_2 : CONTRIBUTION TO THE STATE OF THE	
ART	150
DIRECTIONS OF FUTURE RESEARCH.....	153
<i>Understanding the Mn cycle to understand its role to the C cycle</i>	153
<i>Coupled biotic and abiotic oxidation of organic molecules by MnO_2</i>	154
<i>Consideration on the level of complexity that we want to approach</i>	155
REFERENCES	156
CHAPTER 7 SUPPLEMENTARY INFORMATION	159
CHAPTER 2.....	159
CHAPTER 3	163

CHAPTER 4	168
CHAPTER 6	173
CHAPTER 8 APPENDIX – RAW DATA.....	175
CHAPTER 2	175
CHAPTER 3.....	181
CHAPTER 4	185

Chapter 1

General Introduction

The soil ecosystem: organo-mineral-microbial interfaces

Soil is a region of continuous exchange between the inorganic and the living world (1). The soil receives a constant input of organic matter from the overlying biological activity, a mineral input from the weathered bedrock and hosts an abundance of living species that orchestrates the biogeochemical activity it harbours.

Figure 1 describes how the fate of minerals is coupled both to the microbial and the carbon domains. Bacterial and fungal species are involved in the chemical weathering of primary minerals (for eg: feldspar, quartz and micas) into secondary minerals (for eg: clays, oxides and carbonates)(1, 2). A number of secondary phase minerals, including carbonates, phosphates and Fe and Mn oxides are precipitated through processes of biomineralization. In turn, anaerobic organisms may use redox active minerals as terminal electron acceptors at oxic-anoxic interfaces, which further couples the reactivity of the mineral to the cycling of a number of elements used as electron-rich substrates (C, N, S). Furthermore, while microorganisms are recognized as the main drivers of organic C decomposition, organo-mineral interactions control the accessibility of the organic residues to the decomposing community, thus becoming a major predictor of C stability.

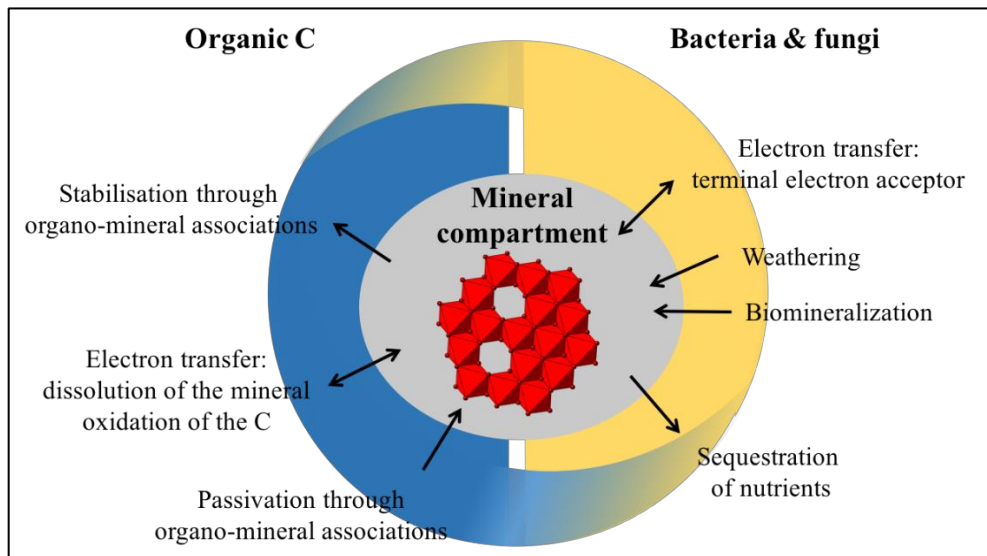


Figure 1 Examples of interactions between the organic, the mineral, and the microbial domains.

Manganese in the environment

Among the secondary minerals that play an important role in soils are manganese oxides (MnO_x). Manganese is the 12th most abundant element, and the 4th most abundant transition metal of the Earth's crust (behind Fe, Al and Ti), with an average concentration of about 1.0 g kg^{-1} (1, 3-5). Manganese is released to the Earth's surface through the weathering of the continental crust, in particular Mn-rich silicate and carbonates (3, 6, 7) and accumulates in the ocean, freshwater bodies, soil and sediments as soluble or solid phase Mn species. Deposits of Mn are extensively found on the ocean floor where it precipitates with Fe to form ferromanganese nodules and crusts (3, 4).

Once mobilised from primary minerals, the cycling of manganese is tightly coupled to the biological domain. Manganese is an essential micronutrient (3, 8), as organisms have evolved to take advantage of its capacity to accept and donate electrons. For example, the active site of the chlorophyll photosynthetic machinery, photosystem II (PSII), features a cluster of Mn atoms, whose redox activity allows to harvest photon energy and transform it to chemical energy (9-11). Manganese is also involved in the attenuation of oxidative stress in plants and animals by acting as the co-factor in superoxide dismutase (12-14). Some dissimilatory-metal reducing organisms take advantage of these redox potentials to harvest energy by using high valent Mn solids as terminal electron acceptors (15, 16). Furthermore, white-rot fungi, which are considered as the main driver of lignin degradation in soils, exploit the abiotic oxidative potential of Mn(III) species to degrade chemically recalcitrant organic polymers (17-19). However, if a wide-variety of microbial species has been found to express Mn(II)-oxidizing traits and to precipitate MnO_2 solids,

the physiological reasons for them to do so remain unclear (6, 8, 20-23). Suggested reasons include the protection against inorganic contaminants, UV or oxidative stress, the storage of electron acceptors, the production of external oxidants for the transformation of biologically refractory molecules to low molecular weight bioavailable substrates (24) or alternatively that Mn(II) oxidation may be a non-specific trait, the non-specific by-product of co-occurring reactions (6).

In the environment, Mn exists in three major valence states, namely Mn(II), Mn(III) and Mn(IV). Lower valent Mn is principally found as the soluble Mn^{2+} ion, but also in insoluble species such as $MnCO_3$ and $MnSO_4$, or sorbed onto Mn oxides (3). Mixed valent Mn(III/IV) oxides occur in various environmental settings (4). From a thermodynamic point of view, Mn(II) is favoured under anoxic conditions and at acidic pH, whereas Mn(III, IV) are favoured under oxic conditions and at higher pH values. However, the homogeneous oxidation of Mn by O_2 is exceedingly slow: Morgan et al. (3) reported that its oxidation at pH 8 and at 25°C was 10^9 times slower than that of Fe(II). Microbial oxidation of Mn(II) by bacteria and fungi, on the other hand, can accelerate the rate of Mn oxidation by up to 5 orders of magnitude (6, 8), which means that most naturally occurring Mn(III, IV) oxides are believed to form from the biotic oxidation of Mn(II) and Mn(III) to Mn(IV) (6, 8, 15, 25, 26).

Structure and composition of MnO_2

Freshly precipitated biogenic MnO_2 are phylломanganates, made of stacks of edge-sharing $Mn^{IV}O_6$ octahedral layers, with a 7–10 Å interlayer spacing occupied by water molecules, Na and Ca (8) (see **Figure 2**). These minerals have a high content of vacancy sites, with up to one out of six Mn(IV) absent from MnO_6 octahedral sites, high surface areas ($> 200 \text{ m}^2 \text{ g}^{-1}$) and average Mn oxidation number (AMON) ranging from 3.7 - 3.9 (8, 26-29).

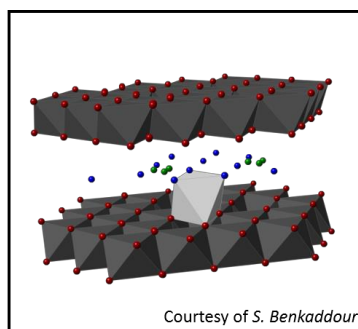


Figure 2 Model of the mineral structure of MnO_2 obtained using the Crystal Maker Software (30), and showing interlayer cations (Na and Ca in blue and green) and interlayer Mn(III) (lighter grey).

Co-occurrence of MnO₂ with Mn(II) is a major pathway of Mn(III)-enrichment of the mineral phase. At high Mn(II)/ Mn(IV) ratio and pH \geq 7.5, the reaction of Mn(II) with hexagonal phyllosulfate has been shown to induce phase transformations to Mn(III)-rich phases such as feitknechtite and manganite (31-35). Under lower Mn(II)/Mn(IV) ratios, and thus under concentration ratios that are more relevant to natural systems, these phase transformations are not observed, but the reaction of Mn(II) with MnO₂ was instead shown to induce modification in the stacking and symmetry of the layers from hexagonal to orthogonal (35-37). This transformation is explained by comproportionation of interlayer Mn(II) with Mn(IV) adjacent to vacancies, thus creating a layer Mn(III) and an interlayer Mn(III) on the vacancy that might later incorporate into the layer (35). High pH values (35, 38-40) and reaction at the edges of the particles may facilitate the enrichment of MnO₂ in structural Mn(III). For lower pH regimes, structural Mn(III) enrichment is likely to be less important, with instead capping of vacancies by interlayer Mn(III).

Reactivity of MnO₂: state of the art

Manganese oxides have a large capacity to sequester metal cations on their surface. The role of MnO₂ on the distribution and bioavailability of natural and anthropogenic inorganic contaminants is recognized to be disproportionately high compared to their occurrence (8) [550 ppm soil concentration reported by Schaklette et al., (41)], which has lead them to be called ‘scavengers of the sea’ (42). Their remarkable sorption properties are explained by a high surface area and a high content of vacancy sites. These defects lead to undersaturation of surface oxygens, which can be charge compensated by the adsorption of cations. The oxygen unsaturation at the lateral edge of MnO₂ layers create additional sorption sites, whose contribution can become important as the particle size decrease (29, 43-46). The effective role of edge sites during metal sorption can be difficult to track due to limitations of traditional X-ray adsorption spectroscopy (XAS) to distinguish interlayer and edge complexes that can have similar second-shell interatomic distances and because of the difficulty in modelling coordination numbers to better than 20 % uncertainty. As a result, studies have therefore reported contradicting views on the relative affinity of edge and interlayer complexes (46-48). The affinity of individual cations for MnO₂ surface reflects the stability of the complex formed on the surface of the mineral, the capacity of the incoming cation to compensate the unsaturation of oxygens surrounding the reactive site, and depend on a number of factors such as the

ionic potential, the electron configuration, acid-base properties and the pH of the solution (1). The incorporation of metals inside the vacancies, observed for cations such as Ni(II) and Co(II) can lead to largely irreversible sorption (39). But for other cations, such as Zn(II) and Pb(II) whose radii and electronic configurations prevent them from entering the layer structure, sorption is a reversible process (39, 50-52).

In addition to their scavenging properties, MnO₂ particles are characterized by a high redox reactivity. High valent Mn species are among the strongest abiotic oxidants found in natural environments (1, 53), as evidenced by the high redox potentials (E_h^0) of the Mn^{IV}O_{2(s)}/ Mn(II)_(aq) and the Mn^{III}₂O_{3(s)}/ Mn(II)_(aq) couples ($E_h^0 = 1.23$ eV and 1.49 eV, respectively)(54, 55). A recent study reported the oxidation of water through photochemical excitation ($\lambda = 400$ nm) of δ -MnO₂ at pH 6.5. Photoreduction of δ -MnO₂ lead to formation of Jahn-Teller distorted Mn(III) sites in the octahedral sheet, followed by migration of the newly formed Mn(III) in the interlayer and increase in the nanosheet stacking (56).

A number of studies have demonstrated the abiotic oxidation of a suite of organic molecules by MnO₂ (57). The studies of Stone et al. (58-65) in particular have provided considerable knowledge of the oxidative reactivity of MnO₂, but some mechanisms remain not fully understood. For example, Simanova et al. (44) have reported a 30 % Mn(III)-enrichment of the solid, with little aqueous Mn released, when reacting δ -MnO₂ with the Good's buffer HEPES (66), whereas other organics are known to reduce MnO₂ extensively and lead to the dissolution of the oxide. Furthermore, if the high redox potentials of Mn(IV, III)/ Mn(II) couples indicate that high valent Mn species may be important oxidants in natural systems, and if stabilised Mn(III) species are recognized as important factor for the litter decomposition (17, 19), there is little consensus on the impact that solid phase Mn oxides can have on the C cycle in soils. Laboratory experiments have shown that MnO₂ can be involved in different chemical reactions when reacting with organic molecules (57). However, some of these reactions can lead the stabilization of organic moieties while others on the contrary can enhance their degradation, and the relevance of these individual reactions in natural systems remains unclear.

Formation of biogenic Mn oxides

A wide range of phylogenetically diverse microorganisms (bacteria and fungi) are known to oxidize Mn(II) [see (6, 8) for reviews of identified Mn(II) oxidizing organisms].

Bacterial models that have been extensively studied include the Gram-positive spore forming *Bacillus* sp. strain SG1 (22, 23, 67), the γ -proteobacteria *Pseudomonas putida* strains MnB-1 and GB-1 (20, 68-70), the β -proteobacterium *Leptothrix discophera* strain SS-1 (6, 8) and the α -proteobacteria *Roseobacter* (71-73). The most studied Mn(II)-oxidizing fungi are the basidiomycota white-rot fungi (74-76). For all these different organisms, Mn(II)-oxidizing activity takes place in the extracellular space, leading to the extracellular accumulation of Mn(III) and Mn(IV) species.

Two main types of enzymes have been associated to the bacterial enzymatic Mn(II)-oxidation (21, 69), namely multicopper oxidases (MCO) and peroxidases. Recently, an MCO from *Bacillus* sp. PL-12 associated to Mn(II) oxidation was successfully expressed and purified (67, 77), which has allowed Soldatova et al. to propose a mechanism for Mn(II) oxidation by MCO (22, 23) that reconciles the known capacity of MCO to conduct 1 electron transfers and the 2-electron transfer required for Mn(II) oxidation to Mn(IV). The authors showed that the oxidation followed two successive 1 electron transfers, with only the oxidation of Mn(II) to Mn(III) taking place in the enzyme's active site. Newly generated Mn(III) was suggested to be displaced to a neighbouring holding site where it forms bi-nuclear Mn(III) complexes $[\text{Mn(III)}(\mu\text{-OH})_2\text{Mn(III)}]$, which then disproportionate to form one Mn(IV) and regenerate one Mn(II). This mechanism is consistent with previous studies that had identified a pyrophosphate-extractable Mn(III) intermediate (78). The Mn(II) oxidation by white-rot fungi is associated to the activity of a Mn peroxidase (MnP) enzyme (74, 76, 79) and of MCO proteins (80, 81). For other organisms, including *Roseobacter* and ascomycete fungi, Mn(II) oxidation has been associated to the indirect abiotic oxidation of Mn(II) by bacterially generated reactive oxygen species (ROS)(71, 72, 74, 82)

Pseudomonas putida GB-1 has been extensively used as a laboratory model for studying Mn(II) oxidation (20, 68-70). This bacterium has been shown to oxidize Mn(II) using both the MCO and the peroxidase pathways, as it encodes genes for two MCOs (*mnxG* and *mcoA*)(20, 68) and one animal-heme peroxidase (*mopA*)(69). One hypothesis that has been proposed for explaining the use of multiple enzymes is that the different enzymes may get activated under different environmental conditions (20, 69, 70). A recent study reported that *Pseudomonas* species may be able not only to oxidize Mn(II), but also ligand-stabilised Mn(III) $[\text{Mn(III)-L}]$, and that in the presence of ligands,

Mn(III)-L is an intermediate in the oxidation of Mn(II)(70). These new findings suggest that *Pseudomonas* species, but most likely other Mn(II)-oxidizing organisms using MCO enzymes, are key controls in the Mn(III)-L intermediates that may accumulate in the aqueous or soil systems.

Reactivity of biogenic MnO₂: state of the art on the impact of bacterial cells and organic molecules on the mineral reactivity

Due to their biotic origin, MnO_x mineral nanoparticles are often embedded in an organic matrix, which contains both intact bacterial cells and extracellular polymeric substances. A common approach to study the reactivity of MnO₂ is to use δ -MnO₂, a synthetic analogue to the biogenic MnO₂ mineral which only contains Mn(IV) (AMON 4)[for eg: (46, 56, 83, 84)]. The use of homogeneous and well-defined pure minerals provides mechanistic understanding of the surface reactivity of MnO₂ in simple systems. But the association of mineral phases with organic and biological components often affects the solid's reactivity. During biomineralization, the presence of an organic matrix has been shown to affect phase transformation and stability of newly-formed particles (85, 86). Furthermore, studies quantifying the loadings of trace metals on bacteria-Fe (hydr)oxides composites commonly report deviations from additivity relative to the loadings on bacteria-only and Fe (hydr)oxides-only sorbents. These differences were explained in part by masking of reactive sites through organo-mineral interactions [for eg: (87, 88)]. For MnO₂ in particular, its co-existence with bacterial cells and extracellular organic molecules can affect its reactivity in four major ways.

1) Additional sorption sites and passivation of reactive sites from organo-mineral interactions

The organic fraction can contribute directly to the sorption capacity of the bio-mineral sorbents (89-94), with high affinity metal interactions occurring predominantly on carboxyl and phosphoryl functional groups (89, 95) and which can compete with sorption sites on the mineral (29, 89, 92, 93, 96). In bio-mineral assemblages, while the biomass is the largest fraction on a mass basis, MnO₂ particles are generally thought to dominate the sorption reactivity. For instance, independent studies of Zn(II) and Ni(II) at circumneutral pH values concluded that partitioning to the organic fraction occurred only at high loadings once all interlayer vacancy sites were saturated (91, 96). However, the relative affinity for the organic and mineral sites depends on the nature of incoming cation, pH and the stability of the complex that can be formed on the mineral surface and

pH (1, 39, 46). Furthermore, if the kinetic accessibility to the mineral surface site is limited, cations may partition on the organic fraction.

Previous studies have concluded that organo-mineral interactions are not strong enough to passivate the vacancy sites of MnO₂ (91, 92, 96), but a recent study suggests that edge sites of MnO₂ particles may be passivated in biomineral composites, thus lowering the overall sorption capacity of the mineral (Simanova et al., *in prep*). The extent to which cations disrupt these organo-mineral interactions may depend on their respective affinities for MnO₂ surface sites.

2) Dynamic redox cycling of Mn: recycling of high valent Mn species

In biomineral assemblages, the presence of cells and enzymes means that the recycling of the high-valent Mn(III) and Mn(IV) centres is possible, and therefore that partially dissolved minerals may be regenerated. The regeneration of high valent Mn species is rarely considered in studies investigating the redox properties of MnO₂ but is expected to have tremendous importance on the effective reactivity of MnO₂.

3) Dynamic cycling of Mn: varying Mn(II, III) content

For biogenic MnO₂, the active biogeochemical cycling of Mn and the heterogeneity in concentration gradients that the biofilm can maintain suggests that local Mn(II) concentrations can be significantly higher near the cells than in the pore water, which exposes MnO₂ particles to an enrichment in Mn(III). For environmentally relevant pH regimes and in particular for biogenic MnO₂, for which the biomass may slow the reaction at the edges relative to abiotic MnO₂, structural Mn(III)-enrichment via abiotic Mn(II) oxidation is expected to be less important, with instead more capping of vacancies by interlayer Mn(III). However, the co-precipitation of the mineral within an organic matrix can lead to structural Mn(III)-enrichment of the mineral due to partial reduction of the oxide by organic residues.

In recent years, the impact the Mn(III)-enrichment can have on the mineral's reactivity has become apparent. It has been shown to affect the mineral's reactivity in two main ways. On one hand, the capping of vacancies by Mn(II) or Mn(III) was shown to affect the sorption reactivity of MnO₂ for Ni(II), Zn(II), Co(II) and Cu(II) (37, 44, 45, 84, 97). Authors have reported a decreasing in the maximal surface excesses and changes in the binding mechanism, with a greater contribution of edge surface complexes. On the other hand, the relative importance of Mn(III) and Mn(IV) centres in governing the redox

reactivity of MnO_x towards inorganic and organic species is unclear. For example, the oxidation of Cr(III), phenols and sulfide by a Mn(III)-enriched δ-MnO₂ (AMON 3.88) was reported to be inhibited by the addition of pyrophosphate, a ligand with a high affinity for Mn(III) species (98, 99). Tentative explanations of the observed inhibition included the higher reduction potential of Mn(III) relative to Mn(IV) (99, 100), and the faster ligand exchange rate of Mn(III) centers relative to Mn(IV) (98-100). However, a recent study reported that at pH 6, the Co(II) oxidation on δ-MnO₂ (AMON 4.0), was higher than that on a Mn(III)-enriched δ-MnO₂ (AMON 3.7) (84, 97). The relative importance of Mn(III) and Mn(IV) reaction sites in reacting with organic molecules thus warrants further investigation.

4) Dynamic response of metabolically active cells can affect solution conditions

The presence of metabolically active cells suggests that biogenic minerals are dynamic systems that may react to external perturbations, such as changes in nutrient availability and exposure to contaminants. The metabolic activity of neighbouring microorganisms can impact the long-term stability of MnO₂, since these are susceptible to partial reduction or dissolution in the presence of reductants and organic acids. These interactions have rarely been accounted for when studying either the scavenging or redox reactivity of MnO₂ minerals.

Research objective and dissertation organization

The objective of this thesis was to study the reactivity of MnO₂, both its affinity towards metals and towards organic reductants, in bio-mineral assemblages. We aimed to investigate the *passive* contributions of cells and organic residues to the reactivity of MnO₂, since these two components interact with the surface sites of oxide particles and offer additional reactive surfaces that may adsorb contaminants (29, 48, 89, 96, 101, 102). In addition, we aimed to account for the *dynamic* contributions of the biomass to the mineral's reactivity and stability. On one hand, the biomass matrix allows direct and indirect mechanisms for redox recycling of Mn, through reduction by organic residues and enzymatic Mn(II)-oxidation, which thus leads to varying Mn(II, III) content. On the other, the cells' metabolic activity can affect the chemical composition of the extracellular solution conditions and have a major impact on the mineral's stability. Therefore, this dissertation addressed the following questions:

- 1) How does the capping of vacancies by Mn(III) affect the sorption of trace metals with different affinities for MnO₂ surface sites? (**Chapter 2**)
- 2) How can the metabolic activity of bacterial cells destabilise MnO₂ in biogenic MnO₂ composites? (**Chapters 3-4**)
- 3) What contribution can biogenic MnO₂ minerals make to the overall C cycling in natural systems? (**Chapters 4-5**)

The thesis is organized in four research chapters. The research questions and approaches for each chapter are described below. Conclusions and future perspectives are discussed in **Chapter 6**.

Chapter 2

Pb, Zn and Mn sorption on biogenic MnO₂: contaminant loading and competitive access to vacancy sites

The scavenging properties of biogenic MnO₂ minerals are largely attributed to sorption on layer structural vacancies. However, the capping of vacancies by Mn(II) or Mn(III) may decrease the extent of metal sorption by competing for the occupancy of vacancy sites. The hypothesis guiding this work is that the position of cations on the affinity series relative to Mn(II) and Mn(III) governs the cation exchange mechanism and thus their sorption capacity on MnO₂. In this study, we investigated the sorption of Zn(II) and Pb(II), two common contaminants that are found on both sides of Mn on the affinity sequence for MnO₂, using the biogenic MnO₂ suspension precipitated by *Pseudomonas putida* GB-1. Batch sorption experiments conducted at pH 5.5 and extended X-ray absorption fine structure (EXAFS) spectroscopy were used to determine the sorption mechanisms of these metals. The displacement of Mn(III) by metals with higher affinity for MnO₂ surface sites may allow for greater loading for these specific cations, whereas the inability of metals with lower affinity to displace sorbed Mn(III) may enhance metal partitioning onto the biomass.

Chapter 3

Abiotic oxidation of glucose and gluconate by δ -MnO₂

The high redox potentials of Mn(IV)/ Mn(II) and Mn(III)/ Mn(II) couples means that these species are among the strongest oxidants present in natural systems (1, 53) and that they can oxidize a range of organic molecules relevant in soil solutions such as organic acids and sugars. However kinetics constraints will eventually largely control the rates

and extent of these reactions. In this study, we compared the dissolution of δ -MnO₂, the synthetic analogue of the natural biogenic MnO₂, when reacted with glucose and gluconate at pH values of 4.5, 5.5 and 6.5 for up to 24 h. Measurements of aqueous Mn by Inductively Coupled Plasma – Optical Emission Spectroscopy (ICP-OES) provided an estimate of electron equivalents transferred to the mineral that led to dissolution of the mineral, whereas colorimetric assays and Attenuated Total Reflection – Fourier Transformed Infrared (ATR-FTIR) spectra provided qualitative measure of changes in glucose or gluconate concentrations. Understanding the reactivity of MnO₂ towards simple organic compounds relevant to soil systems, decoupled from any biological contribution, provides knowledge of the impact the oxide could have on C transformations in natural systems.

Chapter 4

*Glucose metabolism in *Pseudomonas putida* GB-1 induces the dissolution of MnO₂*

Biogenic MnO₂ particles are susceptible to changes in biogeochemical conditions imposed by the cells' metabolic activity. In light of the significant pH-dependence of the redox reactivity of MnO₂, the stability of MnO₂ is expected to be strongly sensitive to extracellular modifications of the solution conditions. This study therefore aimed to characterise the response of stationary-phase *Pseudomonas putida* GB-1 and *Pseudomonas putida*-MnO₂ suspensions to the addition of glucose, chosen as a representative readily bioavailable carbon source, to understand the extent to which the microbial metabolism could induce the reductive dissolution of the Mn oxides. Understanding how bioavailable C substrates can impact the stability of MnO₂ has important implications regarding the fate and reactivity of the oxide in natural systems exposed to variations in the C content.

Chapter 5

Coupled C and Mn dynamics in soil systems

Due to their lower abundance, and despite their high reactivity, the importance of Mn in the context of the soil C cycle, has been less studied in the soil chemistry community relative to that of Al and Fe-bearing minerals, even though some studies suggest that adsorption of organic residues on MnO₂ may be more important than commonly thought and that the high redox potential of Mn species may drive the oxidation of natural organic molecules. Therefore, the goal of this literature review was to assess the ecosystem-scale importance of Mn species on C cycling, in order to identify knowledge gaps to be filled

and testable hypotheses to allow for a better understanding the coupled cycles of Mn and C in soils.

REFERENCES

1. Sposito G. The chemistry of soils: Oxford university press; 2008.
2. Gadd GM. Metals, minerals and microbes: geomicrobiology and bioremediation. *Microbiology*. 2010;156(3):609-43.
3. Morgan JJ. Manganese in natural waters and earth's crust: Its availability to organisms. *Metal ions in biological systems*. 2000;37:1-34.
4. Post JE. Manganese oxide minerals: Crystal structures and economic and environmental significance. *Proc. Nat. Acad. Sci.*, 1999;96(7):3447-54.
5. Wedepohl KH. The composition of the continental crust. *Geochim Cosmochim Ac.* 1995;59(7):1217-32.
6. Tebo BM, Johnson HA, McCarthy JK, Templeton AS. Geomicrobiology of manganese (II) oxidation. *Trends Microbiol.*, 2005;13(9):421-8.
7. Templeton A, Knowles E. Microbial transformations of minerals and metals: recent advances in geomicrobiology derived from synchrotron-based X-ray spectroscopy and X-ray microscopy. *Ann. Rev. Earth Planet. Sci.*, 2009;37:367-91.
8. Tebo BM, Bargar JR, Clement BG, Dick GJ, Murray KJ, Parker D, et al. Biogenic manganese oxides: properties and mechanisms of formation. *Annu Rev Earth Planet Sci.* 2004;32:287-328.
9. Brudvig GW, Crabtree RH. Mechanism for photosynthetic O₂ evolution. *Proc. Nat. Acad. Sci.*, 1986;83(13):4586-8.
10. Haumann M, Müller C, Liebisch P, Iuzzolino L, Dittmer J, Grabolle M, et al. Structural and oxidation state changes of the photosystem II manganese complex in four transitions of the water oxidation cycle (S₀→ S₁, S₁→ S₂, S₂→ S₃, and S₃, 4→ S₀) characterized by X-ray absorption spectroscopy at 20 K and room temperature. *Biochem.*, 2005;44(6):1894-908.
11. Umena Y, Kawakami K, Shen J-R, Kamiya N. Crystal structure of oxygen-evolving photosystem II at a resolution of 1.9 Å. *Nature*. 2011;473(7345):55-60.
12. Bowler C, Montagu Mv, Inze D. Superoxide dismutase and stress tolerance. *Ann. Rev. Plant Biol.*, 1992;43(1):83-116.
13. Macmillan-Crow LA, Cruthirds DL. Manganese superoxide dismutase in disease. *Free radical research*. 2001;34(4):325-36.
14. Bowler C, Van Camp W, Van Montagu M, Inze D, Asada K. Superoxide dismutase in plants. *Critical Rev. Plant Sci.*, 1994;13(3):199-218.
15. Tebo BM, Clement BG, Dick GJ. Biotransformations of manganese. *Manual Environ. Microbiol.*, 2007;3:1223-38.
16. Lovley DR, Phillips EJ. Novel mode of microbial energy metabolism: organic carbon oxidation coupled to dissimilatory reduction of iron or manganese. *Applied Environ. Microbiol.*, 1988;54(6):1472-80.
17. Berg B, Steffen K, McLaugherty C. Litter decomposition rate is dependent on litter Mn concentrations. *Biogeochem.*, 2007;82(1):29-39.
18. Davey MP, Berg B, Emmett BA, Rowland P. Decomposition of oak leaf litter is related to initial litter Mn concentrations. *Botany*. 2007;85(1):16-24.
19. Keiluweit M, Nico P, Harmon ME, Mao J, Pett-Ridge J, Kleber M. Long-term litter decomposition controlled by manganese redox cycling. *Proc. Nat. Acad. Sci.*, 2015;112(38):5253-60.

20. Geszvain K, McCarthy JK, Tebo BM. Elimination of manganese (II, III) oxidation in *Pseudomonas putida* GB-1 by a double knockout of two putative multicopper oxidase genes. *Applied Environ. Microbiol.*, 2013;79(1):357-66.
21. Geszvain K, Butterfield C, Davis RE, Madison AS, Lee S-W, Parker DL, et al. The molecular biogeochemistry of manganese (II) oxidation. Portland Press Limited; 2012.
22. Soldatova AV, Romano CA, Tao L, Stich TA, Casey WH, Britt RD, et al. Mn (II) oxidation by the multicopper oxidase complex Mnx: A coordinated two-stage Mn (II)/(III) and Mn (III)/(IV) mechanism. *J. Am. Chem. Soc.*, 2017;139(33):11381-91.
23. Soldatova AV, Tao L, Romano CA, Stich TA, Casey WH, Britt RD, et al. Mn (II) oxidation by the multicopper oxidase complex Mnx: A binuclear activation mechanism. *J. Am. Chem. Soc.*, 2017;139(33):11369-80.
24. Sunda WG, Kieber DJ. Oxidation of humic substances by manganese oxides yields low-molecular-weight organic substrates. *Nature*. 1994.
25. Spiro TG, Bargar JR, Sposito G, Tebo BM. Bacteriogenic manganese oxides. *Acc. Chem Res.*, 2009;43(1):2-9.
26. Santelli CM, Webb SM, Dohnalkova AC, Hansel CM. Diversity of Mn oxides produced by Mn(II)-oxidizing fungi. *Geochim Cosmochim Ac.* 2011;75(10):2762-76.
27. Webb S, Tebo B, Bargar J. Structural characterization of biogenic Mn oxides produced in seawater by the marine *Bacillus* sp. strain SG-1. *Am. Mineral.*, 2005;90(8-9):1342-57.
28. Villalobos M, Toner B, Bargar J, Sposito G. Characterization of the manganese oxide produced by *Pseudomonas putida* strain MnB1. *Geochim- Cosmochim Ac.*, 2003;67(14):2649-62.
29. Droz B, Dumas N, Duckworth OW, Pena J. A comparison of the sorption reactivity of bacteriogenic and mycogenic Mn oxides nanoparticles. *Environ. Sci. Technol.*, 2015.
30. CrystalMaker®. CrystalMaker Software Limited, Oxford, England.
31. Mandernack KW, Post J, Tebo BM. Manganese mineral formation by bacterial spores of the marine *Bacillus*, strain SG-1: Evidence for the direct oxidation of Mn (II) to Mn (IV). *Geochim Cosmochim Ac.* 1995;59(21):4393-408.
32. Bargar JR, Tebo BM, Bergmann U, Webb SM, Glatzel P, Chiu VQ, et al. Biotic and abiotic products of Mn (II) oxidation by spores of the marine *Bacillus* sp. strain SG-1. *Am. Mineral.*, 2005;90(1):143-54.
33. Elzinga EJ. Reductive transformation of birnessite by aqueous Mn(II). *Environ. Sci. Technol.*, 2011;45(15):6366-72.
34. Lefkowitz JP, Rouff AA, Elzinga EJ. Influence of pH on the reductive transformation of birnessite by aqueous Mn (II). *Environ. Sci. Technol.*, 2013;47(18):10364-71.
35. Zhao H, Zhu M, Li W, Elzinga EJ, Villalobos M, Liu F, et al. Redox reactions between Mn (II) and hexagonal birnessite change its layer symmetry. *Environ. Sci. Technol.*, 2016;50(4):1750-8.
36. Hinkle MA, Flynn ED, Catalano JG. Structural response of phyllomanganates to wet aging and aqueous Mn (II). *Geochim Cosmochim Ac.* 2016;192:220-34.
37. Hinkle MA, Dye KG, Catalano JG. Impact of Mn (II)-Manganese Oxide Reactions on Ni and Zn Speciation. 2017.
38. Miyata N, Tani Y, Sakata M, Iwahori K. Microbial manganese oxide formation and interaction with toxic metal ions. *J. Biosci. Bioeng.*, 2007;104(1):1-8.
39. Kwon KD, Refson K, Sposito G. Understanding the trends in transition metal sorption by vacancy sites in birnessite. *Geochim Cosmochim Ac.* 2013;101:222-32.
40. Zhu M, Ginder-Vogel M, Parikh SJ, Feng X-H, Sparks DL. Cation effects on the layer structure of biogenic Mn-oxides. *Environ. Sci. Technol.*, 2010;44(12):4465-71.
41. Shacklette HT, Boerngen JG. Element concentrations in soils and other surficial materials of the conterminous United States. 1984.
42. Goldberg ED. Marine geochemistry 1. Chemical scavengers of the sea., *J. Geol.*, 1954;62(3):249-65.

43. Manceau A, Lanson B, Drits VA. Structure of heavy metal sorbed birnessite. Part III: Results from powder and polarized extended X-ray absorption fine structure spectroscopy. *Geochim Cosmochim Ac.* 2002;66(15):2639-63.
44. Simanova AA, Kwon KD, Bone SE, Bargar JR, Refson K, Sposito G, et al. Probing the sorption reactivity of the edge surfaces in birnessite nanoparticles using Nickel (II). *Geochim Cosmochim Ac.* 2015;164:191-204.
45. Peña J, Bargar JR, Sposito G. Copper sorption by the edge surfaces of synthetic birnessite nanoparticles. *Chem Geol.* 2015;396:196-207.
46. van Genuchten CM, Peña J. Sorption selectivity of birnessite particle edges: a d-PDF analysis of Cd(II) and Pb(II) sorption by δ -MnO₂ and ferrihydrite. *Environ. Sci. Process. Impacts.*, 2016.
47. Takahashi Y, Manceau A, Geoffroy N, Marcus MA, Usui A. Chemical and structural control of the partitioning of Co, Ce, and Pb in marine ferromanganese oxides. *Geochim Cosmochim Ac.* 2007;71(4):984-1008.
48. Villalobos M, Bargar J, Sposito G. Mechanisms of Pb (II) sorption on a biogenic manganese oxide. *Environ. Sci. Technol.*, 2005;39(2):569-76.
49. Kraemer SM, Cheah SF, Zapf R, Xu JD, Raymond KN, Sposito G. Effect of hydroxamate siderophores on Fe release and Pb(II) adsorption by goethite. *Geochim Cosmochim Ac.* 1999;63(19-20):3003-8.
50. Tani Y, Ohashi M, Miyata N, Seyama H, Iwahori K, Soma M. Sorption of Co (II), Ni (II), and Zn (II) on biogenic manganese oxides produced by a Mn-oxidizing fungus, strain KR21-2. *J. Environ. Sci. Health, Part A.* 2004;39(10):2641-60.
51. Kwon KD, Refson K, Sposito G. Zinc surface complexes on birnessite: A density functional theory study. *Geochim Cosmochim Ac.* 2009;73(5):1273-84.
52. Kwon KD, Refson K, Sposito G. Surface complexation of Pb (II) by hexagonal birnessite nanoparticles. *Geochim Cosmochim Ac.* 2010;74(23):6731-40.
53. Luther GW. *Inorganic Chemistry for Geochemistry and Environmental Sciences: Fundamentals and Applications*: John Wiley & Sons; 2016.
54. Bricker O. Some stability relations in system MnO₂-H₂O at 25 degrees and 1 atmosphere total pressure. *Am. Mineral.*, 1965;50(9):1296-.
55. Jenkins S. *CRC Handbook of Chemistry and Physics*. Chemical Engineering. 2012;119(9):9-10.
56. Marafatto FF, Strader ML, Gonzalez-Holguera J, Schwartzberg A, Gilbert B, Peña J. Rate and mechanism of the photoreduction of birnessite (MnO₂) nanosheets. *Proc. Nat. Acad. Sci.*, 2015; 112(15):4600-5.
57. Remucal CK, Ginder-Vogel M. A critical review of the reactivity of manganese oxides with organic contaminants. *Environ. Sci. Process Impacts.*, 2014;16(6):1247-66.
58. Stone AT. The reduction and dissolution of Mn (III) and Mn (IV) oxides by organics. 1983.
59. Stone AT, Morgan JJ. Reduction and Dissolution of Manganese(III) and Manganese(IV) Oxides by Organics 1. Reaction with Hydroquinone. *Environ. Sci. Technol.*, 1984;18(6):450-6.
60. Stone AT, Morgan JJ. Reduction and dissolution of manganese (III) and manganese (IV) oxides by organics. Part 2. Survey of the reactivity of organics. *Environ Sci Technol.* 1984;18(8).
61. Stone AT. Microbial Metabolites and the Reductive Dissolution of Manganese Oxides - Oxalate and Pyruvate. *Geochim Cosmochim Ac.* 1987;51(4):919-25.
62. Stone AT. Reductive dissolution of manganese(III/IV) oxides by substituted phenols. *Environ. Sci. Technol.*, 1987;21(10):979-88.
63. Stone AT, Ulrich H-J. Kinetics and reaction stoichiometry in the reductive dissolution of Mn(IV) dioxide and Co(III) oxide by hydroquinone. *J. Coll. Interf. Sci.*, 1989;132(2):509-22.
64. Wang Y, Stone AT. The citric acid-Mn^{III},^{IV}O₂ (birnessite) reaction. Electron transfer, complex formation, and autocatalytic feedback. *Geochim Cosmochim Ac.* 2006;70(17):4463-76.
65. Wang Y, Stone AT. Reaction of Mn^{III},^{IV} (hydr)oxides with oxalic acid, glyoxylic acid, phosphonoformic acid, and structurally-related organic compounds. *Geochim Cosmochim Ac.* 2006;70(17):4477-90.
66. Ferguson WJ, Braunschweiger K, Braunschweiger W, Smith JR, McCormick JJ, Wasmann CC, et al. Hydrogen ion buffers for biological research. *Analytical Biochem.*, 1980;104(2):300-10.

67. Butterfield CN, Soldatova AV, Lee S-W, Spiro TG, Tebo BM. Mn (II, III) oxidation and MnO₂ mineralization by an expressed bacterial multicopper oxidase. *Proc. Nat. Acad. Sci.*, 2013; 110(29): 11731-5.
68. Geszvain K, Tebo BM. Identification of a two-component regulatory pathway essential for Mn (II) oxidation in *Pseudomonas putida* GB-1. *Applied Environ. Microbiol.*, 2010;76(4):1224-31.
69. Geszvain K, Smesrud L, Tebo BM. Identification of a third Mn (II) oxidase enzyme in *Pseudomonas putida* GB-1. *Applied Environ. Microbiol.*, 2016;82(13):3774-82.
70. Wright MH, Geszvain K, Oldham VE, Luther III GW, Tebo BM. Oxidative Formation and Removal of Complexed Mn (III) by *Pseudomonas* Species. *Front. Microbiol.*, 2018;9:560.
71. Hansel CM, Francis CA. Coupled photochemical and enzymatic Mn (II) oxidation pathways of a planktonic *Roseobacter*-like bacterium. *Applied Environ. Microbiol.*, 2006;72(5):3543-9.
72. Learman D, Voelker B, Vazquez-Rodriguez A, Hansel C. Formation of manganese oxides by bacterially generated superoxide. *Nature Geoscience*. 2011;4(2):95.
73. Andeer PF, Learman DR, McIlvin M, Dunn JA, Hansel CM. Extracellular haem peroxidases mediate Mn (II) oxidation in a marine *Roseobacter* bacterium via superoxide production. *Environ. Microbiol.*, 2015;17(10):3925-36.
74. Hansel CM, Zeiner CA, Santelli CM, Webb SM. Mn (II) oxidation by an ascomycete fungus is linked to superoxide production during asexual reproduction. *Proc. Nat. Acad. Sci.*, 2012;109(31): 12621-5.
75. Ziegenhagen D, Hofrichter M. Degradation of humic acids by manganese peroxidase from the white-rot fungus *Clitocybula dusenii*. *J. Basic Microbiol.*, 1998;38(4):289-99.
76. Hofrichter M. Review: lignin conversion by manganese peroxidase (MnP). *Enzyme and Microbial technology*. 2002;30(4):454-66.
77. Butterfield CN, Tebo BM. Substrate specificity and copper loading of the manganese-oxidizing multicopper oxidase Mnx from *Bacillus* sp. PL-12. *Metallomics*. 2017;9(2):183-91.
78. Webb SM, Dick GJ, Bargar JR, Tebo BM. Evidence for the presence of Mn(III) intermediates in the bacterial oxidation of Mn(II). *Proc. Nat. Acad. Sci.*, 2005;102(15):5558-63.
79. Ten Have R, Teunissen PJ. Oxidative mechanisms involved in lignin degradation by white-rot fungi. *Chemical Rev.*, 2001;101(11):3397-414.
80. Schlosser D, Höfer C. Laccase-catalyzed oxidation of Mn²⁺ in the presence of natural Mn³⁺ chelators as a novel source of extracellular H₂O₂ production and its impact on manganese peroxidase. *Applied Environ. Microbiol.*, 2002;68(7):3514-21.
81. Höfer C, Schlosser D. Novel enzymatic oxidation of Mn²⁺ to Mn³⁺ catalyzed by a fungal laccase. *FEBS letters*. 1999;451(2):186-90.
82. Learman D, Wankel S, Webb S, Martinez N, Madden A, Hansel C. Coupled biotic–abiotic Mn (II) oxidation pathway mediates the formation and structural evolution of biogenic Mn oxides. *Geochim Cosmochim Ac.* 2011;75(20):6048-63.
83. Lanson B, Drits VA, Gaillot A-C, Silvester E, Plançon A, Manceau A. Structure of heavy-metal sorbed birnessite: Part I. Results from X-ray diffraction. *Am. Mineral.*, 2002;87(11-12):1631-45.
84. Simanova AA, Peña J. Time-resolved investigation of cobalt oxidation by Mn(III)-rich δ-MnO₂ using quick X-Ray absorption spectroscopy. *Environ. Sci. Technol.*, 2015;49(18):10867-76.
85. Mikutta C, Kretzschmar R. Synthetic coprecipitates of exopolysaccharides and ferrihydrite. Part II: Siderophore-promoted dissolution. *Geochim Cosmochim Ac.* 2008;72(4):1128-42.
86. Mikutta C, Mikutta R, Bonneville S, Wagner F, Voegelin A, Christl I, et al. Synthetic coprecipitates of exopolysaccharides and ferrihydrite. Part I: Characterization. *Geochim Cosmochim Ac.* 2008;72(4):1111-27.
87. Moon EM, Peacock CL. Modelling Cu (II) adsorption to ferrihydrite and ferrihydrite–bacteria composites: deviation from additive adsorption in the composite sorption system. *Geochim Cosmochim Ac.* 2013;104:148-64.
88. Kulczycki E, Fowle D, Fortin D, Ferris F. Sorption of cadmium and lead by bacteria–ferrihydrite composites. *Geomicrobiol J.* 2005;22(6):299-310.

89. Toner B, Manceau A, Marcus MA, Millet DB, Sposito G. Zinc sorption by a bacterial biofilm. *Environ. Sci. Technol.*, 2005;39(21):8288-94.
90. Haack EA, Warren LA. Biofilm hydrous manganese oxyhydroxides and metal dynamics in acid rock drainage. *Environ. Sci. Technol.*, 2003;37(18):4138-47.
91. Toner B, Manceau A, Webb SM, Sposito G. Zinc sorption to biogenic hexagonal-birnessite particles within a hydrated bacterial biofilm. *Geochim Cosmochim Ac.* 2006;70(1):27-43.
92. Nelson YM, Lion LW, Shuler ML, Ghiorse WC. Lead binding to metal oxide and organic phases of natural aquatic biofilms. *Limnology and Oceanography.* 1999;44(7):1715-29.
93. Peña J, Kwon KD, Refson K, Bargar JR, Sposito G. Mechanisms of nickel sorption by a bacteriogenic birnessite. *Geochim Cosmochim Ac.* 2010;74(11):3076-89.
94. Zhu M, Ginder-Vogel M, Sparks DL. Ni (II) sorption on biogenic Mn-oxides with varying Mn octahedral layer structure. *Environ. Sci. Technol.*, 2010;44(12):4472-8.
95. Guiné V, Spadini L, Sarret G, Muris M, Delolme C, Gaudet J-P, et al. Zinc sorption to three gram-negative bacteria: combined titration, modeling, and EXAFS study. *Environ. Sci. Technol.*, 2006; 40(6):1806-13.
96. Peña J, Bargar JR, Sposito G. Role of bacterial biomass in the sorption of Ni by biomass-birnessite assemblages. *Environ. Sci. Technol.*, 2011;45(17):7338-44.
97. Wang Y, Benkaddour S, Marafatto F, Pena J. Diffusion-and pH-dependent reactivity of layer-type MnO₂: Reactions at particle edges versus vacancy sites. *Environ. Sci. Technol.*, 2018.
98. Nico PS, Zasoski RJ. Importance of Mn (III) availability on the rate of Cr (III) oxidation on δ -MnO₂. *Environ. Sci. Technol.*, 2000;34(16):3363-7.
99. Nico PS, Zasoski RJ. Mn (III) center availability as a rate controlling factor in the oxidation of phenol and sulfide on δ -MnO₂. *Environ. Sci. Technol.*, 2001;35(16):3338-43.
100. Ukrainczyk L, McBride MB. Oxidation of phenol in acidic aqueous suspensions of manganese oxides. *Clays and Clay Minerals.* 1992;40(2):157-66.
101. Toner B, Sposito G. Reductive dissolution of biogenic manganese oxides in the presence of a hydrated biofilm. *Geomicrobiol J.* 2005;22(3-4):171-80.
102. Peña. Contaminant Metal Immobilization by Biogenic Manganese Oxide Nanoparticles: Implications for Natural Attenuation and Bioremediation (Dissertation). 2009.

Chapter 2

Pb, Zn and Mn sorption on biogenic MnO₂: contaminant loading and competitive access to vacancy sites

The wet chemical and spectroscopic data presented in this chapter were contributed by members of the Environmental Geochemistry Lab. In particular, the sorption isotherms and Mn release data were collected by Imelda Dossou Etui [“Effect of glucose on the adsorption of Pb(II) and Zn(II) by a biogenic Mn oxide for use as a remediation method for wastewater treatment”, Master thesis in Environmental Sciences, Université de Lausanne, 2015].

ABSTRACT

The scavenging properties of biogenic MnO₂ minerals are largely attributed to sorption on layer structural vacancies. The co-occurrence of lower-valent Mn in abiotic MnO₂ has been shown to affect the reactivity of the mineral, either by modifying the structure of the mineral and its Mn(III) content or by competing for the occupancy of vacancy sites. However, incoming cations may displace Mn(III) if the affinity of the metal for the mineral surface is higher than that of Mn(III), and given the instability of Mn(III), if the metal can promote its disproportionation. Here we studied the sorption of Zn(II) and Pb(II) on biogenic MnO₂ precipitated by *Pseudomonas putida* GB-1, through batch sorption experiments and EXAFS spectroscopy. Sorption isotherms on biomass-only and biogenic MnO₂ at pH 5.2 ± 0.3 showed considerably higher loadings for Pb(II) ($0.49 \text{ mol Pb mol}^{-1}$

Mn) than for Zn(II) ($0.12 \text{ mol Zn mol}^{-1} \text{ Mn}$). For $q > 0.1 \text{ mol mol}^{-1} \text{ Mn}$, Zn(II) and Pb(II) sorption was concomitant, albeit to different extents, with the accumulation of Mn(II) in solution. Based on wet chemical measurements and the analysis of Zn K-edge and Pb L₃-edge EXAFS spectra, we concluded that the difference in Zn(II) and Pb(II) loadings and extent of Mn(II) accumulation in solution was related to the capacity of the cations to displace interlayer Mn(III). Our findings demonstrate that the capacity of incoming cations to displace any previously sorbed metal ions ultimately determines the effective capacity of MnO₂ to influence the fate of different, often co-occurring, contaminants in natural systems.

INTRODUCTION

The distribution and bioavailability of inorganic species in environmental systems is regulated by their sorption to solid phases (1-4). Layer-type manganese oxides (MnO₂) are ubiquitous nanoparticulate minerals that are characterised by an unusually high affinity for metal cations. Most naturally occurring Mn oxides precipitate upon the biologically-mediated oxidation of Mn(II) and Mn(III) to Mn(IV) (5-8). Biogenic MnO₂ are phyllosulfates with hexagonal sheet symmetry, have up to one out of every six Mn(IV) absent from MnO₆ octahedral layer sites, and average Mn oxidation numbers ranging from 3.7- 3.9 (5, 7-11). The presence of vacancy sites in these oxides leads to local undersaturation of surface oxygen atoms, which can be charge-compensated by cation adsorption upon their diffusion to the mineral interlayers (7, 12). Oxygen undersaturation at the lateral edges of MnO₂ layers creates additional sorption sites that become increasingly abundant as particle size decreases (12-15). These scavenging properties ensure layer-type Mn oxides a major role in the mobility and bioavailability of contaminants and trace elements in natural systems (16, 17) and motivates their use for the remediation of metal-polluted environments (18-21).

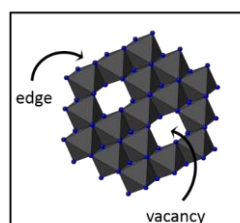


Figure 3 Model of the mineral structure of MnO₂ obtained using the Crystal Maker software (22), and showing reactive sites for the sorption of cations : edges and vacancies

In regions of active redox cycling, Mn(II, III) often co-occurs with MnO_{2(s)}. The sorption of Mn(II), which increases with increasing pH (23, 24), can be a major pathway for Mn(III)-enrichment of MnO₂. Specifically, comproportionation between Mn(II) and Mn(IV) (25-27) results in both layer and interlayer Mn(III). Under low Mn(II)/Mn(IV) ratios relevant to natural systems, comproportionation does not cause phase transformations (28-30). However interlayer Mn(III) may incorporate inside a vacancy and the Jahn-Teller distortion of the newly incorporated Mn(III) modifies the stacking and symmetry of the layers from hexagonal to orthogonal (28-30). High pH values (24, 28, 31, 32) and reaction of Mn(II) at the edges of the particles may facilitate the enrichment of structural Mn(III). For lower pH regimes and in particular for biogenic MnO₂, where microbial biomass may slow the reaction at the edges relative to abiotic MnO₂, structural Mn(III)-enrichment is likely to be less important than the capping of vacancies by interlayer Mn(III).

The capping of vacancies by Mn(II) or Mn(III) may decrease the extent of metal sorption and promotes greater partitioning of metals to the particle edges, as shown for Ni(II) and Zn(II) in abiotic systems (30, 33). However, based on the position of the adsorbing metal on the affinity sequence for MnO₂ relative to Mn(II) and Mn(III), incoming metals may be able to displace adsorbed Mn(II, III). Selectivity sequences have been established through macroscopic measurements for a number of metals (34-37). The selectivity sequence $\text{Ni} < \text{Zn} \leq \text{Co} \leq \text{Mn} < \text{Cu} < \text{Pb}$ has been determined for MnO₂ through sorption experiments (34-36). This sequence is consistent with that obtained through competitive sorption experiments on biogenic MnO₂ at pH 7 (37). While Mn is reported in these selectivity sequences, the affinity of Mn(II) and Mn(III) was not differentiated in these studies. Furthermore, Mn(II) and Mn(III) sorption and desorption is dynamic given the various redox processes that can produce, consume or displace these species in biogenic MnO₂.

The hypothesis guiding this work is that the position of cations on the affinity series relative to Mn(II) and Mn(III) governs the cation exchange mechanism and thus their sorption capacity on MnO₂. Furthermore, depending on the accessibility of metals to vacancy sites, metal cations may partition to other surface sites, including those on the biomass (11, 18, 38-43) or at the mineral particle edges (12-15), depending on the availability of the latter in biogenic MnO₂. To test these hypothesis, we compared the relative sorption behaviour of Zn(II) and Pb(II) on biogenic MnO₂. These common contaminants are found on both sides of Mn on the affinity sequence for MnO₂ surfaces (34, 35) and therefore are ideal probes of mineral reactivity. Furthermore, spectroscopic studies have

identified the coordination geometries of Zn(II) and Pb(II) sorbed by MnO₂. Specifically, Zn(II) adsorbs as triple-corner-sharing (TCS) complexes at vacancy sites, adopting a tetrahedral geometry (Zn^{IV}) at low loading and an octahedral coordination (Zn^{VI}) at high loading (12, 15, 30, 39, 44). For Pb(II), in addition to TCS complexes, stable complexes on the edges of MnO₂ have been described (14, 15, 45, 46).

In the current study, sorption isotherms of Zn(II) and Pb(II) were measured on the biogenic MnO₂ precipitated by the bacterium *Pseudomonas putida* GB-1 at pH 5.2 ± 0.3. Since neither Zn(II) nor Pb(II) undergoes redox changes upon reaction with biogenic MnO₂ (12, 39, 45), aqueous Mn(II) was used to measure the displacement of lower-valent Mn(II, III) by Zn(II) and Pb(II). Sorption isotherms were also measured on biomass-only sorbents to estimate the highest surface loadings of the metals to the organic fraction on the bio-mineral sorbent. Finally, Zn K-edge and Pb L₃-edge EXAFS spectroscopy was used to identify the sorption mechanism as a function of the affinity of the metal cations for MnO₂ and availability of reactive surface sites.

MATERIAL AND METHODS

All solutions were prepared using ultrapure water (> 18 mΩ cm) and ACS-grade reagents. The Mn(II)-oxidizing bacterium *Pseudomonas putida* GB-1 (*P. putida*) was used to produce biomass-only and biogenic MnO₂ suspensions. All cultures were propagated under sterile conditions in a nutrient-rich growth medium (38, 43, 47). Leptothrix medium was prepared by dissolving glucose (1.0 g L⁻¹, 5.5 mM), casamino acids (0.50 g L⁻¹), yeast extract (0.50 g L⁻¹) and HEPES acid (2.38 g L⁻¹, 10 mM) in ultrapure water and autoclaved at 120 °C for 20 minutes. After cooling, the medium was amended with filter-sterilised CaCl₂ (0.5 mM), MgSO₄ (0.83 mM), FeCl₃ (3.7 μM), CuSO₄ (40 nM), ZnSO₄ (152 nM), CoCl₂ (84 nM), Na₂MoO₄ (54 nM), and either 0 or 1 mM MnCl₂, which are denoted as (-)Mn or (+)Mn cultures, respectively.

Preparation of sorbent suspensions

Biomass-only and biogenic MnO₂ suspensions were prepared by inoculating (-)Mn or (+)Mn growth medium (125 mL) in Erlenmeyer flasks (250 mL) capped with foam stoppers and incubating on a table-top shaking incubator in the dark (27 °C, 150 RPM). The inocula for biomass-only and biogenic MnO₂ suspensions were transferred from *P. putida* suspensions grown in (-)Mn or (+)Mn medium, respectively, for 30 ± 12h. The

resulting sorbents were harvested after 120 ± 24 h of incubation and washed from their spent growth media by centrifuging the suspensions (3700 RCF, 10°C, 30 min) and re-suspending the pellets in a NaCl solution (10 mM), with 30 min equilibration between centrifuge cycles on an end-to-end rotator. The washing procedure was repeated twice, and the washed sorbents were suspended in 10 mM NaCl.

Sorbent concentrations (c_{sorbent} , kg L⁻¹) were determined gravimetrically. A 10 mL aliquot of the biomass-only or biogenic MnO₂ suspensions was sampled and the sorbent was collected in Epi-Tubes 1 mL at a time by centrifuging (14'000 RCF, 5 min) and discarding the supernatant. The pellets were oven-dried for 48h at 45°C. Reported c_{sorbent} values are the average of triplicate measurements. The concentration of MnO₂ in biogenic MnO₂ was measured by ICP-OES (Perkin-Elmer Optima 8300) as described below.

Zn(II) and Pb(II) sorption by biomass-only and biogenic MnO₂ sorbents

Zinc(II) and Pb(II) isotherms were measured at pH 5.2 ± 0.3 . Biomass-only and biogenic MnO₂ suspensions (15 ± 0.1 mL) were transferred to opaque high-density polyethylene (HDPE) bottles (30 mL) from the sorbent suspension under vigorous stirring (43). Zn(II) and Pb(II) additions were made from stock solutions of ZnCl₂ (10 mM and 100 mM) and Pb(NO₃)₂ (10 mM and 100 mM) to yield metal concentrations ranging from 0 μM to 600 μM. All experiments were performed in triplicate. Sorption samples were equilibrated for 24h on an end-to-end rotator before sampling for chemical analysis.

Concentrations of Mn, Zn(II) and Pb(II) were measured by ICP-OES (Perkin-Elmer Optima 8300) using 2 or 3 emission lines for each element. Aqueous metal concentrations (c_{Pb} , c_{Zn} , and c_{Mn}) were measured from 5 mL aliquots obtained by filtration (0.20 μm pore size, polyethersulfone) and acidification with 50 μL of HNO₃ 65 %. To determine the total metal concentrations in biomass and biogenic MnO₂ suspensions ($c_{\text{Pb_TOT}}$, $c_{\text{Zn_TOT}}$, $c_{\text{Mn_TOT}}$), 1 mL aliquots of the suspensions were acid-digested for 10 min with 50 μL of 1 M oxalic acid and 50 μL of HNO₃ 65 % to achieve complete dissolution of the mineral phase and/or release of all metal ions to solution. After centrifugation of the digested suspensions (14'000 RCF, 5 min), the supernatants were diluted and analysed for Zn(II), Pb(II) and Mn(II).

All solutions were undersaturated with respect to common oxide and hydroxide minerals [ZnO, Zn(OH)₂, Pb₂(OH)₃Cl_(s), PbCl(OH)_(s), Pb₂O(OH)_{2(s)}, PbO_(s), Pb(OH)_{2(s)}] as determined by speciation calculations in MINEQL+ (48). Because Pb can easily

precipitate, additional controls were collected in triplicate to verify the absence of Pb precipitates when adding 10, 50, 100, 250, 450 and 650 μM PbNO_3 to 10 mM NaCl (pH 5.5 maintained by NaOH addition). Control samples were equilibrated for 24h before sampling (0.2 μm PES filter) and were not diluted prior to chemical analysis. The difference between concentration of Pb in solution and that obtained after acid digestion of any solid (50 μL of 1 M oxalic acid and 50 μL of HNO_3 65 % added to 5 mL sample) were within instrument uncertainty (< 2.6 %) (see **Table 2-A3**), confirming the absence of homogeneous precipitation of Pb solid.

Surface excess q_i (with $i = \text{Zn}$ or Pb), which is defined as the number of moles of i partitioned to the sorbent relative to its concentrations in the supernatant, normalised by the quantity of sorbent (49), was expressed in both units of $\text{mol } i \text{ kg}^{-1}$ sorbent and $\text{mol } i \text{ mol}^{-1} \text{ Mn}$. Values of q_i were calculated according to $(c_{i_TOT} - c_{i_aq})/c_{\text{sorbent}}$ OR $(c_{i_TOT} - c_{i_aq})/(c_{\text{Mn_TOT}} - c_{\text{Mn_aq}})$. The distribution coefficient $K_d = q_i/c_i$ as a function of q_i was plotted to evaluate the category of the isotherms and test whether a maximum surface excess (q_{max}) was achieved on the sorbents (49).

Zn K-edge and Pb L₃-edge X-ray absorption spectroscopy

Separate samples for X-ray absorption spectroscopy were prepared as described above and are named according to: metal_% loading ($\text{mol } i \text{ mol}^{-1} \text{ Mn}$)_pH (see **Table 2S1** in the Supporting Information). Metals were added dropwise from 10 mM ZnCl_2 and $\text{Pb}(\text{NO}_3)_2$ solutions to the sorbent suspensions and equilibrated for 26h on an end-to-end rotator before chemical analysis. Finally, the pellets were collected through successive centrifugation cycles. Excess moisture was removed with a Kim-wipe before freezing the samples in a 1.5 mL EpiTube at -4°C . At the beamline, wet pastes were thawed, homogenised and loaded on aluminium sample holders sealed with Kapton tape.

X-ray absorption spectra were collected at beamline 4-1 of the Stanford Synchrotron Radiation Lightsource (SSRL, Stanford, US) using a Si(220) $\phi = 90^\circ$ crystal monochromator. The monochromator energy was calibrated using Zn(0) and Pb(0) foils with binding energies of 9659 eV and 13035 eV respectively, in a double-transmission configuration. Data were acquired under liquid-nitrogen conditions (77 K) using a Lytle ion chamber detector in fluorescence mode. Scattering of the incident beam was attenuated by Cu-3 and Ga-3 filters for Zn(II) and Pb(II) analysis respectively, and soller slits. Three to four replicate spectra were collected for individual samples.

The EXAFS spectra were analysed using the SixPack program (50) which is built on the IFEFFIT engine (51). Replicate spectra were aligned to a common energy scale and averaged. The averaged spectra were then background subtracted with the following parameters for Zn K-edge and Pb L₃-edge respectively: $E_0 = 9659$ (Zn) and 13035 (Pb) eV, $R_{bkg} = 1$, no clamps, splined between 1.0 and 11 \AA^{-1} (Zn) and 1.0 and 10.8 \AA^{-1} (Pb) with a linear pre-edge function and a quadratic post-edge function, a Kaiser-Bessel Fourier-transform window and $k\text{-weight} = 3$.

Zinc K-edge EXAFS spectra of the Zn-biogenic MnO₂ samples were analysed by linear combination fitting (LCF) of reference spectra using the least-square fitting module in SixPack to determine the partitioning of Zn(II) between the biomass and mineral fractions of the sorbent, as well as the distribution of Zn(II) between tetrahedral (Zn^{IV}) and octahedral (Zn^{VI}) coordination geometries. The sum of components was allowed to vary during the fitting of the experimental spectra, and the R-value and reduced chi-squared (χ^2_{red}) were used to evaluate the quality of the fits. Reference spectra collected for Zn(II)-sorbed on *P. putida* biomass (Ref. 1: $q \sim 0.1 \text{ mol Zn kg}^{-1}$ biomass, pH 6.0, 10 mM NaCl and HEPES) and on biogenic MnO₂ (Ref. 2: $q = 0.09 \text{ Zn mol}^{-1} \text{ Mn}$, pH 6.5, 10 mM NaCl and HEPES, 100 % Zn^{IV} and Ref. 3: $q = 0.12 \text{ mol Zn mol}^{-1} \text{ Mn}$, pH 7.0, 10 mM NaCl and HEPES, 59 % Zn^{IV} / 41 % Zn^{VI}). The fraction of Zn^{IV} in Ref. 2 was inferred from shell-by-shell fitting, which showed characteristic structural parameters for tetrahedral Zn [$R_{(\text{Zn-O})} = 1.96 \pm 0.01 \text{ \AA}$, $\text{CN}_{(\text{Zn-O})} = 3.72 \pm 0.66$; $\sigma^2 = 0.005 \pm 0.002 \text{ \AA}^2$; $R_{(\text{Zn-Mn})} = 3.34 \pm 0.01 \text{ \AA}$, $\text{CN}_{(\text{Zn-Mn})} = 7.12 \pm 1.61$, $\sigma^2 = 0.008 \pm 0.002 \text{ \AA}^2$](52). For Ref. 3, the average coordination of Zn(II) was determined by LCF using Ref. 2 and chalcophanite (ZnMn₃O₇·3H₂O, 100 % Zn^{VI}) as reference spectra.

Due to the lack of reference spectra acquired under the same conditions as the experimental samples, the Pb L₃-edge EXAFS spectra of Pb-sorbed biogenic MnO₂ were analysed by shell-by-shell fitting using the FEFF EXAFS fitting interface in SixPack. The CrystalMaker® software (22) was used both to visualise the coordination environments of Pb(II) on MnO₂ and to generate a list of atomic coordinates needed as an input to FEFF6 (51, 53) to calculate phase and amplitude scattering paths for the Pb-MnO₂ cluster. An amplitude reduction factor (S_0^2) of 0.84 was used in all fits, which was determined previously for Pb(II) sorbed on δ -MnO₂ (45). All EXAFS spectra were fitted in R-space over the k -range of $3\text{-}10.8 \text{ \AA}^{-1}$ and R -range $1\text{-}4 \text{ \AA}$, and plotted alongside reference EXAFS spec-

tra for Pb(II) sorbed on abiotic δ -MnO₂ [0.2 mol Pb mol⁻¹ MnO₂, pH 5.8, 7 days equilibration, collected at room temperature (45)] and Pb(II) sorbed on *Penicillium chrysogenum* cell wall powder [0.01 mol Pb kg⁻¹, pH 6.0, 24h of equilibration, collected at room temperature on dried samples (54)].

RESULTS

Sorption of Pb(II) and Zn(II) by *P. putida* biomass and biogenic MnO₂

The sorption isotherms of Zn(II) and Pb(II) on the biomass-only sorbent are presented in **Figure 1A**. Both isotherms are L-type, which show moderate sorption of the metals by organic functional groups on the biomass. The maximal surface excesses reached for Zn(II) and Pb(II) were 0.07 ± 0.04 and 0.20 ± 0.02 mol kg⁻¹ respectively. The greater sorption capacity of the biomass for Pb(II) as compared to Zn(II) is consistent with the soft character of Pb(II). At high metal concentrations, large scatter was observed in the surface excess values measured for replicate experiments. This variability in Zn(II) loadings was especially pronounced at $c_{Zn} > 200$ μ M and may arise from a biological response of the bacteria to high Zn(II) concentrations. On the contrary, the high toxicity of Pb(II) may inhibit any biological activity during the sorption experiments. Similar scattering observed in analogous sorption isotherms studies conducted in our group (43, 55) was ascribed to a non-linear biological response to high concentrations of toxic contaminants.

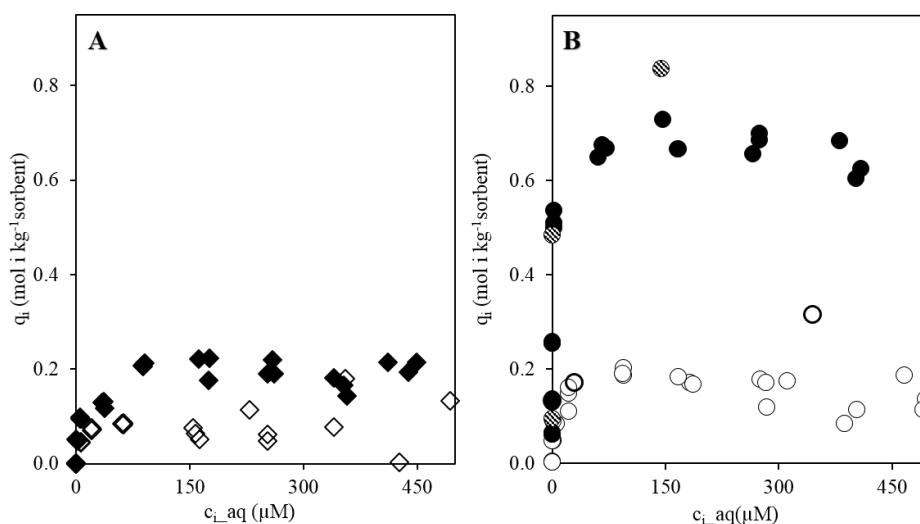


Figure 2 Sorption isotherms for Zn(II) (open symbols) and Pb(II) (filled symbols) on biomass-only (A) and biogenic MnO₂ (B), plotted in units of mol i kg⁻¹ sorbent, with i = Zn(II) or Pb(II). Samples with thicker lines (Zn-samples) and dashed fillings (Pb-samples) are those analysed by EXAFS spectroscopy.

Sorption isotherms for Zn(II) and Pb(II) on biogenic MnO₂ are presented in **Figure 2B**. Both isotherms are H-type, which demonstrates the extremely high affinity of MnO₂ for these divalent metal cations. The sorption isotherms showed a significantly higher sorption affinity and capacity for Pb(II) compared to Zn(II), which is consistent with previous studies (14, 17, 39, 42, 45, 56). While the mass of sorbent only increased by only 16 – 24 % in biogenic MnO₂ compared to biomass-only suspensions, the sorption capacity of the bio-mineral assemblages was 2 – 3 times greater than in the biomass-only sorbent, with surface excesses reaching $0.15 \pm 0.04 \text{ mol Zn kg}^{-1}$ and $0.67 \pm 0.03 \text{ mol Pb kg}^{-1}$. The large increase in loadings attained in the presence of MnO₂ is consistent with significant partitioning of both metals to the inorganic phase. The sorption isotherms on biogenic MnO₂ showed less scatter in replicate experiments at high loadings relative to the biomass-only sorbent. This difference likely reflects the reduced exposure of the bacterial cells to the contaminants in the biogenic MnO₂, either due to differences in cell viability between the two sorbents or physico-chemical protection of the cells by the mineral.

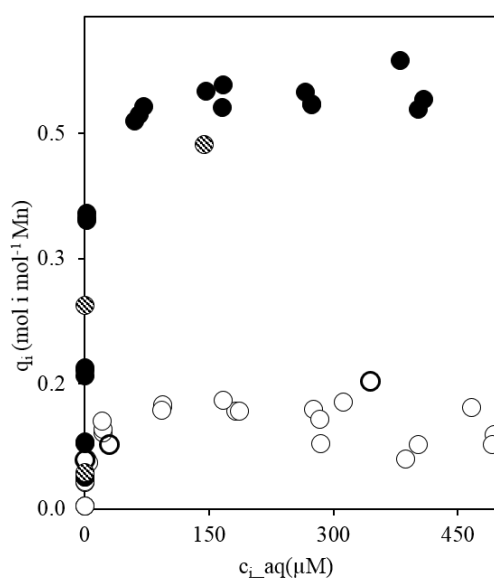


Figure 3 Sorption isotherms for Zn(II) (open symbols) and Pb(II) (filled symbols) on biogenic MnO₂, plotted in units of mol i mol⁻¹ MnO₂. Samples with thicker lines (Zn-samples) and dashed fillings (Pb-samples) are those analysed by EXAFS spectroscopy.

Because of the significant sorption of Zn(II) and Pb(II) to the inorganic phase inferred from **Figure 2**, surface excess is expressed in units of mol i mol⁻¹ Mn in **Figure 3**. The lack of a clear x-intercept in plots of K_d versus q_i (see **Figures 2-S2A-B**) did not support the calculations of a q_{max} values. Thus, we defined q_{max} for Zn(II) and Pb(II) as the highest loading measured (\pm standard deviation of the 7 and 12 highest loadings), with $c_{Zn} <$

200 μM for Zn(II). The sorption isotherms showed q_{max} of $0.12 \pm 0.01 \text{ mol Zn mol}^{-1} \text{ Mn}$ and $0.49 \pm 0.02 \text{ mol Pb mol}^{-1} \text{ Mn}$ and indicated the presence of 0.06 and 0.35 moles of high affinity surface sites per mole of MnO_2 ($c_{i_aq} < 3.0 \mu\text{M}$) for Zn(II) and Pb(II) respectively.

Release of Mn to solution upon Zn(II) and Pb(II) sorption

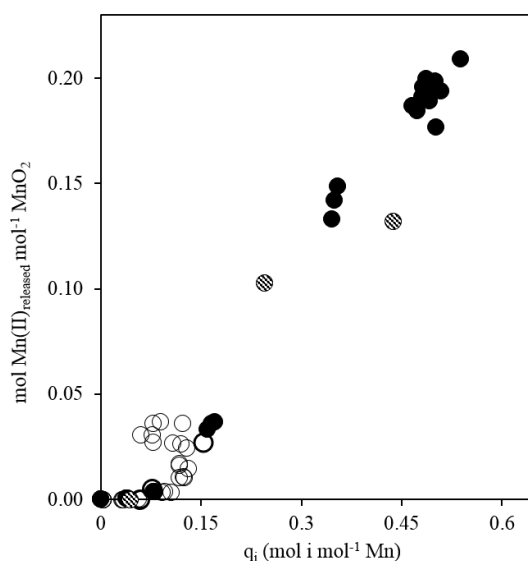


Figure 4 Concentration of Mn(II) released ($\text{mol mol}^{-1} \text{ MnO}_2$) as a function of surface excess for Zn(II) (open circles) and Pb(II) (filled circles). Samples with thicker lines show are those analysed by EXAFS spectroscopy.

Figure 4 shows that the sorption of Zn(II) and Pb(II) was accompanied by a loading-dependent accumulation of aqueous Mn(II). However, Mn(II) released was significantly higher in the Pb(II) experiments than in Zn(II) experiments. For both metals, no Mn(II) was released at loadings below $0.10 \text{ mol mol}^{-1}$. For Zn(II), up to $0.04 \text{ mol Mn(II) mol}^{-1} \text{ Mn}$ was measured at loadings greater than $0.10 \text{ mol Zn mol}^{-1} \text{ Mn}$. The large scatter in $q_{\text{Zn(II)}}$ values at $c_{\text{Zn(II)}} > 150 \mu\text{M}$ was also seen in **Figure 4**. For Pb(II), the data showed three distinct trends (R1, R2, R3): no release of Mn(II) for $0.0 - 0.1 \text{ mol Pb mol}^{-1} \text{ Mn}$ (R1), then Mn(II) increased linearly with increasing loading up to $q_{\text{Pb}} = 0.49 \pm 0.02 \text{ mol Pb mol}^{-1} \text{ Mn}$, with a slope of $0.60 \text{ mol Mn(II)}_{\text{released}} \text{ mol}^{-1} \text{ Pb}_{\text{sorbed}}$ ($R^2 = 0.97$)(R2). Finally, no more Mn(II) was released once the maximal surface excess was reached (R3).

The release of Mn upon metal sorption by MnO_2 has been modelled previously (43) as a cation exchange process described in terms of a Vanselow selectivity coefficient K_{app} (49) (**Eq. 1**).

$$K_{app} = [\equiv i][Mn] / [\equiv Mn][i(II)] \quad \text{Eq. 1}$$

where the surface concentrations of specie *i* [$\equiv i$] are equal to the surface excess q_i , and the aqueous specie concentrations [$i(II)$] is equal to c_i . The selectivity coefficient can thus be re-written to yield **Eq. 2**.

$$K_{app} = q_i c_{Mn(II)} / q_{Mn} c_i \quad \text{Eq. 2}$$

such that a value of $K_{app} > 1$ indicates selectivity for *i* over Mn. Assuming that the total number of reactive sites on MnO₂ remains constant, we can write a mass balance for the surface sites (**Eq. 3**) and rewrite **Eq. 2** to yield **Eq. 4**.

$$q_{TOT} = q_i + q_{Mn} \quad \text{Eq. 3}$$

$$q_i / (c_i / c_{Mn}) = -K_{app} q_i + K_{app} q_{TOT} \quad \text{Eq. 4}$$

For q_i values $> 0.1 \text{ mol } i \text{ mol}^{-1} \text{ Mn}$, when sorption of *i* is associated to the displacement of sorbed Mn, a plot of $q_i / (c_i / c_{Mn})$ versus q_i should yield a straight line with a slope of $-K_{app}$. Because of the large variability in q values at high Zn(II) concentrations, $q_{Zn} / (c_{Zn} / c_{Mn})$ versus q_{Zn} were plotted only for $c_{Zn} < 200 \mu\text{M}$ (see **Figures 2S2 A-B**). The selectivity coefficients K_{app} for Zn(II) and Pb(II) were 0.11 ± 0.12 (95 % confidence interval, $R^2 = 0.41$) and 108.19 ± 16.65 (95 % confidence interval, $R^2 = 0.93$) respectively, indicating no selectivity for Zn(II) over Mn and a very large selectivity of Pb(II) relative to Mn at pH 5 (49). For Pb(II), the total number of reactive sites estimated was $0.49 \pm 0.02 \text{ mol reactive sites mol}^{-1} \text{ MnO}_2$.

Coordination environment of Zn(II) on biogenic MnO₂

The loadings of Zn(II) on the organic and inorganic fractions of the sorbent were determined by scaling the surface loading by the fractions obtained from LCF. We found between 0.06 and 0.09 mol Zn kg⁻¹ sorbent partitioned to the biomass. The significant contribution of the biomass to Zn(II) sorption in the lowest loading sample suggests the presence of some high affinity surface sites in the organic fraction. These EXAFS-derived loadings of Zn(II) on the organic fraction of biogenic MnO₂ are consistent with the data for the biomass-only system, which show a q_{max} of $0.07 \pm 0.04 \text{ mol Zn kg}^{-1} \text{ biomass}$. This agreement suggests that Zn(II) sorption by the biomass is similar in both sorbents. In the biogenic MnO₂ samples, the EXAFS-derived loading of Zn(II) on the mineral fraction increased with increasing loading and ranged from 0.07 to 0.21 mol Zn kg⁻¹ sorbent (0.03

to 0.10 mol Zn mol⁻¹ Mn). This trend is consistent with studies that place Zn(II) towards the low-affinity end of the selectivity sequence for MnO₂.

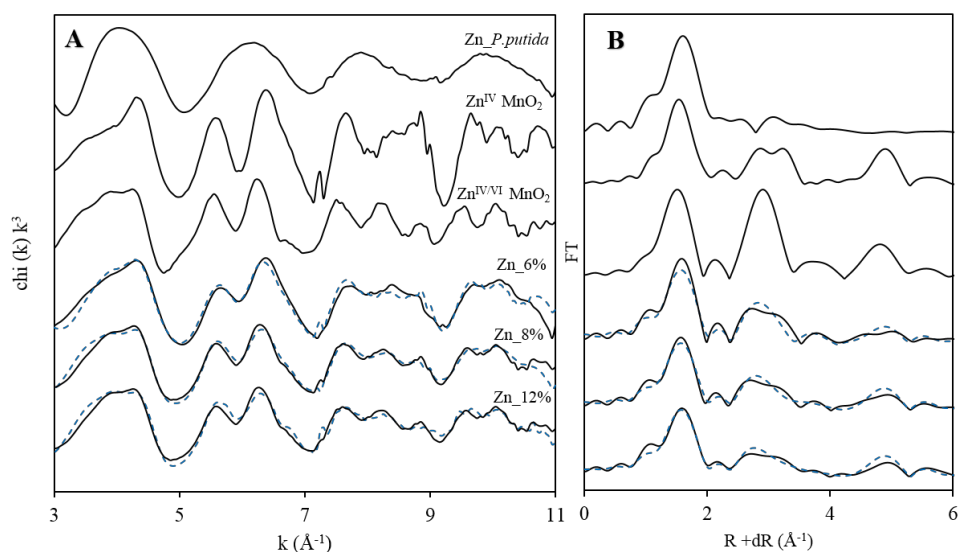


Figure 5 EXAFS spectroscopic spectra (A) and their Fourier transforms (B) of Zn(II) loaded on biogenic MnO₂, modelled by linear combination fitting of reference spectra. The references were chosen to represent the Zn(II) coordination environment on the organic fraction and on the mineral, in a tetrahedral (Zn^{IV}) and in an octahedral (Zn^{VI}) geometries. The data is plotted as a black line, the fittings as the blue dotted lines. Spectra were fitted in Six-Pack using the least square fitting module, from k 1 to k 11 Å⁻¹ with no restrictions on the component sum. The Fourier transform of the samples and fits were obtained using the FEFF EXAFS fitting module in Sixpack, from k 3 to 11 Å⁻¹, R_{\min} 1 to R_{\max} 4, using a Kaiser-Bessel window.

Table 1 Fitting parameters for Zn(II) sorption on biogenic MnO₂, for samples with loadings (q_{sample}) of 0.06, 0.08 and 0.12 mol Zn mol⁻¹ Mn. Fractions (f) of LCF reference spectra [Zn sorbed on biomass and Zn sorbed on MnO₂, either with tetrahedral (Zn^{IV}) and octahedral geometries (Zn^{VI})] are reported. The values of q_x (with x = biomass or vacancies) represent the loading on the different binding sites as determined by LCF. The values for q_{biomass} are obtained as $q_{\text{biomass}} = q_{\text{sample}} \times f_{\text{Zn-biomass}}$ and assume that $q_{\text{edges}} = 0$. The values of $q_{\text{vacancies}}$ are obtained as $q_{\text{vacancies}} = q_{\text{sample}} \times f_{\text{Zn-MnO}_2}$ and assume that $q_{\text{edges}} = 0$.

	Zn 6 % 0.06 mol mol ⁻¹ 0.13 mol kg ⁻¹	Zn 8 % 0.08 mol mol ⁻¹ 0.17 mol kg ⁻¹	Zn 15 % 0.15 mol mol ⁻¹ 0.32 mol kg ⁻¹	
LCF	$f_{\text{Zn-biomass}}$*	0.44	0.26	0.29
	$f_{\text{Zn-MnO}_2}$ (mixed Zn ^{IV} /Zn ^{VI})**	0.13	0.46	0.52
	$f_{\text{Zn-MnO}_2}$ (100 % Zn ^{IV})***	0.42	0.23	0.13
	$f_{\text{Zn-MnO}_2}$	0.55	0.69	0.65
	χ^2_{red}	0.69	0.41	0.29
	$\sum_{\text{components}}$	0.98	0.95	0.94
speciation	q_{biomass} (mol kg ⁻¹)	0.06	0.04	0.09
	$q_{\text{vacancies}}$ (mol kg ⁻¹)	0.07	0.12	0.21
	$q_{\text{vacancies}}$ (mol mol ⁻¹)	0.03	0.06	0.10

* Zn(II) sorbed on biomass, pH 6.0, 10 mM NaCl, 10 mM HEPES

** Zn(II) sorbed on biogenic MnO₂, pH 7.0, 41 % Zn^{IV}/59 % Zn^{VI}, 10 mM NaCl, 10 mM HEPES

*** Zn(II) sorbed on biogenic MnO₂, pH 6.5, ~ 100 % Zn^{VI}, 10 mM NaCl, 10 mM HEPES

The above interpretation assumes that Zn(II) does not partition to the particle edges. Because the Zn-Mn distances in the Zn-TCS complex on vacancies and for Zn(II) sorbed on particles edges are too similar to be distinguished by EXAFS, the LCF analysis cannot distinguish sorption on edges to that on biomass. The linear combination of spectra for Zn-TCS complex on vacancies ($C_{N_{Zn-Mn}} 6$) and of Zn on biomass ($C_{N_{Zn-Mn}} 0$) would indeed yield a spectrum very similar to that expected for Zn(II) sorbed on edges ($C_{N_{Zn-Mn}} 2$) (11, 57). However, the references for Zn(II) sorbed on biogenic MnO₂ have similar loadings to those measured in this study, and shell-by-shell fittings did not indicate any sorption of Zn(II) on edge sites. Furthermore, as the loadings of Zn(II) on biomass in biogenic MnO₂ as predicted by LCF are consistent with those measured for the biomass-only sorbent, it also argues against significant partitioning of Zn(II) to edge sites.

Coordination environment of Pb(II) on biogenic MnO₂

The Pb L₃-edge EXAFS spectra and corresponding Fourier transforms (FT) for Pb(II) sorbed on biogenic MnO₂ are reported in **Figure 6**, alongside reference spectra for Pb(II) sorbed on bacterial biomass and δ -MnO₂. The EXAFS spectrum of Pb(II) sorbed on biomass showed one main oscillation and no significant second-shell structure in the FT. The EXAFS spectra from biogenic MnO₂ samples showed a strong splitting of the second oscillation around $k = 5.5 - 6.0 \text{ \AA}^{-1}$ and large amplitude in the second-shell (Pb-Mn) peak in the FT. This splitting was much more pronounced in the EXAFS spectrum from biogenic MnO₂ than δ -MnO₂, where the latter was reported as having 75 % of the Pb(II) adsorbed at the particle edges and 25 % adsorbed at vacancy sites. The shape of this oscillation, which correlates with the second-shell amplitude, indicates greater partitioning of Pb(II) to vacancy sites in biogenic MnO₂ compared to δ -MnO₂. The EXAFS spectra for the experimental samples were similar to each other irrespective of the Pb(II) loading, which ranged from 0.04 to 0.44 mol Pb mol⁻¹ Mn. The EXAFS spectrum from the lowest loading sample, however, appeared slightly shifted to lower k values relative to the higher loading samples. The superposition of the rising edge across all samples, as seen by plotting the first derivative of the μ spectra in **Figure S3**, confirmed that the differences did not originate from energy misalignment, but indicate a slightly different coordination environment for Pb(II) at low loading.

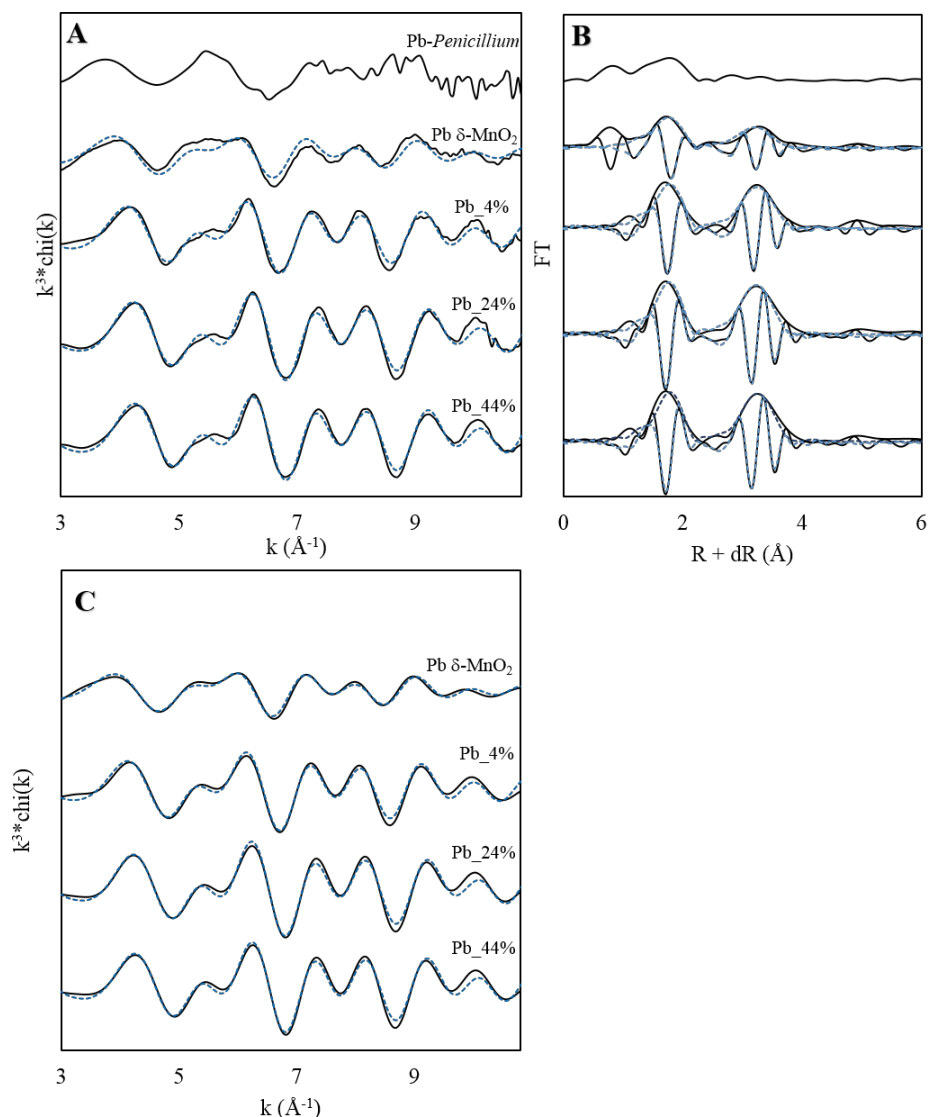


Figure 6 EXAFS spectroscopic spectra (A) and their Fourier transforms (B) of Pb(II) loaded on biogenic MnO₂, modelled by shell-by-shell fittings using a two shells model. The data is plotted alongside references for Pb(II) sorbed on biomass [*Penicillium chrysogenum*, pH 6.0, 0.01 mol Pb kg⁻¹ (54)] and Pb(II) loaded on δ-MnO₂ [0.2 mol Pb mol⁻¹ MnO₂, pH 5.5, (45)]. Figure (C) shows the Fourier-filtered chi spectra. The data is plotted as a black line, the fittings as the blue dotted lines.

The high disorder inherent to the Pb(II) ion, which leads to low Pb-Mn CNs, together with the lack of a distinct features in the Pb-biomass EXAFS spectrum limits our ability to evaluate the extent to which the biomass or even MnO₂ particle edges may sorb Pb(II) in biogenic samples. Given the extremely high affinity of Pb(II) for MnO₂ [0.40 mol Pb mol⁻¹ Mn reported for Pb(II) sorbed on δ-MnO₂ at pH 5.5 (14)], Pb(II) is expected to be largely adsorbed at vacancies sites. Although sorption at particle edges has been reported in abiotic samples (12, 45, 56), these studies reported CNs that were even lower than the ones obtained in this study. A large contribution of the biomass to Pb(II) sorption would also be expected to reduce the CN of the Pb-Mn shell significantly. While the 0.04 mol Pb

mol⁻¹ Mn low loading sample returned a CN of 3.42 ± 1.20 that was lower by 0.5 to 0.7 relative to the higher loading samples, all three CNs were the same if considering the fitting uncertainty. Because we could not determine unambiguously the contribution, if any, from the biomass and particle edges from EXAFS spectroscopy, we discuss plausible scenarios below as constrained by the sorption isotherms, the measurements of Mn(II) in solution as a function of Pb(II) loading and the modelling of the EXAFS spectra.

Table 2 Fitting parameters for Pb sorption on biogenic MnO₂ by shell-by-shell fitting, for samples with loadings (q_{sample}) of 0.04, 0.24 and 0.44 mol Pb mol⁻¹ Mn, obtained by shell-by-shell fitting of EXAFS spectra using a two-shells model. Fittings were run with a value for s^0_2 fixed to 0.843 and 7 other unconstrained variables.

Shell		Pb_4 %	Pb_24 %	Pb_44 %	Pb_δ-MnO ₂
Pb-O	R (Å)	2.29 ± 0.02	2.26 ± 0.01	2.27 ± 0.01	2.27 ± 0.01
	N	2.58 ± 0.70	2.46 ± 0.61	2.43 ± 0.63	2.46 ± 0.62
	σ^2 (Å)	0.009 ± 0.003	0.008 ± 0.002	0.008 ± 0.003	$0.008 \pm .003$
Pb-Mn	R (Å)	3.73 ± 0.02	3.70 ± 0.02	3.71 ± 0.02	3.72 ± 0.02
	N	3.42 ± 1.20	4.06 ± 1.26	3.81 ± 1.23	2.08 ± 0.91
	σ^2 (Å)	0.009 ± 0.003	0.009 ± 0.002	0.009 ± 0.002	$0.011 \pm .003$
	E _o	-4.11 ± 2.00	-3.11 ± 1.82	-1.74 ± 1.88	-9.48 ± 2.21
	R	0.054	0.045	0.049	0.056
	χ^2_{red}	240.72	206.00	1172.31	0.01

DISCUSSION

Cation exchange at interlayer vacancies and selectivity sequence

In natural and engineered systems, the sorption capacity of MnO₂ particles towards an incoming metal cation depends on the capacity of the latter to displace any cation already present on the sorption sites. The competition for these sites is expected to reflect both the relative concentrations of different metal cations and their relative affinity for the mineral's reactive sites. Because of the active redox cycling of Mn, interlayer Mn(II, III) is often found above and below structural vacancies. A consequence of the ready access of Mn(II, III) to interlayer vacancies is that these lower-valent Mn species can restrict the access to these sites to other metal cations. The positions of incoming cations relative to Mn(II, III) on the affinity serie for MnO₂ surface sites is thus expected to govern the cation exchange mechanism and the effective sorption capacity of MnO₂. Depending on the accessibility of

vacancy sites, metal cations may also partition to other sites, including organic functional groups on the biomass or surface sites at the particle edges.

In this study, we investigated the sorption of Zn(II) and Pb(II) on biogenic MnO₂, two metals found on both sides of Mn(II) and Mn(III) on the affinity series for MnO₂ vacancies. Sorption isotherms showed a much larger loading of Pb(II) compared to Zn(II). The 3 – 4 folds higher q_{\max} reached upon Pb(II) sorption compared to Zn(II) indicates that Pb(II) had access to 0.38 mol binding sites mol⁻¹ Mn inaccessible to Zn(II). The absence of Mn release during the sorption of the initial 0.10 mol i mol⁻¹ Mn indicate that the bio-mineral offered 0.10 mol mol⁻¹ Mn of reactive sites available to the two metals. Access to additional binding sites was restricted for Zn(II), but not for Pb(II). The accumulation of Mn(II) in solution that accompanied the sorption of Pb(II) for $q_{\text{Pb}} > 0.1$ mol Pb mol⁻¹ Mn indicates that Pb(II) can displace any Mn(II, III) occupying vacancy sites, thus explaining the high loading achieved for Pb(II). This result is consistent with the affinity sequence for MnO₂ with Zn(II) < Mn(II), Mn(III) < Pb(II) and a competitive access to sorption sites (34, 35, 56).

To identify the nature of the sorption sites that were seemingly inaccessible to Zn(II) but occupied by Pb(II) at high loading, we conducted EXAFS spectroscopic analysis of the coordination environment of Zn(II) and Pb(II) sorbed on biogenic MnO₂ at different loadings. The fittings of the Zn(II) and Pb(II) data suggested that TCS complexation on vacancy sites was the dominant coordination environment for the two contaminants. For Pb(II), very similar coordination environments were measured in the three loading regimes, highlighting the dominant role of TCS complexation on vacancies for Pb(II) sorption on biogenic MnO₂. This was supported by the greater splitting between 5.5 to 6.0 Å⁻¹, observed in the biogenic MnO₂ samples relative to that observed for the Pb(II) on δ -MnO₂ sample, for which edge complexes are believed to be the dominant coordination mode (45). The secondary role played by edge sites and organic functional groups on the biomass for both Zn(II) and Pb(II) sorption are discussed below, but these end-membered scenarios remain consistent with a dominant partitioning to MnO₂ vacancies.

Contribution of secondary sites, edge and biomass, for Zn(II) and Pb(II) sorption

The effective role of edge sites during metal sorption on MnO₂ can be difficult to track due to limitations of traditional EXAFS spectroscopy to distinguish interlayer and edge complexes that can similar second-shell interatomic distances (14, 30), and studies have reported contradicting views on the relative affinity of edge and interlayer complexes (14,

15, 33). In biogenic MnO₂, the presence of the biomass further complicates the identification of the sorption mechanism because the linear combination of vacancy sites (CN = 6) and biomass (CN = 0) may artificially suggest partitioning to edge sites (CN = 2). Despite these limitations, our data does indicate some contribution from edge sites and biomass in the sorption of Zn(II) and Pb(II).

The biofilm contains metal binding organic functional groups, in particular carboxyl, phosphoryl functional groups that can contribute to the sorption of Zn(II) and Pb(II) (11, 38, 58-60). Toner et al. (38) studied the sorption of Zn(II) on *P. putida* suspensions at pH 6.9 and reported a maximal loading of 0.64 ± 0.05 mol Zn kg⁻¹ of biosorbent. EXAFS analysis demonstrated that the metal binding capacity was dominated by phosphoryl (85 ± 10 mol %) and carboxyl (23 ± 10 mol %) functional groups. At lower pH, and in particular at pH 5.5 as in our study, the relative contribution from carboxyl groups (pK_a ~ 4 - 5) is however expected to increase as phosphoryl group become protonated (pK_a ~ 7.0). In the present study (pH 5.2 ± 0.3), loadings of 0.07 ± 0.04 mol Zn kg⁻¹ biosorbent and 0.20 ± 0.02 mol Pb kg⁻¹ biosorbent were measured for Zn and Pb respectively. For Zn(II), LCF analysis clearly demonstrated a non-negligible partitioning to the biomass and/ or particle edges. This observation likely reflects the limited accessibility of Zn(II) to interlayer vacancies, which thus encourages the partitioning to alternative binding sites. LCF analysis of the highest loading Zn EXAFS spectra (0.12 mol Zn mol⁻¹ Mn or 0.32 mol Zn kg⁻¹ sorbent) showed that 22 to 33 % of Zn(II) was not sorbed on vacancies, depending on the relative contribution of the biomass (CN = 0) and edges (CN = 2) to Zn(II) sorption. One study demonstrated that organo-mineral interactions passivates edge sites for Ni(II) sorption (pH 6.5) on δ -MnO₂ particles equilibrated in bacterial biofilms (Simanova et al., *in prep*), which would suggest minimal sorption of Zn(II) on particle edges. Under this assumption, 22 % of the total Zn(II) loaded on the bio-mineral sorbent would thus be partitioned on the biomass (0.07 mol Zn kg⁻¹ sorbent). This loading is consistent with the q_{\max} reached for Zn(II) sorption in the biomass-only isotherm (0.07 ± 0.04 mol Zn kg⁻¹ sorbent; see **Figure 2**). The good agreement between the wet-chemistry and the spectroscopy therefore supports the assumption of a limited contribution from edges for Zn(II) sorption, and suggests that the organic fractions in the biomass-only and in the biogenic MnO₂ sorbents have similar binding sites and site densities. However, these findings are insufficient to rule out completely a contribution from edges for Zn(II) sorption.

The LCF analysis of the lowest loading sample surprisingly indicated that Zn(II) partitioned first on high affinity sorption sites on the biomass rather than on the mineral. This result is in contradiction with the study by Toner et al. (39) on Zn(II) sorption on biogenic MnO₂ that reported a large preferential sorption on the mineral relative to the organic fraction. This study was however conducted at higher pH (7.0 versus 5.5 in our experiment), and their samples were equilibrated for longer prior to filtration (48h, versus 24h in our experiment). Slow diffusion of Zn(II) into the interlayer to reach vacancy sites at low Zn(II) concentrations may explain the greater partitioning of Zn(II) to the biomass observed in our study. The discrepancy between the two studies however warrants further investigation.

For Pb(II) sorption, while EXAFS analysis identified TCS complexes on vacancies as the main coordination environment, q_{\max_Pb} on biogenic MnO₂ (0.49 ± 0.02 mol Pb mol⁻¹ Mn or 0.67 ± 0.03 mol Pb kg⁻¹ sorbent) exceeded what could be reached by occupying only interlayer sites above and below vacancies. Based on structural considerations, the maximal vacancy content for phyllosulfate is 16 % (9), which means that, while the loading measured are typical for Pb(II) sorption on MnO₂ (14, 42, 61), only up to 65 % of the surface excess can be explained by sorption on vacancies. This consideration leaves 0.17 mol Pb mol⁻¹ Mn (0.23 mol Pb kg⁻¹ sorbent) of the maximal surface excess observed that needs to be explained by sorption on the organic compartment or on particle edges.

The extremely high affinity of Pb(II) for MnO₂ argues against significant partitioning to the biomass (42). The good agreement between the maximal surface excess reported for Pb(II) sorption on δ -MnO₂ (14) and those reported in this study for biogenic MnO₂ further supports a limited contribution of the organic fraction. Therefore, up to 35 % q_{\max} of Pb(II) (0.17 mol Pb mol⁻¹ Mn (0.23 mol Pb kg⁻¹ sorbent)) is likely sorbed on the edge sites. While we argued that organo-mineral interactions may prevent Zn(II) from accessing particle edges, we expect Pb(II) to more easily displace any weakly bound organic molecules to access particle edges because of the reported high affinity of the Pb(II) edge complex (15). In an EXAFS analysis of Pb(II) sorbed on δ -MnO₂, Takahashi et al. (15) were able to resolve two Pb-Mn distances as a doublet in the Pb-Mn shell of the Fourier transform. They were thus able to distinguish an edge complex (CN= 2, Pb-Mn 3.2Å) from the interlayer complex (TCS, CN= 6, Pb-Mn 3.7Å). Their data showed the prevalence of the edge complex at low loading and a shift to the TCS complex at higher loading, highlighting the high affinity of the former complex. Sorption of Pb(II) on edges of δ -MnO₂ was

supported by a differential pair-distribution-analysis study, which however argued for the appearance of the edge complex only when vacancy sites were saturated (14). Because a second Pb-Mn distance that could be attributed to the Pb(II) edge complex could not be resolved, the contribution of edges to the sorption of Pb(II) on biogenic MnO₂ was not quantified directly. Therefore, while the data supported a greater partitioning of Pb(II) to vacancy sites, in particular from the large splitting in the EXAFS between 5.5 to 6.0 Å⁻¹ observed at all loadings, a minor contribution of edge sites was expected to accompany the loading on vacancies, throughout the sorption isotherm.

Pb(II) sorption on biogenic MnO₂ and displacement of interlayer Mn(III)

Because Mn(IV) is insoluble and Mn(III) is unstable in solution unless stabilised by strong ligands, the accumulation of aqueous Mn(II) can result from three processes: i) the reductive dissolution of Mn^{IV}O₂; ii) the desorption of adsorbed Mn(II) from the mineral phase; or iii) disproportionation of two Mn(III) metal centres into Mn(II) and Mn(IV). The reductive dissolution of MnO₂ is unlikely both because of the plateau reached in the amount of Mn(II) released upon reaching q_{\max} , and because Manceau et al. (12) showed no oxidation of Pb(II) during the sorption on MnO₂. Surface oxidation of sorbed Mn(II) means that limited Mn(II) is expected to dwell on MnO₂. The release of Mn therefore likely originates from the disproportionation of interlayer Mn(III), destabilised by Pb(II) approaching from the other side of the vacancies. The displaced Mn(III) could then disproportionate, either with a layer-Mn(III) or with interlayer-Mn(III) located on neighbouring vacancies (see **Figure 7 A-B**).

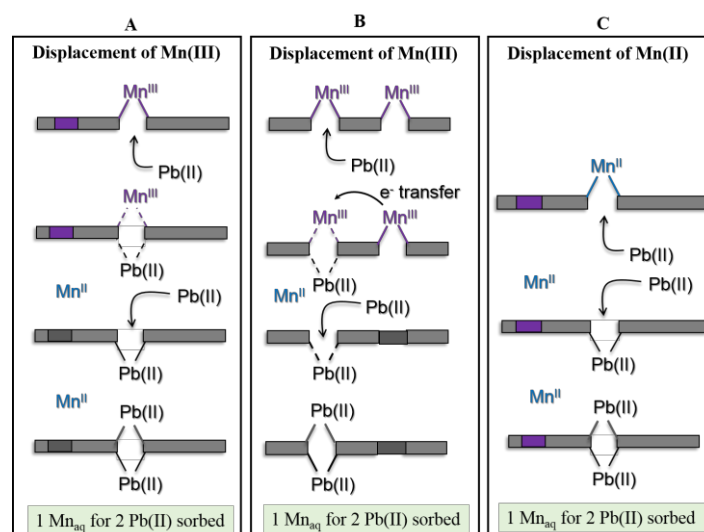


Figure 7 Mechanisms of sorption of Pb(II) on vacancy sites, associated to the displacement of Mn(III) (A & B) and Mn(II) (C). Mn(III) centres are represented in purple, Mn(II) in blue, and Mn(IV) in grey. Purple and grey boxes represent Mn(III) and Mn(IV) centres within the layer.

The slope of Mn(II) accumulated in solution as a function of Pb(II) sorbed (0.60, $R^2 = 0.97$) can be used to constrain possible sorption mechanisms. The sorption of Pb(II) on available free vacancies does not require the displacement of any Mn (slope of 0). Similarly, sorption on edges of particles and on biomass would yield a slope of 0. These three sorption mechanisms could therefore in principle take place in the R1 phase of sorption ($q_i \leq 0.10 \text{ mol i mol}^{-1} \text{ Mn}$). As discussed above, sorption of Pb(II) on biomass is however likely to be minimal. Loadings above $0.10 \text{ mol i mol}^{-1} \text{ Mn}$ were possible for Pb(II) because it was able to displace Mn(III) occupying vacancies, which induced a linear accumulation of Mn(II) in solution with increasing Pb(II) loading. The binding of Pb(II) on both sides of vacancies has been observed on dPDF study of Pb(II) sorption on δ -MnO₂ (14). Therefore, two Pb(II) atoms are expected to be able to occupy a vacancy site formally occupied by one Mn(III). Because Mn(III) is unstable, displaced Mn(III) will disproportionate with a neighbouring Mn(III) [$2x \text{ Mn(III)} \rightarrow 1x \text{ Mn(II)}$ and $1x \text{ Mn(IV)}$]. Disproportionation with layer Mn(III) (**Figure 7A**) and interlayer Mn(III) (**Figure 7B**) will result in the sorption of two Pb(II) for 1 Mn(II) released (slope of 0.5). This ratio is close to the ratio of 0.60 of Mn displaced per Pb(II) sorbed observed in **Figure 4**, which suggests these mechanisms are dominant in the R2 phase. Minor contributions from edge sites (slope of 0) and direct desorption of Mn(II) (slope of 0.5) are also reflected in the slope measured. Single occupancy of vacancy sites (slope of 1.0) will increase the value of the slope above 0.5. Further mechanistic data are however required to gain further insight into the relative importance of these disproportionation mechanisms.

Limitation of the dataset for the validation of the proposed mechanism

The proposed mechanism where Mn(III) is displaced by incoming Pb(II) is consistent with current knowledge concerning biogenic MnO₂: 1) biogenic MnO₂ are enriched in Mn(III), with average manganese oxidation number (AMON) reported to be close to 3.7 (5, 8-11). Although measurements of the Mn(III)-content of the biogenic MnO₂ suspensions used in this study were not made, measurements of pyrophosphate extractable Mn(III) and potentiometric titrations have been carried multiple times in our group on biogenic MnO₂ suspensions obtained from cultures of *P. putida* GB-1 in the same conditions as those used in our study, and show a Mn(III) content of ~ 30 % 2) interlayer Mn(III) has been shown to occupy vacancy sites (13, 14, 33, 62) 3) the observed accumulation of 150 μM of Mn(II) suggests an initial 30 % Mn(III) content, which is consistent with reported AMON values for biogenic MnO₂ and 4) affinity sequences for Zn(II), Mn(II), Mn(III)

and Pb(II) have been reported in the order of Zn(II) < Mn(II), Mn(III) < Pb(II), for MnO₂ vacancy sites (35-37, 63).

However, to confirm the proposed mechanism, the current dataset should be complemented with direct measurements of changes in the Mn(III)-content of the mineral as a function of Zn(II) and Pb(II) loading. These measurements would allow to confirm the displacement of Mn(III) by incoming cations, and the different sorption mechanism observed in the low loading regimes [$q < 10\%$ for Zn(II) and Pb(II)] and the higher loading regimes [$q > 10\%$ for Pb(II)]. Measurements of the Mn(III)-content would furthermore help to distinguish the contribution from the direct desorption of Mn(II) and displacement of Mn(III). Potentiometric titrations as a function of loading should furthermore identify a change in AMON towards 4 supporting the displacement Mn(III) and associated disproportionation reactions.

Environmental implications

This study suggests that the initial Mn(III) content of MnO₂ particles dictates the effective sorption capacity of MnO₂ particles for metal cations that are found lower than MnO₂ on the affinity sequence for MnO₂ vacancies. The incorporation of metals inside the vacancies, which is observed for cations such as Ni(II) and Co(II), can lead to largely irreversible sorption barring large decreases in solution pH (31, 32, 64, 65). However, for cations such as Zn(II) (32, 37) or Pb(II) (66), whose ionic radii and electronic configurations prevent them from entering the layer structure, adsorption is a reversible process. Displacement of contaminants sorbed on MnO₂ by incoming ones with greater affinity for the mineral surface sites has important implications for the effective reactivity of MnO₂ towards different, often co-occurring contaminants, considering the role MnO₂ plays as a contaminant scavenger both in natural and engineering systems.

Another consequence of the proposed sorption mechanism is that the removal of layer and interlayer Mn(III) during sorption of cations with higher affinity for MnO₂ vacancies will increase the oxidation state of the mineral towards an AMON of 4.0 (see **Figure 7A**). A change in the oxidation state of the mineral will likely affect the oxidative reactivity of the mineral towards organic and inorganic species. Recent methods combining pyrophosphate extractions and potentiometric titrations could be developed to track changes in average Mn oxidation state during Pb(II) sorption to further verify the proposed mechanism. Furthermore, depending on the disproportionation mechanism that prevails following the displacement of Mn(III), the vacancy content of the mineral is likely to be

modified. For example, an unstable Mn(III) may receive an electron from a neighbouring interlayer Mn(III), followed by incorporation of newly Mn(IV) into the layer which would result in the loss of a vacancy (see **Figure 7B**).

The competition for reactive sites between incoming contaminants and Mn(III) is expected to be especially relevant where MnO₂ particles is part of a dynamic biomineral assemblage. Biogenic MnO₂ contains metabolically active cells that can respond to external perturbation, such input of nutrients or exposure to contaminants (for example illustrated by the scattering of the sorption data at high Zn(II) loadings), which will have an important impact on the structure, interlayer occupancy and long-term stability of biogenic MnO₂ particles. Partial reduction of Mn(IV) to Mn(III), reduction of Mn(IV) directly to Mn(II) and enzymatic re-oxidation to Mn(IV) are all expected to affect interlayer Mn(II, III) and therefore the reactivity of the mineral towards incoming cations.

ACKNOWLEDGMENTS

The authors thank F.F. Marafatto and L. Monbaron for laboratory support, Y. Wang, S. Benkaddour and D. Hausladen for EXAFS data collection, as well as M. Villalobos and G. Sarret for sharing the spectra for Pb(II) sorbed on δ -MnO₂ and on biomass, respectively. JP acknowledges funding support from the Sandoz Foundation and the BCV Foundation. Portions of this research were carried out at the Stanford Synchrotron radiation Lightsource, a national use facility operated by Stanford University on the behalf of the U.S. Department of Energy, Office of Basic Sciences.

REFERENCES

1. Brown GE. How minerals react with water. *Science*. 2001;294(5540):67-9.
2. Bradl B. Adsorption of heavy metal ions on soils and soils constituents. *J. Coll. Interf. Sci.*, 2004;277(1):1-18.
3. Stumm W, Morgan JJ. *Aquatic chemistry: chemical equilibria and rates in natural waters*: John Wiley & Sons; 2012.
4. Xyla AG, Sulzberger B, Luther III GW, Hering JG, Van Cappellen P, Stumm W. Reductive dissolution of manganese (III, IV)(hydr)oxides by oxalate: The effect of pH and light. *Langmuir*. 1992;8(1):95-103.
5. Tebo BM, Bargar JR, Clement BG, Dick GJ, Murray KJ, Parker D, et al. Biogenic manganese oxides: properties and mechanisms of formation. *Annu. Rev. Earth Planet. Sci.* 2004;32:287-328.
6. Tebo BM, Johnson HA, McCarthy JK, Templeton AS. Geomicrobiology of manganese (II) oxidation. *Trends in Microbiology*. 2005;13(9):421-8.
7. Spiro TG, Bargar JR, Sposito G, Tebo BM. Bacteriogenic manganese oxides. *Acc. Chem. Res.*, 2009;43(1):2-9.
8. Santelli CM, Webb SM, Dohnalkova AC, Hansel CM. Diversity of Mn oxides produced by Mn(II)-oxidizing fungi. *Geochim Cosmochim Ac.* 2011;75(10):2762-76.
9. Webb S, Tebo B, Bargar J. Structural characterization of biogenic Mn oxides produced in seawater by the marine *Bacillus* sp. strain SG-1. *Am. Mineral.*, 2005;90(8-9):1342-57.

10. Villalobos M, Toner B, Bargar J, Sposito G. Characterization of the manganese oxide produced by *Pseudomonas putida* strain MnB1. *Geochim Cosmochim Ac.* 2003;67(14):2649-62.
11. Droz B, Dumas N, Duckworth OW, Pena J. A comparison of the sorption reactivity of bacteriogenic and mycogenic Mn oxides nanoparticles. *Environ. Sci. Technol.*, 2015.
12. Manceau A, Lanson B, Drits VA. Structure of heavy metal sorbed birnessite. Part III: Results from powder and polarized extended X-ray absorption fine structure spectroscopy. *Geochim Cosmochim Ac.* 2002;66(15):2639-63.
13. Peña J, Bargar JR, Sposito G. Copper sorption by the edge surfaces of synthetic birnessite nanoparticles. *Chem Geol.* 2015;396:196-207.
14. van Genuchten CM, Peña J. Sorption selectivity of birnessite particle edges: a d-PDF analysis of Cd(II) and Pb(II) sorption by δ -MnO₂ and ferrihydrite. *Environ. Sci. Process. Impact.*, 2016.
15. Takahashi Y, Manceau A, Geoffroy N, Marcus MA, Usui A. Chemical and structural control of the partitioning of Co, Ce, and Pb in marine ferromanganese oxides. *Geochim Cosmochim Ac.* 2007;71(4):984-1008.
16. Post JE. Manganese oxide minerals: Crystal structures and economic and environmental significance. *Proc. Nat. Acad. Sci.*, 1999;96(7):3447-54.
17. Villalobos M, Bargar J, Sposito G. Trace metal retention on biogenic manganese oxide nanoparticles. *Elements.* 2005;1(4):223-6.
18. Haack EA, Warren LA. Biofilm hydrous manganese oxyhydroxides and metal dynamics in acid rock drainage. *Environ. Sci. Technol.*, 2003;37(18):4138-47.
19. Gardner TG, Santelli C, Johnston T, Droz B, Andrews M, Rivera N, et al. Microbially mediated formation of manganese oxides at a superfund site remediation system. *Soil Sci. Soc. Am.* 2013.
20. Fuller CC, Bargar JR. Processes of zinc attenuation by biogenic manganese oxides forming in the hyporheic zone of Pinal Creek, Arizona. *Environ. Sci. Technol.*, 2014;48(4):2165-72.
21. Han R, Zou W, Zhang Z, Shi J, Yang J. Removal of copper (II) and lead (II) from aqueous solution by manganese oxide coated sand: I. Characterization and kinetic study. *J. Haz. Mat.*, 2006;137(1):384-95.
22. CrystalMaker®. CrystalMaker Software Limited, Oxford, England.
23. Lefkowitz JP, Rouff AA, Elzinga EJ. Influence of pH on the reductive transformation of birnessite by aqueous Mn (II). *Environ. Sci. Technol.*, 2013;47(18):10364-71.
24. Zhu M, Ginder-Vogel M, Parikh SJ, Feng X-H, Sparks DL. Cation effects on the layer structure of biogenic Mn-oxides. *Environ. Sci. Technol.*, 2010;44(12):4465-71.
25. Mandernack KW, Post J, Tebo BM. Manganese mineral formation by bacterial spores of the marine *Bacillus*, strain SG-1: Evidence for the direct oxidation of Mn (II) to Mn (IV). *Geochim Cosmochim Ac.* 1995;59(21):4393-408.
26. Bargar JR, Tebo BM, Bergmann U, Webb SM, Glatzel P, Chiu VQ, et al. Biotic and abiotic products of Mn (II) oxidation by spores of the marine *Bacillus* sp. strain SG-1. *Am. Mineral.*, 2005;90(1):143-54.
27. Elzinga EJ. Reductive transformation of birnessite by aqueous Mn(II). *Environ. Sci. Technol.*, 2011;45(15):6366-72.
28. Zhao H, Zhu M, Li W, Elzinga EJ, Villalobos M, Liu F, et al. Redox reactions between Mn (II) and hexagonal birnessite change its layer symmetry. *Environ. Sci. Technol.*, 2016;50(4):1750-8.
29. Hinkle MA, Flynn ED, Catalano JG. Structural response of phyllo-manganates to wet aging and aqueous Mn (II). *Geochim Cosmochim Ac.* 2016;192:220-34.
30. Hinkle MA, Dye KG, Catalano JG. Impact of Mn (II)-Manganese Oxide Reactions on Ni and Zn Speciation. *Environ. Sci. Technol.*, 2017.
31. Miyata N, Tani Y, Sakata M, Iwahori K. Microbial manganese oxide formation and interaction with toxic metal ions. *J. Biosci Bioeng.*, 2007;104(1):1-8.
32. Kwon KD, Refson K, Sposito G. Understanding the trends in transition metal sorption by vacancy sites in birnessite. *Geochim Cosmochim Ac.* 2013;101:222-32.

33. Simanova AA, Kwon KD, Bone SE, Bargar JR, Refson K, Sposito G, et al. Probing the sorption reactivity of the edge surfaces in birnessite nanoparticles using Nickel (II). *Geochim Cosmochim Acta*. 2015;164:191-204.
34. Murray JW. The interaction of metal ions at the manganese dioxide-solution interface. *Geochim Cosmochim Acta*. 1975;39(4):505-19.
35. McKenzie R. The adsorption of lead and other heavy metals on oxides of manganese and iron. *Soil Research*. 1980;18(1):61-73.
36. Tamura H, Furuichi R. Adsorption affinity of divalent heavy metal ions for metal oxides evaluated by modeling with the Frumkin isotherm. *J. Coll. Interf. Sci.*, 1997;195(1):241-9.
37. Tani Y, Ohashi M, Miyata N, Seyama H, Iwahori K, Soma M. Sorption of Co (II), Ni (II), and Zn (II) on biogenic manganese oxides produced by a Mn-oxidizing fungus, strain KR21-2. *J. Environ. Sci. Health, Part A*. 2004;39(10):2641-60.
38. Toner B, Manceau A, Marcus MA, Millet DB, Sposito G. Zinc sorption by a bacterial biofilm. *Environ. Sci. Technol.*, 2005;39(21):8288-94.
39. Toner B, Manceau A, Webb SM, Sposito G. Zinc sorption to biogenic hexagonal-birnessite particles within a hydrated bacterial biofilm. *Geochim Cosmochim Acta*. 2006;70(1):27-43.
40. Peña J, Bargar JR, Sposito G. Role of bacterial biomass in the sorption of Ni by biomass-birnessite assemblages. *Environ. Sci. Technol.*, 2011;45(17):7338-44.
41. Zhu M, Ginder-Vogel M, Sparks DL. Ni (II) sorption on biogenic Mn-oxides with varying Mn octahedral layer structure. *Environ. Sci. Technol.*, 2010;44(12):4472-8.
42. Nelson YM, Lion LW, Shuler ML, Ghiorse WC. Lead binding to metal oxide and organic phases of natural aquatic biofilms. *Limnol. Oceanography*. 1999;44(7):1715-29.
43. Peña J, Kwon KD, Refson K, Bargar JR, Sposito G. Mechanisms of nickel sorption by a bacteriogenic birnessite. *Geochim Cosmochim Acta*. 2010;74(11):3076-89.
44. Kwon KD, Refson K, Sposito G. Zinc surface complexes on birnessite: A density functional theory study. *Geochim Cosmochim Acta*. 2009;73(5):1273-84.
45. Villalobos M, Bargar J, Sposito G. Mechanisms of Pb (II) sorption on a biogenic manganese oxide. *Environ. Sci. Technol.*, 2005;39(2):569-76.
46. Kwon KD, Refson K, Sposito G. Surface complexation of Pb (II) by hexagonal birnessite nanoparticles. *Geochim Cosmochim Acta*. 2010;74(23):6731-40.
47. Tebo BM, Clement BG, Dick GJ. Biotransformations of manganese. *Manual Environ. Microbiol*. 2007;3:1223-38.
48. C. WJ. MINEQL: A computer program for the calculations of chemical equilibrium composition of aqueous systems. Massachusetts Institute of Technology: Water Quality Laboratory; 1976.
49. Sposito G. *The chemistry of soils*: Oxford university press; 2008.
50. Webb S. SIXpack: a graphical user interface for XAS analysis using IFEFFIT. *Physica Scripta*. 2005; 2005(T115):1011.
51. Newville M. EXAFS analysis using FEFF and FEFFIT. *Journal of synchrotron radiation*. 2001;8(2):96-100.
52. Pena J, Sposito G, Bargar J, editors. *Structure of Zn Surfaces Complexes on Biogenic Hexagonal Birnessite*. AGU Fall Meeting Abstracts; 2010.
53. Rehr J, Mustre de Leon J, Zabinsky S, Albers R. Theoretical X-ray absorption fine structure standards. *J. Am. Chem. Soc.*, 1991;113(14):5135-40.
54. Sarret G, Manceau A, Spadini L, Roux J-C, Hazemann J-L, Soldo Y, et al. Structural determination of Zn and Pb binding sites in *Penicillium chrysogenum* cell walls by EXAFS spectroscopy. *Environ. Sci. Technol.*, 1998;32(11):1648-55.
55. Droz B, Dumas N, Duckworth OW, Peña J. A comparison of the sorption reactivity of bacteriogenic and mycogenic Mn oxide nanoparticles. *Environ. Sci. Technol.*, 2015;49(7):4200-8.

56. Matocha CJ, Elzinga EJ, Sparks DL. Reactivity of Pb(II) at the Mn(III, IV)(oxyhydr)oxide-water interface. *Environ. Sci. Technol.*, 2001;35(14):2967-72.
57. Pena J, Bargar JR, Sposito G. Role of bacterial biomass in the sorption of Ni by biomass-birnessite assemblages. *Environ. Sci. Technol.*, 2011;45(17):7338-44.
58. Fein JB, Daughney CJ, Yee N, Davis TA. A chemical equilibrium model for metal adsorption onto bacterial surfaces. *Geochim Cosmochim. Acta.* 1997;61(16):3319-28.
59. Fein JB, Martin AM, Wightman PG. Metal adsorption onto bacterial surfaces: development of a predictive approach. *Geochim Cosmochim. Acta.* 2001;65(23):4267-73.
60. Fein JB, Boily J-F, Yee N, Gorman-Lewis D, Turner BF. Potentiometric titrations of *Bacillus subtilis* cells to low pH and a comparison of modeling approaches. *Geochim Cosmochim. Acta.* 2005;69(5):1123-32.
61. Nelson YM, Lion LW, Ghiorse WC, Shuler ML. Production of biogenic Mn oxides by *Leptothrix discophora* SS-1 in a chemically defined growth medium and evaluation of their Pb adsorption characteristics. *Appl. Environ. Microbiol.*, 1999;65(1):175-80.
62. Wang Y, Feng X, Villalobos M, Tan W, Liu F. Sorption behavior of heavy metals on birnessite: relationship with its Mn average oxidation state and implications for types of sorption sites. *Chem Geol.* 2012;292:25-34.
63. Murray JW. The surface chemistry of hydrous manganese dioxide. *J. Coll. Interf. Sci.*, 1974;46(3):357-71.
64. Simanova AA, Peña J. Time-resolved investigation of cobalt oxidation by Mn(III)-rich δ -MnO₂ using quick X-Ray absorption spectroscopy. *Environ. Sci. Technol.*, 2015;49(18):10867-76.
65. Peacock CL. Physicochemical controls on the crystal-chemistry of Ni in birnessite: Genetic implications for ferromanganese precipitates. *Geochim Cosmochim. Acta.* 2009;73(12):3568-78.
66. Zhao W, Cui H, Liu F, Tan W, Feng X. Relationship between Pb²⁺ adsorption and average Mn oxidation state in synthetic birnessites. *Clays and Clay Minerals.* 2009;57(5):513-20.

Chapter 3

Abiotic oxidation of glucose and gluconate by MnO₂

ABSTRACT

The high redox potentials of Mn(IV)/ Mn(II) and Mn(III)/ Mn(II) couples mean that these species are among the strongest oxidants present in natural systems and that they can oxidize a range of organic molecules relevant in soils, such as organic acids and sugars. However kinetics constraints will eventually control the rates and extent of these reactions. In this study, we compared the dissolution of δ -MnO₂, the synthetic analogue of the natural biogenic MnO₂, when reacted with glucose and gluconate at pH 4.5, 5.5 and 6.5 for up to 24 h. Measurements of aqueous Mn by ICP-OES provided an estimate of electron equivalents transferred to the mineral that led to dissolution of the mineral, whereas colorimetric assays and ATR-FTIR spectra provided qualitative measures of changes in glucose or gluconate concentrations. We measured significant pH dependence of the rates and extent of reductive dissolution of MnO₂ with both substrates. After 24 h of reaction, we observed similar extent of reduction for glucose and gluconate, suggesting that the chemical nature of the organic reductant reacting with MnO₂ may be less important than the chemical conditions, such as pH, in which the reaction takes place. Coupled ATR-FTIR spectroscopy of the supernatant and aqueous Mn(II) measurements showed only partial oxidation of the glucose pool, suggesting extensive oxidation of the organic substrates by MnO₂, with multiple electrons ($> 2e^-$) transferred from the reductants to the mineral. Understanding the reactivity of MnO₂ towards simple organic compounds

relevant to soil systems, decoupled from any biological contribution, provides knowledge of the impact the oxide could have on C transformations in natural systems.

INTRODUCTION

The soil interstitial water contains low molecular-weight organic substrates, including organic acids and carbohydrates, excreted by plant roots and microorganisms. The accumulation of these rhizodeposits arise from a number of processes, including passive and active diffusion across the lipid bilayer of plant cells, the microbial exudation of secondary metabolites and extracellular enzymes, and the decay of dead organic material (1, 2). Large concentrations of these substrates are routinely measured in the rhizosphere, forming a pool of chemically labile organic molecules (2). These substrates can be used as nutrients by microorganisms but may also interact with co-occurring soil minerals. Interactions with mineral surfaces may lead to stabilization of the organic substrates through sorption processes (1, 3-6), but soil minerals may also participate in the transformations of these substrates (7-11).

High valent Mn species are among the strongest abiotic oxidants found in natural environments (12, 13), as evidenced by the high redox potentials ($E_h^0 = 1.23$ eV and 1.49 eV) of the $\text{Mn}^{\text{IV}}\text{O}_{2(\text{s})}/\text{Mn}(\text{II})_{(\text{aq})}$ and the $\text{Mn}^{\text{III}}_2\text{O}_{3(\text{s})}/\text{Mn}(\text{II})_{(\text{aq})}$ couples (14, 15). The cycling between soluble Mn(II), sparingly soluble Mn(III) and insoluble Mn(IV) therefore has the potential to drive the abiotic oxidation of natural organic molecules. Reactions of Mn oxides with a number of small organic molecules have been reported (16-19) and typically lead to the dissolution of the mineral phases. Mn(IV) can be reduced to Mn(III) or further reduced to Mn(II), leading to Mn(III)-enrichment or to reductive dissolution of the oxide. When present in the mineral phase, Mn(III) may be complexed by strongly chelating ligands, leading to ligand-assisted dissolution. However, few ligands are strong enough chelators to stabilise aqueous Mn(III). The dissolution of Mn oxides is therefore often reductive, and there is a large thermodynamic driving force for its coupling to the oxidation of chemical species, such as small organic acids and sugars, that are found on the opposite end of the redox ladder.

Electron transfer between organic substrates and MnO_2 requires the formation of a surface complex (13, 20, 21). The redox reaction between organic substrates and solid phase Mn oxides is thus understood to follow the steps: i) the formation of a precursor surface complex ii) electron transfer between the surface complex and the mineral and iii)

detachment of the oxidized surface residue (17, 22-25). Because of poor electrostatic and leaving group capacity of O²⁻ and OH⁻, it is energetically difficult for organic substrates to form inner-sphere coordination complexes on the basal surface of MnO₂ (19). Overall, the reaction kinetics is controlled either by the rates of formation of the surface complex, or the rates of electron transfer, with the relative speed of the two processes varying with the nature of the organic substrates (26).

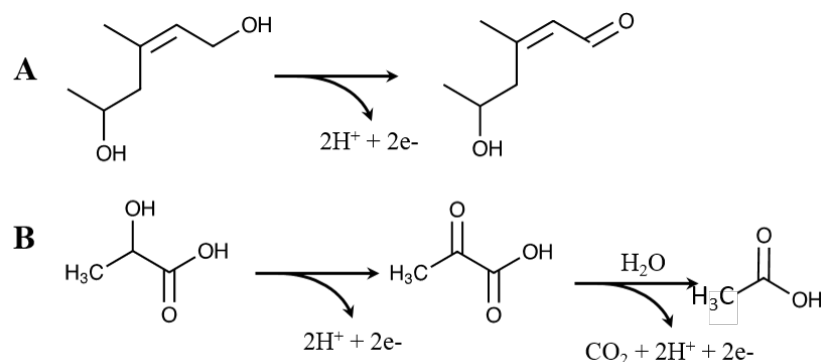


Figure 1 Oxidative transformations of organic molecules by MnO₂ **A**) Selective oxidation of allylic alcohols catalyzed by MnO₂ **B**) Schemes proposed by Wang and Stone (2006) for the oxidation of 2 electrons reductants by MnO₂.

Studies on the oxidation of organic molecules by MnO₂ show a few prevailing mechanisms. For instance, allylic or benzylic alcohols are selectively oxidized to ketones by MnO₂ (27) (**Figure 1A**). Carboxylic acids featuring a carbonyl group in the α -position commonly undergo C-C bond cleavage through decarboxylation reactions, as reported by Wang and Stone (18, 19). For α -hydroxy carboxylic or α -hydroxy ketone substrates, C-C bond cleavage is preceded by the oxidation of the α -hydroxyl group, which then facilitates the C-C bond cleavage through decarboxylation (**Figure 1B**). These reaction pathways, together with consideration of surface complex formation, can be extrapolated to predict the reactivity of MnO₂ and simple sugars, which has scarcely been studied under environmentally relevant conditions. Specifically, MnO₂ may first oxidize sugar aldehydes to carboxylic functional groups, thus creating reactive substrates that can then undergo oxidative transformations through the pathways described in **Figure 1**. The cyclic structure adopted by a number of simple sugars is however likely to limit the formation of a surface complex. For example Olsson and Person (28) showed that only little glucose sorbed on FeOOH ($q_{\max} = 14.7 \mu\text{mol glucose g}^{-1} \text{FeOOH}$ at pH 7.0) through hydrogen bonding interactions and an intact ring, despite the high IEP of FeOOH (~ 9) that should favour inner-sphere coordination.

In this study, we investigated the oxidation of glucose ($C_6H_{12}O_6$, a hydroxyaldehyde) and its 2-electrons oxidation product gluconate ($C_6H_{12}O_7$, a hydroxycarboxylate, pKa 3.8)(29) (see **Figure 2**) upon reaction with MnO_2 . We hypothesized that the carboxylic functional group should result in higher reactivity of gluconate relative to its parent compound because the carboxylic moiety is likely to facilitate the formation of a surface complex. Based on the oxidative decarboxylation pathway reported by Wang and Stone, (2006), we further hypothesize that both molecules may undergo a cascade of multi-electrons (more than 2) oxidative transformations, which may lead to CO_2 evolution. However, the cyclic structure of glucose [99 : 1 ratio between its ring and open conformation (27)] likely hinders surface complexation. Thus, the transformation of glucose to gluconate is expected to be the rate-determining oxidative step upon reaction with MnO_2 .

To test these hypotheses, we compared the extent and rates of dissolution of δ - MnO_2 , a synthetic analogue of the natural biogenic MnO_2 , when reacted with glucose and gluconate at pH values of 4.5, 5.5 and 6.5 for up to 24 h. Measurements of aqueous Mn by ICP-OES provided an estimate of electron equivalents transferred to the mineral, whereas colorimetric assays and ATR-FTIR spectra provided qualitative measure of changes in glucose or gluconate concentrations. Based on our data, we discussed the relative importance of the chemical structure of the substrates and the reaction conditions to govern the pathways of transformations and the products formed.

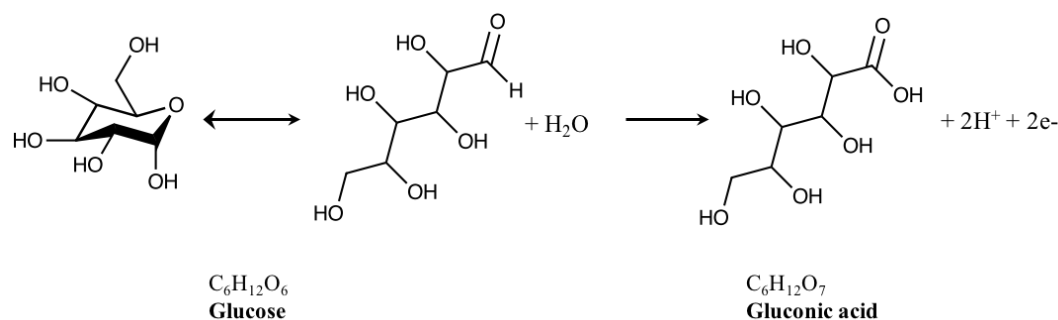


Figure 2 Equilibrium between the cyclic and acyclic forms (99 : 1) of glucose and its oxidation to gluconic acid.

MATERIAL AND METHODS

Solutions of glucose ($C_6H_{12}O_6$, Sigma-Aldrich, > 99.5 %) and sodium-gluconate ($C_6H_{11}NaO_7$, Sigma-Aldrich, > 99.5 %) solutions were prepared using ultrapure water (> 18 $M\Omega$ cm). The synthesis of δ - MnO_2 was carried out through the reaction of

stoichiometric amounts of MnCl₂ with KMnO₄ in excess NaOH as described elsewhere (30, 31). The oxide has a layer-type structure with hexagonal sheet symmetry, an average manganese oxidation number (AMON) of 4.03 ± 0.01 , a Mn(III) content determined by pyrophosphate extraction of 2.07 ± 0.52 %, a BET - SSA of $140 \text{ m}^2 \text{ g}^{-1}$ and a Na/ Mn ratio of 30 %. After synthesis, the solids were stored as an aqueous stock suspension (approx. 70 mM) in a Nalgene bottle in the dark at 4°C. Individual experimental suspensions were prepared from the stock solution without prior sonication.

Dissolution experiments

All batch dissolution experiments were conducted in 250 mL glass beakers at room temperature (25 °C) and kept open to the atmosphere. Reactor contents were stirred with a Teflon coated magnetic stir bar and covered loosely with parafilm for up to 24 h. Glucose solutions were prepared with a NaCl background electrolyte (10 mM), Na-gluconate solutions without NaCl background electrolyte. Throughout the experiment, the pH of the suspensions was maintained constant by use of a pH stat (Metrohm Titrino 718 or Titrand 888) through automatic addition of HCl (24 or 50 mM). The pH was monitored with a pH electrode (Metrohm) calibrated using 3 standard buffers (pH 4, 7 and 10).

To begin an experiment, an aliquot of a concentrated suspension of δ -MnO₂ was added to 5.5 mM glucose or gluconate solutions to yield a 1.1 ± 0.2 mM MnO₂ suspensions. The pH of the suspensions was manually pre-adjusted, within 0.5 pH unit above target 4.5, 5.5 and 6.5 pH values by the addition of HCl (250 mM). The pH was then finely adjusted (± 0.1 pH unit) through automatic addition of HCl by pH stats as describe above. Aliquots of the suspensions were collected at different time-points. A control experiment was performed to ensure the lack of release of aqueous Mn(II) from MnO₂ in the absence of reductant, by acidifying with HCl a suspension of δ -MnO₂ to pH 4.5 ± 0.3 . The flask was capped with a cellulose cap, and placed in the incubator (27 °C, 150 RPM) for 24 h. The pH of the suspension was measured every couple of hours to ensure it stayed at pH 4.5 and did not need further adjustment. After 24 h, filtered aliquots were sampled and aqueous Mn(II) concentrations were measured by ICP-OES. Aqueous Mn(II) was measured by ICP-OES in filtered (0.20 μm pore size, polyethersulfone), diluted and acidified (50 μL HNO₃ 66 % in 5 mL samples). The initial MnO₂ concentration was determined by sampling 1 mL of the suspensions and acid digesting the solids using concentrated nitric acid (50 μL , 65 %) and excess oxalic acid (50 μL , 1 M), and diluted with ultrapure water.

Manganese concentrations were determined by ICP-OES (Perkin-Elmer Optima 8300) at three emission lines and using Sc as an internal standard. All gluconate experiments were conducted in duplicate, glucose pH 4.5 was conducted in triplicate and glucose pH 5.5 and 6.5 were only measured once.

Glucose consumption in glucose solutions reacted with δ -MnO₂ as a function of pH

Separate suspensions of δ -MnO₂ (1.3 ± 0.3 mM) were prepared in 100 mL flasks by diluting an aliquot of the stock solution in a NaCl solution (10 mM). The pH of the suspensions was manually pre-adjusted (within 0.5 pH unit) to 4.5, 5.5 and 6.5 by the addition of HCl (250 mM). The pH was finely adjusted (± 0.1 pH unit) by pH stats (Metrohm Titrino 718 or Titrand 888). Once pH equilibrated, the suspensions were spiked an aliquot of a glucose stock solution (500 mM), to yield a 5.5 mM initial glucose concentration (t0h). Aliquots of the suspensions were collected at different time points (t0h – 24h) and filtered immediately (0.20 μ m pore size, polyethersulfone). Duplicate sets of measurements were carried out for all three pH conditions.

Glucose concentrations were measured using a colorimetric assay (GAGO 20, Sigma-Aldrich), following the protocol described by the manufacturer and using a UV-Vis spectrophotometer (Shimadzu UV-2600). Briefly, filtered aliquots were diluted (DF 20) and reacted for 30 min in a water bath (37 ± 2 °C) with a colorimetric reagent containing glucose oxidase, reduced o-dianisidine (colorless) and peroxidase. The oxidation of glucose by oxidases yielded gluconic acid and H₂O₂. The later reacts with reduced o-dianisidine in the presence of peroxidase to form oxidised o-dianisidine, which has a brown color. The reaction was quenched by the addition of 12 N H₂SO₄, which stabilises o-dianisidine, yielding a pink color. Glucose concentration were determined from the absorbance of the o-dianisidine formed, measured against a reagent blank at 540 nm using 1 cm path-length disposable plastic cuvettes. A calibration curve was obtained from 4 standards following the protocol provided by the manufacturer. The calibration curve was linear from 0 – 0.40 mM glucose ($\epsilon = 2.65 \text{ mM}^{-1} \text{ cm}^{-1}$, $R^2 = 0.99$). Blank samples (n = 6) yielded a concentration of 0.01 ± 0.01 mM glucose and 5.5 mM check standards (n = 8) yielded a concentration of 5.6 ± 0.2 mM. Because the sensitivity of the assay was not sufficient to quantify the glucose consumption, we did not attempt gluconate measurements with another enzymatic assay.

Reaction of δ -MnO₂ with glucose and gluconate monitored by ATR-FTIR

Suspensions of glucose or gluconate (2.2 mM) + δ -MnO₂ (~ 1.5 mM) were prepared in a 10 mM NaCl background electrolyte. Compared to the dissolution experiments, the organic substrate to oxide molar ratio was decreased from about 5 : 1 to 2 : 1 to better track the transformation of the organic substrates. The pH of the suspensions was manually pre-adjusted, within 0.5 pH unit above target 4.5, 5.5 and 6.5 pH values by the addition of HCl (250 mM). The pH was then finely automatically adjusted (\pm 0.1 pH unit) by pH stats as described above. After 3 h and 24 h (t_{3h} and t_{24h}), aliquots of the suspensions were collected and filtered twice (0.20 μ m poresize, polyethersulfone). Samples for ATR-FTIR analysis were prepared by placing 3 mL of the filtered solutions in 25 mL beakers that were left opened under a closed fume-hood overnight. When fully dried, the crystallised solid materials were re-hydrated with 150 μ L of ultrapure water, to obtain solutions concentrated 20x. No control samples, which could have included pure glucose and gluconate solutions dried and resuspended, were collected.

ATR-FTIR spectra were recorded using a Perkin Elmer 100 FTIR spectrometer equipped with a universal attenuated total reflectance (ATR) accessory (ZnSe diamond). A drop of sample was deposited on the crystal and the spectra were recorded open to the atmosphere at wavenumbers 500 - 4000 cm⁻¹. A total of 124 scans were collected and averaged before background subtraction of the FTIR signal from that measured for ultrapure water. As water adsorbs strongly around 1640 cm⁻¹, some experimental spectra show noise in this region. All spectra were baseline-corrected using the Perkin-Elmer Spectrum software. ATR-FTIR spectra were plotted from 950 – 1850 cm⁻¹ to focus on the relevant features of glucose and gluconate.

RESULTS

Reductive dissolution of MnO₂

The release of Mn(II) as a function of time when δ -MnO₂ was reacted with 5.5 mM glucose and gluconate at pH 4.5, 5.5 and 6.5 are reported in **Figure 3A** and **Figure 3B** respectively, and in **Table 3-A1** and **Table 3-A2**. The reductive dissolution of δ -MnO₂ increased with decreasing pH, such that up to 0.73 and 0.75 aqueous Mn(II) mol⁻¹ MnO₂ was measured in solution after 24 h for glucose and gluconate at pH 4.5. At pH 6.5, 0.11 mol Mn(II) mol⁻¹ MnO₂ were measured in solution after 24 h for both glucose and gluconate.

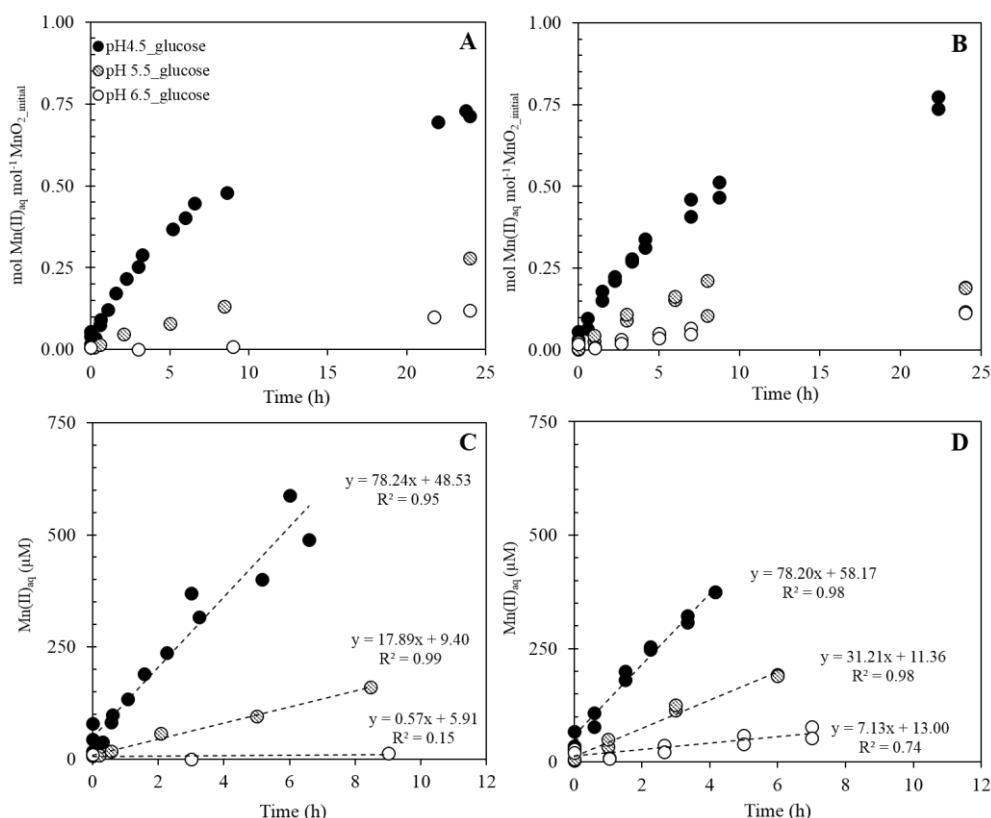


Figure 3 Release of Mn(II) as function of time when δ -MnO₂ (1.1 ± 0.2 mM) was stirred in 5.5 mM solutions of glucose (A) or gluconate (B) under fixed pH conditions. Rates of release of aqueous Mn(II) during the initial 4 - 9h of reaction between δ -MnO₂ and glucose (C) and gluconate (D). All gluconate experiments were conducted in duplicate, glucose pH 4.5 was conducted in triplicate and glucose pH 5.5 and 6.5 were only measured once.

Initial rates of dissolution were obtained by plotting changes in aqueous Mn(II) as a function of time for pH 6.5, 5.5 and 4.5 (see **Figure 3C** and **Figure 3D**). These values were obtained by linear regression of aqueous Mn against time for the initial 4 – 9 h of reaction (22). At longer reaction time, the measured dissolution rates could be influenced by sorption or re-oxidation of Mn(II), which is favoured under high concentrations of dissolved Mn (32-35). However, surface-catalysed oxidation of Mn(II) by MnO₂ should be limited at pH < 5.5 (36). The initial rates of release of Mn(II) in the glucose and gluconate solutions were similar at pH 4.5 ($78 \mu\text{M h}^{-1}$). Under acidic conditions, the reductive dissolution of MnO₂ appeared to be independent of the substrate structure. However, for the pH 5.5 and 6.5 experiments, these initial rates were greater for gluconate than for glucose, with $31 \mu\text{M h}^{-1}$ (pH 5.5) and $7 \mu\text{M h}^{-1}$ (pH 6.5) measured for gluconate compared to $18 \mu\text{M h}^{-1}$ (pH 5.5) and $1 \mu\text{M h}^{-1}$ (pH 6.5) measured for glucose. For some samples, and in particular for the lowest pH conditions, the concentration of Mn(II) at t0h deviated from 0 μM . The fact that this deviation was particularly important for the pH 4.5 sample strongly suggests extremely rapid reductive dissolution of MnO₂ upon spiking with

glucose and gluconate, already before sampling the aliquot for the t₀h measurement. Alternatively, this deviation could be ascribed to colloidal MnO₂ passing through the 0.2 μm pore size filter.

No release of Mn(II) was measured when acidifying a δ-MnO₂ suspension to pH 4.5 for 24 h (see **Table 1**).

Table 1: Control experiment to verify the extent of release of Mn(II) that can be observed when δ-MnO₂ suspensions are equilibrated at pH 4.5.

	Mn _{Filt} (μM)	Mn _{TOT} = Mn _{aq} and Mn _{solid} (μM)	Mn _{Filt} / Mn _{TOT}
δ-MnO ₂ _pH4.5_control_1	< 1.0	1179.3	0.00
δ-MnO ₂ _pH4.5_control_2	< 1.0	1166.6	0.00
δ-MnO ₂ _pH4.5_control_3	< 1.0	1251.2	0.00

Glucose consumption upon reaction with δ-MnO₂

Changes in glucose concentrations when reacted with δ-MnO₂ during 24 h at pH 4.5, 5.5 and 6.5 are reported in **Figure 4**. Within measurement error (± 0.2 mM) no changes in glucose concentrations were measured over 24 h for samples reacted at pH 6.5 and 5.5. A decrease of 0.5 ± 0.2 mM of glucose was measured after 24 h for duplicate samples reacted at pH 4.5.

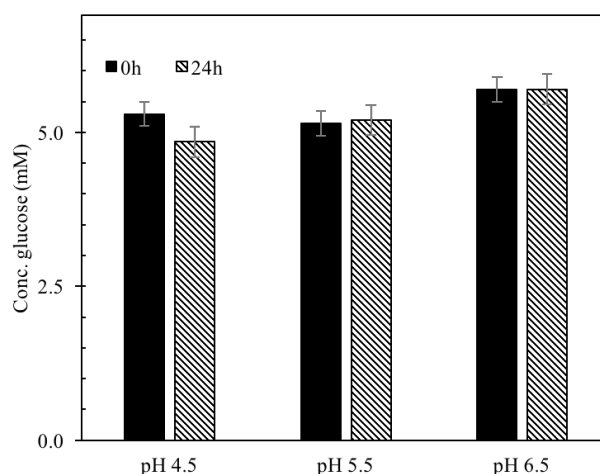


Figure 4 Glucose concentrations at t₀h and t₂₄h upon reaction of δ-MnO₂ (1.3 ± 0.3 mM) suspensions with glucose (5.5 mM) at pH 4.5, 5.5 and 6.5. Glucose concentrations were measured with an enzymatic colorimetric assay (GAGO, Sigma-Aldrich). Measurements were collected in duplicate for each pH condition. The initial glucose (glucose t₀h) was measured directly following the addition of glucose to a δ-MnO₂ suspension. Blank samples (n = 6) yielded a concentration of 0.01 ± 0.01 mM glucose and 5.5 mM check standards (n = 8) yielded a concentration of 5.6 ± 0.02 mM. No similar gluconate measurements were collected.

Reaction of glucose with δ -MnO₂ monitored by ATR-FTIR

Characterisation of glucose and gluconate ATR-FTIR spectra are described in the **Supplementary Information (SI)** and in **Figure 3-S1**. The ATR-FTIR spectra of the supernatant of a δ -MnO₂ suspensions reacted with glucose for 3 h and 24 h at pH 4.5, 5.5 and 6.5 are plotted in **Figure 5**. The concentration of glucose remained constant, within the sensitivity of the measurement, between the earlier and later samplings at all the pH conditions investigated. The predicted concentration from the absorbance at 1035 cm⁻¹ was 45 mM, and when corrected by the concentration factor, 2.3 ± 0.5 mM. This value is close to the 2.2 mM glucose added at t0h. Based on the sensitivity of the measurement, these measurements thus confirm that less than 0.5 mM glucose was consumed over the reaction period. Attempts to further quantify glucose consumption were unsuccessful given the poor sensitivity of these measurements (0.5 mM, see **SI**) and small changes in glucose concentrations over the reaction period.

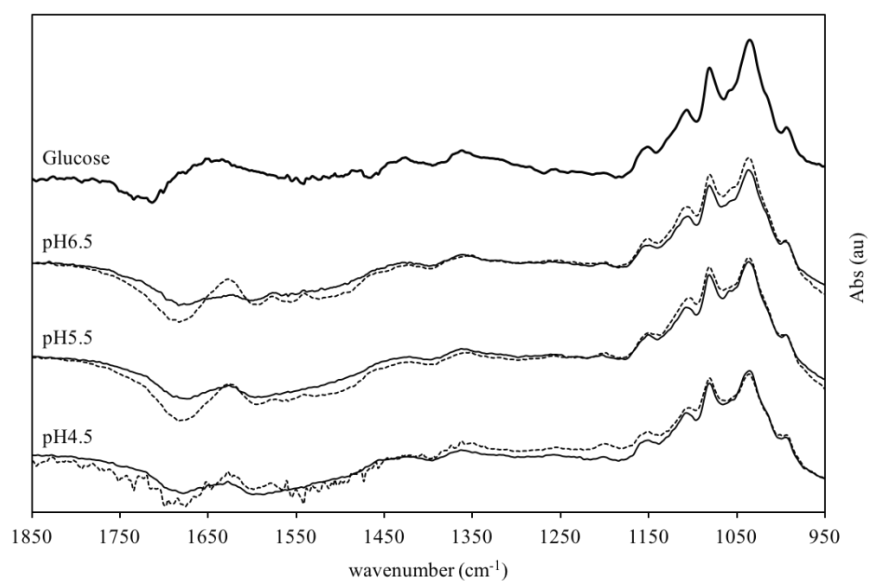


Figure 5 ATR-FTIR spectra of concentrated samples from suspensions of glucose (2.2 mM) reacted with δ -MnO₂ (~ 1.5 mM) at pH 6.5, 5.5 and 4.5, sampled after 3 h (t_{3h}, solid lines) and 24 h (t_{24h}, dotted lines) of reaction. Experimental spectra are plotted alongside a reference spectrum for glucose.

Reaction of gluconate with δ -MnO₂ monitored by ATR-FTIR

The ATR-FTIR spectra of the supernatant of δ -MnO₂ suspensions reacted with gluconate at pH 4.5, 5.5 and 6.5 for 3 h and 24 h are plotted in **Figure 6**. Gluconate standards at pH 4.7 and 7.6 are plotted alongside the data. At pH 4.7, where 89 % of the substrate remains deprotonated, no significant shift is observed in the position of the vibration bands associated to the carboxylic acid functional group (see **SI** and **Figure 3-S1B**).

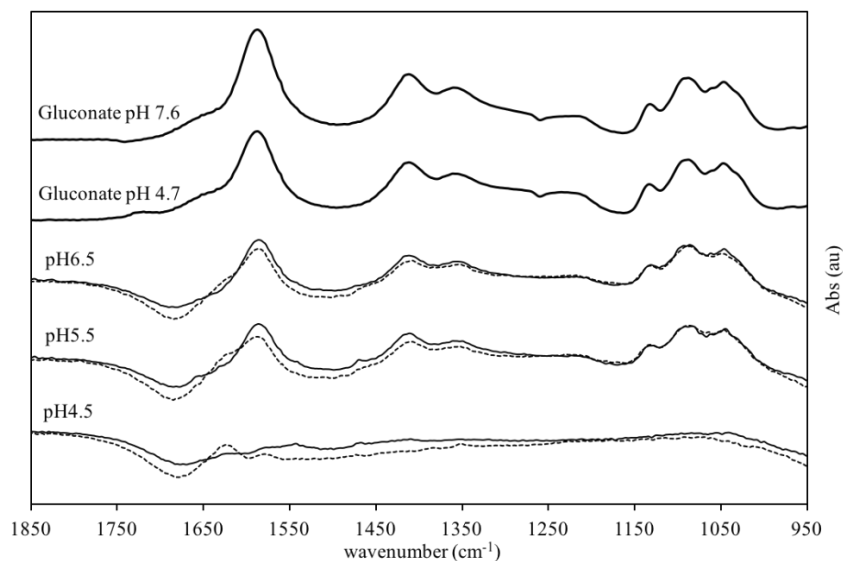


Figure 6 ATR-FTIR spectra of concentrated samples from suspensions of gluconate (2.2 mM) reacted with δ -MnO₂ (~ 1.5 mM) at pH 6.5, 5.5 and 4.5, sampled after 3 h (t3h, solid lines) and 24 h (t24h, dotted lines) of reaction. Experimental spectra are plotted alongside reference spectra for gluconate at pH 7.6 and 4.7.

Attempts to quantify gluconate consumption were unsuccessful given the high detection limit for these measurements (1.0 mM, see **SI**). For the gluconate solutions reacted at pH 5.5 and 6.5, the intensity of the signal did not change during the reaction period. The predicted concentration from the absorbance at 1092 cm⁻¹ was 56 mM, and when corrected by the concentration factor, 2.8 ± 1.0 mM. This value is relatively close to the 2.2 mM glucose added at t0h. Based on the sensitivity of the measurement, these measurements thus confirm that less than 1.0 mM gluconate was consumed over the reaction period. When reacted at pH 4.5 however, the gluconate signal was significantly reduced in both 3 h and 24 h samples indicating a loss of at least 1.2 mM gluconate from solution.

DISCUSSION

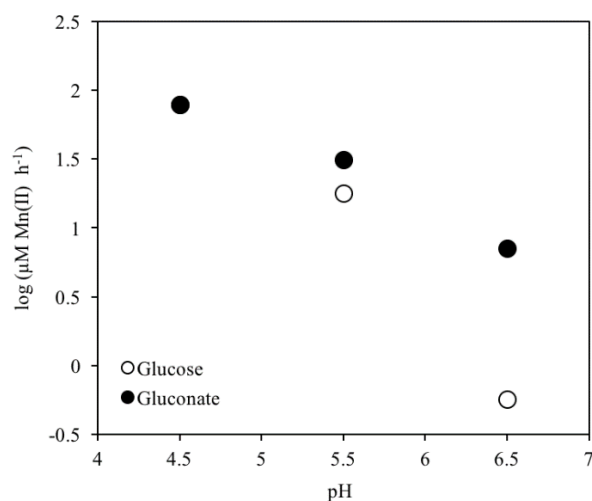
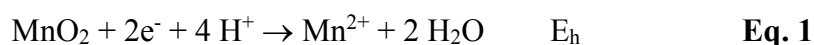
Reductive dissolution of δ -MnO₂

Figure 7 Initial rates of release of Mn(II) as a function at pH 4.5, 5.5 and 6.5 upon reaction between glucose (open circles) and gluconate (filled circle) with δ -MnO₂.

The trends in the initial rates of δ -MnO₂ dissolution upon reaction with glucose and gluconate were relatively similar (see **Figure 7**), despite their respective cyclic and acyclic forms and the presence of a carboxylic acid functional group in gluconate that is absent in glucose. For both substrates, the reductive dissolution of MnO₂, and therefore the concomitant oxidation of the organic substrates, showed a strong pH-dependence. At pH 6.5, at most 11 % of the solid dissolved after 24 h of reaction. This stability was observed despite the 3 : 2 molar ratio between the organic substrates and MnO₂, which is located at the opposite end of the redox ladder relative to glucose and gluconate (13). On the other hand, at pH 4.5, extensive dissolution was observed after 24 h of reaction with both substrates, with 71 – 77 % dissolution of the solid phase. The strong pH-dependence of the reductive dissolution of MnO₂ coupled to the oxidation of small organic molecules can be explained by both thermodynamic and kinetic factors.

The position of MnO₂ on the redox ladder relative to glucose and gluconate indicates that MnO_{2(s)} reduction is energetically favourable between pH 4.5 and 6.5. However, the half-equation for the reduction of Mn(IV) to Mn(II) (**Eq. 1**) and the E_h-pH diagram of Mn species (see **Figure 3-S3**) show that the redox potential (E_h) of the Mn(IV/ II) becomes increasingly high with decreasing pH.



The pH dependence of the E_h for the $MnO_2 / Mn(II)$ couple is particularly important due to the power 4 at which the proton activity is raised in the Nernst equation. The thermodynamic driving force for the reaction of MnO_2 with organic molecules thus increases significantly with decreasing pH (14, 37). At pH 6.5, even though the reduction of MnO_2 by both glucose and gluconate remains thermodynamically favourable, we measured only limited dissolution of MnO_2 . Furthermore, because gluconate is more oxidized than glucose, glucose oxidation is expected to be, from a thermodynamic point of view, more favourable than gluconate oxidation. However, initial rates of dissolution of MnO_2 in glucose solutions were lower than those in gluconate solutions at pH 5.5 and 6.5. These two observations suggest that at these pH conditions, electron transfer from both reductants to MnO_2 is kinetically hindered.

Surface complex formation, and electron transfer from the reductants to MnO_2 can kinetically limit the reaction, especially at higher pH. If electron transfer through outer-sphere coordination is poorly efficient, the reductive dissolution of MnO_2 may be dependent on the formation of inner-sphere surface complexes. The low pH_{pzc} often reported for MnO_2 basal sites [~ 2.8 (38)] suggests that MnO_2 surface sites are deprotonated under all environmentally relevant pH. Because O^{2-} and OH^- are poor leaving groups, inner-sphere coordination of organic substrates on MnO_2 surface when $pH > pH_{pzc}$ is not favorable (19). However, higher values ranging from 6 - 7 have been reported for pH_{pzc} of singly coordinated oxygen atoms at edge sites (39, 40), which suggests different protonation states between pH 6.5 and 4.5 and thus more favourable inner-sphere complexation of the substrates at pH 4.5 than at 6.5. Furthermore, the facilitated ring-opening of glucose under acidic conditions (41, 42) may contribute to align the reactivity of glucose to that of gluconate at pH 4.5, by facilitating its binding to the surface of MnO_2 . Once glucose oxidation is started, any gluconate formed can further react through the cascade described in **Figure 8**.

The role of protons in catalysing the dissolution of MnO_2 also likely contributes to the observed pH-dependence of the redox reactions with glucose and gluconate. In oxide minerals, structural ions are held together by strong lattice energies that hinder dissolution of the mineral. Proton-catalysis however lowers the lattice energy barrier for mineral dissolution, as protonation of oxygen atoms pull away the electron density from Mn-O bonds, weakening the bond and therefore facilitating dissolution (43, 44). At pH 4.5, proton catalysis is expected to lower the lattice energy barrier. This means that mineral

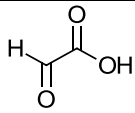
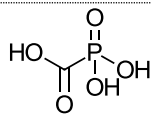
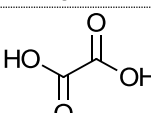
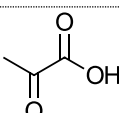
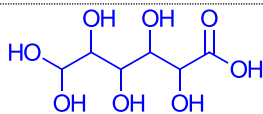
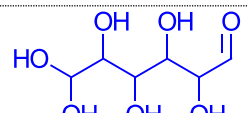
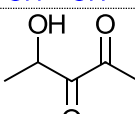
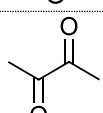
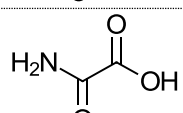
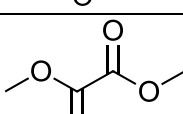
dissolution may become too favourable to discriminate between the two organic substrates, and thus contribute to explain rates of dissolution observed for glucose and gluconate. At high pH, the lattice energy sufficiently hinders mineral dissolution, such that the surface complex formation governs the initial reactivity observed. In other words, when the dissolution of the mineral is kinetically favoured at low pH, the formation and nature of the surface complex is not rate-determining. However at higher pH, when the lattice energy is higher and thus kinetically hinders dissolution, the formation of the surface complex of the substrate becomes important as it affects the formation of the surface complex.

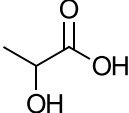
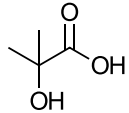
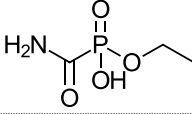
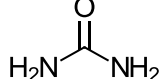
The similarity in reactivity observed in the extent of Mn reduction after 24 h of reaction with either glucose and gluconate brings into question the importance of the chemical nature of organic molecules when reacting with highly reactive phases such as MnO₂. In **Table 2**, the initial rates of dissolution measured for glucose and gluconate reacting with δ -MnO₂ at pH 5.0 (as extrapolated from rates measured at pH 4.5, 5.5 and 6.5) are compared with those reported by Wang and Stone (19) for a suite of organic substrates reacting with MnO₂ at pH 5.0. The range of initial rates reported illustrate the extent to which the abiotic oxidation of organic substrate by MnO₂ may depend on the intrinsic chemical nature of the reductant. In particular, Wang and Stone highlighted that the adsorptive, the complexant and the reductant properties of the organic substrates all control their reactivity with Mn oxides. For Mn(III)-enriched or Mn(III)-only Mn oxides, the ability of some molecules to form a complex with Mn(III) may allow the detachment of Mn(III) through ligand-assisted dissolution. However, in the list of organic molecules reported in **Table 2**, only oxalic acid, and only under high concentration, was found to be able to react with MnO₂ through ligand-assisted dissolution. All other molecules, including oxalic acid at lower concentration, reacted by reductively dissolving MnO₂. Alcohol, carbonyl, carboxylic acid and phosphonic acid groups in the α -position relative to carbonyl or carboxylic acid groups were suggested to allow one electron-transfers since the radical generated can be resonance-stabilised. Overall, the rate of Mn(II) production and accumulation into solution depends either on rate of surface complex formation or the rate of electron transfer which itself depends on the identity of the organic molecule (45). For example, Wang and Stone reported that carboxylate and phosphonate groups should facilitate adsorption of the organic substrate on the mineral.

Based on these considerations, it is reasonable to expect that gluconate should form a surface complex more easily than glucose because it features a carboxylic functional group

that glucose lacks. The ring structure of adopted by glucose may further slow down its reaction with MnO₂, especially at higher pH as the ring opening is slower than under acid conditions. However overall, the two molecules are sufficiently similar to suggest that they likely undergo similar oxidative transformations. Furthermore, both molecules feature an alcohol functional group in the α -position relative to a carbonyl or carboxylic, which indicates that radical intermediates may be formed for the two molecules.

Table 2 Initial rate of MnO₂ dissolution when reacted with a suite of organic molecules at pH 5.0, as reported by Wang and Stone (19) [MnO₂ comprising 22 % Mn(III) and 78 % Mn(IV), AMON 3.78, BET specific surface are 174 m² g⁻¹]. The initial rates obtained in the present study for the reaction of δ -MnO₂ [100 % Mn (IV), AMON 4] with glucose and gluconate at pH 5.0 [obtained from extrapolation of the data collected at pH 4.5,5.5 and 6.5] are included for comparison.

Chemical name	Chemical structure	R ₀ ($\mu\text{M h}^{-1}$)	pH
glyoxylic acid		$> 3.0 \times 10^3$	5.0
phosphonoformic acid		$\sim 1.4 \times 10^3$	5.0
oxalic acid		4.6×10^2	5.0
pyruvic acid		6.8×10^1	5.0
gluconate		4.7×10^1	5.0
glucose		3.2×10^1	5.0
glycolic acid		1.4×10^1	5.0
2,3-butanedione		3.0×10^1	5.0
oxamic acid		4.8×10^0	5.0
dimethyl oxalate		2.7×10^0	5.0

lactic acid		1.6×10^0	5.0
2-hydroxyisobutyric acid		2.7×10^{-1}	5.0
fosamine		7.0×10^{-2}	5.0
urea		$< 1.0 \times 10^{-2}$	5.0

While the chemical nature of molecules is an important factor in controlling the rate of reaction with MnO_2 , our observations of the reaction of glucose and gluconate with δ - MnO_2 suggest that for this pair of molecules, pH may be more important than the chemical nature of the organic reductants in controlling the rates of the reaction taking place. In natural systems, microbial activity and metabolic processes will strongly modulate biogeochemical conditions and consequently exert a strong influence on MnO_2 -assisted oxidation of organic molecules. Furthermore, the extensive reductive dissolution of MnO_2 observed when reacted with glucose and gluconate suggests that MnO_2 will undergo significant reductive dissolution in C-rich areas. This reactivity has environmental implications regarding the fate of nutrient or contaminant elements sorbed by MnO_2 , since dissolution of MnO_2 will be also lead to their associated release into solution.

Electron transfer to MnO_2 : aqueous and surface-bound Mn

Electron transfer from glucose and gluconate will result in aqueous or solid-phase Mn(II) or Mn(III) . While the formation of stable aqueous Mn(III) -organic complexes is possible, we excluded this possibility, because compounds that able to solubilize Mn(III) , such as desferrioxamine B, pyrophosphate and phosphonoformic acid, all feature multiple hydroxamate, phosphonate or carboxylic groups that allow them to stabilize Mn(III) . Wang and Stone (19) dismissed the possibility that ligands featuring only one carboxylic acid or phosphonate monoester group could form sufficiently strong complexes with Mn(III) to solubilize it. There has been some report of electrochemical formation of Mn(III) -gluconate complexes in alkaline conditions (46-48), but in these pH regimes ($> \text{pH } 13$), deprotonation of α -hydroxyl groups allows bidentate binding of Mn(III) . Under environmentally relevant pH conditions, glucose, gluconate and any of the derivatives that

can form from oxidative transformation on MnO₂ are unlikely to be strong enough chelators for stabilising Mn(III). Therefore, aqueous Mn can be considered to be Mn(II).

Changes in aqueous Mn can therefore be used as a probe for the oxidation of the organic substrates by MnO₂. Considering that two electrons are required to reduce Mn(IV) to Mn(II), the concentration of aqueous Mn was scaled by a factor of two to estimate the minimum number of electron equivalents transferred from glucose or gluconate to MnO₂ at a given time (**Eq. 2**).

$$n_{\text{min_e-transferred_t}} = \text{Mn(II)}_{\text{aq_t}} \times 2 \quad \text{Eq. 2}$$

At pH 4.5, minimum 1.66 mM electrons were transferred from glucose and gluconate to MnO₂ after 24 h, whereas at pH 5.5 and pH 6.5, at least 0.58 mM and 0.30 mM electrons were transferred respectively.

The solid phase, however, may store electrons in the form of reduced Mn. In particular, reduced Mn may accumulate in the solid phase at short reaction times where no or little aqueous Mn is observed. For instance, up to 34 % pyrophosphate-extractable Mn(III) was shown to accumulate in δ -MnO₂ when equilibrated at pH 6.6 with HEPES buffer (49, 50), and 32 % Mn(III) was reported to accumulate in δ -MnO₂ equilibrated at pH 3 (51). In addition, some Mn(II) may remain sorbed on the mineral depending on the pH (36, 52). Lefkowitz et al. (2013) have reported a maximum 16 % adsorption (mol : mol) of Mn(II) on MnO₂ at pH 6 under oxic conditions (36). Therefore, if the maximal sorption of Mn(II) on MnO₂ can be considered as negligible for the pH 4.5 condition relative to the aqueous Mn concentration, for the pH 6.5 condition, up to 0.16 mol Mn(II) mol⁻¹ MnO₂ can be sorbed on the solid phase. Furthermore, small quantities of aqueous Mn(II) may readsorb on MnO₂ vacancies and disproportionate with neighbouring Mn(IV), leading to further Mn(III)-enrichment of the oxide. These additional electron storage reservoirs can lead to underestimation of the extent of electron transfer from the organic substrates to the mineral when looking only at aqueous Mn. The absence of measurable aqueous Mn(II) measured in solution during the first 9h of reaction between glucose and MnO₂ at pH 6.5 therefore does not preclude Mn(IV) reduction, as it could only reflect the build-up of Mn(III) in the mineral phase. To verify these hypotheses solid-phase analysis of Mn oxidation state, as can be achieved by potentiometric titration or with pyrophosphate extractions of Mn(III) and subsequent quantification of Mn(III)-pyrophosphate complexes by UV-vis spectroscopy, may be carried (49, 53).

The accumulation of Mn(III) in the solid phase can be accounted for to yield a maximal number of electrons transferred to the mineral at a given time t (**Eq. 3**).

$$n_{\max_e\text{-transferred}_t} = \text{Mn(II)}_{\text{aq}_t} \times 2 + 0.34 \times [1 - (\text{Mn(II)}_{\text{aq}_t} \times \text{MnO}_{2_i}^{-1})] \times \text{MnO}_{2_i} \quad \text{Eq. 3}$$

where $\text{Mn(II)}_{\text{aq}_t}$ is the concentration of Mn(II) measured in solution at a time t , MnO_{2_i} is the initial MnO_2 concentration and assuming 34 % is the maximal Mn(III) content that the $\delta\text{-MnO}_2$ structure can accommodate. **Eq. (2-3)** thus provide a range for the number of electrons transferred between the organic substrate and MnO_2 . When the pH is lowered and the extent of reductive dissolution of the mineral increases, the amount of Mn(III) the remaining solid phase can hold necessarily decreases, and the window therefore becomes narrower. At pH 4.5, 1.71 ± 0.13 mM electrons were transferred from glucose and gluconate to MnO_2 after 24 h of reaction, whereas at pH 5.5 and pH 6.5, 0.73 ± 0.21 mM and 0.50 ± 0.26 mM electrons were transferred respectively.

Oxidation of the organic substrates

Despite extensive reductive dissolution of MnO_2 observed upon reaction with glucose and gluconate, both the colorimetric assay and FTIR spectra showed ≤ 0.5 mM glucose consumed at all pH conditions, and ≤ 1.0 mM gluconate at pH 6.5 and 5.5 during their reactions with $\delta\text{-MnO}_2$. These results suggest that when these substrates encounter MnO_2 , they transfer multiple electrons to the solid phase, thus leaving a large pool of unreacted organic substrate in solution.

The cascade of 2 electrons oxidation steps that may transform glucose to CO_2 , through a gluconate intermediate, is presented in **Figure 8**. One molecule of glucose can provide up to 24 moles of electron equivalents to the solid phase, whereas gluconate can provide 22 electrons. The extent of oxidation glucose and gluconate will experience when reacting with MnO_2 depends on their intrinsic stability relative to that of any oxidized intermediates that may form, as well as the relative stabilities of the surface complexes formed by either of these species on the surface of the oxide. Because of the methods employed in this study to measure glucose and gluconate concentrations and their poor sensitivity, the consumption of glucose and gluconate could not be quantified. Furthermore, the identity of the products formed remained unknown. Therefore, neither a mass balance nor an electron balance could be established, and only end-membered scenarios could be inferred based on **Figure 8**. The oxidation of glucose to gluconic acid requires the transfer of two electrons to the oxidant. The oxidation of 275 μM of glucose to gluconic acid would thus

be sufficient to explain the 550 μM Mn(II) released in solution after 6 h of reaction at pH 4.5 [assuming no Mn(III) accumulate in the mineral]. One study reported the formation of formic acid (HCOOH) upon reaction (6 h, 90 °C, 2 % H₂SO₄) of glucose (0.27 g L⁻¹, 15 mM) with MnO₂ (1 g L⁻¹, 12 mM) (54). Lower concentrations of monocarboxylic polyhydroxyacids such as gluconic acid, glyceric acid (CH₂OH-CHOH-COOH) and glycolic acid (CH₂OH-COOH) were also measured. Upon oxidation to formic acid, glucose transfers 22 electrons to MnO₂, which means that the oxidation of 25 μM glucose down to formic acid would be sufficient to explain the 550 μM Mn(II) released in solution after 6h of reaction at pH 4.5. The reason why the oxidative transformation cascade should stop at formic acid is however unclear, considering the strong entropic driving force associated to CO₂ evolution upon oxidising formic acid.

Similar reaction pathways are likely taking place during the reaction between gluconate and $\delta\text{-MnO}_2$ in all pH conditions, despite the loss of the FTIR signal observed at pH 4.5. Considering the sensitivity of the ATR-FTIR, the loss of the signal suggests that at least 1.2 mM was removed from the solution. However, this disappearance of the signal cannot be ascribed to complete mineralization, since that would require the transfer of 26.4 mM electrons to MnO₂, which largely exceeds the total electron accepting capacity of the 1.5 mM MnO₂ initially added. The loss of the signal at pH 4.5 therefore points toward an organo-mineral interaction, resulting in the removal of the substrate upon filtration or which prevents to re-suspend Mn(II)-gluconate after drying. Supplementary experiments are needed to test this hypothesis.

The extensive oxidative transformations of glucose and gluconate upon reaction with $\delta\text{-MnO}_2$ demonstrate that this highly oxidising specie can lead to the extensive oxidation of C species in engineering (37, 55, 56) and natural systems (7, 8, 57, 58). In addition, the limited consumption of glucose and gluconate demonstrates that MnO₂ is unlikely to compete efficiently with bacterial cells for the transformation of bioavailable C substrates, especially when these minerals are precipitated within a metabolically active biofilm matrix, since rates of 4.77 ± 0.33 mmol glucose g⁻¹ bacteria h⁻¹ are reported for common bacterial strains (21, 59, 60). The potential role of MnO₂ to participate in the soil C cycle is therefore likely focused on the transformation of biologically refractory molecules, for which the MnO₂ particles would not have to compete with metabolic processes.

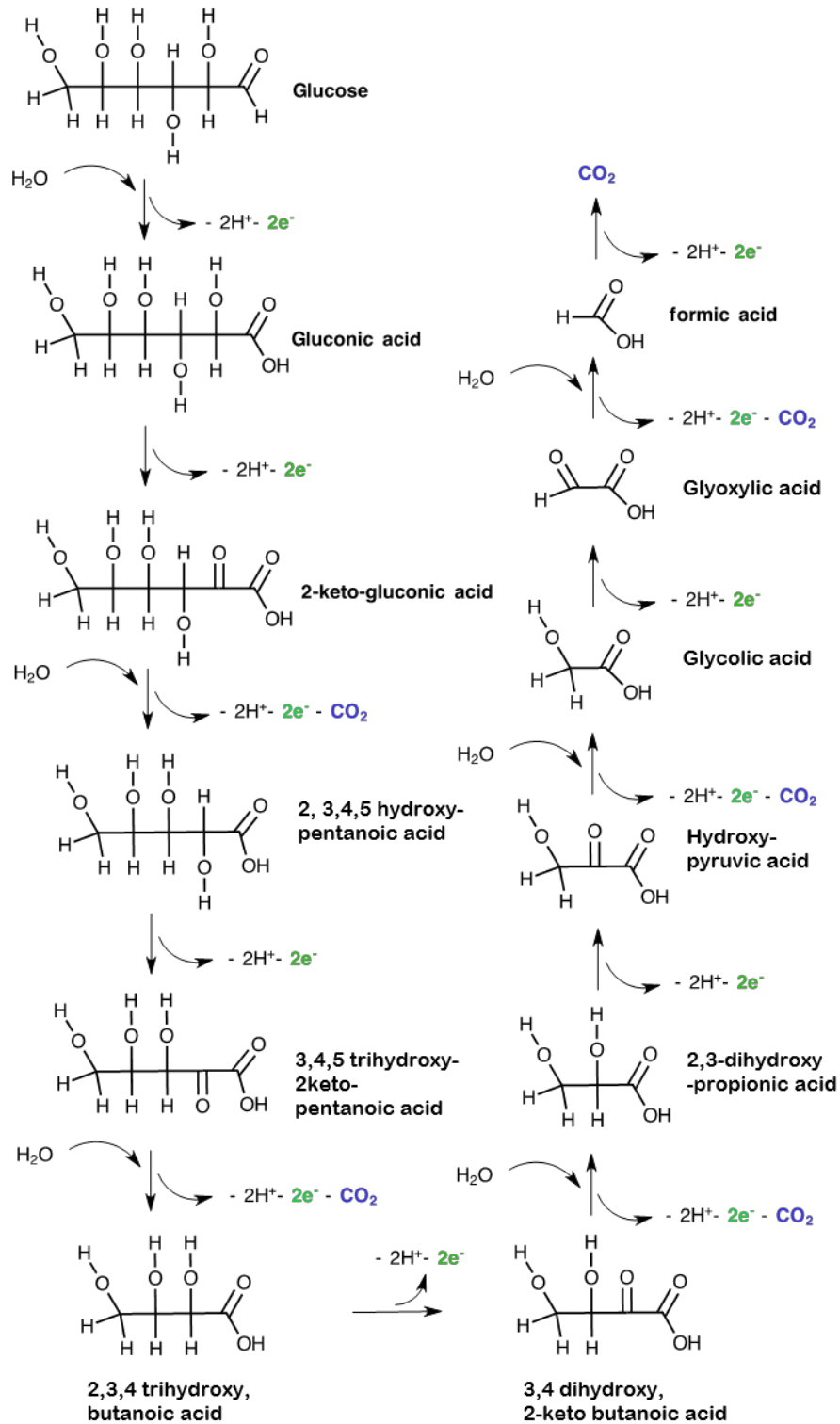


Figure 8 Cascade of 2 electrons oxidative steps for the complete mineralization of glucose to CO₂, predicted based on the 2-electrons oxidation scheme of similar hydroxy-carbonyl/ carboxylic acids reported by Wang and Stone (19) The complete mineralization yields 6 moles of CO₂, 24 moles H⁺ and 24 moles of electrons per mole of glucose transformed.

Abiotic oxidation of glucose and gluconate by biogenic MnO₂

Glucose and gluconate are generally good carbon substrates for bacteria [for eg: (21, 60, 61)]. When biogenic MnO₂ suspensions, which contain stationary phase bacteria, are provided with an input of these organic substrates, the bacterial cells are expected to feed on these substrates, thus competing with the abiotic oxidation carried by the mineral, modifying the extracellular solution or possibly provide alternative reductants, either due to the direct extracellular oxidation these substrates or secretion of new molecules (see **Chapter 4**). Decoupling the biological reactivity from the purely abiotic oxidation requires that biological activity be inactivated without denaturing the mineral, either by modifying its structure or its oxidation state (AMON). In light of this consideration, the extremely high reactivity of MnO₂ prevents the use of chemicals, such as sodium-azide, to inactivate the cells [for eg: (52, 62, 63)]. The use of physical means, such as γ -radiation, may be more appropriate to preserve the integrity of the mineral.

Compared to the δ -MnO₂ used in this study, biogenic MnO₂ can have up to a 30 % enrichment in Mn(III)(AMON of 4.0 and \sim 3.7 respectively)(30, 64-67). The presence of Mn(III) in the mineral corresponds to a pool of electrons already stored in the mineral and may affect the mechanism of release of Mn(II). Furthermore, the relative importance of Mn(III) and Mn(IV) centres in governing the redox reactivity of MnO_x towards both organic inorganic species is unclear. For example, the oxidation of Cr(III), phenols and sulfide by a Mn(III)-enriched δ -MnO₂ (AMON 3.88) was reported to be inhibited by the addition of pyrophosphate, a ligand with a high affinity for Mn(III) species (68, 69). Tentative explanations of the observed inhibition included the higher reduction potential of Mn(III) relative to Mn(IV) (69, 70), and the faster ligand exchange rate of Mn(III) centers relative to Mn(IV) (68-70). However, a recent study reported that at pH 6, the Co(II) oxidation on δ -MnO₂ (AMON 4.0), was higher than that on a Mn(III)-enriched δ -MnO₂ (AMON 3.7) (50, 71). The relative importance of Mn(III) and Mn(IV) reaction sites in reacting with organic molecules thus warrants further investigation. This knowledge is required to understand how to translate the data collected on abiotic MnO₂ to biogenic MnO₂.

In addition to the intrinsic differences in the reactivity of the mineral phases for δ -MnO₂ and biogenic MnO₂, the occurrence of the mineral particles within a biofilm matrix in biogenic MnO₂ may slow the diffusion of the organic substrates to the mineral surface.

Furthermore, existing organo-mineral interactions with moieties from the biofilms may passivate the mineral surface by preventing surface complex formation between glucose or gluconate and surface hydroxyls. These considerations highlight the importance of better understanding how organic molecules may arrange on MnO₂ surface in organo-mineral suspensions, to understand how the pre-exposure to organic molecules can affect the reaction of MnO₂ with incoming organic substrates (see **Chapter 5**).

REFERENCES

1. Dungait JA, Hopkins DW, Gregory AS, Whitmore AP. Soil organic matter turnover is governed by accessibility not recalcitrance. *Global Change Biol.*, 2012;18(6):1781-96.
2. Jones DL. Organic acids in the rhizosphere—a critical review. *Plant and soil.* 1998;205(1):25-44.
3. Kleber M, Mikutta R, Torn M, Jahn R. Poorly crystalline mineral phases protect organic matter in acid subsoil horizons. *Europ. J. Soil Sci.*, 2005;56(6):717-25.
4. Lützw Mv, Kögel-Knabner I, Ekschmitt K, Matzner E, Guggenberger G, Marschner B, et al. Stabilization of organic matter in temperate soils: mechanisms and their relevance under different soil conditions—a review. *Europ. J. Soil Sci.*, 2006;57(4):426-45.
5. Kögel-Knabner I, Guggenberger G, Kleber M, Kandeler E, Kalbitz K, Scheu S, et al. Organo-mineral associations in temperate soils: Integrating biology, mineralogy, and organic matter chemistry. *J. Plant Nutri. Soil Sci.*, 2008;171(1):61-82.
6. Kleber M, Eusterhues K, Keiluweit M, Mikutta C, Mikutta R, Nico PS. Chapter One-Mineral–Organic Associations: Formation, Properties, and Relevance in Soil Environments. *Adv. Agron.*, 2015;130:1-140.
7. Sunda WG, Kieber DJ. Oxidation of humic substances by manganese oxides yields low-molecular-weight organic substrates. *Nature*, 1994.
8. Chorover J, Amistadi MK. Reaction of forest floor organic matter at goethite, birnessite and smectite surfaces. *Geochim Cosmochim Ac.* 2001;65(1):95-109.
9. Mitchell MB, Sheinker V, Mintz EA. Adsorption and decomposition of dimethyl methylphosphonate on metal oxides. *J. Phys. Chem. B.*, 1997;101(51):11192-203.
10. Baldwin DS, Beattie JK, Coleman LM, Jones DR. Phosphate ester hydrolysis facilitated by mineral phases. *Environ. Sci. Technol.*, 1995;29(6):1706-9.
11. Reardon PN, Chacon SS, Walter ED, Bowden ME, Washton NM, Kleber MW. Abiotic protein fragmentation by manganese oxide: implications for a mechanism to supply soil biota with oligopeptides. *Environmental Science and Technology.* 2016;50(PNNL-SA--108407).
12. Luther GW. *Inorganic Chemistry for Geochemistry and Environmental Sciences: Fundamentals and Applications*: John Wiley & Sons; 2016.
13. Sposito G. *The chemistry of soils*: Oxford university press; 2008.
14. Bricker O. Some stability relations in system MnO₂-H₂O at 25 degrees and 1 atmosphere total pressure. *Am. Mineral.*, 1965;50(9):1296-.
15. Jenkins S. *CRC Handbook of Chemistry and Physics. Chemical Engineering.* 2012;119(9):9-10.
16. Stone AT. Microbial Metabolites and the Reductive Dissolution of Manganese Oxides - Oxalate and Pyruvate. *Geochim Cosmochim Ac.* 1987;51(4):919-25.
17. Stone AT, Morgan JJ. Reduction and dissolution of manganese (III) and manganese (IV) oxides by organics. Part 2. Survey of the reactivity of organics. *Environ Sci Technol.*; 1984;18(8).
18. Wang Y, Stone AT. The citric acid–Mn^{III},^{IV}O₂ (birnessite) reaction. Electron transfer, complex formation, and autocatalytic feedback. *Geochim Cosmochim Ac.* 2006;70(17):4463-76.
19. Wang Y, Stone AT. Reaction of Mn^{III},^{IV} (hydr)oxides with oxalic acid, glyoxylic acid, phosphonoformic acid, and structurally-related organic compounds. *Geochim Cosmochim Ac.* 2006;70(17):4477-90.

20. Stumm W. Chemistry of the solid-water interface: processes at the mineral-water and particle-water interface in natural systems: John Wiley & Son Inc.; 1992.
21. Fuhrer T, Fischer E, Sauer U. Experimental identification and quantification of glucose metabolism in seven bacterial species. *J. Bacteriol.* 2005;187(5):1581-90.
22. Matocha CJ, Sparks DL, Amonette JE, Kukkadapu RK. Kinetics and mechanism of birnessite reduction by catechol. *Soil Sci. Soc. Am. J.*, 2001;65(1):58-66.
23. Stone AT, Morgan JJ. Reduction and Dissolution of Manganese(III) and Manganese(IV) Oxides by Organics 1. Reaction with Hydroquinone. *Environ. Sci. Technol.*, 1984;18(6):450-6.
24. Luther III GW. Manganese (II) oxidation and Mn (IV) reduction in the environment—two one-electron transfer steps versus a single two-electron step. *Geomicrobiol J.* 2005;22(3-4):195-203.
25. Xyla AG, Sulzberger B, Luther III GW, Hering JG, Van Cappellen P, Stumm W. Reductive dissolution of manganese (III, IV)(hydr)oxides by oxalate: The effect of pH and light. *Langmuir.* 1992;8(1):95-103.
26. Zhang H, Chen W-R, Huang C-H. Kinetic modeling of oxidation of antibacterial agents by manganese oxide. *Environ. Sci. Technol.*, 2008;42(15):5548-54.
27. Clayden J, Greeves N, Warren S, Wothers P. *Organic Chemistry*: Oxford University Press; 2001.
28. Olsson R, Giesler R, Persson P. Adsorption mechanisms of glucose in aqueous goethite suspensions. *J. Coll. Interf. Sci.*, 2011;353(1):263-8.
29. Besson M, Lahmer F, Gallezot P, Fuertes P, Fleche G. Catalytic oxidation of glucose on bismuth-promoted palladium catalysts. *J. Catalysis.* 1995;152(1):116-21.
30. Villalobos M, Toner B, Bargar J, Sposito G. Characterization of the manganese oxide produced by *Pseudomonas putida* strain MnB1. *Geochim. Cosmochim. Ac.*, 2003;67(14):2649-62.
31. Marafatto FF, B. Lanson and J. Peña. Crystal growth and aggregation in suspensions of δ -MnO₂ nanoparticles: Implications for surface reactivity. In press, *Environ. Sci. Nano.* 2017.
32. Zhao H, Zhu M, Li W, Elzinga EJ, Villalobos M, Liu F, et al. Redox reactions between Mn (II) and hexagonal birnessite change its layer symmetry. *Environmental science & technology.* 2016;50(4):1750-8.
33. Mandernack KW, Post J, Tebo BM. Manganese mineral formation by bacterial spores of the marine *Bacillus*, strain SG-1: Evidence for the direct oxidation of Mn (II) to Mn (IV). *Geochim Cosmochim Ac.* 1995;59(21):4393-408.
34. Hinkle MA, Flynn ED, Catalano JG. Structural response of phyllo-manganates to wet aging and aqueous Mn (II). *Geochim Cosmochim Ac.* 2016;192:220-34.
35. Elzinga EJ. Reductive transformation of birnessite by aqueous Mn(II). *Environ. Sci. Technol.*, 2011; 45(15)
36. Lefkowitz JP, Rouff AA, Elzinga EJ. Influence of pH on the reductive transformation of birnessite by aqueous Mn (II). *Environ. Sci. Technol.*, 2013;47(18):10364-71.
37. Remucal CK, Ginder-Vogel M. A critical review of the reactivity of manganese oxides with organic contaminants. *Environ. Sci. Process Impacts.*, 2014;16(6):1247-66.
38. Murray JW. The surface chemistry of hydrous manganese dioxide. *J. Coll. Interf. Sci.*, 1974;46(3):357-71.
39. van Genuchten CM, Peña J. Sorption selectivity of birnessite particle edges: a d-PDF analysis of Cd(II) and Pb(II) sorption by δ -MnO₂ and ferrihydrite. *Environ. Sci. Process. Impacts.* 2016.
40. Villalobos M. The role of surface edge sites in metal(loid) sorption to poorly-crystalline birnessites. *Advances in the Environmental Biogeochemistry of Manganese Oxides*: ACS Publications; 2015. p. 65-87.
41. Plazinski W, Plazinska A, Drach M. The water-catalyzed mechanism of the ring-opening reaction of glucose. *Phys. Chem. Chem. Phys.*, 2015;17(33):21622-9.
42. Wrolstad RE. Reactions of sugars. *Food carbohydrate chemistry.* 2012:35-47.
43. Stumm W. Reactivity at the mineral-water interface: dissolution and inhibition. *Colloids and Surfaces A: Physicochemical and Engineering Aspects.* 1997;120(1):143-66.
44. Grassian VH. *Environmental catalysis*: CRC press; 2005.
45. Zhang H, Huang C-H. Oxidative transformation of triclosan and chlorophene by manganese oxides. *Environ. Sci. Technol.*, 2003;37(11):2421-30.
46. Bodini ME, Willis LA, Riechel TL, Sawyer DT. Electrochemical and spectroscopic studies of manganese (II),-(III), and-(IV) gluconate complexes. 1. Formulas and oxidation-reduction stoichiometry. *Inorg. Chem.*, 1976;15(7):1538-43.

47. Sawyer DT, Bodini ME. Manganese (II) gluconate. Redox model for photosynthetic oxygen evolution. *J. Am. Chem. Soc.*, 1975;97(22):6588-90.
48. Richens DT, Smith CG, Sawyer DT. Sorbitol and related polyol complexes of manganese (II),-(III), and-(IV): redox and oxygenation equilibria. *Inorg. Chem.*, 1979;18(3):706-12.
49. Simanova AA, Kwon KD, Bone SE, Bargar JR, Refson K, Sposito G, et al. Probing the sorption reactivity of the edge surfaces in birnessite nanoparticles using Nickel (II). *Geochim Cosmochim Acta*. 2015;164:191-204.
50. Simanova AA, Peña J. Time-resolved investigation of cobalt oxidation by Mn(III)-rich δ -MnO₂ using quick X-Ray absorption spectroscopy. *Environ. Sci. Technol.*, 2015;49(18):10867-76.
51. Manceau A, Marcus MA, Grangeon S, Lanson M, Lanson B, Gaillot A-C, et al. Short-range and long-range order of phyllosilicate nanoparticles determined using high-energy X-ray scattering. *J. Applied Crystal.*, 2013; 46(1)
52. Zhu M, Ginder-Vogel M, Parikh SJ, Feng X-H, Sparks DL. Cation effects on the layer structure of biogenic Mn-oxides. *Environ. Sci. Technol.*, 2010;44(12):4465-71.
53. Klewicki J, Morgan J. Dissolution of β -MnOOH particles by ligands: pyrophosphate, ethylenediaminetetraacetate, and citrate. *Geochim Cosmochim Acta*. 1999;63(19):3017-24.
54. Furlani G, Pagnanelli F, Toro L. Reductive acid leaching of manganese dioxide with glucose: identification of oxidation derivatives of glucose. *Hydrometallurgy*. 2006;81(3):234-40.
55. De Rudder J, Van de Wiele T, Dhooge W, Comhaire F, Verstraete W. Advanced water treatment with manganese oxide for the removal of 17 α -ethynylestradiol. *Water Research*. 2004;38(1):184-92.
56. Forrez I, Carballa M, Verbeken K, Vanhaecke L, Ternes T, Boon N, et al. Diclofenac oxidation by biogenic manganese oxides. *Environmental science & technology*. 2010;44(9):3449-54.
57. Johnson K, Purvis G, Lopez-Capel E, Peacock C, Gray N, Wagner T, et al. Towards a mechanistic understanding of carbon stabilization in manganese oxides. *Nature Comm.*, 2015;6.
58. Allard S, Gutierrez L, Fontaine C, Croué J-P, Gallard H. Organic matter interactions with natural manganese oxide and synthetic birnessite. *Sci. Tot. Environ.*, 2017;583:487-95.
59. Sasnow SS, Wei H, Aristilde L. Bypasses in intracellular glucose metabolism in iron-limited *Pseudomonas putida*. *MicrobiologyOpen*. 2015.
60. del Castillo T, Ramos JL, Rodríguez-Herva JJ, Fuhrer T, Sauer U, Duque E. Convergent peripheral pathways catalyze initial glucose catabolism in *Pseudomonas putida*: genomic and flux analysis. *J Bacteriol*. 2007;189(14).
61. de Werra P, Pechy-Tarr M, Keel C, Maurhofer M. Role of gluconic acid production in the regulation of biocontrol traits of *Pseudomonas fluorescens* CHA0. *Applied Environ. Microbiol.*, 2009;75(12):4162-74.
62. Zhu M, Ginder-Vogel M, Sparks DL. Ni (II) sorption on biogenic Mn-oxides with varying Mn octahedral layer structure. *Environ. Sci. Technol.*, 2010;44(12):4472-8.
63. Miyata N, Maruo K, Tani Y, Tsuno H, Seyama H, Soma M, et al. Production of biogenic manganese oxides by anamorphic ascomycete fungi isolated from streambed pebbles. *Geomicrobiol J*. 2006;23(2):63-73.
64. Tebo BM, Bargar JR, Clement BG, Dick GJ, Murray KJ, Parker D, et al. Biogenic manganese oxides: properties and mechanisms of formation. *Annu Rev Earth Planet Sci*. 2004;32:287-328.
65. Santelli CM, Webb SM, Dohnalkova AC, Hansel CM. Diversity of Mn oxides produced by Mn(II)-oxidizing fungi. *Geochim Cosmochim Acta*. 2011;75(10):2762-76.
66. Webb S, Tebo B, Bargar J. Structural characterization of biogenic Mn oxides produced in seawater by the marine *Bacillus* sp. strain SG-1. *Am. Mineral.*, 2005;90(8-9):1342-57.
67. Droz B, Dumas N, Duckworth OW, Pena J. A comparison of the sorption reactivity of bacteriogenic and mycogenic Mn oxides nanoparticles. *Environ. Sci. Technol.*, 2015.
68. Nico PS, Zasoski RJ. Importance of Mn (III) availability on the rate of Cr (III) oxidation on δ -MnO₂. *Environ. Sci. Technol.*, 2000;34(16):3363-7.
69. Nico PS, Zasoski RJ. Mn (III) center availability as a rate controlling factor in the oxidation of phenol and sulfide on δ -MnO₂. *Environ. Sci. Technol.*, 2001;35(16):3338-43.
70. Ukrainczyk L, McBride MB. Oxidation of phenol in acidic aqueous suspensions of manganese oxides. *Clays and Clay Minerals*. 1992;40(2):157-66.
71. Wang Y, Benkaddour S, Marafatto F, Pena J. Diffusion-and pH-dependent reactivity of layer-type MnO₂: Reactions at particle edges versus vacancy sites. *Environ. Sci. Technol.*, 2018.

Chapter 4

Glucose metabolism in *Pseudomonas putida* GB-1 induces the dissolution of MnO₂

ABSTRACT

Naturally-occurring MnO₂ is precipitated by microorganisms, and therefore often occurs admixed with metabolically active cells. Consequently, mineral particles are exposed to changes in biogeochemical conditions imposed by the cells' metabolic activity. In light of the pH-dependence of the redox reactivity of MnO₂, the stability of MnO₂ is expected to be strongly sensitive to extracellular modification of the solution conditions. This study therefore aimed to characterise the response of stationary-phase *Pseudomonas putida* GB-1 and *Pseudomonas putida*-MnO₂ to the addition of glucose, chosen as a model for readily bioavailable carbon source, to understand the extent to which the microbial response could result in the reductive dissolution of the Mn oxides. We measured glucose consumption rates and changes in pH and dissolved oxygen. We then used chemical equilibria calculations to model the extent of extracellular acidification due to respiration relative to glucose-derived organic acids. We observed significant reductive dissolution of MnO₂ in bio-mineral assemblages spiked with glucose, with implications for the

scavenging and redox properties of MnO_2 in systems amended with a bioavailable C source.

INTRODUCTION

In soil systems, local physico-chemical conditions, including nutrient availability, hydration, oxygenation, pH and temperature control the microbial communities that can thrive in a given environment (1-3). However, these communities themselves modulate the characteristics of the surrounding extracellular solution. In particular, the metabolic activity of aerobic heterotrophic bacteria can impact soil functioning (2, 4) by altering the physical characteristics of the soils (5, 6) and/or its chemical characteristics. Chemical alterations may for example arise from respiration, which increases pCO_2 and decreases O_2 concentrations (7, 8), the activation of metabolic pathways that use alternative electron acceptors such as NO_3^- , SO_4^{2-} , Mn(III, IV) or Fe(III) oxides and thus drive important biogeochemical cycling (9, 10) or the secretion of secondary metabolites (11-13).

The metabolism of glucose, which is both a significant component of organic polymers and root exudates and a common C source for a number of microorganisms (14-16), can have significant impact on local extracellular chemical conditions. In addition to the uptake of glucose into the cytoplasm, the extracellular oxidation of glucose to gluconic acid has been reported for a number of bacterial species (17-20) (see **Figure 1**).

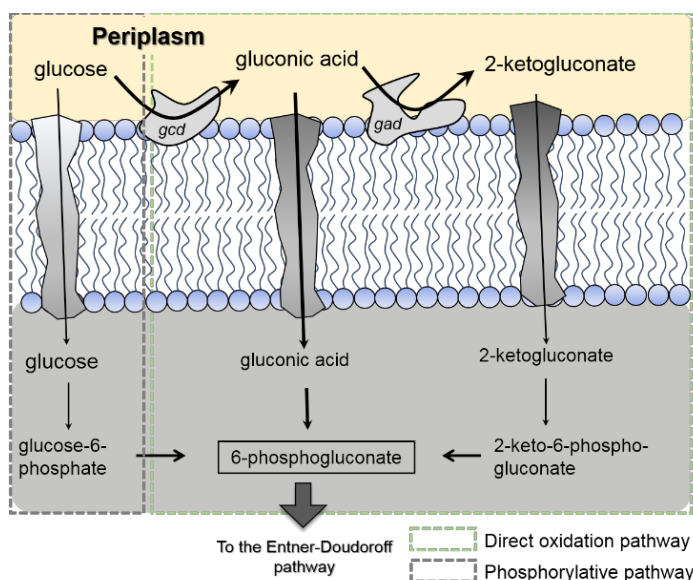


Figure 1 Glucose metabolism in *Pseudomonas putida* GB-1. Glucose diffuses from the extracellular solution to the periplasm through Opr porins (not shown). In the periplasm, glucose can either directly be transported to the cytoplasm, where it is phosphorylated and oxidized to 6-phosphogluconate. Alternatively, glucose can be oxidized by membrane bound periplasmic glucose dehydrogenase (*gcd*) to gluconate. Gluconate is then either directly uptaken to the cytoplasm where it is phosphorylated, or it can

be further oxidized by membrane-bound gluconate dehydrogenase (*gad*) to 2-ketogluconate, which is uptaken and further transformed in the cytoplasm to 6-phosphogluconate.

In this pathway, glucose diffuses through the outer-membrane into the periplasm through Opr porins (19, 21), where it is oxidised by membrane bound dehydrogenase enzymes (*gcd* and *gad*) (21) to gluconate and subsequently to 2-ketogluconate. Gluconate and 2-ketogluconate can therefore accumulate in the periplasm, and then can passively diffuse back in the extracellular solution. For example, Schleissner et al. (18) measured near complete extracellular conversion of glucose to gluconic acid when 10 mM glucose was added to stationary phase *Pseudomonas putida* U. Gluconic and 2-ketogluconic acid have low pKa values [3.6 and 2.4 respectively (22)], and therefore can acidify the extracellular solution. Furthermore, their open structures and carboxylic acid functional groups may allow for higher reactivity and complex formation with mineral surfaces relative to glucose (23, 24).

The acidic and chelating properties of microbially-derived organic acids can promote the weathering of mineral surfaces. For example, the periplasmic oxidation of glucose, and therefore the extracellular accumulation of gluconic acid and 2-ketogluconic acid, has been suggested to be the metabolic basis for efficient phosphate solubilisation by gram-negative bacteria (17, 22, 25). The microbial weathering of aluminosilicates (26-28), in particular bytownite feldspar but also other silicate minerals such as quartz and kaolinite (27), was also observed upon addition of glucose to various bacterial strains grown in the presence of these minerals. For example, Welch et al. (28) measured 70 μM Si in solution after 3 days when 1 mM glucose was added to a biomineral suspension containing 20 g L⁻¹ feldspar and 10⁸ cells mL⁻¹, whereas less than 5 μM Si was measured in solution in a no-glucose control. These studies ascribed the dissolution of the aluminosilicates to the extracellular accumulation of gluconic acid and enhanced dissolution by both proton- and ligand- promoted mechanisms (26-28). In addition to its chelating and acidic properties, gluconic acid can also act as a reductant, that can reductively dissolve Fe(III) and Mn(III, IV) oxides (29, 30) (see **Chapter 3**).

Biogenic Mn oxides, which are precipitated by bacteria and fungi (31-33) and are thus physically close to metabolically active bacteria (31-36), may be particularly susceptible to reductive dissolution when organic acids are secreted by the cells. Therefore, microbial carbon metabolism may exert significant control over the stability of these minerals. Although the reactivity of biogenic MnO₂ has been investigated using laboratory Mn(II)-oxidizing microbial models [for eg:(37-39)], these studies were conducted on stationary

phase suspensions, under conditions of C-starvation. Thus, the impact the metabolic activity of the bacteria can have on the stability and reactivity of the oxides has not been considered to date.

To investigate the extent to which the input of a readily available carbon source such as glucose can lead to dissolution of Mn oxides, we characterised the response of stationary-phase *Pseudomonas putida* GB-1 (*P. putida*) and *P. putida*-MnO₂ suspensions to the addition of glucose. In these suspensions, only 15 % of the total organic carbon provided in the growth medium as glucose, casamino acids and yeast extract at the time of inoculation is left (*personal communication*), and this pool of carbon is expected to be poorly available to the bacteria. The rates of glucose consumption as well as the changes in dissolved oxygen and pH that accompanied the glucose uptake were measured. The accumulation of gluconic acid in solution was also measured in *P. putida* suspensions. We then used chemical equilibria calculations to model the extent of extracellular acidification due to respiration [i.e., CO_{2(aq)}] versus glucose-derived organic acids. In experiments where glucose was added to biomass-MnO₂ assemblages, reductive dissolution of MnO₂ was measured by tracking the aqueous concentration of Mn(II). The implications of these results for the formation and reactivity of MnO₂ particles in natural systems were then discussed.

MATERIAL AND METHODS

All solutions were prepared using ultrapure water (> 18 mΩ cm) and ACS-grade reagents. The Mn(II)-oxidizing bacterium *Pseudomonas putida* GB-1 (*P. putida*) was used as a model organism. All bacterial suspensions were grown under sterile conditions. Once harvested, and unless stated otherwise, experiments were conducted in glass beakers or Erlenmeyer flasks at room temperature, kept open to the atmosphere and loosely covered with parafilm. Synthetic MnO₂ (δ-MnO₂) was obtained by the reaction of stoichiometric amounts of MnCl₂ with KMnO₄ in excess NaOH as described elsewhere (40, 41). The oxide has a layer-type structure with hexagonal sheet symmetry, an average manganese oxidation number (AMON) of 4.03 ± 0.01 , a Mn(III) content determined by pyrophosphate extraction of 2.07 ± 0.52 %, a BET - SSA of 140 m² g⁻¹ and a Na/ Mn ratio of 30 %. After synthesis, the solids were stored as an aqueous suspension (approx. 70 mM) in a Nalgene bottle in the dark at 4°C. Suspensions of δ-MnO₂ were prepared from the stock solution without prior sonication. A summary of all measurements

collected, with details on the conditions and replicates is provided in **Table 4-S1** (see **Supplementary Information - SI**).

Preparation of bacterial suspensions

Suspensions of *P. putida* (referred thereafter as biomass) were obtained from pure cultures grown under sterile conditions in Leptothrix growth medium (35, 42, 43), in the absence of any aqueous Mn(II). Leptothrix medium was prepared by dissolving glucose (1.0 g L⁻¹, 5.5 mM), casamino acids (0.50 g L⁻¹), yeast extract (0.50 g L⁻¹) and HEPES acid (2.38 g L⁻¹, 10 mM) in ultrapure water and autoclaved at 120°C for 20 minutes. After cooling to room temperature and before inoculation, the medium was completed with filter-sterilised CaCl₂ (0.5 mM), MgSO₄ (0.83 mM), FeCl₃ (3.7 μM), CuSO₄ (40 nM), ZnSO₄ (152 nM), CoCl₂ (84 nM), Na₂MoO₄ (54 nM). Cultures were propagated in 125 mL or 50 mL of growth medium, contained in 250 mL or 100 mL Erlenmeyer flasks capped with foam or cellulose stoppers in a table-top shaking incubator in the dark (27°C, 150 RPM). Experimental suspensions were inoculated from stationary-phase suspensions (30h ± 12h) grown in Leptothrix growth medium.

Cells were harvested at stationary phase 120 ± 24h after inoculation. Bacterial suspensions were either used directly in their spent growth medium, or cells were washed and resuspended in an electrolyte. For the latter condition, suspensions were centrifuged (3700 RCF, 10°C, 30 min), the pellets were resuspended in NaCl (10 mM) and equilibrated for 30 min on an end-to-end rotator. The washing procedure was repeated twice, and the washed cells were then re-suspended in inorganic electrolyte solutions described in **Table 1**. Suspensions were equilibrated for 30 min in the incubator (27°C, 150 RPM) before use.

We distinguish two major sets of conditions used in experiments with biomass suspensions: cells were either kept in the spent Leptothrix media, or cells were washed and resuspended in an inorganic electrolyte. Electrolytes 1 - 4 (see **Table 1**) were chosen to approximate the conductivity of spent medium but avoid the influence of HEPES buffer or other undefined organics. For cells resuspended in inorganic electrolytes, all the nutrients beside glucose (and any cations added such as Mg²⁺ and Ca²⁺), in particular N, P and trace metals, have to be obtained from the bacteria reserves, or within extracellular polymeric substances. In the spent media, these nutrients and other carbon sources can be provided by the solution. This distinction limits the comparison between the experiments run in the spent media relative to those collected in electrolytes. Nonetheless, the

assumption is made that the metabolic activity is similar in these different conditions and the results are thus discussed interchangeably. The validity of this assumption is discussed in **Table 4**.

Table 1 Characteristics of the inorganic electrolyte solutions in which the washed bacterial pellets were suspended. The reported ionic concentrations for ions in Electrolyte 3 are the gravimetric ions added to *Leptothrix* growth medium before inoculation. The reported ionic concentrations in Electrolyte 4 are the major ions measured in duplicate by ion chromatography in *Leptothrix* growth medium after 120h of growth of *P. putida* growth, with $Mn_{TOT} = 0$ mM.

Electrolyte	Ions in solution	Description	Conductivity
Electrolyte 1	10 mM NaCl, 570 μ M MgSO ₄ , 480 μ M CaCl ₂	-	~1.4 mS cm ⁻¹ *
Electrolyte 2	10 mM NaCl	-	1.19 mS cm ⁻¹
Electrolyte 3	0.50 mM CaCl ₂ , 0.83 mM MgSO ₄ , 3.7 μ M FeCl ₃ , 40 nM CuSO ₄ , 152 nM ZnSO ₄ , 84 nM CoCl ₂ , 54 nM Na ₂ MoO ₄	Ions from <i>Leptothrix</i>	0.23 mS cm ⁻¹
Electrolyte 4	2.9 mM Cl ⁻ , 530 μ M SO ₄ ²⁻ , 2.14 mM Na ⁺ , 1.1 mM NH ₄ ⁺ , 70 μ M K ⁺ , 550 μ M Mg ²⁺ , 480 μ M Ca ²⁺	Spent <i>Leptothrix</i>	0.70 mS cm ⁻¹

* Estimated as the sum of the conductivity of Electrolytes 2 and 3

Preparation of bacteria-MnO₂ suspensions

Biomass-mineral assemblages were prepared either by mixing biomass with δ -MnO₂ or directly by the biomass, which produces MnO₂ at stationary phase when amended with Mn(II). The former sorbent was prepared by adding an aliquot of a δ -MnO₂ stock solution (~ 70 mM) to a washed biomass suspension (120 \pm 12h) resuspended in NaCl (10 mM). The resulting suspensions were covered with a cellulose stopper and equilibrated for 30 min in a table-top incubator before use (27°C, 150 RPM). Biogenic MnO₂ suspensions were prepared through the same protocol as biomass suspensions, but 1.0 mM MnCl₂ was added to the *Leptothrix* growth medium before inoculation. The inoculum was sampled from a *P. putida* culture grown in *Leptothrix* growth medium containing 1.0 mM MnCl₂ for 30 \pm 10h. After 5 days of incubation, 90 – 100 % of the aqueous Mn(II)_{aq} provided was oxidised to MnO_{2(s)}, yielding biogenic MnO₂. At this time (120 \pm 24h), biogenic MnO₂ suspensions were harvested and measurements were either collected directly in the spent *Leptothrix* medium or alternatively biominerals suspensions were washed and resuspended in an inorganic electrolyte following the protocol described above.

Glucose, gluconate and 2-keto-gluconate consumption and production

Suspensions of biomass and biogenic MnO₂ (120 ± 12h), prepared in 100 or 250 mL Erlenmeyer flasks and kept in *Leptothrix* spent medium, were spiked with an aliquot of a glucose stock solution (500 mM) to yield an initial glucose concentration of 5.5 mM. Suspensions were kept in the table-top incubator (27°C, 150 RPM) in between sampling and throughout the experiment. Aliquots of the suspensions were collected at different time-points for up to 24h after the glucose addition and filtered immediately (0.20 µm pore size, polyethersulfone) for chemical analysis. Gluconate concentrations were measured in separate duplicate biomass suspensions kept in *Leptothrix* spent medium and spiked with an aliquot of a stock solution of gluconate (500 mM) to yield an initial 5.5 mM gluconate concentration. Aliquots of the suspensions were collected at different time-points over 30 min and filtered immediately (0.20 µm pore size, polyethersulfone).

Glucose concentrations were measured using a colorimetric assay (GAGO-20, Sigma-Aldrich), following the protocols described by the manufacturers and using a UV-Vis spectrophotometer (Shimadzu UV-2600). Briefly, filtered aliquots were reacted for 30 min in a water bath (37 ± 2°C) with a colorimetric reagent containing glucose oxidase, reduced o-dianisidine (colorless) and peroxidase. The oxidation of glucose by oxidases yielded gluconic acid and H₂O₂. The later reacts with reduced o-dianisidine in the presence of peroxidase to form oxidised o-dianisidine, which has a brown color. The reaction was quenched by the addition of 12 N H₂SO₄, which stabilises o-dianisidine, yielding a pink color. Glucose concentration were determined from the absorbance of the o-dianisidine formed, measured against a reagent blank at 540 nm using 1 cm path-length disposable plastic cuvettes. The calibration curve was obtained from 4 standards following the protocol provided by the manufacturer. The calibration curve was linear from 0.00 – 0.40 mM glucose ($\epsilon = 2.87 \text{ mM}^{-1} \text{ cm}^{-1}$, $R^2 = 0.99$) with an error of < 5 % up to 0.40 mM glucose. Blank samples (n = 6) yielded a concentration of 0.01 ± 0.01 mM glucose and 5.5 mM check standards (n = 8) yielded a concentration of 5.6 ± 0.2 mM. The absorbance of all samples was measured against a reagent blank (ie: reagent not containing any glucose).

Gluconate and 2-keto-gluconate were measured using an enzymatic colorimetric assay (d-Gluconate/ d-Glucono- δ -lactone, Megazymes) following the protocol described by the manufacturers and using a UV-Vis spectrophotometer (Shimadzu UV-2600). Briefly, filtered samples were mixed with reagents containing nicotinamide-adenine dinucleotide

phosphate (NADP^+), adenosine-5'-triphosphate (ATP) and 6-phosphogluconate dehydrogenase in a buffered solution (pH 7.6) containing sodium azide (0.02 % w/v) for 5 minutes. The absorbance of the solution (A1) was measured at 340 nm. The addition of gluconate kinase (GCK) to the solution then catalysed the phosphorylation of d-gluconic acid into d-gluconate-6-phosphate in the presence of ATP. In the presence of NADP^+ , d-gluconate-6-phosphate is decarboxylated by 6-phosphogluconate dehydrogenase to form ribulose-5-phosphate and reduced nicotinamide-adenine dinucleotide phosphate (NADPH). After 6 min of reaction, the absorbance was measured at 340 nm (A2). Considering that the initial gluconic acid concentration was stoichiometric with the quantity of NADPH formed, the formation of the latter was tracked by changes in the absorbance at 340 nm (A2-A1). Concentrations of keto-gluconic acids were measured in some samples using the same protocol, but first hydrolysing the solutions to transform keto-gluconic acid to gluconic acid, and determining the concentration of the former from the difference between the gluconic acid concentration in hydrolysed and non-hydrolysed samples. The hydrolysis was carried by increasing the pH of the filtered solution to about 11 with 2 M NaOH for 10 min in a water bath at 25°C. The calibration was obtained from 3 standards and was linear from 0.0 – 0.5 g L⁻¹ (0.0 – 2.4 mM) gluconate ($R^2 = 0.99$, $\epsilon = 0.30 \text{ mM}^{-1} \text{ cm}^{-1}$) with an associated error < 3 %. Blank samples (n = 4) yielded a concentration of $0.01 \pm 0.02 \text{ mM}$ gluconate. A control run in duplicate in which glucose (5.5 mM) was spiked into the spent growth medium, where removal of biomass was achieved by centrifugation (3700 RCF, 10°C, 30 min) yielded a concentration of $0.00 \pm 0.00 \text{ mM}$ gluconate after 2h, demonstrating that spontaneous conversion of glucose to gluconate was not observed in the absence of bacteria.

Glucose-induced changes in dissolved oxygen and pH

Glucose induced changes in dissolved oxygen

Separate suspensions of biomass ($120 \pm 24\text{h}$) kept in the *Leptothrix* spent medium were prepared in 250 mL Erlenmeyer and fitted with a galvanic dissolved oxygen sensor (Oxi-Cal, WTW). Suspensions were spiked with an aliquot of a stock solution of glucose (500 mM), to yield a 5.5 mM initial glucose concentration. The dissolved oxygen concentration of the suspensions was then measured over 37h. For the first 5 - 7h, during which the recording frequency was particularly high, the flask was gently shaken on the table-top shaker (~100 RPM) at room temperature and the sensor was left in the flask in between measurements. At longer times, the sensor was removed in between measure-

ments and the flasks were put in a table-top incubator (150 RPM, 27°C) in between measurements. We assume that the stirring of the flasks in the table-top shaker and in the incubator was sufficiently similar to minimize differences in the rate of O₂ replenishment from the overlaying atmosphere.

Glucose-induced acidification in different electrolytes

Separate biomass suspensions (120 ± 12h), left in *Leptothrix* spent medium, were prepared in 250 mL flasks, fitted with a pH electrode and a Teflon-coated magnetic stir bar cleaned with ethanol (70 %). The pH of the suspensions was measured for about 10 min to establish an initial baseline pH. The suspensions were then spiked an aliquot of a stock solution of glucose (500 mM), to yield an 5.5 mM initial glucose concentration. The pH of the suspensions was measured automatically (± 0.1 pH units) over 40h using pH stats (Metrohm Titrino 718 and Titrando 888). The pH was measured every 60s during the first 4h, then every 180s for the next 36h. The pH was monitored with a pH electrode (Metrohm) calibrated using 3 standard buffers (pH 4, 7 and 10) at the start of the experiment and after 20h of measurement, when it was removed from the flasks and washed with distilled water to prevent passivation of the electrode from the build-up of biofilm on the electrode surface.

Leptothrix growth medium contains 10 mM of HEPES, a Good's buffer with a pKa of 7.5 (44) which has a strong influence on the pH. The pH measurements were thus repeated for washed biomass suspensions (120 ± 24h), poured in 100 mL beakers, suspended in inorganic electrolytes (Electrolyte 2-3, see **Table 1**). The pH was measured automatically every 60 to 300s for the first three hours following glucose addition, after which it was measured manually over the next 45h (Titrino 718, Metrohm).

Additional experiments were conducted to measure the glucose-induced acidification of bacterial suspensions as a function of the concentration of glucose added. Separate washed biomass suspensions (120 ± 12h), suspended in Electrolyte 3 were prepared in 100 mL beakers, fitted with a pH electrode and a Teflon-coated magnetic stir bar cleaned with ethanol (70 %). An aliquot of a stock solutions (250 or 500 mM) was spiked in the suspensions to yield initial glucose concentrations of 0.01, 0.10, 0.55, 1.0, 5.5 mM. The pH of the suspensions was measured automatically over 20h using pH stats (Metrohm Titrino 718 and Titrando 888).

Calculation of changes in dissolved oxygen and pH

Glucose metabolism can acidify the extracellular solution by two main processes. On one hand, mineralization of glucose to CO₂ leads to the accumulation of carbonic acid in solution. On the other hand, organic acids, either metabolic intermediates or secondary metabolites, can accumulate in the extracellular solution. To constrain the origin of acidification measured upon spiking glucose to *P. putida* suspensions, we used chemical speciation calculations to model the extent of extracellular acidification due to respiration [i.e., CO_{2(aq)}] versus glucose-derived organic acids.

CASE 1: Acidification due to CO₂

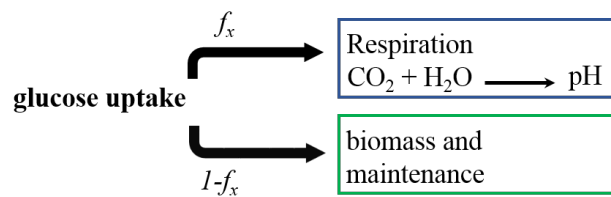


Figure 2 Schematic showing the fraction of glucose invested in respiration (f_x) and biomass and maintenance ($1-f_x$).

Figure 2 shows the partitioning in the use of glucose by bacterial cells. Some of the carbon substrate is fully oxidised to CO₂ and gives its electron to a terminal electron acceptor (**Eq. 1**) to harvest energy. The rest of the carbon is used for biomass synthesis and maintenance (**Eq. 2**)(45). The fraction of C invested in either pathway (f_x and $1-f_x$, see **Figure 2**) depends, amongst other things, on the nature of the bacteria, the growth substrate and the nutrient availability (45, 46).



The concentration of CO₂ released in solution is therefore directly related both to the O₂ and the glucose consumed (**Eq. 3-4**).

$$\text{CO}_2_{\text{produced}} = \text{O}_2_{\text{consumed}} \quad (\text{Eq. 3})$$

$$\text{CO}_2_{\text{produced}} = 6 f_x \text{ glucose}_{\text{consumed}} \quad (\text{Eq. 4})$$

The use of **Eq. 3** to determine CO₂ produced was not feasible due to lack of measurements on the rate of O₂ resupply (which depends on its volume and contact surface area with the overlaying atmosphere, at the experimental stirring rate and temperature). We instead used the measured glucose consumption to determine the CO₂

produced. The use of **Eq. 4**, however requires a value of f_x . This fraction f_x was calculated by combining **Eq. (3-4)**, from linear regression of O₂ consumed against glucose consumed, in the first minutes following the glucose spike. In this short time-range ($t < 5$ min), O₂ is largely available for respiration and O₂ re-supply with the atmosphere can be considered negligible. A sensitivity test was performed on f_x and the calculated f_x was compared to values reported in the literature for *P. putida* grown with glucose (46).

The speciation of CO₂ in solution is summarized in **Table 2**. Assuming that no organic acids are released, and that the pH is thus only affected by the release of CO₂ to solution, **Eq. (5-7)** can be combined to calculate the solution pH according to **Eq. 8**. This calculation assumes that the system presented no buffering capacity and that the degassing of CO₂ to the atmosphere was slow relative to the CO₂ production. These assumptions may lead to overestimated accumulation of CO₂ in solution and thus modelling greater acidification. However this approach yields the maximum acidification that can be due to the accumulation of carbonic acid.

Table 2 Carbonic acid speciation.

Chemical speciation	$\text{CO}_{2(\text{aq})} + \text{H}_2\text{O} \rightleftharpoons \text{H}_2\text{CO}_3$	(Eq. 5)	
	with $\text{H}_2\text{CO}_3^* = \text{CO}_{2(\text{aq})} + \text{H}_2\text{CO}_3$		
	$\text{H}_2\text{CO}_3^* \rightleftharpoons \text{HCO}_3^- + \text{H}^+ \quad K_1 = 4.5 \times 10^{-7}$	(5.1)	
	$\text{HCO}_3^- \rightleftharpoons \text{CO}_3^{2-} + \text{H}^+ \quad K_2 = 4.7 \times 10^{-11}$	(5.2)	
Mass balance	$\text{CO}_{2_ \text{produced}} = [\text{H}_2\text{CO}_3^*] + [\text{HCO}_3^-] + [\text{CO}_3^{2-}]$	(Eq. 6)	At pH < 6
	$\text{CO}_{2_ \text{produced}} \approx [\text{H}_2\text{CO}_3^*] + [\text{HCO}_3^-]$	(6.1)	$[\text{CO}_3^{2-}] \approx 0$
Charge balance	$[\text{H}^+] = [\text{HCO}_3^-] + 2[\text{CO}_3^{2-}] + [\text{OH}^-]$	(Eq. 7)	At pH < 6
	$[\text{H}^+] \approx [\text{HCO}_3^-]$	(7.1)	$[\text{OH}^-] \approx 0$
(5.1) + (6.1)	$\text{CO}_{2_ \text{produced}} \approx \frac{[\text{H}^+][\text{HCO}_3^-]}{K_1} + [\text{HCO}_3^-]$	(6.2)	
(6.2) + (7.1)	$[\text{H}^+]^2 + K_1[\text{H}^+] - K_1 \text{CO}_{2_ \text{produced}} = 0$ One natural solution: $[\text{H}^+] = \frac{-K_1 + \sqrt{K_1^2 + 4K_1 \text{CO}_{2_ \text{produced}}}}{2}$	(Eq. 8)	Assuming CO ₂ degassing ≈ 0

CASE 2: Acidification due to organic acids

The acidification of the extracellular solution resulting from the accumulation of an organic acid in solution will depend on the concentration of the acid and on its pKa. The

speciation in solution of a generic organic acid (HA) is summarized in **Table 3**. Combining **Eq. (9-11)** yields **Eq. 12**, which expresses the protons released in solution as a function of the concentration of organic acids. **Eq. 12** was used to calculate a pH based on measured concentrations of gluconic acid. It was also used to calculate the concentration of organic acid (c_{HA}) required to achieve the measured extent of acidification.

Table 3 Speciation of generic carboxylic acids.

Chemical speciation	$\text{HA} \rightleftharpoons \text{A}^- + \text{H}^+ \quad K_a$	(Eq. 9)
Mass balance	$c_{\text{HA}} = \text{HA} + \text{A}^-$	(Eq. 10)
Charge balance	$[\text{H}^+] = [\text{A}^-]$	(Eq. 11)
(Eq. 9) + (Eq.10) + (Eq.11)	$[\text{H}^+]^2 + K_a [\text{H}^+] - K_a c_{\text{HA}} = 0$ One natural solution: $[\text{H}^+] = \frac{-K_1 + \sqrt{K_1^2 + 4K_1 c_{\text{HA}}}}{2}$ $\Leftrightarrow c_{\text{HA}} = \frac{[\text{H}^+]^2}{K_a} + [\text{H}^+]$	(Eq. 12)

Glucose-induced reductive dissolution of MnO_2

Suspensions of synthetic bio-mineral assemblages and biogenic MnO_2 suspended in electrolyte 1 (see **Table 1**) were poured in 100 mL beakers. Suspensions were spiked an aliquot of stock glucose solutions (250 and 500 mM) to yield initial concentrations of 0.01, 0.55 and 5.5 mM. Suspensions were kept in the incubator in the dark throughout the experiment and in between sampling (150 RPM, 27°C). Aliquots of the suspensions were collected at different time-points. Aqueous Mn(II) was measured by ICP-OES in filtered (0.20 μm pore size, polyethersulfone), diluted and acidified (50 μL HNO_3 66% in 5 mL samples). Initial MnO_2 concentrations were determined by sampling 1 mL of the suspensions and acid digesting the solids using concentrated nitric acid (50 μL , 66 %) and excess oxalic acid (50 μL , 1 M), and diluting the resulting solution with ultrapure water. Manganese concentrations were determined by ICP-OES (Perkin-Elmer Optima 8300) at three emission lines and using Sc as an internal standard.

Control experiments were performed to test whether in the absence of glucose, the biomass provided any reducing equivalents, either from the reducing capacity of the organic moieties displayed or through metabolites secreted as a response to the extracellular acidification. Separate suspensions of washed biomass ($120 \pm 12\text{h}$) were poured in 100 mL Erlenmeyer flasks and fitted with a Teflon-coated magnetic stir bar

cleaned with ethanol (70 %). Suspensions were then spiked an aliquot of a δ -MnO₂ stock suspension to yield a bio-mineral suspension containing $716 \pm 108 \mu\text{M}$ MnO₂. The pH of the suspension was immediately pre-adjusted to \sim pH 5 by the addition of HCl (250 mM). The pH was then lowered to $\text{pH } 4.5 \pm (0.1 \text{ pH unit})$ by use of a pH stat (Metrohm Titrino 718 or Titrando 888) through automatic addition of HCl (24 or 50 mM). The pH was monitored with a pH electrode (Metrohm) calibrated using 3 standard buffers (pH 4, 7 and 10). Aliquots of the suspensions were collected at different time-points and immediately filtered (0.20 μm pore size, polyethersulfone). Aqueous Mn(II) and the initial MnO₂ concentration were measured by ICP-OES as described above.

Table 4: Summary and discussion of the assumptions made in this study

The interpretations of the results collected in this study are based on a number of assumptions that are listed here and discussed to evaluate the strength of the conclusions reached. The weakness of each assumption is graded with stars (★★★= poor assumption, ★= ok assumption).

Some of the results described in the following section can balance the importance of these assumptions. Since results have not yet been described, comments based on results are reported in *black italic font*.

Assumptions made:

*1. We assume that the rate of glucose uptake by *P. putida* is independent of the concentration of glucose provided. ★★★*

The modelling of the CO₂-induced acidification, calculated for different concentrations of glucose, relies heavily on this assumption. This is a poor assumption, as the first order kinetics that describes glucose uptake when biomass suspensions in spent growth medium are spiked with 5.5 mM glucose demonstrates that the glucose uptake rate is indeed dependent on concentration.

We expect the rate of glucose uptake to decrease at lower concentrations, which means the contribution of CO₂ might be further overestimated for lower initial concentration of glucose. *Overall, the conclusion reached that the accumulation of CO₂ is not the major source of acidification remains valid.*

*2. We assume that the rate of glucose uptake of *P. putida* in inorganic electrolytes is similar to that measured in the spent media. ★★*

This assumption is likely problematic because the concentrations of nutrients available for the cells when left in the spent growth medium and when washed and resuspended in a minimal electrolyte are likely to be very different. Because they were grown in a nutrient-rich growth media (*Leptothrix*), cells may however have reserves of nutrients, intracellularly or within the extracellular polymeric substances, especially in the first hour of the experiment.

*3. We assume that the metabolic activity of *P. putida* is similar in all inorganic electrolytes. ★*

We use interchangeably the data collected from washed suspensions, irrespective of the electrolyte solution used. We assumed that these electrolytes were however sufficiently similar to elicit similar response relative to the cells kept in the spent media. *The similarity in the extent of acidification measured in different electrolytes (Electrolyte 2-3, see **Figure 4**) supports the assumption that the cells respond similarly to the glucose addition in the different media.*

4. We assume no delay between the time of glucose uptake and mineralization ★

This assumption is problematic, as demonstrated by the accumulation of gluconic acid in solution during the first 30 min. However, the f_x value obtained was consistent with that reported in the literature. Furthermore, we performed a sensitivity analysis which confirmed that the value of f_x was not a dominant factor in our model.

5. We assume that the factor f_x is the same in the spent medium than in the electrolyte suspensions ★

The value calculated was in the expected range (45, 46). Furthermore, we performed a sensitivity analysis which confirmed that the value of f_x was not a dominant factor in our model.

6. We assume that CO_2 production is rapid relative to CO_2 degassing ★

The rapid rate of dissolved oxygen depletion following the glucose spike suggest rapid CO_2 production. Not accounting for the degassing of CO_2 gives an overestimation of the accumulation of carbonic acid but allows to determine the maximum acidification that could be ascribed to respiration.

7. We use the concentrations of glucose and gluconate measured in biomass suspensions and assume that these measurements represent the evolution of these parameters in biomineral suspensions (δ - MnO_2 -biomass and biogenic MnO_2) ★

The presence of Mn, as $Mn(II)_{aq}$ or Mn solids, can affect the cells in a number of ways. For example:

- The cell viability may be different.
- Sorption of nutrients on the mineral surface may affect their accessibility by the cells.
- The presence of mineral particles may facilitate gas and mass transfer through the suspension, as the aggregation of organic molecules from the biofilm around mineral particles can reduce the viscosity of the suspension by segregating organic molecules away from the solution.

All these factors may affect the rate of uptake of glucose, and possibly also the value fraction of glucose uptaken that is invested in respiration. *However, the pH trace measured in biogenic MnO_2 suspensions in spent growth medium spiked with glucose (see **Figure 4-S5**) was sufficiently similar to those measured in the biomass suspension, to justify discussing the impact of glucose metabolism on MnO_2 stability based on the data collected for the latter suspensions.*

RESULTS

Glucose consumption and changes in solution pH and dissolved oxygen

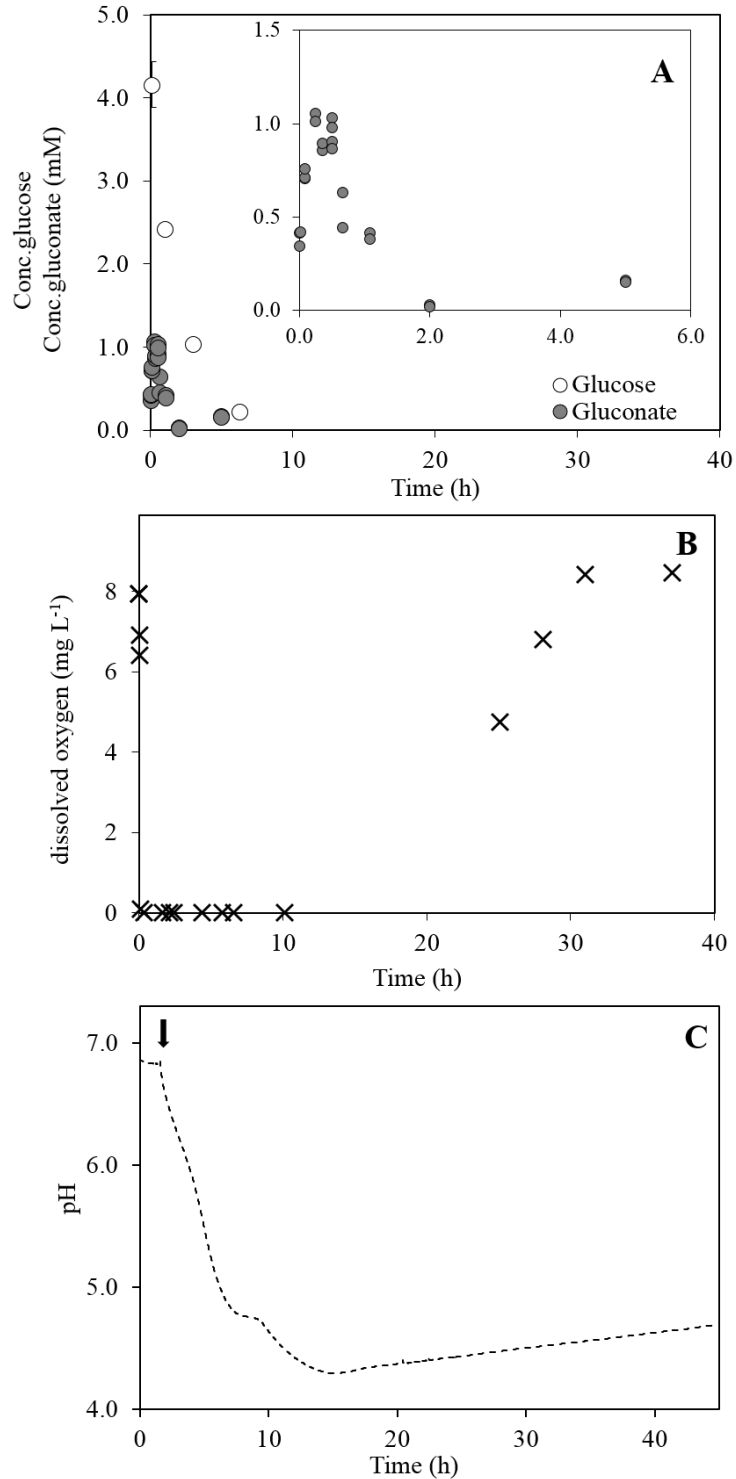


Figure 3 Changes in extracellular conditions following the addition of glucose (5.5 mM initial concentration) to biomass suspensions (kept in spent growth media) **A)** Concentrations of glucose (empty circles) and gluconate (filled circles). The inset focus on the gluconate measurements. **B)** Changes in dissolved oxygen concentrations **C)** Change in pH.

Figure 3A and **Table 4-A3** shows the concentrations of glucose measured in solution as a function of time t (c_{glucose_t}) after the addition of 5.5 mM glucose to biomass suspensions ($\sim 0.40 \text{ g L}^{-1}$) kept in spent growth medium. Glucose concentrations decreased exponentially, with less than 0.2 mM glucose measured in solution 6h30 after the glucose spike. A plot of $\ln(c_{\text{glucose}_t})$ as a function of t (see **Figure 4-S1**; $R^2 = 0.99$) showed that glucose consumption rates followed the 1st order kinetics described by **Eq. 13**. During the first hour, the cells consumed glucose at a rate of $4.8 \text{ mmol h}^{-1} \text{ g}^{-1}$, which is consistent with reported glucose uptake rate for *Pseudomonas putida* and *fluorescens* [$4.71 \pm 0.30 \text{ mmol g}^{-1} \text{ h}^{-1}$ (46); $4.79 \pm 0.39 \text{ mmol g}^{-1} \text{ h}^{-1}$ (19); $4.81 \pm 0.17 \text{ mmol g}^{-1} \text{ h}^{-1}$ (20)]. In our study, rate of glucose uptake however slowed down at longer times, as it showed first order kinetics and was thus dependent on the glucose concentration. Limitation of O_2 supply or nutrient (e.g., N) may also contribute to slow down the rate of glucose uptake.

$$c_{\text{glucose}_t} = c_{\text{glucose}_{\text{initial}}} e^{-0.47 t} \quad \text{Eq. 13}$$

Glucose consumption was accompanied by the appearance and disappearance of gluconate in solution (see **Figure 3A** and **Table 4-A4**). We measured $0.95 \pm 0.08 \text{ mM}$ of gluconate in solution $24 \pm 7 \text{ min}$ ($n = 8$) after the pulse of glucose. After 1h, we measured $0.40 \pm 0.02 \text{ mM}$ gluconate ($n = 2$), $0.02 \pm 0.01 \text{ mM}$ ($n = 2$) after 2h, and $0.17 \pm 0.01 \text{ mM}$ after 5h. No measurable keto-gluconate ($< 0.03 \text{ mM}$) was detected 15 min and 5h after glucose addition.

Despite the recognised importance of the 2-ketogluconate intermediate for glucose metabolism by *P. putida* (15, 17, 21, 22, 47), studies report limited extracellular accumulation of 2-ketogluconate. For example, del Castillo et al. (19) reported 70 % more gluconate than 2-ketogluconate measured in solution after spiking *P. putida* suspensions with glucose. The limited extracellular accumulation of 2-ketogluconate either suggests low rate of activity of the *gad* enzyme (see **Figure 1**), or faster rate of 2-ketogluconate uptake relative to that of gluconate, and therefore limited diffusion of the former to the extracellular solution. The measured rate of gluconate uptake when C-limited biomass was spiked with an aliquot of gluconate ($\sim 4.5 \text{ mM}$) was $9.5 \text{ mmol h}^{-1} \text{ g}^{-1}$ (see **Table 4-A5**), which is twice as large as glucose consumption rate and much larger than gluconate uptake following glucose addition to the cultures (-0.55 mM h^{-1} , $R^2 = 0.91$, $n = 14$).

The dissolved oxygen concentrations measured over 40h in biomass suspensions kept in their spent growth medium and spiked with 5.5 mM glucose are shown in **Figure 3B**

and in **Table 4-A6**. The initial dissolved oxygen concentration was close to 8 mg L⁻¹ before the glucose addition. After 5 minutes, the O₂ concentration decreased to < 1 mg L⁻¹. It remained close to 0 mg L⁻¹ for over 10h, indicating that the O₂ consumption rate was equal to the O₂ re-supply rate from the overlaying atmosphere. After ~ 17h, the O₂ concentration gradually equilibrated with the atmosphere, at a rate of 0.62 mg dissolved oxygen h⁻¹ L⁻¹ (0.02 mM h⁻¹) ($R^2 = 0.99$).

The pH measured over 40h in biomass suspensions kept in their spent growth medium and spiked with 5.5 mM glucose are shown in **Figure 3C**. The initial pH of the suspension was close to 6.8. A rapid linear decrease in pH was measured during the first 9h hours following glucose addition ($- 0.3 \text{ pH h}^{-1}$, $R^2 = 0.97$) reaching a pH of 4.8. The pH then remained constant for 2 hours, and the dropped linearly (-0.07 pH h^{-1} , $R^2 = 0.95$) to reach a minimum value of 4.3 15h after the glucose addition, with coincides with the time at which the dissolve oxygen concentration started to increase. The pH then steadily increased back to 4.7 (0.01 pH h^{-1} , $R^2 = 0.998$), however the system did not recover its initial pH of 6.8 over the timescale of the measurement.

Extracellular acidification of biomass suspended in defined electrolytes

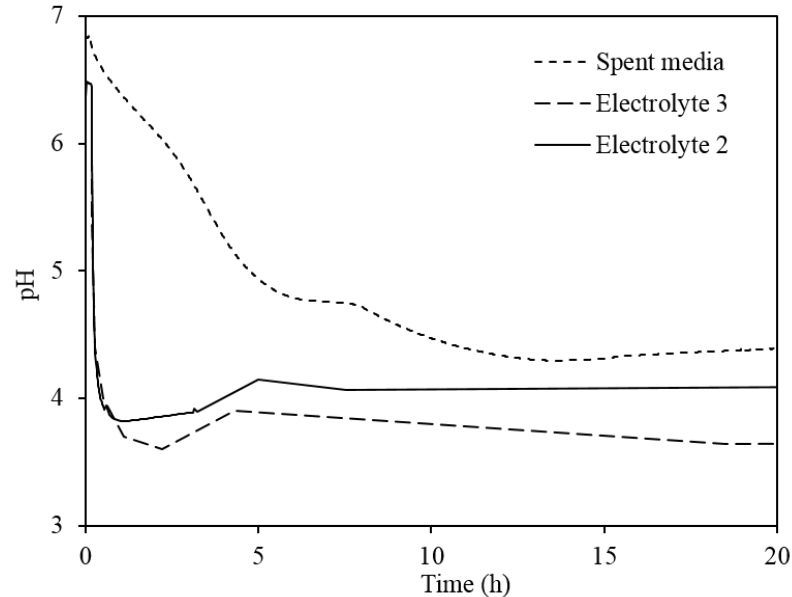


Figure 4 Acidification of biomass suspensions spiked an aliquot of glucose (5.5 mM initial glucose concentration) directly in spent growth medium or washed and resuspended in defined inorganic electrolytes.

Figure 4 shows the pH measured over 24h following the addition of glucose (5.5 mM) to biomass suspensions suspended inorganic electrolyte (Electrolyte 2-3), alongside the pH trace measured for biomass in the spent medium. While the acidification observed in

the spent medium was progressive, reaching a minimum of 4.3 in about 15h, the acidification measured in the washed suspensions was significantly faster, reaching a minimum pH of 4.0 ± 0.1 30 min after the glucose addition. This difference is either related to differences in the C-metabolism or of the initial buffering capacity of the two suspensions and is further discussed below.

Extracellular acidification as function of glucose added

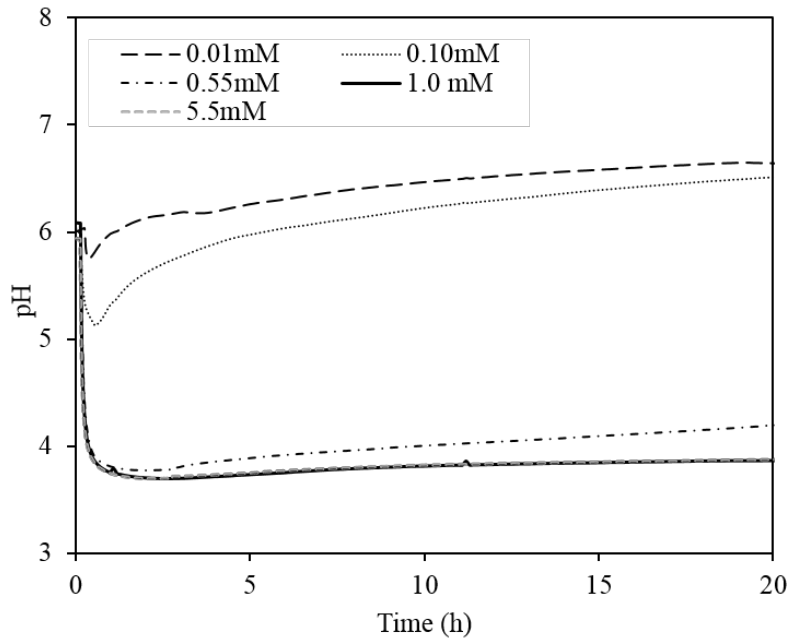


Figure 5 Changes in pH measured after the addition of glucose (0.01-5.5 mM initial concentrations) of glucose to washed biomass-only suspensions resuspended in electrolyte 2 (10 mM NaCl).

The measured acidification of biomass suspended in an inorganic electrolyte (Electrolyte 2) spiked with glucose concentrations in the range of 0.01 – 5.50 mM are reported in **Figure 5**. From 0.0 to 1.0 mM, the extent of acidification observed depended on the concentration of glucose provided. No difference in the pH traces was however observed following the addition of 1.0 and 5.5 mM glucose. For the addition of 0.01 and 0.10 mM of glucose, the pH reached minima of 5.7 and 5.2, in 8 min and 42 min respectively, before gradually increasing back to pH > 6 20h after the glucose addition. For the addition of 0.55 mM to 5.5 mM, the pH reached a minimum of about 3.7 1h20 after the glucose addition. For the addition of 0.55 mM, the pH of the system started to increase but was unable to recover to the initial pH over 20h. For the addition of 1.0 and 5.5 mM, the pH remained at the minimum value over the timescale of the measurement

Modelling the acidification induced by glucose metabolism

A plot of the concentrations of O₂ consumed at a time *t* against that of glucose, for O₂ concentration ≥ 0.10 mg L⁻¹ (≥ 0.003 mM), is plotted in **Figure 4-S2**. It shows a slope of 2.17 ± 0.58 (95 % confidence interval). When accounting for the stoichiometry of the mineralization of glucose, we obtain a value for *f_x* of 0.36 ± 0.10. This approach to determine *f_x* assumes that there is no time delay between the time of glucose uptake and that of complete glucose mineralization. The transient accumulation of gluconic acid in solution, which represents ~ 20 % of the total glucose, demonstrates that this assumption is flawed. However, the value of 0.36 is consistent with the fractions of glucose uptaken lost as CO₂ reported by Sasnow et al. (46) for *Pseudomonas putida* KT2240 for Fe-depleted and Fe-repleted cells (0.31 ± 0.02 and 0.38 ± 0.07 respectively), even when the former were significantly limited in their biomass growth.

To determine the maximum acidification that can be expected solely based on the accumulation of carbonic acid in solution, we used the value of *f_x*, and the equation describing glucose consumption (**Eq. 13**) to calculate the CO₂ produced as a function of time after glucose addition (see **Eq. 14**).

$$\text{CO}_2 \text{ produced} = 6f_x \times c_{\text{glucose_consumed_t}} = 6f_x \times (c_{\text{glucose_initial}} - c_{\text{initial}} e^{-0.47 t}) \quad \text{Eq. 14}$$

Within the assumptions made in this model, **Figure S4** shows the calculated pH as a function of time based for initial glucose concentrations ranging from 0.01 – 5.5 mM, alongside the pH traces measured. The calculated pH traces under-estimated the extent of acidification for glucose concentrations above 0.1 mM, confirming that the extracellular acidification cannot be solely explained by accumulation of carbonic acid in the extracellular solution. Because of the assumptions associated to the determination of *f_x*, we performed a sensitivity test on the *f_x* value by varying its value within the range of the confidence interval (± 0.10). This test showed that the modelled acidification due to CO₂ efflux was not strongly sensitive to the *f_x* value (see **Figure 4-S3**). For the 5.5 mM initial glucose concentration, the modelled acidification is plotted in **Figure 6B**. We then used the solution from **Eq. 7**, to calculate the pH that the measured concentration of gluconic acid could lead to in unbuffered suspensions (see **Figure 6D**). The data reported in **Figure 6** confirms that the extracellular accumulation of gluconic acid is sufficient to explain the observed acidification.

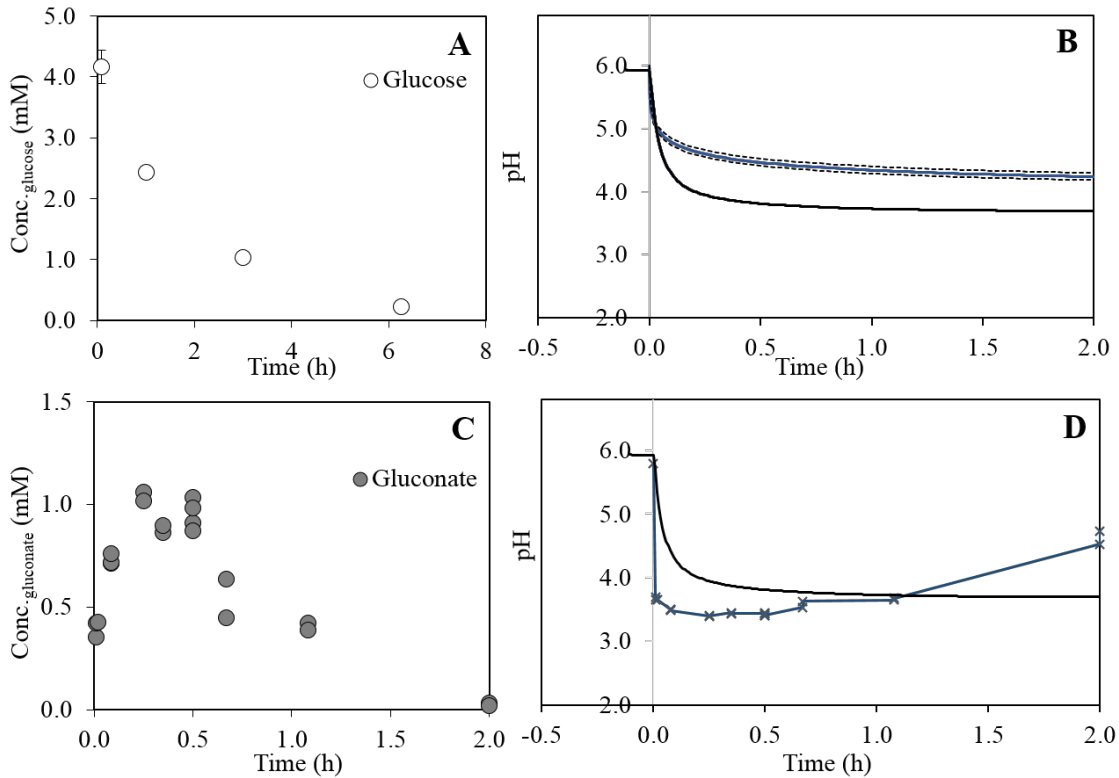


Figure 6 Sources of extracellular acidification, when biomass suspensions were spiked with 5.5 mM glucose. **A-B)** A fraction of glucose consumed is invested in respiration, which leads to the accumulation of carbonic acid, which is modelled and represented in blue. The modelled acidification is not sufficient to explain the measured acidification (black line). The dashed lines represent the values obtained when performing a sensitivity test on f_x (0.36 ± 0.10). **C-D)** Gluconic acid is measured in solution. The calculated associated acidification (blue line) is sufficient to explain measured pH trace (black line).

Since we cannot exclude the secretion of other acids, and because gluconate was quickly consumed from the extracellular solution, **Figure 7** shows the concentration of generic organic acids with pKa of 2.4, 3.6 or 4.5, calculated with **Eq. 12**, needed in solution to match the pH trace measured upon the addition of 5.5 mM of glucose to the biomass suspension. If the accumulation of H_2CO_3 is accounted for, the concentrations of acids required is slightly reduced. The error bars therefore represent the range of concentration of acids required, with the lower limit accounting for the maximal calculated contribution from the accumulation of H_2CO_3 . For organic acids with pKa of 4.5, the accumulation of up to 1484 μM would be necessary to explain the pH trace measured 2h after the addition of glucose. When considering the putative contribution of H_2CO_3 , this concentration falls to 804 μM . For lower pKa values, the contribution H_2CO_3 can have becomes less important. Only 365 μM of organic acids with pKa of 3.6 and 212 μM of organic acids with pKa of 2.4 would be required to explain the measured pH trace. When the contribution of glucose mineralization is included, these concentrations decrease to 230 μM and 151 μM respectively.

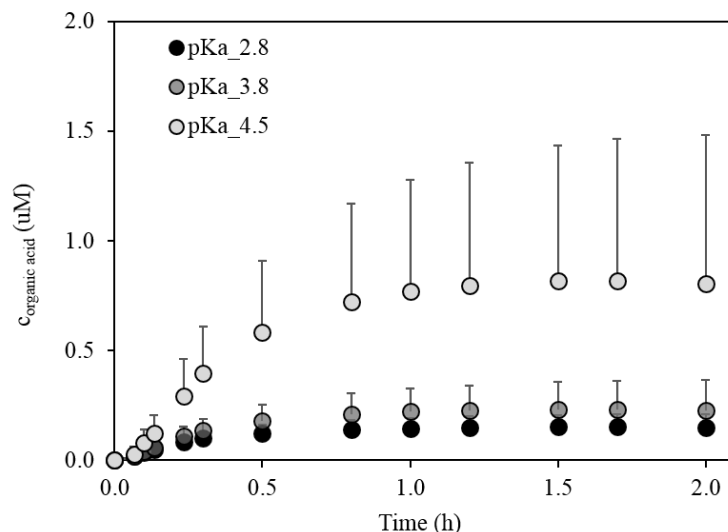


Figure 7 Calculated concentration of organic acids with pKa of 2.8, 3.8 and 4.5 required to explain the measured extracellular acidification in washed biomass suspensions spiked with glucose (5.5 mM initial concentration). The lower end of the error bar of each data point shows the concentrations of acids required when the calculated contribution of H₂CO₃ accumulation to acidification is included.

Impact of glucose metabolism on MnO₂ stability

Glucose addition to biomass-MnO₂ suspensions

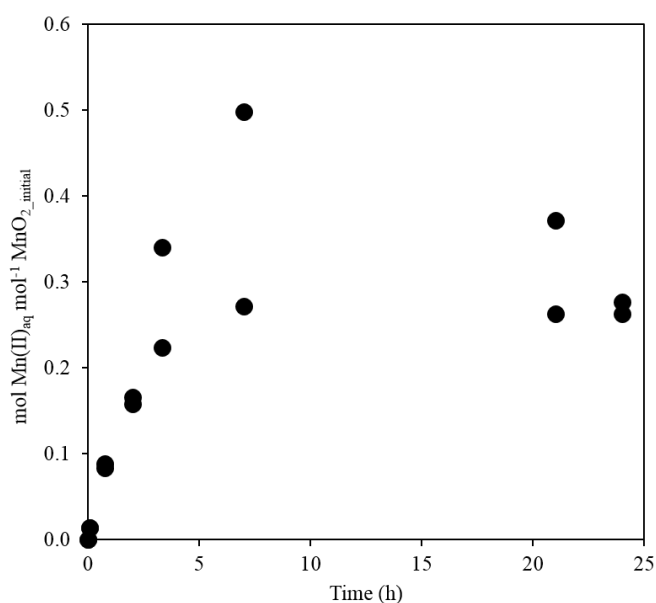


Figure 8 Release of Mn(II) as a function of time when a synthetic bio-mineral assemble of biomass and δ -MnO₂ was spiked with glucose (5.5 mM initial concentration).

The net release of Mn(II) as a function of time when composites of δ -MnO₂-biomass in electrolyte were spiked with glucose is reported in **Figure 8** and in **Table 4-A7**. Up to 0.38 aqueous Mn(II) mol⁻¹ MnO₂_i was measured in solution 7h after the addition of glucose. The initial rates of net release of aqueous Mn(II), calculated from the data collected in the first three hours, was 46 μ M h⁻¹. This rate is lower than that measured for

dissolution of δ -MnO₂ in glucose solution ($78 \mu\text{M h}^{-1}$ for 5.5: 1.3 mM ratio for glucose: MnO₂) at pH 4.5 (see **Chapter 2**). The release of Mn(II)_{aq} was balanced at longer times by the removal of Mn(II) from solution. Only $0.28 \text{ aqueous Mn(II) mol}^{-1} \text{ MnO}_{2_i}$ was measured after 24h. At pH 4.5, Mn(II) adsorption of MnO₂ is minimal (48), thus enzymatic re-oxidation of Mn(II) is the only reasonable explanation for the removal of Mn(II) at longer timescales.

The release of aqueous Mn(II) when a composite of δ -MnO₂-biomass was acidified to pH 4.5 over 24h is reported in **Figure 9** and in **Table 4-A9**. We observed significant scattering of the data over the three independent replicates. At short timescale (< 10h), little dissolution of the oxide is observed. The data point showing 14 % dissolution of the mineral after 6h is likely to be erroneous, as points at longer time from the same series showed lower dissolution (5 % dissolution after 9h). At longer timescale, we observed dissolution of MnO₂, with up to $0.11 \pm 0.09 \text{ mol Mn(II) mol}^{-1} \text{ MnO}_2$ released in solution after 24h. The significant increase at longer timescales is possibly explained as the results of the prolonged exposure of the cells to acidic conditions, which may cause the secretion of metabolites, either actively secreted by the cells or released in solution following cell lysis. However the large scattering of the data over the three replicates prevents reaching any strong quantitative conclusions.

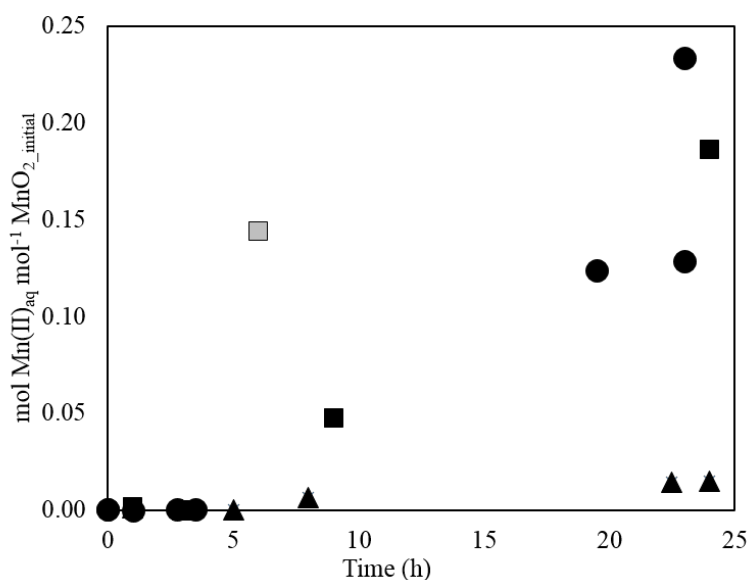


Figure 9 Release of aqueous Mn(II) when δ -MnO₂-biomass biomineral assemblage was kept to pH 4.5 over 24h. Data points are reported from three independent replicate measurements and showed important scattering of the data. We measured to $0.11 \pm 0.09 \text{ mol Mn(II) mol}^{-1} \text{ MnO}_2$ released in solution after 24h. At shorter timescale (< 10h), little dissolution of the oxide is observed. The data point showing 14 % dissolution of the mineral after 6h is likely to be erroneous, as points at longer time from the same series showed lower dissolution (5 % dissolution after 9h). It was therefore coloured in grey not to hide the overall trend of the data.

Glucose addition to biogenic-MnO₂ suspensions

The net release of Mn(II) as a function of time in biogenic MnO₂ suspensions spiked aliquots of glucose to yield 0.01, 0.55 and 5.5 mM concentrations are reported in **Figure 10** and in **Table 4-A8**. The initial rates of net release of aqueous Mn(II), calculated from the data collected in the first three hours, varied non-linearly for the different concentrations tested : close to 0.0 $\mu\text{M h}^{-1}$ for 0.01 mM, 22 $\mu\text{M h}^{-1}$ for 0.55 mM and 21 $\mu\text{M h}^{-1}$ for 5.5 mM. These rates are significantly lower than those measured for dissolution of $\delta\text{-MnO}_2$ in glucose solution (5.5: 1.3 mM ratio for glucose: MnO₂) at pH 4.5 (78 $\mu\text{M h}^{-1}$)(see **Chapter 2**) and for $\delta\text{-MnO}_2$ -biomass (46 $\mu\text{M h}^{-1}$). After the first 6h, based on the rate of glucose consumption measured in biomass suspensions, the ratio of reductant: MnO₂ in the present experiment is estimated to be close to 1:10. Limitation of the reductant may contribute the lower rate of dissolution measured in this experiment. Up to 0.02, 0.11 and 0.27 aqueous Mn(II) mol⁻¹ MnO₂_{initial} were measured after the additions of 0.01, 0.55 and 5.5 mM glucose. Similarly to that observed in the synthetic $\delta\text{-MnO}_2$ -biomass assemble, the release of Mn(II) was balanced at longer times by its removal from solution, which was ascribed to biotic Mn(II) oxidation.

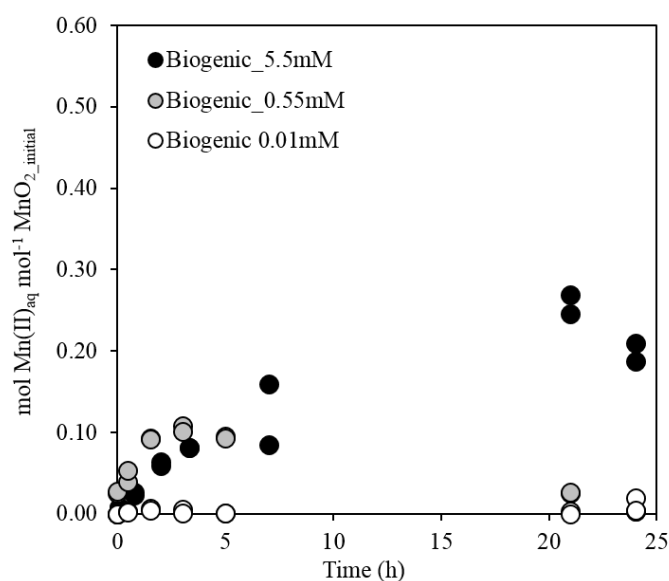


Figure 10 Release of Mn(II) as a function of time when biogenic MnO₂ suspensions were spiked aliquots of glucose (0.01, 0.55 and 5.5 mM initial concentrations).

DISCUSSION

Glucose metabolism results in extracellular acidification

Glucose is a major constituent of natural polymers and rhizodeposits in soils, and is representative of other easily bioavailable C substrates (16, 49). We observed that glucose

metabolism of *P. putida* GB-1, both in the absence and presence of MnO_2 , lead to significant medium acidification. The accumulation of both carbonic acid (H_2CO_3), resulting from respiration (50), and organic acids, due to extracellular glucose oxidation, can lead to acidification of the extracellular medium. The contribution of each of these processes to medium acidification was not quantified directly in this study. However, we constrained the origin of the acidification through chemical speciation modelling. Based on our simplified model, the maximum acidification that could be ascribed to respiration (i.e., H_2CO_3) was largely below the measured acidification for glucose concentrations above 0.10 mM, thus confirming that the secretion of organic acids played a major role in governing the decrease in pH from 6.5 to 4.0.

Of possible organic acids, gluconate was expected to be relevant and was therefore measured. Many others may also be excreted but were not screened for. We measured 0.95 ± 0.08 mM gluconate in solution 24 ± 7 min ($n = 8$) after a 5.5 mM pulse of glucose was added to a biomass suspension, when 1.7 – 2.1 mM glucose had been consumed. These measurements indicate that at least 45 – 55 % of the glucose consumed during this time was transformed through the periplasmic oxidation pathway. This fraction may, however, be largely underestimated due to the amount of acids that could remain in the periplasm. In addition to gluconic acid ($\text{pK}_a = 3.8$) and 2-keto gluconic acid ($\text{pK}_a = 2.4$), *Pseudomonas* commonly secrete a suite of other small organic acids, including acetic ($\text{pK}_a 4.8$), pyruvic ($\text{pK}_a 2.50$), formic ($\text{pK}_a 3.8$), malic ($\text{pK}_a 3.4$ and 5.2), and succinic acids ($\text{pK}_a 4.2$ and 5.6)(17, 25). We calculated the concentrations of organic acids required to reproduce acidification we measured following the addition of 5.5 mM glucose. For low pK_a (< 3.8) acids, concentrations of a few hundred μM were sufficient to drive the observed acidification.

In natural systems, bacterial metabolism may be less likely to induce the extensive acidification observed in this study due to the presence of buffering agents, such as dissolved carbonate species and negatively charged particles. If the bulk soil solution can resist acidification, the physical and chemical heterogeneity of soil at the microscale can however create microsites where redox and pH conditions differ significantly from the bulk solution (51, 52). In particular, biofilms can form diffusion-limited domains when confined structures, such as pores, cleavage steps or edges of mineral grains are colonized by microorganisms (13, 26, 53), with heterogeneous gradients of pH or organic acids relative to the bulk solution. For example, Liermann et al. (13) measured ΔpH of over

1.1 pH unit between biofilm and bulk solution. Biogenic minerals such as MnO₂, which are precipitated in a biofilm matrix and thus retained close to metabolically active bacteria, are therefore expected to be highly exposed to micro-scale variations in pH, dissolved oxygen and organic acids.

Reductive dissolution of MnO₂ upon metabolic transformation of glucose

Given their high redox potential ($E_h^0 = 1.23$ eV for Mn^{IV}O₂/ Mn(II)_{aq} couple)(54), Mn oxides minerals can readily accept electrons from a wide range of organic molecules. However, biogenic Mn oxides are stable in stationary-phase cultures of Mn(II)-oxidizing bacteria. In these systems, there is no evidence for net reductive dissolution of MnO₂ even if the oxides are embedded in a biofilm that contains a variety of organic moieties that could provide electrons to reduce MnO₂ particles (surfaces of bacterial cells, extracellular polymeric substances, residual compounds from the growth medium). This absence of observable redox activity means that the conditions, in terms of pH and/or nature of the reductants are not favourable for reductive dissolution of the mineral. Although cryptic redox recycling of MnO₂, with partial reduction of the oxide by the biomass/medium and concomitant Mn(II)-reoxidation by the bacteria or Mn(III)-enrichment of the solid cannot be excluded (55-57), any net reductive dissolution of the oxide is sufficiently slow that the system is in steady-state relative to solid phase MnO₂.

The acidification of the growth medium and the accumulation of reductants following the glucose spike caused extensive reductive dissolution of MnO₂, both in δ -MnO₂-biomass composite and biogenic MnO₂ suspensions. The decrease in the solution pH to values below 4.0 makes the conditions particularly favourable for reductive dissolution of the mineral if reductants are present, as observed in **Chapter 3**. Potential reductants include the C directly supplied to the cells (here 5.5 mM glucose) and metabolic intermediates that may accumulate in solution, such as gluconate and other organic acids. It also includes any reductants in the extracellular polymeric substances secreted by the cells independently of its metabolism.

We observed a lag of a few hours (5 - 15h) between the time at which the solution C substrate concentrations were highest and the time at which maximal dissolution was observed. While maximum aqueous concentrations of Mn(II) were measured 7 – 20h after the biomineral suspensions were spiked with glucose, highest concentrations of potential reductants were measured in the first few hours following the spike. For example, glucose was consumed in the first few hours, leaving less than 220 μ M glucose in solution 6h30

after its addition and likely less than 50 μM after 10h. Similarly, only 150 μM gluconic acid was measured after 5h. The reasons governing this disconnection are not easy to pinpoint, especially considering that the measured concentrations of these substrates in biomass suspensions may not be fully representative of biomineral suspensions.

The extensive dissolution observed when the MnO_2 suspensions kept in their spent media were spiked with 5.5 mM glucose ($> 0.80 \text{ mol Mn(II) mol}^{-1} \text{ MnO}_2$, after 20–40 h, see **Figure 4-S4**), which is significantly higher than that observed when washed and suspended in an inorganic electrolytes, suggests that dissolution of MnO_2 in washed conditions was likely limited by the concentration of reductants. Nutrient limitations may further indirectly contribute to the lower dissolution of the oxide, as it limits the synthesis of potential reductants. However, the concentration of reductants required to dissolve MnO_2 is not necessarily very high. For example, one mole of glucose or gluconic acid can provide respectively up to 24 moles or 22 moles of electrons to an oxidant, meaning that 91 μM gluconic acid could in principle be sufficient to reduce 1 mM of MnO_2 . Furthermore, the accumulation of Mn(II) in biomass suspensions acidified to pH 4.5 suggest that the biomass itself may cause dissolution of MnO_2 , although these measurements are highly uncertain.

At longer timescale, we observed a decrease of aqueous Mn(II) both in the $\delta\text{-MnO}_2$ -biomass composite and in biogenic MnO_2 ($-15 \mu\text{M Mn(II) h}^{-1}$, $R^2 = 0.87$). The regeneration of MnO_2 demonstrates that the net rates of dissolution of MnO_2 measured are likely biased by underlying Mn(II) oxidation. In other words, the turnover of Mn between its aqueous Mn(II) and solid phase Mn(IV) may be higher than that suggested through measurements of the steady-state concentrations of these two species. Concomitant bacterially mediated Mn(II) oxidation further complicates the understanding of the relation between the time at which the solution C substrate concentrations and metabolites were highest and that of maximal dissolution was observed.

Differences observed in the synthetic biomineral and biogenic MnO_2 suspensions

The dissolution of MnO_2 was significantly greater in $\delta\text{-MnO}_2$ -biomass composites than in biogenic MnO_2 suspensions spiked an equivalent amount of glucose. Up to 40 % dissolution of the solid phase was measured 7h after the addition of 5.5 mM glucose in the synthetic assemblage, compared to less than 15 % in the biogenic MnO_2 suspension. It is however not evident to directly compare the extent of dissolution in the two systems

because 1) we do not have measurements of the pH and gluconic acid concentration following glucose addition in neither system and 2) the evolution of these parameters is estimated from measurements on biomass suspensions. In addition, the metabolic state of bacterial cells and the cell number in the presence and absence of MnO₂ may differ, even if we aimed to prepare the bacterial suspensions in similar conditions. The presence of 1 mM Mn, as Mn(II)_{aq} or as MnO₂ solids, may affect the viability of the cells. The number of viable cells in the two biomineral suspensions could thus differ and were not measured. The difference observed in the pH traces measured upon spiking a biomass and a biogenic MnO₂ suspensions with 5.5 mM glucose (see **Figure 3C** and **Figure S4**) support that the representability of the δ -MnO₂-biomass composite relative to biogenic MnO₂ may be limited. Furthermore, the types of organo-mineral interactions obtained when mineral particles are co-precipitated within a matrix of exopolymeric substances and in close vicinity to cell walls are not likely to be re-created when an aliquot of δ -MnO₂ is equilibrated in a biomass suspension. These factors can affect both the extent of acidification and the types of reductants available, as well as their diffusion to the surface of the mineral, and therefore the net dissolution of the oxide. Furthermore, net release of Mn(II) are biased by co-occurring Mn(II) re-oxidation, which may differ in the two systems if the metabolic state and/or the number of cells differ. These factors should be considered in future experimental work to compare rates of dissolution in the synthetic biomineral assemblage and that of biogenic MnO₂ suspensions.

Implications for the redox cycling of MnO₂ in natural systems

Implications for the scavenging properties of MnO₂

Because MnO₂ is recognized to extensively sorb trace and contaminant metals [for eg: (58-63)] its dissolution can have direct environmental consequences. Previous studies on sorption of contaminants on biogenic MnO₂ suspensions have highlighted processes such as passivation of the minerals surface sites by organo-mineral interactions (*Simanova et al., in prep*) or partitioning of contaminants on the organic fraction (38, 42, 43, 64, 65). These studies were however conducted on-metabolising, stationary-phase suspensions, under conditions of C-starvation. The impact their metabolic activity could have on the reactivity of the oxides was therefore not considered. Our study demonstrate that metabolic activity can compromise the stability of the minerals, with dissolution of MnO₂ leading to the release of contaminants sorbed on the surface of the mineral. When extrapolated to natural systems, these results suggest that an input of bioavailable C

substrates may result in a point release of inorganic contaminants, with an impact on the temporal cycling of contaminants.

Implications for Mn cycling

A number of authors have noted that manganese oxide accumulation by *P. putida* only takes place in stationary phase or under C starvation (66-68), thus underlining a link between metabolic activity and bio-mineralization. The results from this study indicate that the chemical composition of the extracellular medium with respect to carbon speciation creates favourable or unfavourable conditions for mineral stability. It implies that MnO₂ particles will only precipitate under conditions of C-limitation, when the rate of bacterial Mn(II) oxidation offsets the rate of MnO₂ reductive dissolution. However a cryptic cycling of Mn (55-57) between low valent and high valent species may be possible until the conditions become favourable for the persistence of the oxide.

Implications for C cycling

While MnO₂ is recognized to oxidatively transform a number of organic molecules [for eg: (69-72)], the impact MnO₂ can have on the C cycle in soils has not been carefully assessed. As laboratory-based studies have highlighted the pH dependence of the redox reactivity of MnO₂, pH variations need to be considered to evaluate the reactivity of these minerals in soils. The results collected in this study suggest a mechanism that could couple biotic mineralization of C substrate and MnO₂ reductive dissolution and that could contribute to enhanced soil organic carbon mineralization following the addition of fresh C substrate to soils (see **Figure 11**).

Upon input of fresh C, metabolic transformation of the labile fraction is expected to drive local drops in pH (**A**). This localised acidification will facilitate the reductive dissolution of MnO₂ and enhance its Lewis acidity, thus facilitating the abiotic oxidation of native C by MnO₂ (**B**). The perturbations of the extracellular chemical conditions resulting from the microbial response to the input of bioavailable carbon substrates may thus tip the assemblage from an equilibrium *stationary bio-mineral* to an actively cycling machinery for C transformation through coupled-biotic and abiotic oxidative transformation (**B-C**). The effective contribution of MnO₂ to C oxidation in soils, however, depends on an efficient concomitant Mn(II)-reoxidation scheme to restore the oxidative capacity of high valent Mn (**D**).

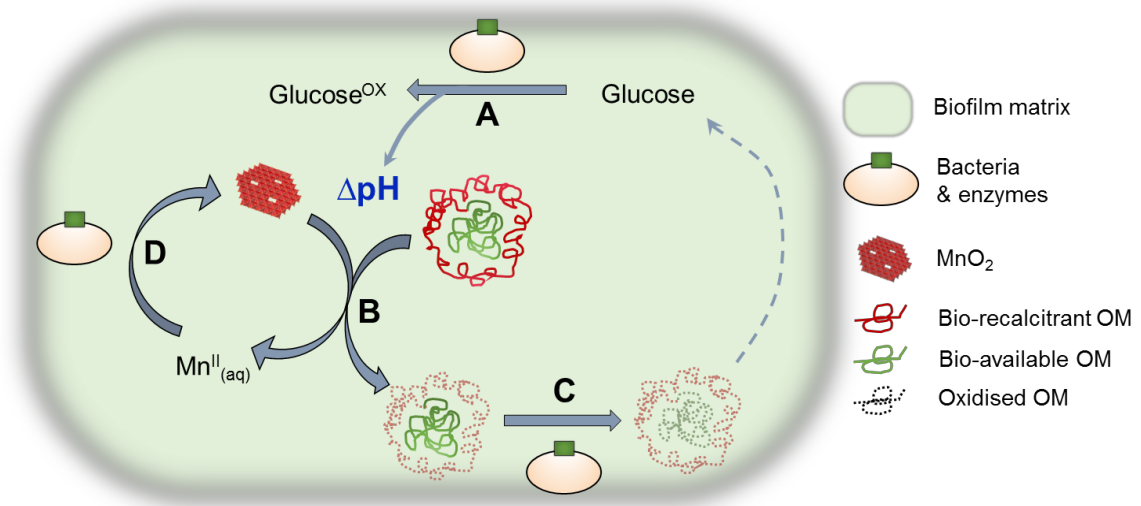


Figure 11 This diagram illustrates how mineralization of complex natural organic molecules can pass through coupled biotic and abiotic transformations. **A)** Metabolic transformation of bioavailable C substrates induces acidification of the extracellular solution **B)** Under favourable pH conditions, bio-recalcitrant molecules are abiotically oxidized by MnO₂. This reaction exposes bioavailable chemical moieties **C)** Partially oxidized substrates become bioavailable

REFERENCES

1. Torsvik V, Sørheim R, Goksøyr J. Total bacterial diversity in soil and sediment communities—a review. *J. Ind. Microbiol. Biotechnol.*, 1996;17(3):170-8.
2. Crawford JW, Harris JA, Ritz K, Young IM. Towards an evolutionary ecology of life in soil. *Trends in ecology & evolution*. 2005;20(2):81-7.
3. Or D, Smets BF, Wraith J, Dechesne A, Friedman S. Physical constraints affecting bacterial habitats and activity in unsaturated porous media—a review. *Adv. Water Res.*, 2007; 30(6): 1505-27.
4. Nannipieri P, Ascher J, Ceccherini M, Landi L, Pietramellara G, Renella G. Microbial diversity and soil functions. *Eur. J. Soil Sci.*, 2003;54(4):655-70.
5. Preston S, Griffiths BS, Young IM. Links between substrate additions, native microbes, and the structural complexity and stability of soils. *Soil Biol. Biochem.*, 1999;31(11):1541-7.
6. Martens D, Frankenberger W. Decomposition of bacterial polymers in soil and their influence on soil structure. *Biol. Fertil. Soils.*, 1992;13(2):65-73.
7. Jandl R, Sollins P. Water-extractable soil carbon in relation to the belowground carbon cycle. *Biol Fertil Soils*. 1997;25(2):196-201.
8. Raich JW, Tufekciogul A. Vegetation and soil respiration: correlations and controls. *Biogeochem.*, 2000;48(1):71-90.
9. Falkowski PG, Fenchel T, Delong EF. The microbial engines that drive Earth's biogeochemical cycles. *Science*. 2008;320(5879):1034-9.
10. Young IM, Crawford JW. Interactions and self-organization in the soil-microbe complex. *Science.*, 2004;304(5677):1634-7.
11. Duckworth OW, Sposito G. Siderophore-promoted dissolution of synthetic and biogenic layer-type Mn oxides. *Chem. Geol.*, 2007;242(3):497-508.

12. Liermann LJ, Kalinowski BE, Brantley SL, Ferry JG. Role of bacterial siderophores in dissolution of hornblende. *Geochim. Cosmochim. Ac.*, 2000;64(4):587-602.
13. Liermann LJ, Barnes AS, Kalinowski BE, Zhou X, Brantley SL. Microenvironments of pH in biofilms grown on dissolving silicate surfaces. *Chem. Geol.*, 2000;171(1):1-16.
14. Maier RM, Pepper IL, Gerba CP. *Environmental microbiology*: Academic press; 2009.
15. de Werra P, Pechy-Tarr M, Keel C, Maurhofer M. Role of gluconic acid production in the regulation of biocontrol traits of *Pseudomonas fluorescens* CHA0. *J. Appl. Environ. Microbiol.*, 2009; 75(12): 4162-74.
16. Derrien D, Marol C, Balesdent J. The dynamics of neutral sugars in the rhizosphere of wheat. An approach by ¹³C pulse-labelling and GC/C/IRMS. *Plant and Soil*. 2004;267(1):243-53.
17. Buch A, Archana G, Kumar GN. Metabolic channeling of glucose towards gluconate in phosphate-solubilizing *Pseudomonas aeruginosa* P4 under phosphorus deficiency. *Res. Microbiol.*, 2008;159(9):635-42.
18. Schleissner C, Reglero A, Luengo JM. Catabolism of D-glucose by *Pseudomonas putida* U occurs via extracellular transformation into D-gluconic acid and induction of a specific gluconate transport system. *Microbiol.*, 1997;143:1595-603.
19. del Castillo T, Ramos JL, Rodríguez-Herva JJ, Fuhrer T, Sauer U, Duque E. Convergent peripheral pathways catalyze initial glucose catabolism in *Pseudomonas putida*: genomic and flux analysis. *J. Bacteriol.*, 2007;189(14):5142-52.
20. Fuhrer T, Fischer E, Sauer U. Experimental identification and quantification of glucose metabolism in seven bacterial species. *J. Bacteriol.*, 2005;187(5):1581-90.
21. Daddaoua A, Krell T, Ramos J-L. Regulation of glucose metabolism in *Pseudomonas* : The phosphorylative branch and Entner-Doudoroff enzymes are regulated by a repressor containing a sugar isomerase domain. *J. Biol. Chem.*, 2009;284(32):21360-8.
22. Goldstein AH. Recent progress in understanding the molecular genetics and biochemistry of calcium phosphate solubilization by gram negative bacteria. *Biological Agriculture & Horticulture*. 1995;12(2):185-93.
23. Olsson R, Giesler R, Persson P. Adsorption mechanisms of glucose in aqueous goethite suspensions. *J. Colloid Interface Sci*. 2011;353(1):263-8.
24. Sposito G. *The chemistry of soils*: Oxford university press; 2008.
25. Vyas P, Gulati A. Organic acid production in vitro and plant growth promotion in maize under controlled environment by phosphate-solubilizing fluorescent *Pseudomonas*. *BMC microbiology*. 2009;9(1):174.
26. Barker W, Welch S, Chu S, Banfield J. Experimental observations of the effects of bacteria on aluminosilicate weathering. *Am. Mineral.*, 1998;83:1551-63.
27. Vandevivere P, Welch S, Ullman W, Kirchman D. Enhanced dissolution of silicate minerals by bacteria at near-neutral pH. *Microbial ecology*. 1994;27(3):241-51.
28. Welch S, Ullman W. The effect of microbial glucose metabolism on bytownite feldspar dissolution rates between 5 and 35°C. *Geochim. Cosmochim. Ac.*, 1999;63(19):3247-59.
29. Stone AT. The reduction and dissolution of Mn (III) and Mn (IV) oxides by organics. 1983 (Dissertation).
30. Stone AT, Morgan JJ. Reduction and dissolution of manganese (III) and manganese (IV) oxides by organics. Part 2. Survey of the reactivity of organics. *Environ. Sci. Technol.*, 1984; 18(8).
31. Tebo BM, Johnson HA, McCarthy JK, Templeton AS. Geomicrobiology of manganese (II) oxidation. *Trends in Microbiology*. 2005;13(9):421-8.

32. Spiro TG, Bargar JR, Sposito G, Tebo BM. Bacteriogenic manganese oxides. *Acc. Chem. Res.*, 2009; 43(1):2-9.
33. Santelli CM, Webb SM, Dohnalkova AC, Hansel CM. Diversity of Mn oxides produced by Mn(II)-oxidizing fungi. *Geochim. Cosmochim. Ac.*, 2011;75(10):2762-76.
34. Tebo BM, Bargar JR, Clement BG, Dick GJ, Murray KJ, Parker D, et al. Biogenic manganese oxides: properties and mechanisms of formation. *Annu. Rev. Earth Planet Sci.*, 2004;32:287-328.
35. Tebo BM, Clement BG, Dick GJ. Biotransformations of manganese. *Manual of Environmental Microbiology*. 2007;3:1223-38.
36. Emerson D, Fleming EJ, McBeth JM. Iron-oxidizing bacteria: an environmental and genomic perspective. *Annu. Rev. Microbiol.*, 2010;64:561-83.
37. Toner B, Manceau A, Webb SM, Sposito G. Zinc sorption to biogenic hexagonal-birnessite particles within a hydrated bacterial biofilm. *Geochim. Cosmochim. Ac.*, 2006;70(1)
38. Peña J, Bargar JR, Sposito G. Role of bacterial biomass in the sorption of Ni by biomass-birnessite assemblages. *Environ. Sci. Technol.*, 2011;45(17):7338-44.
39. Zhu M, Ginder-Vogel M, Sparks DL. Ni (II) sorption on biogenic Mn-oxides with varying Mn octahedral layer structure. *Environ. Sci. Technol.*, 2010;44(12):4472-8.
40. Villalobos M, Toner B, Bargar J, Sposito G. Characterization of the manganese oxide produced by *Pseudomonas putida* strain MnB1. *Geochim. Cosmochim. Ac.* 2003;67(14):2649-62.
41. Marafatto FF, B. Lanson and J. Peña. Crystal growth and aggregation in suspensions of δ -MnO₂ nanoparticles: Implications for surface reactivity. *Environ Sci Nano*. 2017.
42. Toner B, Manceau A, Marcus MA, Millet DB, Sposito G. Zinc sorption by a bacterial biofilm. *Environ. Sci. Technol.*, 2005;39(21):8288-94.
43. Peña J, Kwon KD, Refson K, Bargar JR, Sposito G. Mechanisms of nickel sorption by a bacteriogenic birnessite. *Geochim. Cosmochim. Ac.*, 2010;74(11):3076-89.
44. Ferguson WJ, Braunschweiger K, Braunschweiger W, McCormick JJ, Wasmann CC, et al. Hydrogen ion buffers for biological research. *Anal. Biochem.*, 1980; 104(2): 300-10.
45. Rittman B.E. MPL. *Environmental Biotechnology: Principles and Applications*, Chapter 2: *Stoichiometry and Bacterial Energetics*. In: Editions M-HI, editor.2001.
46. Sasnow SS, Wei H, Aristilde L. Bypasses in intracellular glucose metabolism in iron-limited *Pseudomonas putida*. *MicrobiologyOpen*. 2015.
47. Lessie T, Phibbs Jr P. Alternative pathways of carbohydrate utilization in pseudomonads. *Ann. Rev. Microbiol.*, 1984;38(1):359-88.
48. Lefkowitz JP, Rouff AA, Elzinga EJ. Influence of pH on the reductive transformation of birnessite by aqueous Mn (II). *Environ. Sci. Technol.*, 2013;47(18):10364-71.
49. Kuzyakov Y. Priming effects: interactions between living and dead organic matter. *Soil Biol. Biochem.*, 2010;42(9):1363-71.
50. Mookerjee SA, Goncalves RL, Gerencser AA, Nicholls DG, Brand MD. The contributions of respiration and glycolysis to extracellular acid production. *Biochim Biophys Acta - Bioenergetics*. 2015;1847(2):171-81.
51. Keiluweit M, Bougoure JJ, Nico PS, Pett-Ridge J, Weber PK, Kleber M. Mineral protection of soil carbon counteracted by root exudates. *Nature Climate Change*. 2015.
52. De Gryze S, Jassogne L, Six J, Bossuyt H, Wevers M, Merckx R. Pore structure changes during decomposition of fresh residue: X-ray tomography analyses. *Geoderma*. 2006;134(1):82-96.

53. Flemming H-C, Wingender J. The biofilm matrix. *Nat Rev Microbiol* 2010; 8(9): 623-33.
54. Bricker O. Some stability relations in system $\text{MnO}_2\text{-H}_2\text{O}$ at 25 degrees and 1 atmosphere total pressure. *Am. Mineral.*, 1965;50(9):1296-.
55. Berg JS, Michellod D, Pjevac P, Martinez-Perez C, Buckner CR, Hach PF, et al. Intensive cryptic microbial iron cycling in the low iron water column of the meromictic Lake Cadagno. *Environ Microbiol.* 2016;18(12):5288-302.
56. Hansel CM, Ferdelman TG, Tebo BM. Cryptic cross-linkages among biogeochemical cycles: novel insights from reactive intermediates. *Elements.* 2015;11(6):409-14.
57. Kappler A, Bryce C. Cryptic biogeochemical cycles: unravelling hidden redox reactions. *Environ. Microbiol.*, 2017;19(3):842-6.
58. Villalobos M, Bargar J, Sposito G. Trace metal retention on biogenic manganese oxide nanoparticles. *Elements.* 2005;1(4):223-6.
59. Manceau A, Lanson B, Drits VA. Structure of heavy metal sorbed birnessite. Part III: Results from powder and polarized extended X-ray absorption fine structure spectroscopy. *Geochim. Cosmochim. Ac.*, 2002; 66(15):2639-63.
60. Grangeon S, Manceau A, Guilhermet J, Gaillot A-C, Lanson M, Lanson B. Zn sorption modifies dynamically the layer and interlayer structure of vernadite. *Geochim. Cosmochim. Ac.*, 2012; 85:302-13.
61. van Genuchten CM, Peña J. Sorption selectivity of birnessite particle edges: a d-PDF analysis of Cd(II) and Pb(II) sorption by $\delta\text{-MnO}_2$ and ferrihydrite. *Environ. Sci. Process. Impact* 2016.
62. Simanova AA, Kwon KD, Bone SE, Bargar JR, Refson K, Sposito G, et al. Probing the sorption reactivity of the edge surfaces in birnessite nanoparticles using Nickel (II). *Geochim. Cosmochim. Ac.*, 2015;164:191-204.
63. Peña J, Bargar JR, Sposito G. Copper sorption by the edge surfaces of synthetic birnessite nanoparticles. *Chem. Geol.*, 2015;396:196-207.
64. Droz B, Dumas N, Duckworth OW, Pena J. A comparison of the sorption reactivity of bacteriogenic and mycogenic Mn oxides nanoparticles. *Environ. Sci. Technol.*, 2015.
65. Nelson YM, Lion LW, Shuler ML, Ghiorse WC. Lead binding to metal oxide and organic phases of natural aquatic biofilms. *Limnology and Oceanography.* 1999;44(7):1715-29.
66. Schweisfurth R. Manganoxydierende Bakterien. I. Isolierung und Bestimmung einiger Stämme von Manganbakterien. *Zeitschrift für allgemeine Mikrobiologie.* 1973;13(4):341-7.
67. DePalma SR. Manganese oxidation by *Pseudomonas putida*. (Dissertation). 1993;1:114.
68. Geszvain K, McCarthy JK, Tebo BM. Elimination of manganese (II, III) oxidation in *Pseudomonas putida* GB-1 by a double knockout of two putative multicopper oxidase genes. *Appl. Environ. Microbiol.*, 2013;79(1):357-66.
69. Remucal CK, Ginder-Vogel M. A critical review of the reactivity of manganese oxides with organic contaminants. *Environ. Sci. Process. Impact.*, 2014;16(6):1247-66.
70. Stone AT. Reductive dissolution of manganese(III/IV) oxides by substituted phenols. *Environ. Sci. Technol.*, 1987;21(10):979-88.
71. Wang Y, Stone AT. The citric acid– $\text{Mn}^{\text{III}}, \text{IV}}\text{O}_2$ (birnessite) reaction. Electron transfer, complex formation, and autocatalytic feedback. *Geochim. Cosmochim. Ac.* 2006;70(17):4463-76.
72. Wang Y, Stone AT. Reaction of $\text{Mn}^{\text{III}}, \text{IV}}$ (hydr)oxides with oxalic acid, glyoxylic acid, phosphonoformic acid, and structurally-related organic compounds. *Geochim. Cosmochim. Ac.*, 2006; 70(17):4477-90.

Chapter 5

Coupled C and Mn dynamics in soil systems

ABSTRACT

Similarly to clays and Fe and Al oxides, Mn (oxy)(hydr)oxides are highly reactive minerals that occur widely in soils. Due to their lower abundance, and despite their high reactivity, the importance of Mn in the context of the soil C cycle, however, has been less studied in the soil chemistry community relative to that of Al and Fe-bearing minerals, even though some studies suggest that adsorption of organic residues on MnO₂ may be more important than commonly thought and that the high redox potential of Mn species may drive the oxidation of natural organic molecules. Therefore, the goal of this literature review was to assess the ecosystem-scale importance of Mn species on C cycling. We review the interactions that are reported to take place between Mn and C species. We then discuss the relevance of these interactions and the specific conditions necessary to make them relevant in soil systems, namely the need for Mn(III) and Mn(IV) re-generation at sufficiently large rates to compete with other abiotic and biotic processes that contribute to carbon stabilization or mineralization. Finally, we identify knowledge gaps to be filled and testable hypotheses to allow for a better understanding the coupled cycles of Mn and C in soils.

1. INTRODUCTION

1.1 Cycling of soil organic C

Soil organic matter (SOM) is a heterogeneous mixture of organic molecules originating from plant, microbial and animal tissues in various stages of alteration (1, 2). Soil organic C is not only a critical factor for plant growth, but also the largest reservoir of non fossil fuel organic C on Earth (3). The mechanisms controlling soil C turnover rates therefore have a tremendous impact both on the long-term fertility of soils and on global C dynamics. Early concepts of SOM stability focused on the concept of chemical recalcitrance to explain the existence of C pools with different residence times in soils (4-6). The emerging consensus among the soil science community is that the persistence of soil C cannot be predicted solely from the intrinsic chemical properties of its component molecules (7), but is instead a function of more global properties of the ecosystem, which include the climatic, microbial and mineralogical signatures (8). From the perspective of soil C chemistry, two major mechanisms control organic matter dynamics in soils: those that lead to its mineralization and those that lead to its stabilization.

Microorganisms are the main drivers of soil organic C cycling (1, 9). The degradation of dead biomass begins with the hydrolytic depolymerisation of large fragments, which are turned into bioavailable low molecular weight (LMW) ones. These transformations are facilitated by extracellular enzymes (eg: oxidoreductases, hydrolases) secreted by the decomposing community. Small organic substrates are then taken up by microbial cells, where they are further mineralized to CO₂ through redox coupling with an available terminal electron acceptor. Initial resistance of macromolecules to decomposition is largely associated to the absence of hydrolytic bonds and to high content of aromatic and aliphatic moieties (9). However, irrespective of chemical structure, the accessibility of organic molecules to the decomposing community is the main driver of C cycling in soils (10, 11).

In soil, OM accessibility to the decomposing community is restricted by the formation of stable organo-mineral aggregates and complexation and adsorption of organic molecules onto mineral surfaces. Several studies have summarized the current knowledge on organo-mineral interactions (9, 12-16). Physical entrapment within organo-mineral aggregates and sorption of organic molecules on mineral surfaces offer protection against oxidative degradation by sequestering these molecules away from the soil solution and extracellular enzymes (17) and restricting O₂ diffusion to smaller pores

(18). Aggregate organisation in soils spans different scales given the continuum of classes of binding agents and sizes of organic and inorganic constituents. In macroaggregates ($> 250 \mu\text{m}$), mixtures of more labile and less transformed organic fragments are held together by roots and hyphae. Microaggregates ($20 - 250 \mu\text{m}$) are themselves formed from the chemical interactions of organic fragments and mineral particles ($< 20 \mu\text{m}$) as a result of adsorption, electrostatic binding and bridging interactions governed by clay minerals, metal oxides and polyvalent cations (19-21).

Stabilised organic matter is thought to be mainly associated to Fe and Al oxy(hydr)oxides and clay minerals. These minerals are characterised by high surface area and surface chemistries that allow the adsorption of negatively charged organic residues, either through the displacement of surface hydroxyls followed by inner-sphere complexation at the surface of metal oxides, or through polyvalent cation-bridging (13). Organic residues may further accumulate on mineral surfaces through hydrophobic interactions. Reported values for surface excesses (mass of adsorbed material per mass of sorbent material or mass of adsorbed material per unit area of sorbent material) of soil organic C on Fe oxides and Al silicates vary widely : Murphy et al. (22) reported between 0.9 mg C m^{-2} and 46 mg C m^{-2} on haematite, Chorover et al. (23) reported loading of $0.2 - 0.3 \text{ mg C m}^{-2}$ on montmorillonite and goethite and Eusterhues et al. (24) reported 1.3 mg C m^{-2} .

Based on the finding that that organic carbon is composed of amphiphilic molecules (2), that it does not accumulate evenly on mineral surfaces (25-27), that it accumulates on mineral surfaces with capacity exceeding those expected for monolayer coverage ($\sim 1 \text{ mg C m}^{-2}$)(24, 28), and that isolated hydrophobic fractions adsorb extensively to mineral surfaces (29, 30), Kleber et al. (31) proposed a conceptual model of entropically-driven chemical self-arrangement of organic C on mineral phases. According to this *zonal* model, polar functional groups attach to hydroxyl surface groups on oxy(hydr)oxides and phyllosilicate edges through ligand exchange reactions in the *contact zone*. In the *hydrophobic zone* large apolar moieties are retained through hydrophobic interactions, offering further sites for binding to similarly apolar organic molecules. In the *kinetic zone* polar head groups provide additional low affinity sorption sites in rapid exchange with the soil solution.

1.2 Manganese and soil organic C

Similarly to clays and Fe and Al oxides, Mn (oxy)(hydr)oxides are highly reactive minerals that occur widely in soils (32-34). Because of their high surface areas and high affinity for metal cations, Mn (oxy)(hydr)oxides are recognized to influence the mobility and bioavailability of trace metals in terrestrial and marine environments [for eg: (35-41)]. Manganese (oxy)(hydr)oxides however differ from these other secondary minerals by being on average less abundant than Fe and Al oxides. For instance, average soil concentration of 72 000 ppm for Al, 26 000 ppm for Fe and 550 ppm for Mn reported by Shacklette et al (42). Furthermore, MnO₂ are characterised by high redox reactivity, as evidenced by the high redox potential of the Mn^{IV}O_{2(s)}/ Mn(II)_(aq) couple [$E_h^0 = 1.23$ eV, relative to 0.77 eV for α -FeO(OH)/ Fe²⁺], which places them amongst the strongest oxidants in natural systems (43-46).

Due to its lower abundance, and despite its high reactivity, the importance of Mn has been less studied in the soil chemistry community relative to that of Al and Fe-bearing minerals. A number of studies investigating the reaction of solid-phase Mn species in natural systems have focused on the metal scavenging properties of MnO₂ [for eg: (35, 39, 40, 47-57)]. Several kinetic studies on the oxidation of model organic compounds by MnO₂ have also been carried out, but these studies often used small organic compounds and/ or focused on the reductive dissolution of the MnO₂ (58-67). In a well-cited paper published in 1994, Sunda and Kieber (68) suggested that MnO₂ in soils could serve to increase the pool of accessible growth substrates for neighbouring microorganisms by turning high molecular weight organic acids into lower molecular weight fragments. Other studies have demonstrated the ability of MnO₂ to lyse high molecular weight organic into low molecular substrates (23, 69). However while this hypothesis remains highly cited, its applicability in natural systems has not been confirmed.

Based on electrostatic consideration, the sorption of organic C on Mn oxides is expected to be significantly lower than on Al and Fe oxides. The high surface area and hydroxylated surface of MnO₂ provide a high concentration of ligand exchangeable sites, but the low p*H*_{pzc} (~ 2) of their basal surface oxygens is expected to hinder sorption due to unfavourable electrostatic interactions and protonation state. However, the p*H*_{pzc} of edge sites is estimated to be significantly higher than that of its basal sites, with values ranging between 6 - 8 (40, 57). In addition, the zonal model proposed by Kleber et al.,

(31) highlights the importance of hydrophobic interactions and thus puts less emphasis on the role of electrostatic interactions in governing organo-mineral interactions for Mn oxides. These two factors thus suggest that more C can be retained on MnO₂ than might be expected when considering only the overall pH_{pzc} typically cited for MnO₂ [\sim 2-3 (70)]. Recent work on organo-mineral interactions in biogenic MnO₂ suspensions and the observation that biogenic MnO₂ particles accumulate and persist in biofilm matrices rich in organic carbon suggests that this hypothesis needs to be evaluated (see **Chapter 2 & 4**)(53, 65, 71-73).

The Mn literature provides evidence that the high redox reactivity of high valent Mn species may impact the soil C dynamics at the ecosystem scale. In soils, correlations have been reported between litter Mn content and decomposition rates in a number of forest ecosystems (74-76). This relationship has been associated to the activity of white-rot fungi, which use transient Mn(III) as oxidative agents that degrade chemically and biologically recalcitrant molecules such as lignin (74, 76, 77). Recent studies have reported that appreciable quantities of Mn(III)-L complexes are found in various coastal locations (78-81) whereas they were historically considered too unstable to be relevant (82, 83). Chemically synthesized MnO₂ minerals have also been shown to oxidize a wide range of natural and anthropogenic organic compounds in laboratory settings (58). The active cycling of Mn between Mn(II) and Mn(III) maintained by white-rot fungi (76), as well as recent discussions on the cryptic cycling of highly reactive intermediate species (84-86), suggests that the redox reactivity of Mn may be important at the ecosystem level despite its low abundance and the resulting electron imbalance between the electron accepting capacity of high valent Mn species and the reservoir of electron reducing equivalents provided by soil organic C.

1.3 Objective of the review

The goal of this review is to assess the role Mn species can play on C cycling at the ecosystem-scale. By systematically reviewing the pathways reported in the literature through which Mn species can react with organic residues in soils, this study aims to identify the respective limitation and/ or relevance of these individual pathways and to provide the critical insight required to identify the major gaps of understanding.

Figure 1 summarizes the different processes that can couple the Mn and the C cycle in soils to illustrate the organization of this review. We first reviewed reactions through which MnO₂ can contribute to the stabilization of organic fragments, i.e., adsorption and oxidative polymerization reactions. We reviewed the reactions that, on the contrary, favour the oxidative degradation of organic fragments through reduction of high valent Mn species. We then reviewed current knowledge on the natural occurrence of Mn in order to assess the relative importance of Mn(III) versus Mn(IV) in governing its redox reactivity and hence its influence on organic matter oxidation. In light of the lower abundance of Mn relative to Fe and Al, the ability of Mn to cycle between three oxidation states [Mn(II), Mn(III) and Mn(IV)], and the intimate association of biomass and organic residues and MnO₂ particles in biogenic MnO₂, we finally examined the conditions under which the processes highlighted in **Figure 1** may be relevant in natural systems and whether these should be incorporated into the discussion of mineral control on soil organic C dynamics. In the conclusion section, we thus provide recommendations for research directions in this field.

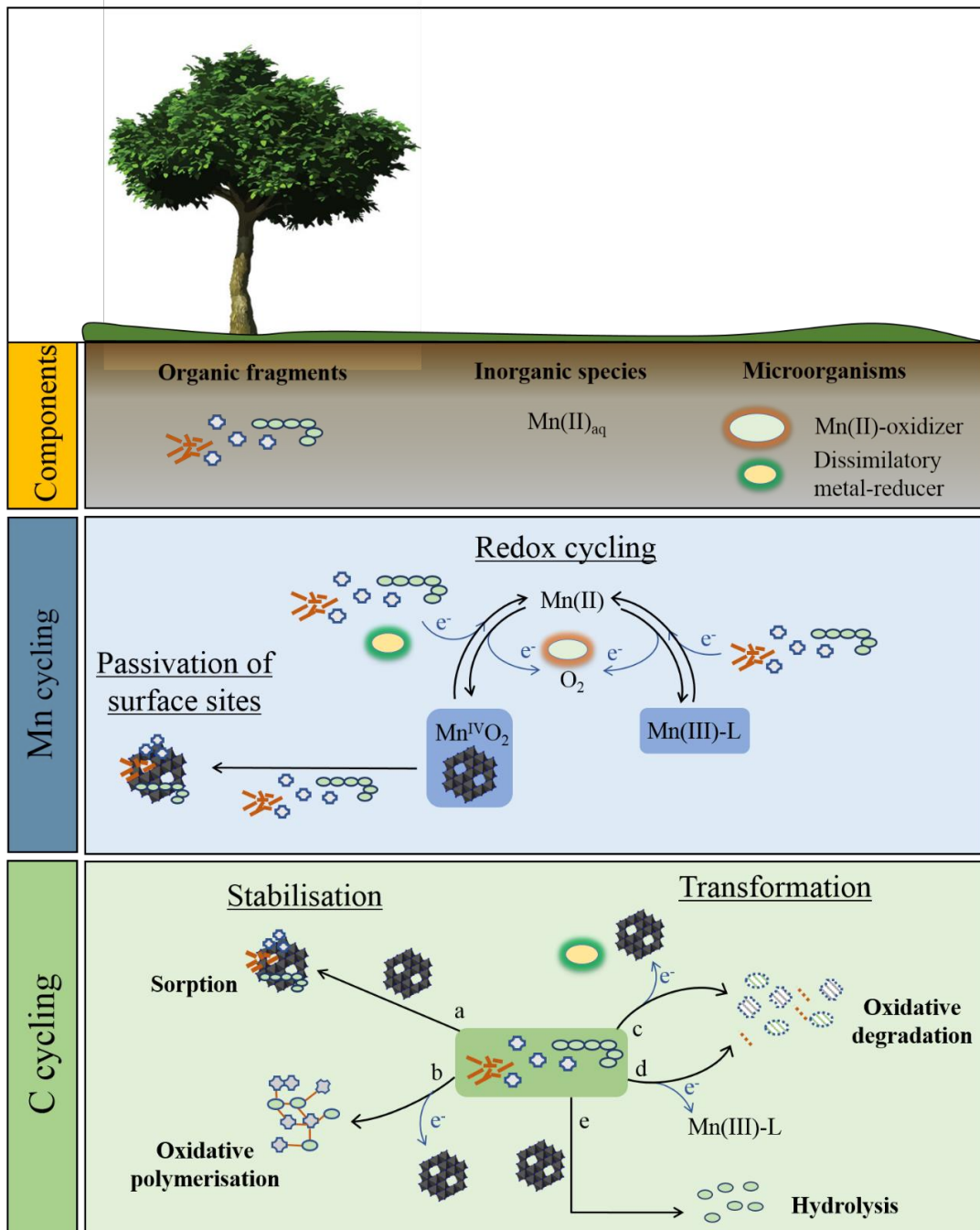


Figure 1 Schematic that describes the coupled cycling of C and Mn in soils. Blue curly arrows represent transfer of electrons from a reducers/ to an oxidant. The *soil components* are brought together to run the *Mn redox cycling*. Mn(II)-oxidizing organisms (bacteria and fungi) secrete enzymes that catalyse the electron transfer from Mn(II) to O_2 , thus generating stabilized Mn(III)-ligands complexes [Mn(III)-L] or MnO_2 . These high valent Mn species can in turn accept electrons from reduced organic components, regenerating Mn(II). Solid phase MnO_2 can additionally be reduced biotically by dissimilatory metal reducers that couple the oxidation of the organic components to the reduction of MnO_2 . Sorption of organic components on the mineral surface may passivate mineral surface sites. The *C cycling* can be influenced by high valent Mn components [Mn(III)-L and MnO_2] through different reactions that may contribute either to the stabilisation of organic residues, or to their transformation : a) sorption of organic molecules on the mineral surface b) polymerization of oxidized residues c) abiotic and biotic oxidative degradation of organic residues, when electrons are either transferred directly to the mineral or through the metabolism of the metal reducers, respectively d) abiotic oxidative degradation by Mn(III)-L complexes and e) surface catalysed hydrolysis reactions.

Table 3 Measured sorption capacity on different mineral phases of natural organic molecules. The values directly transcribed from the original study are reported in **bold**. Values calculated from the characteristics provided are reported in *italic*. The molecular formula of humic substance is taken as $C_{187}H_{186}O_{89}N_{9}S_1$. Organic carbon is abbreviated as OC and Natural Organic Matter as NOM in the table.

Minerals	Mineral characteristics	Organic molecules	$C_{\text{sorbbed}}/\text{mass mineral}$	$C_{\text{sorbbed}}/\text{surface area}$	Experimental Condition	Ref.
Montmorillonite (SWy-2)	N_2 -BET SSA: $36.4 \pm 0.9 \text{ m}^2 \text{ g}^{-1}$ (596 $\text{m}^2 \text{ g}^{-1}$ including interlayer)	Oak NOM	> 11 g C kg ⁻¹	<i>0.30 mg C m⁻²</i> (from N_2 -BET SSA)	dark, pH 4	
Goethite α -FeOOH	N_2 -BET SSA: $50.1 \pm 0.2 \text{ m}^2 \text{ g}^{-1}$	Pine NOM Oak NOM	9g C kg⁻¹ 11 g C kg⁻¹	<i>0.18 mg C m⁻²</i> <i>0.22 mg C m⁻²</i>	dark, pH 4	(23)
Binnessite MnO_2 (Synthetic)	N_2 -BET SSA: $83.8 \pm 0.7 \text{ m}^2 \text{ g}^{-1}$ AMON: na	Oak NOM	1.5 g C kg⁻¹	<i>0.02 mg C m⁻²</i>	dark, pH 4	
Goethite α -FeOOH	N_2 -BET SSA: $58.0 \pm 0.8 \text{ m}^2 \text{ g}^{-1}$ XRD shows trace of hematite	Great Dismal Swamp & Suwannee River NOM	<i>14.5 g C kg⁻¹</i> <i>17.4 g C kg⁻¹</i>	0.25 mg C m⁻² 0.30 mg C m⁻²	dark, pH 4, 24h	(30)
Goethite α -FeOOH	SSA: $15 \text{ m}^2 \text{ g}^{-1}$ pH _{lep} : 7.9	Isolated humic substance from Esthwaite Water	30 mg HS g⁻¹ <i>~ 17 g C kg⁻¹</i> 55 mg HS g⁻¹ <i>~ 31 mg C g⁻¹</i>	<i>2.0 mg HS m⁻²</i> <i>1.1 mg C m⁻²</i> <i>3.6 mg HS m⁻²</i> <i>2.1 mg C m⁻²</i>	pH 7, I = 2mM (Na ⁺ , Cl ⁻ , HCO ₃ ⁻) pH 7, I = 2mM (Mg ²⁺ , Ca ²⁺ , Na ⁺ , SO ₄ ²⁻ , Cl ⁻ , HCO ₃ ⁻)	(87)
Fer ^{10r} (dithionite-citrate-bicarbonate)	Goethite (200 $\text{m}^2 \text{ g}^{-1}$) Ferrhydrite (800 $\text{m}^2 \text{ g}^{-1}$)	Soil sample from Haplic Podzol Soil sample from Dystric Cambisol	<i>~ 220 g C kg⁻¹</i> <i>~ 880 g C kg⁻¹</i> <i>~ 220 g C kg⁻¹</i> <i>~ 1040 g C kg⁻¹</i>	1.1 mg C m⁻² 1.3 mg C m⁻²	na na	(24)
Mn ₃ O ₄	SSA (Strohlein): $65 \text{ m}^2 \text{ g}^{-1}$ pH _{lep} : 5.4 AMON: 2.7	Isolated humic substance from Esthwaite Water	<i>52 g HS kg⁻¹</i> <i>29 g C kg⁻¹</i> <i>111 g HS kg⁻¹</i> <i>62 g C kg⁻¹</i>	0.8 mg HS m⁻² <i>0.4 mg C m⁻²</i> 1.7 mg HS m⁻² <i>1.0 mg C m⁻²</i>	pH 6.7, 0 mM CaCl ₂ pH 6.7, 1 mM CaCl ₂	(88)
Oxide B (~β-MnOOH)	SSA (Strohlein): $75 \text{ m}^2 \text{ g}^{-1}$ pH _{lep} : 2.8		<i>45 g HS kg⁻¹</i> <i>25 g C kg⁻¹</i>	0.6 mg HS m⁻² <i>0.3 mg C m⁻²</i>	pH 6.7, 0 mM CaCl ₂	

	AMON: 3.4		113 g HS kg^{-1} 63 g C kg^{-1}	1.5 mg HS m^{-2} 0.9 mg C m^{-2}	pH 6.7, 1 mM CaCl ₂	
Biogenic MnO ₂	<i>Roseobacter</i> , <i>Erythrobacter</i> (bacteria), <i>Pyrenochaeta</i> , <i>Stagnospora</i> (fungi) SSA: na AMON: na pH _{pzc} : na	Culture media or Brackish water from Oyster Pond (Falmouth, MA)	4-17 mol OC kg⁻¹	/	96h, dark, non-filtered	(89)
δ-MnO ₂	SSA: na AMON: na pH _{pzc} : na	Brackish water from Oyster Pond (Falmouth, MA)	5.0 mol OC kg⁻¹ 60 g OC kg^{-1}	/	4 weeks, dark, non-filtered	
MnO ₂ coating on sand grain from WTW	SSA : na pH _{pzc} : na AMON : na	Water treatment work DOM	30 g OC kg⁻¹ $2.8 \text{ mol OC kg}^{-1}$	/	10 mg L ⁻¹ DOM 2 mg L ⁻¹ Mn(II)	(90)
δ-MnO ₂	N ₂ -BET SSA: 140 m ² g ⁻¹ AMON: 3.8 (MnO _{1.87})	Suwannee River hydrophobic fraction (24% aromatic C)	3.25 g C kg^{-1}	0.02 mg m^{-2}	pH 5, 10mM NaOClO ₄	(69)

2. STABILISATION OF ORGANIC MOLECULES BY MnO₂

Among the different types of interactions reported for MnO₂ with organic residues, two pathways can lead to their stabilisation in natural systems: adsorption of organic residues on MnO₂ and oxidative polymerization of organic residues. These two pathways are shown schematically in the bottom panel of **Figure 1**. In the section that follows, we review the chemistry governing these two pathways.

2.1 Adsorption of organic C on MnO₂

2.1.1 Quantification of OM sorption by MnO₂

One approach to evaluate the relevance of sorption of organic matter to MnO₂ is to compare the quantitative loadings reported on MnO₂ relative to that reported for other minerals (see **Table 1**). Reported values for surface loadings, however, vary enormously. Consequently, drawing quantitative conclusions about the relative importance of different mineral phases is difficult, especially given the wide range of experimental conditions used in published studies. To provide greater context for the values reported in **Table 1**, we use **Table 2** to summarize the challenges associated with quantification of the surface excesses of organic residues on mineral surfaces.

The study of Chorover and Amistadi (23), who compared the sorption of dissolved organic C derived from forest soil leachates ($c_i = 0 - 140 \text{ g C m}^{-3}$) on MnO₂, goethite and montmorillonite (pH 4), allows us to compare directly the sorption affinity and capacity of organic residues on these minerals and thus evaluate the importance of sorption on MnO₂ relative to these other phases. They reported a maximum loading of $\sim 2 \text{ g C kg}^{-1} \text{ MnO}_2$ (equivalent to $\sim 0.2 \text{ mol C kg}^{-1} \text{ MnO}_2$) relative to $\sim 10 \text{ g C kg}^{-1}$ for goethite and montmorillonite (23). The sorption isotherm for MnO₂ showed a gentle initial slope, which indicates the absence of high affinity sorption site for organic C. Higher affinity was observed for both goethite and montmorillonite. This study therefore suggests a limited role for MnO₂ for C sequestration through sorption interactions. However, the relatively low surface area of MnO₂ particles used in this study ($83 \text{ m}^2 \text{ g}^{-1}$) does not represent the most reactive MnO₂ phases. Furthermore, other studies have reported significantly higher loadings on MnO₂ mineral, with values ranging from 2.8 – 17.0 mol C kg⁻¹ MnO₂.

Table 2 Summary of the methodological challenges associated to the quantification of C loadings on mineral phases, both from the both from the carbon perspective and from the mineral perspective.

Carbon perspective	Different pools of C may bind to the mineral surfaces via different types of interactions (e.g., ligand exchange, electrostatic, hydrophobic), and therefore display different stabilities. Therefore, depending on the extraction method used, different pools of C can be mobilised or preserved (91).
	Because of the formation multilayer organic C on mineral surfaces, sorption isotherms often do not show maximum surface excess values at high concentrations of organic C. The assembly of the layers depends on a multitude of factors, which include the cation concentrations, pH, the nature of the organic molecule. This complexity limits the ability to make cross-study comparisons.
Mineral perspective	The mass of the mineral is a poor indication of mineral phase and mineral properties. For example, it gives no indication on the sizes of crystallite and on the specific surface area available for sorption.
	Measurements of the total Fe, Al, or Mn concentrations are not trivial because different mineral phases may resist different chemical treatment (24).
	The <i>zonal</i> model for the sorption of organic residues on mineral surfaces, which refutes a homogeneous monolayer covering of mineral phases, implies that specific surface area is a poor indicator of propensity for OM to accumulate at the mineral surface (92).

2.1.2 Mechanism of OM sorption on MnO₂

Because of the acidity of MnO₂ basal surface sites (70), sorption of organic molecules on the surface of MnO₂ is commonly considered to be insignificant. Unfavourable electrostatic interactions between negatively charged organic molecules and MnO₂ basal surface sites ($\text{pH}_{\text{pzc}} < 3$) are expected to hinder organo-mineral interactions relative to other environmentally relevant mineral oxide such as goethite ($\text{pH}_{\text{pzc}} \sim 8$), which are protonated at these pH conditions. Furthermore, the deprotonation of surface bound oxygen at typical environmental pH values means that it is energetically difficult for organic substrates to form an inner-sphere coordination complex on MnO₂ surface because O²⁻ and OH⁻ are poorer leaving ligands than H₂O (67). However, the pH_{pzc} of edge sites of MnO₂ particles have recently been estimated to be significantly higher than that of its basal sites, with values ranging between 6 – 8 (40, 57). Such differences in pH_{pzc} values

for basal and edge sites suggest a very different reactivity of these two sites, and higher sorption capacity on MnO_2 relative to that which can be predicted by considering only overall pH_{pzc} of the mineral phase. Simanova et al., (*in prep*), for example, observed that extracellular polymeric substance (EPS) may passivate edge sites of biogenic MnO_2 and $\delta\text{-MnO}_2$, but leave basal sites free for cation sorption. Considering that MnO_2 particles can be extremely small (3 – 10 nm along the basal plane and 2 – 4 nm along the stacking direction, $\text{SSA}_{\text{max}} \approx 200 \text{ m}^2 \text{ g}^{-1}$) (93-97) the density of reactive surface sites at the particle edges can be large relative to those on the basal surface. Therefore, the extent of organo-mineral interactions at the surface of MnO_2 will be dependent on the size of the particles.

Alongside ligand exchange reactions, cation bridging and hydrophobic interactions can contribute to organo-mineral interaction on MnO_2 surface. The presence of Ca^{2+} has been shown to increase the retention of organic residues on MnO_2 , Mn_3O_4 and a Mn(IV)-enriched $\beta\text{-MnOOH}$, through cation bridging of the negatively charged humic acid and mineral surfaces and by reducing the electrostatic repulsion between humic acids (69, 88). Furthermore, a few studies have reported preferential loading of high molecular weight, hydrophobic rich organic molecules on MnO_2 (23, 69). Allard et al. 2017 (69) reported that the loading of organic C on a Mn sand was reduced upon removing its original OC content (0.99 mg C g^{-1}), and that the loading of C on this Mn sand was not dependent on pH. Both observations are consistent with hydrophobic interactions governing the sorption of organic molecules on MnO_2 . Because of the low affinity of organic C for exchangeable surface sites of MnO_2 , the vertical accumulation of patches of hydrophobic C, as described in Kleber's zonal model (31), can enhance the potential for C sequestration on MnO_2 (see **Figure 2**).

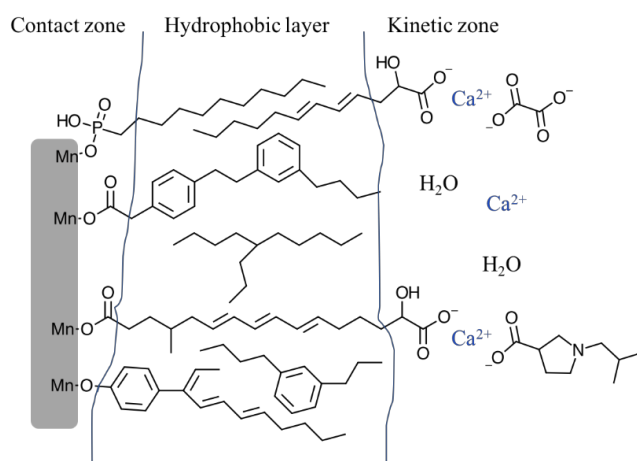


Figure 2 Schematic illustrating the zonal model of organo-mineral interactions. Adapted from Kleber et al. (31). The grey box represents the surface of MnO_2 mineral.

Of candidate organic molecules that may accumulate on mineral surfaces, amphiphilic molecules like proteins play an important role in structuring the zonal architecture of organic C on mineral surfaces (31). This observation is in agreement with the known affinity of N-rich compounds on mineral surfaces (31, 98). In fact, proteins appear to be selectively sorbed by MnO₂, and in particular by biogenic MnO₂, both because hydrophobic interactions are expected to be favourable at MnO₂ surfaces (69) and because biogenic MnO₂ will be in close contact with protein-rich extracellular polymeric substances (71). For instance, Estes et al. (89) reported that the organic carbon associated to biogenic MnO₂ (4.1 – 17.0 mol OC kg⁻¹ MnO₂) precipitated from bacteria and fungi grown in cultures media or in field-collected brackish water was primarily proteinaceous (bacteria) and proteinaceous and lipopolysaccharides (fungi) (40 - 188 mg proteins g⁻¹ mineral). A large fraction of the proteins (> 55%) were identified as being related to heme peroxidase, suggesting that proteins involved in Mn(II) oxidation may remain sorbed on MnO₂. Johnson et al. (90) also reported significant retention of proteins on MnO₂, where the OC associated to MnO₂-coated grain sand collected from a water treatment work [dissolved organic content (DOC) content ~10 mg L⁻¹ and ~0.2 mg L⁻¹ of Mn(II), 3 % w/w C, calculated as 2.8 mol OC kg⁻¹ mineral] showed a lower C: N ratio than the original DOC (15: 1 versus 60: 1 respectively)(90).

2.2 Oxidative polymerization

2.2.1 Reaction of MnO₂ with polyphenols

A number of studies have shown that MnO₂ can oxidize polyphenols, thus leading to the oxidative polymerization of phenols (63, 99-104). These studies are directly relevant to soil systems because polyphenols are a ubiquitous class of organic molecules secreted by plants (105-108). One electron transfer at the surface of MnO₂ leads to the formation of phenoxy radicals, facilitated by the stabilization of radicals conferred by the benzene ring. The relative positions of the –OH functional groups also has a direct impact on the rate of radical formation, with *ortho* –OH being more efficient than *para* –OH, themselves more efficient than *meta* –OH to react with MnO₂ (61, 100, 102, 103). This difference is attributed to the respective capacity of the three polyphenols to form inner-sphere surface complexes on MnO₂. Upon binding of catechol to the mineral surface through one –OH, hydrogen bonding from the neighbouring *ortho* –OH may further stabilize the complex as a 5-membered ring.

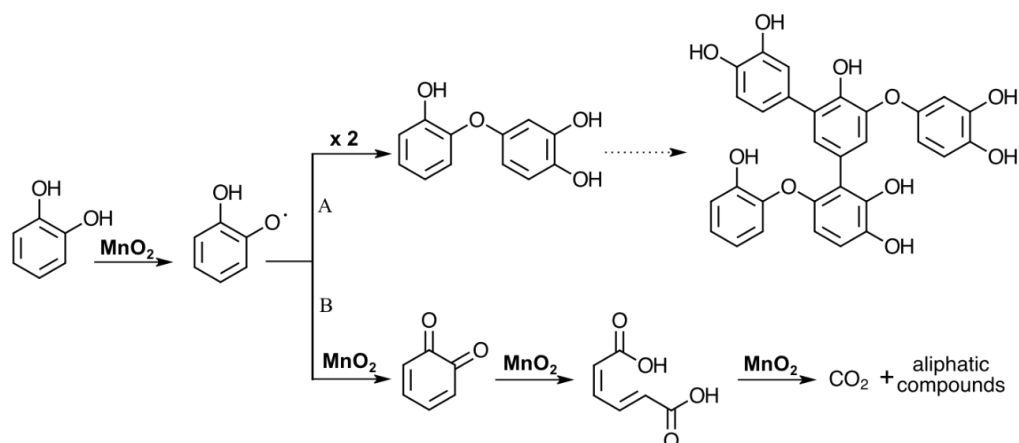


Figure 3 Oxidative transformation of phenols induced by MnO₂. A polyphenol is represented here (catechol). Surface complexation of phenol results in the formation of phenoxy radical, which is stabilized by resonance throughout the benzene ring. Two further reaction pathways are then possible. Pathway A) Two phenoxy radicals can couple to form phenolic dimers. Further coupling reactions with phenoxy radicals leads to polymerisation. Pathway B) An additional electron transfer to MnO₂ results in the formation of quinones. These can be further oxidized, resulting in ring opening, and eventually CO₂ evolution and formation of aliphatic compounds.

As shown in **Figure 3**, phenoxy radicals may either undergo radical coupling and polymerisation (109), or lead to ring opening by breaking of the aromatic C-C bond, and subsequently to partial mineralization to CO₂ and accumulation of aliphatic fragments (99)(see **Figure 3**, *Pathways A* and *B* respectively). *Pathway B*, which is an oxidative degradation pathway is discussed further in **Section 3.1** The C-stabilization pathway (A) is favoured under conditions of high phenol concentrations since high concentrations of radicals favour coupling reactions (63). Majcher et al. (99) reacted ¹⁴C-labelled catechol (2.3 mmol L⁻¹) with MnO₂ (1 g L⁻¹) at pH 4 over 24h and measured 5 - 16 % of the initial catechol ¹⁴C evolved as CO₂, but the largest fraction (55 – 83 %) of C was turned into a stable solid C residue. High concentrations of other types of organic molecules may also favour polymerization reactions. For example, Li et al. (103) observed that the mineralization of ¹⁴C catechol decreased from 28.5 to 6.5% at pH 5 and from 10.5 to 4.3% at pH 8 when two different humic acids were added to a ¹⁴C-catechol–MnO₂ reactions. The use of ¹³C-labelling of the humic acids showed the binding between phenoxy radicals and humic acids with intact aromatic ring.

2.2.2 Reaction of MnO₂ with sugars and amino acids

Manganese oxides are known to enhance other polymerisation reactions, notably the Maillard reaction, which involves the condensation of saccharides and amino acids through nucleophilic attack from the amine to the carbonyl (110). Uncatalyzed, this reaction is too slow to be significant under environmental conditions since protonation of the amino acids [pK_a ~ 8.5 – 10.2 (111, 112)] at environmentally relevant pH conditions

reduces their nucleophilic character and thus slows the nucleophilic attack on the carbonyl centre (113). In the presence of MnO_2 , however, the Maillard reaction proceeds at significant rates at 25°C and pH 6 – 7 as measured by the increased absorbance of the solution over a 30 day period (114). The oxidation of glucose to open-chained aliphatic carbonyl compounds by MnO_2 , which facilitates the subsequent coupling of the sugar and the amino acids, is thought to explain the enhanced rates of condensation (109, 115).

Because MnO_2 enhances the rates of both polyphenol condensation and the Maillard reaction, and because polyphenols, sugars and amino acids co-occur in most ecosystems, Jokic et al. (115) investigated the MnO_2 -catalysed integrated polyphenol-Maillard reaction as a link between the two individual pathways. They reacted equimolar mixtures (0.05 M) of catechol (11 g L⁻¹), glycine (4 g L⁻¹) and glucose (9 g L⁻¹) with $\delta\text{-MnO}_2$ (10 g L⁻¹). An increase in darkening, taken as an indication of oxidative coupling, was measured as an increase in absorbance at 400 and 600 nm (25°C, 60 days, pH 6.5 – 7.5, mass yield of lyophilised product = 28 mg L⁻¹) relative to a control without $\delta\text{-MnO}_2$ (mass yield of lyophilised product < 20 mg L⁻¹). The observed enhancement in polymerisation of saccharides, amino acids and polyphenols in the presence of MnO_2 , and the FTIR, UV-Vis, $E_{465\text{nm}}/E_{665\text{nm}}$ ratio, atomic force microscopic, ¹H and ¹³C-NMR signatures of the products formed, lead the authors to suggest that these oxidative polymerisation reactions catalysed by MnO_2 could be considered as appreciable mechanisms of humification of soil organic molecules (109, 114-120).

2.3 Synergy between OM sorption and oxidative polymerization

Stabilization of organic residues can also be enhanced through coupled sorption and oxidative reactions. Because of the high E_h of the Mn(IV/II) couple and the characteristically high reactivity of freshly precipitated MnO_2 , electrons are expected to be transferred between organic substrates complexed to the mineral surface through inner-sphere coordination and highly oxidizing $\text{Mn}^{\text{III,IV}}$ centres. Providing that electron transfer does not lead to the dissolution of the oxide, the adsorption of organic molecules onto the mineral surface thus favours further redox reaction. Sorption and oxidative transformations of organic molecules are therefore likely to occur simultaneously.

Johnson et al. (90) studied the onion-like arrangement of organic residues associated to MnO_2 layers on sand grains collected from water treatment works. In this system, the layer arrangement of organics and MnO_2 provided the opportunity to study the changes in the chemistry of the molecules preserved within the bulk of the organo-mineral

aggregate relative to those sorbed at the surface of the aggregate. X-ray photoelectron spectrometry-C1 (XPS-C1) analysis of thermally labile (< 550°C) and thermally refractory (> 550°C) fractions showed that the latter fraction contained relatively higher concentrations of carboxyls, consistent with stabilization through carboxylate binding to the surface of MnO₂. The authors, however, noted that upon complexation of organic residues to the mineral surface, neighbouring phenolic functional groups were brought close to the surface. Oxidation of phenols to phenolic radicals could then either lead to polymerisation or breaking of aromatic C-C bonds, with the relative importance of the two pathways depending on the concentration of reactants (63) (see **Section 2.2**).

The burial of aromatic and other unsaturated molecules within a thick layer of hydrophobic molecules may favour the polymerization pathway, thus further stabilizing the hydrophobic layer through cross-linking between molecules. Indeed, considering that hydrophobic molecules are often rich in aromatic and unsaturated chains, the hydrophobic layer may favour efficient electron transfer. The phenoxy radicals formed at the surface of MnO₂ may therefore act as redox mediator that transfer radicals from the surface of the mineral to the hydrophobic layer. The authors noted that polymerisation within the bulk would lead to new C-C and C-O bonds, and thus should increase the aliphatic content. However their XPS C1 results showed that the alkene/aromatic: aliphatic ratio for surface OM was lower than for bulk OM buried within the layers (1: 4 versus 3: 2), which is not consistent with their interpretation. However, they did not consider that these new bonds may further stabilize the hydrophobic layer, thus favouring the accumulation of more hydrophobic molecules, which would then be coherent with the increased alkene/aromatic: aliphatic ratio measured. This type of enhanced polymerization reactions through the hydrophobic layer is consistent with the results from Li et al. (103) who reacted polyphenols and humic acids in the presence of δ -MnO₂ and observed significant binding of the two organic constituents, with intact aromatic rings. The aggregate formation mechanisms and the *zonal* model described by Kleber et al. (31) could therefore be updated to show redox reactions on mineral surfaces that can lead to further OM stabilization.

3. DEGRADATION OF ORGANIC MOLECULES BY MN(III) AND MN(IV)

Among the different types of interactions that are reported for MnO₂ with OM, three main pathways are suggested to lead to the degradation of organic C in natural systems:

the abiotic oxidation of organic residues by MnO₂, the biotic oxidation of organic residues by dissimilatory metal reducing bacteria that use of MnO₂ as a terminal electron acceptor, and through surface-catalysed hydrolysis reactions. These pathways are shown schematically in the bottom panel of **Figure 1**. In the following section, we review these three pathways.

3.1 Abiotic oxidation of organic C

3.1.1 Direct oxidation of organic substrates by Mn oxides

The redox reaction between organic substrates and solid phase Mn oxides is understood to follow: i) the formation of a precursor surface complex ii) electron transfer between the surface complex and the mineral and iii) detachment of the oxidized surface residue (60, 61, 100, 121, 122). Because of poor electrostatic and leaving group capacity of O²⁻ and OH⁻, it is energetically difficult for organic substrates to form inner-sphere coordination complexes on the basal surface of MnO₂ (67). Overall, the reaction kinetics is controlled either by the rates of formation of the surface complex, or the rates of electron transfer, with the relative speed of the two processes varying with the nature of the organic substrates (123). The slow rate of surface complexation may be balanced by a fast rate of electron transfer. As discussed above (**Section 2.1.2**), inner-sphere coordination is expected to be easier on particles edges [$\text{pH}_{\text{pzc}} \sim 6 - 8$ (40, 57)] than on the basal surface.

The solution pH is a major control of the redox reactions on MnO₂ surface, as low pH regimes favour the reductive dissolution of the oxide both thermodynamically and kinetically (43, 58, 122, 124, 125)(see also **Chapter 3**). Briefly, redox reactions are favoured at low pH because i) the redox potential of the Mn^{IV}O₂(s)/Mn(II)_{aq} couple increases with decreasing pH, ii) protonation of surface functional groups facilitates surface complex formation as H₂O and H₃O⁺ are better leaving groups than O²⁻ and OH⁻, and iii) protonation of surface functional groups weakens Mn-O bonds, which in turn favours the dissolution of the oxide.

The studies on the oxidation by MnO₂ of small and organic molecules show a few prevailing mechanisms (see **Figure 4**). For instance, allylic or benzylic alcohols are selectively oxidized to ketones by MnO₂ (111). Carboxylic acids featuring a carbonyl group in the α -position commonly undergo C-C bond cleavage through decarboxylation reactions, as reported by Wang and Stone (66, 67). For α -hydroxy carboxylic or α -hydroxy keto substrates, C-C bond cleavage is preceded by the oxidation of the α -

hydroxyl group, which then facilitates the C-C bond cleavage through decarboxylation. The transfer of multiple electrons (>2 electrons) from one molecule to MnO₂ has been reported in a number of studies (67, 126, 127), but one electron oxidation may also take place, depending on the capacity of the product to stabilize radicals (see **Section 3.1.2**) (67).

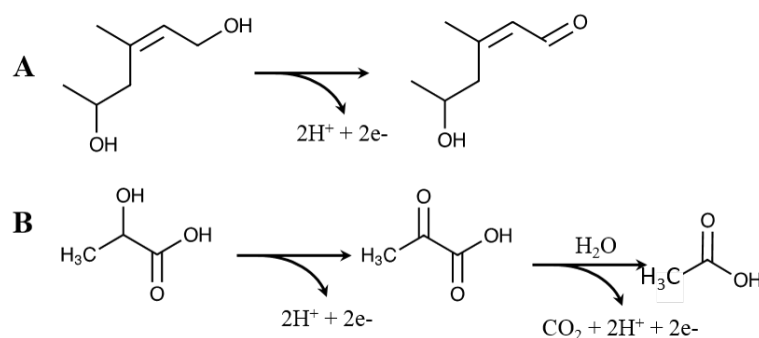


Figure 4 Oxidative transformations of organic molecules by MnO₂ A) Selective oxidation of allylic alcohols catalysed by MnO₂; B) Schemes proposed by Wang and Stone (2006) for the oxidation of two electrons reductants by MnO₂ (see **Chapter 3**).

3.1.2 One electron oxidation of OM by high valent Mn species

Instead of two-electron transfer reactions that cause reductive dissolution of the solid phase, MnO₂ can also undergo one electron transfer reactions, depending on the capacity of the product to stabilize radicals (67). Furthermore, the different orientation of the two empty electron orbitals of Mn(IV) (d_{z²} and d_{x²-y²}) means that the reduction of Mn(IV) is more likely to occur through two individual one electron transfers (121). Single electron transfers to MnO₂ lead to Mn(III)-enrichment of the solid phase and form intermediate organic radicals. For Mn(III) centres, one electron transfers are the only possible pathway for redox reactions with organic substrates.

One electron oxidation by high valent Mn offers an efficient route for C-C bond cleavage (99, 128, 129). For example, when phenols react with MnO₂, single electron transfer at the surface of MnO₂ leads to the formation of phenoxy radicals, facilitated by the stabilization of radicals conferred by the benzene ring. Further oxidation of phenoxy radicals to quinones can then lead to ring opening by breaking aromatic C-C bonds, and mineralization to CO₂ and accumulation of aliphatic fragments (99) (see **Figure 3, Pathway B**). As discussed above (see **Section 2.2.1**), the formation of phenoxy radicals may also lead to coupling and polymerisation reaction (109). The relative importance of the two pathways is dependent on the concentration of phenols reacting with MnO₂ because high concentrations of radicals are expected to favour radical coupling and thus polymerisation reactions (63).

3.1.3 Reaction of MnO₂ with high molecular weight organics

The mechanistic insights gathered from the study of small organic molecules [e.g., (60, 66, 67)] reviewed in **Sections 3.1.1** and **3.1.2** can be extrapolated to the oxidation of larger organic molecules. The reaction of natural OM with MnO_{2(s)} has been shown to transform high molecular weight organic acids into lower molecular weight fragments (23, 68, 69). This observation lead Sunda and Kieber (68) to suggest that MnO₂ in soils could serve to increase the pool of accessible growth substrates for neighbouring microorganisms. Consistent with this hypothesis, Chorover and Amistadi (23) showed that the reaction of DOC ($c_i = 120 \text{ g m}^{-3}$, 17h of reaction in the dark, initial pH 4) with MnO₂ (5 kg m^{-3}) resulted in the formation of $0.20 \text{ mol -COOH m}^{-3}$ and $0.60 \text{ mol -COOH m}^{-3}$ acetic and formic acid respectively, despite low adsorption of organics on the mineral surface. In comparison, the reaction with goethite induced the formation of only $0.12 \text{ mol -COOH m}^{-3}$ acetic acid and negligible formic acid, and none when DOM was reacted with montmorillonite. The MnO₂-induced redox transformations were supported by changes in the FTIR spectra obtained from the DOM solution, and reduction in the molar absorptivity of the DOM solution. The latter observation could be either due to the preferential sorption of high UV-absorbing aromatic moieties despite an overall low adsorption of OM, which would be consistent with the importance of hydrophobic interactions governing organo-mineral interaction at the surface of MnO₂, or to the degradation of high molecular weight molecules into UV-inactive smaller fragments. Changes in the High Performance Size Exclusion Chromatography-UV (HPSEC-UV) chromatogram of the hydrophobic fraction of Suwannee River (SR-HPOA, 5 mg C L^{-1}) reacted with δ -MnO₂ (0.1 g L^{-1}) at pH 5 over 24h showed the loss and the appearance of respectively high and low molecular weight UV absorbing molecules, which is consistent with either preferential adsorption of large organic molecules or their oxidative breakdown to smaller residues, likely a combination of both processes (69).

3.1.4 Reaction of Mn(III)-L species with high molecular weight organics

White-rot fungi are known to use the high reduction potential of Mn(III) to help them degrade lignin (77, 130). White-rot fungi secrete Mn peroxidase enzymes (MnP), which are excellent phenol oxidizing enzymes (77, 130). The MnPs oxidize soluble and unreactive Mn²⁺ to highly reactive Mn³⁺. Transient Mn³⁺ is then stabilized by small organic molecules (e.g., oxalate, tartrate, malonate, lactate, = L)(77), which are also secreted by

the fungi, to yield oxidative agents adapted to degrade phenolic-rich molecules such as lignin (74, 76, 77, 129).

Similarly to the oxidation of phenols by MnO_2 (see **Section 2.2.1**), phenols can be oxidized by Mn(III)-L through 1 electron transfer, thus generating phenoxy radicals. Further 1 electron oxidation and rearrangement result in C-C and C-O bond cleavage and a suite of degradation products (77, 129, 131). Non-phenolic moieties in lignin may also be susceptible to degradation by MnP , in particular in the presence organic sulfur functional groups and unsaturated fatty acids. These molecules can be oxidized by Mn(III)-L , thus forming form highly reactive thiyl and peroxy radicals that can act as co-oxidants. In the presence of O_2 , these radicals can attack non-phenolic moieties that are less susceptible to MnP oxidation (77). In addition, the MnP system has been shown to oxidatively degrade other chemically recalcitrant non-lignin molecules, in some cases showing partial mineralization of the organic substrates [for eg: (132-134)].

3.2 MnO_2 -catalyzed hydrolysis

The surface of mineral oxide, such as Fe, Al and Mg, can act as heterogeneous catalysts for the hydrolysis of ester bonds (135). The process is ascribed to favourable interactions of carbonyl oxygens with hydroxyls functional group at the surface of minerals oxides, which increases the concentration of reactants at the surface of the mineral (135), followed by the nucleophilic attack of surface hydroxyls to the carbonyl C. Fragments then detach from the mineral surface (see **Figure 5** for a generic example) (136). Larger concentration of hydroxide ions in the diffuse layer of metal oxides is also suggested to contribute to the enhanced rate of hydrolysis (137, 138). Similarly to the hydrolysis of carboxylic esters, the hydrolysis of other ester derivatives, and therefore of a number of environmentally relevant bonds such peptidic, phosphoester and thiophosphoester bonds, can be catalysed by mineral surfaces.

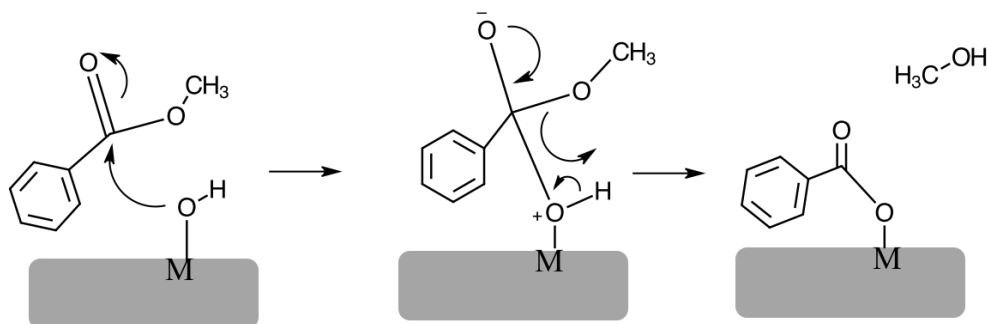


Figure 5 Surface catalyzed hydrolysis of carboxylic esters, by nucleophilic attack of a surface hydroxyl to the carbonyl C. The grey box represents the surface of a generic M oxide.

Baldwin et al. (139) reported that MnO_2 was able to enhance the cleavage of organophosphate ester bonds, despite limited adsorption of the organophosphate on the mineral (see **Figure 6A**). They showed that p-nitrophenyl phosphate was turned into p-nitrophenol and ortho-phosphate in the presence of MnO_2 (32 – 55 μM organophosphate for 11.5 mM MnO_2 , pH 5 – 8). The measured rate of hydrolysis was reported to be one order of magnitude faster than when catalysed by hydrous ferric oxide, as measured in a previous experiment under comparable conditions (140). In a similar study, the hydrolysis of polyphosphates into orthophosphates subunits in the presence of MnO_2 was also reported, with enhanced hydrolysis with decreasing pH (141).

More recently, Reardon et al. (142) used 2D ^1H - ^{15}N -HSQC-NMR (Heteronuclear single quantum coherence spectroscopy-NMR) to track the conformational and structural stability of a well characterised protein Gb1 (B1 domain of protein G) when reacted with MnO_2 (0.4: 20 mg ratio Gb1/ MnO_2 ; pH 5 and 7). At pH 5, they observed within 30 min the loss of the native Gb1 signal, followed by the appearance of a new signal consistent with the release of small peptidic products over 72h. Electrophoretic mobility measured using SDS-PAGE confirmed the protein fragmentation, with complete loss of the band for the original Gb1 protein. Protein fragmentation was also observed at pH 7, although to a lesser extent. The authors suggested that MnO_2 catalysed the irreversible hydrolysis of peptide bonds from Gb1 protein (see **Figure 6B**). By comparison, the reaction of Gb1 reacted with kaolinite under the same conditions lead to large adsorption of the protein on the mineral surface, with no irreversible conformational changes. This result was supported by molecular dynamic simulations that showed little change in the structure of the protein Gb1 upon interaction with kaolinite, montmorillonite and goethite surfaces, while interaction upon Na-birnessite compromised the secondary structure of the proteins (143).

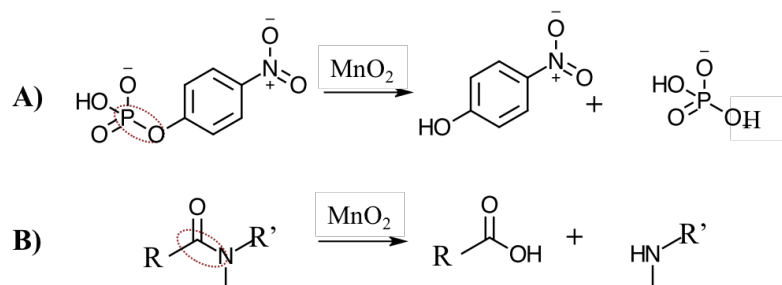


Figure 6 Hydrolysis reactions catalysed by MnO_2 , A) hydrolysis of p-nitrophenyl phosphate into nitrophenol and inorganic phosphate (pKa 12.3, 7.9 and 2.2) and B) Hydrolysis of generic peptidic bonds, forming a carboxylic acid and amine and compromise the secondary structure of proteins. The bonds that are cleaved are circled in red. The blue and red box represent undefined fragments that are bound together through a peptidic bond.

3.3 Organic C oxidation by Mn-reducing organisms

In addition to the abiotic oxidation of organic molecules by MnO_2 , the microbial use of MnO_2 as a terminal electron acceptor (TEA) coupled to oxidation of organic substrate for bacterial growth provides another link between the Mn and C cycles that operates under the suboxic and anoxic conditions encountered in flooded soils or in O_2 -depleted microsites (18). In the late 1980s, two studies demonstrated for the first time the microbial use of MnO_2 reduction to sustain anaerobic growth, coupled to the complete oxidation of a carbon substrate (144, 145). Since then, a number of dissimilatory metal reducing organisms have been identified, both in the *bacteria* and *archaea* domains (146, 147). Most organisms that can use Fe(III) as TEA are able to alternatively reduce high valent Mn species (147). Because of the low concentrations of dissolved Fe and Mn relative to the carbon available, this pathway can impact C cycling if there is an efficient mechanism to recycle high valent Fe or Mn species (148). Diffusion of soluble Fe(II) and Mn(II) to the oxic / anoxic interface allows for the regeneration Fe(III) and Mn(III, IV) species. However for the latter, abiotic oxidation by O_2 is slow. Thus, the redox cycling of Mn requires the co-existence of aerobic Mn oxidizing and anaerobic Mn reducing organisms at oxic/anoxic redox interfaces (146).

4. RELEVANCE OF MN(III) AND MN(IV) SPECIES IN SOIL SYSTEMS

4.1 Biotic oxidation of Mn

A wide range of phylogenetically diverse microorganisms (bacteria and fungi) are known to oxidize Mn(II) [see (94, 149) for reviews of identified Mn(II)-oxidizing organisms]. Because the homogeneous oxidation of Mn(II) by O_2 is exceedingly slow, most of naturally occurring Mn oxides are believed to form from the biotic oxidation of Mn(II) and Mn(III) to Mn(IV) (34, 94, 149-151). Bacterial models that have been extensively studied include the Gram-positive spore forming *Bacillus* sp. strain SG1 (152-154), the γ -proteobacteria *Pseudomonas putida* strains MnB-1 and GB-1 (155-158), the β -proteobacterium *Leptothrix discophera* strain SS-1 (94, 149) and the α -proteobacteria *Roseobacter* (159-161). The most studied Mn(II)-oxidizing fungi are the basidiomycota white-rot fungi (77, 133, 162). For all these different organisms, Mn(II)-oxidizing activity takes place in the extracellular space, leading to the extracellular accumulation of Mn(III) and Mn(IV) species.

Two main types of enzymes have been associated to the bacterial enzymatic Mn(II)-oxidation (157, 163), namely multicopper oxidases (MCO) and peroxidases. Recently, an MCO from *Bacillus* sp. PL-12 associated to Mn(II) oxidation was successfully expressed and purified (152, 164), which has allowed Soldatova et al. to propose a mechanism for Mn(II) oxidation by MCO (153, 154), that reconciles the known capacity of MCO to conduct 1 electron transfers and the 2-electron transfer required for Mn(II) oxidation to Mn(IV). The authors showed that the oxidation followed two successive 1 electron transfers, with only the oxidation of Mn(II) to Mn(III) taking place in the enzyme's active site. Newly-generated Mn(III) was suggested to be displaced to a neighbouring holding site where it forms bi-nuclear Mn(III) complexes $[\text{Mn(III)}(\mu\text{-OH})_2\text{Mn(III)}]$, which then disproportionate to form one Mn(IV) and regenerate one Mn(II). This mechanism is consistent with previous studies that had identified a pyrophosphate-extractable Mn(III) intermediate (165). The Mn(II) oxidation by white-rot fungi is associated to the activity of a Mn peroxidase (MnP) enzyme (77, 130, 162) and of MCO proteins (166, 167). For other organisms, including *Roseobacter* and ascomycete fungi, Mn(II) oxidation has been associated to the indirect abiotic oxidation of Mn(II) by bacterially generated reactive oxygen species (ROS)(159, 160, 162, 168)

4.2 Occurrence of Mn(IV) oxides

Manganese is released to the Earth's surface through the weathering of the continental crust, in particular Mn-rich silicate and carbonates (32, 149, 169). It is thus commonly found in soils of various ages and from different parent material (170).

Freshly precipitated biogenic Mn oxides are typically phyllosulfates, made of stacks of edge-sharing $\text{Mn}^{\text{IV}}\text{O}_6$ octahedral layers, with a 7 – 10 Å interlayer spacing occupied by water molecules and cations (for eg: Na, Ca, K)(94). These minerals have a high content of vacancy sites, with up to one out of six Mn(IV) absent from MnO_6 octahedral sites, high surface areas ($> 200 \text{ m}^2 \text{ g}^{-1}$) and average Mn oxidation states ranging from 3.7 - 3.9 (55, 94, 151, 171, 172). However, the co-occurrence of MnO_2 with Mn(II) and organic reductants rapidly leads to Mn(II)/ Mn(III)-enrichment and phase transformations of the newly precipitated minerals (173-177). In soils, most solid-phase Mn therefore occurs as mixed-valence Mn oxides, such as Mn(III)-enriched birnessite $[(\text{Na}, \text{Ca})(\text{Mn}^{3+}\text{Mn}^{4+})_7\text{O}_{14}\cdot 2.8\text{H}_2\text{O}]$, todorokite $[(\text{Mg}_{0.77}\text{Na}_{0.33})(\text{Mg}_{0.18}\text{Mn}_{0.60}^{2+}\text{Mn}_{5.22}^{4+})\text{O}_{12}\cdot 3.7 \text{H}_2\text{O}]$ and lithiophorite $[\text{Al}_2\text{LiMn}_2^{4+}\text{Mn}^{3+}\text{O}_6(\text{OH})_6]$ (170, 178). Manganese oxides often occur as few mm diameter black nodules or as coatings of rock surfaces. It also

frequently co-occurs with Fe in ferromanganese nodules and concretions in which primary minerals (quartz, feldspar or mica) and clays are cemented with Fe and Mn oxides (178-180). Furthermore, their large affinity for inorganic contaminants means that Mn oxides frequently co-occur with a number of impurities (36, 48, 178, 179, 181, 182). Overall, the diversity of the solid Mn phases, the low concentration of Mn relative to other soil minerals, the nanoscale size and the low crystallinity of some of the naturally-occurring Mn oxides means that the Mn oxide phases found in soils are difficult to characterise (170, 178). However, the vast majority of the studies investigating the reactivity of MnO₂ are laboratory-based, using suspensions of synthetic minerals (93, 172) or biogenic MnO₂ obtained from model Mn(II)-oxidizers (bacteria and fungi)(146, 149).

4.2 Occurrence of Mn(III) complexes

In the last decade there has been a growing recognition of the role of dissolved Mn(III) in coastal oceans systems (79, 81-83). Measurable dissolved Mn(III), stabilized as Mn(III)-ligands complexes, have been measured in suboxic and anoxic waters in a suite of locations (78-80, 82). More recently, the presence of dissolved Mn(III)-L complexes was measured in oxygenated waters, with Mn(III)-L accounting for up to 86 % of dissolved Mn (81), confirming the ubiquitous presence of dissolved Mn(III) in oceans settings. Oldham et al. (81) furthermore identified stabilizing ligands as humic-like substances, which accounted for nearly all stabilizing ligands. Because Mn(III)-L species can act both as oxidative and reductive species, they can affect the redox cycling of a suite of elements. Thus, geochemical redox models should continue to be refined in order to account for their presence.

4.3 Relative importance of Mn(III) and Mn(IV) species

4.3.1 Lignin degradation by Mn(III)

The correlation observed in some forest soils between litter Mn content and decomposition rates (74-76) is associated to the exploitation by white-rot fungi of the redox potential of Mn(III), and not Mn(IV), for lignin degradation (77, 130). Taking advantage of a 7 years litter decomposition experiment, Keiluweit et al. (183) used pyrophosphate Mn(III)-extraction and spectroscopic measurements to show that concentrations of Mn³⁺ increased in the first 3 years of decomposition, whereas the accumulation of solid-phase Mn(III, IV) occurred only after 4 - 6 years. Hotspots of lignin decomposition showed

fungal cycling of Mn between Mn^{2+} and Mn^{3+} , with Mn(III)-L serving as the oxidative agent. The accumulation of solid-phase Mn^{IV} species was observed on dead hyphae, when stabilising ligands were no longer provided for Mn(III) stabilization. Considering that $\text{MnO}_2(\text{s})$ is known to oxidize phenols, the mineral could in principle also participate in the oxidation of phenolic-rich lignin. The observation that MnO_2 only accumulates on dead hyphae, when the fungi-driven decomposition is presumably terminated, questions the role of Mn(III) relative to solid-phase Mn(IV) as the oxidants of choice in rapidly redox cycling systems.

4.3.2 Mn(III) intermediate in the enzymatic oxidation of Mn(II) to Mn(IV)

Recent studies have demonstrated that the bacterially mediated enzymatic oxidation of Mn(II) is a succession of two 1 electron transfer processes, passing through a Mn(III) intermediate (153, 154, 163, 165). Kinetics experiments have demonstrated that this Mn(III) intermediate cannot transfer another electron to the active site. Instead, Mn oxidase are thought to enzymatically oxidize Mn(II) to Mn(III), which are then displaced from the active site as binuclear Mn(II)-Mn(III) complexes. A second Mn(II) oxidation yields a binuclear $\text{Mn(III)(}\mu\text{-OH)}_2\text{Mn(III)}$, which then disproportionates to form Mn(IV) particles and Mn(II) which is recycled back (153, 154). Trapping experiments with pyrophosphate have demonstrated that the Mn(III) intermediate is ligand labile, and may thus leak out of the system, if appropriate stabilizing ligands are available in the local organic fraction. The humic like nature of the ligands found to stabilize Mn(III) measured in marine systems (81) suggest that soil organic matter may be able to offer the stabilization that Mn(III) requires. Like in marine systems, these findings suggest that Mn(III) species may be more present in soils than that originally thought.

4.3.3 Solid-phase Mn(IV) and Mn(III) oxidative centers.

In the solid phase, while the redox chemistry Mn species is generally assumed to be governed by Mn(IV), the role of Mn(III) centers may also be underestimated. While freshly precipitated Mn oxides are mainly composed of Mn(IV), Mn(III)-enrichment of the mineral is rapidly observed [AMON of biogenic $\text{MnO}_2 \approx 3.6 - 3.7$ (55, 94, 151)]. Furthermore, Nico et al., (184, 185) reported that the oxidation of Cr(III), phenols and sulfide by a Mn(III)-enriched $\delta\text{-MnO}_2$ (AMON 3.88) was inhibited by the addition of pyrophosphate, a ligand with a high affinity for Mn(III) species. Tentative explanations of the observed inhibition included the higher reduction potential of Mn(III) relative to

Mn(IV)[$E_h^0 \text{ Mn}^{3+}/\text{Mn}^{2+} = 1.55 \text{ eV}$ and $E_h^0 \text{ Mn}^{\text{IV}}\text{O}_{2(\text{s})}/\text{Mn}(\text{II})_{(\text{aq})} = 1.23 \text{ eV}$](104, 112, 185), and the faster ligand exchange rate of Mn(III) centers relative to Mn(IV) (104, 184, 185). Considering the high redox potential of Mn(III) species (83), the kinetic mobility associated to aqueous species relative, and the lack of lattice energy that may kinetically hinder the reduction of MnO₂ at circumneutral pH, Mn(III)-L species have the potential to compete significantly with solid phase Mn oxidants. The relative importance of Mn(III) and Mn(IV) reaction sites when reacting with organic molecules is unclear and warrants further investigation.

5. OPPORTUNITY FOR COUPLED Mn AND C CYCLES IN SOILS

5.1 Stabilization interactions

5.1.1 Stabilization of organic C through organo-mineral interactions

There are two main reasons that suggest that organo-mineral interactions on the surface of MnO₂ may be more important than that expected based on surface charge considerations: the pH_{pzc} of edge sites is higher than that of basal sites (57) and layers of hydrophobic molecules accumulate on minerals with little dependence on electrostatics (31), as shown for proteins that accumulate extensively on MnO₂ surfaces (89). However, the relevance of these interactions from the point of view of C dynamics is ultimately limited by the abundance of Mn relative to C and to Fe and Al (42, 45). Furthermore, the intrinsic redox reactivity of MnO₂ means that it has the propensity to reductively dissolve, which undermines any long-term stabilization of the organic molecules on the mineral.

5.1.2 MnO₂ as a catalyst for SOM polymerization?

A number of studies have demonstrated that MnO₂ can catalyse the polymerization of a number of organic molecules commonly found in soils. These include the polymerization of polyphenols, sugars and amino acids. Because these products are chemically more stable than the starting material, these reactions were suggested to contribute to the stabilization of organic C in soils (102, 109, 114, 116-119, 186-188). However, the ‘polymer-model’ of humic substances is now widely criticised by soil scientists (2, 189, 190). Soil organic matter is more correctly described as supramolecular association formed from a continuum of different organic compounds originating from plants and biomass present in different sizes, decomposition states and “moving down a thermodynamic gradient” (2, 191). This new view is supported by the absence of an identifiable 2D-NMR signature of humic substances that could be separated from that key

biomolecule components originating from plants and biomass (proteins, polysaccharides, lignin and aliphatic biomolecules)(192). In addition, the type of reactions reported were observed over 30 – 60 days, which means their relevance in natural systems is further constrained by the residence time of the biomolecules involved. Some polymerization reactions, for example catalysed by MnO₂, may happen in soils, but low rates and yields likely render them poorly relevant in the overall C cycling in soils, in particular when occurring aside efficient enzymatically catalysed degradation reactions (189).

5.1.3 Relevance of organo-mineral interactions for the reactivity of Mn

Although organo-mineral interactions at the surface of MnO₂ may not be relevant from the perspective of the C cycle, they have profound consequences for the Mn cycle. Under the E_h and pH regimes that do not favour reductive dissolution of the oxide, organo-mineral interactions are expected to have significant impact on the reactivity of MnO₂. The sorption of organic residues on the surface of MnO₂ may passivate surface sites, slowing the diffusion of both inorganic species and potential reductant to the mineral surface, which is expected to impact both the scavenging property and redox reactivity of MnO₂ (184, 185). Furthermore, the accumulation of organic molecules on the surface of MnO₂, as multiple layers of hydrophobic molecules (2, 31), provides ideal conditions for polymerization reactions (90)(see **Section 2.3**). The surface of Mn oxides could therefore be buried underneath layers of cross-coupled organic residues. A better understanding of how organic residues interact with the mineral surface and the strength of these interactions would shed light on the relevance of this process.

5.2 Degradation interactions

5.2.1 Relevance of the catalysis of hydrolysis reactions

The depolymerisation of a number of natural organic polymers involves hydrolysis reactions. Both phosphorus and nitrogen are plants and biomass macro-nutrients. The concentration of soluble phosphorus in soils is however often low, and cells generally take up phosphate in the forms of inorganic phosphate ions (PO₄³⁻, HPO₄²⁻ or H₂PO₄⁻). While rocks are one important reservoir of phosphate in soils, organic matter is also an important source of soil phosphate. Organic phosphorus is found on the form of organo-phosphate ester molecules, and in particular as phytic acids, inositol hexophosphate ester molecules synthesised by microorganisms and plants as their principal form of phosphorus storage (193, 194). Similarly, mineralization of organic forms of nitrogen into bio-

available nitrates requires as a first step the fragmentation of proteins through hydrolysis of peptidic bonds (195).

The relevance of MnO_2 -catalyzed hydrolyses for the soil C cycling is constrained by both the intrinsic strength of hydrolytic bonds and the existence of alternative pathways for hydrolysis. Hydrolytic bonds are not excessively stable bonds, and their presence is characteristic of easily decomposable macromolecules (9, 18). Microorganisms have evolved to secrete hydrolase enzymes that catalyse specific hydrolysis reactions. However, chemically recalcitrant organic molecules, such as lignin, do not feature hydrolytic bonds but instead feature ethers, long aliphatic chains or aromatic functional groups. Baldwin et al. (139) compared the rates of hydrolysis by MnO_2 to measured enzymatic activity, and argued that MnO_2 hydrolysis could compete with the enzymatic pathways. However, in complex natural systems, the high reactivity of MnO_2 and its poor selectivity for hydrolysis reactions mean that these minerals are likely to be involved in a number of reactions, thus lowering their chances of competing with hydrolase enzymes.

5.2.2 *Circumventing the abundance limitation*

The high redox potential of MnO_2 means that these minerals have the potential to degrade a wide range of organic molecules, either directly through abiotic oxidation of the organic substrate at the surface of the mineral, or indirectly when anaerobic dissimilatory bacteria couple the oxidation of organics to the use of MnO_2 as terminal electron acceptor. However, considering the relative concentrations of soil organic molecules relative to the average Mn soil concentration, it becomes evident that for MnO_2 to have any meaningful impact on oxidative degradation of organic molecules, an efficient concomitant Mn(II)-oxidizing mechanism is required to continuously regenerate the oxidative capacity of high valent Mn species.

In this respect, cryptic cycles (84-86, 196) offer a mechanism through which MnO_2 could play a significant role in C oxidation in natural systems. Despite small total concentrations, the redox cycling of highly reactive species (e.g., Mn(III)-L) may drive important biogeochemical cycles. These cycles may remain 'cryptic' because steady-state concentrations of stable end products or intermediates may not be measurable. Cryptic biogeochemical cycles have been demonstrated for S, P and Fe in marine systems and in lake water column (85, 86). Considering its redox reactivity, the rapid recycling of high valent Mn provides the pathway through which its redox reactivity may be relevant for C

dynamics. In this sense, the recycling of Mn(III)-L maintained by the white-rot fungi (76) illustrates the *sine qua non* condition for Mn to have an impact on the C cycle.

5.3 Recommendations for future studies

From the knowledge gathered in this review regarding the reactivity of Mn towards biomolecules emerge a few major gaps of understanding. In **Table 3** we therefore summarize these knowledge gaps, and propose testable hypotheses that may help to better understand coupled C and Mn dynamics in natural systems.

Table 3 Gaps in understanding and recommendation for future studies

1) Better understanding of the rates of cycling of Mn in natural systems

Looking at steady-state concentrations of Mn(II) or Mn(IV) is insufficient to understand the biogeochemical cycling of Mn because this approach excludes the reactivity of transient Mn(III) species. Similarly, exchanges between aqueous Mn(II) and solid phase Mn(III, IV), through sorption/desorption or through partial reduction /oxidation may be missed.

To apprehend the coupling of the C and Mn in natural systems, it is therefore necessary to get a better understanding of the cycling between Mn(II), Mn(III) and Mn(IV) species. Understanding the role Mn could play in soil C dynamics requires knowledge of i) the relative importance of Mn(III) and Mn(IV) in governing Mn redox reactivity and thus to determine the rates at which high valent Mn species can react with organic molecules and ii) determine the rates at which high valent Mn species may be regenerated (see **Figure 7**). In this redox cycling, the Mn re-oxidation step is expected to be rate-determining in C-rich systems.

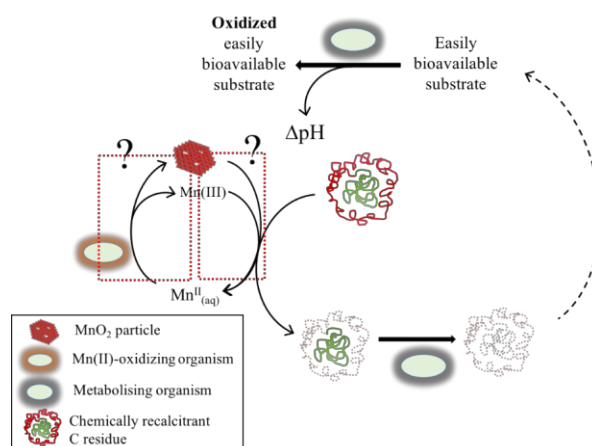


Figure 7 Schematic representation of the coupling between the redox cycling of Mn and transformation of organic residues. The question marks highlight the importance of understanding i) the relative importance of Mn(III) and Mn(IV) to govern the Mn redox reactivity and ii) the rates of regeneration of the high valent Mn species.

2) Cross-coupling of organic molecules sorbed on MnO₂ surface

On redox active minerals such as MnO₂, the self-assembly of multiple layers of heterogeneous organic molecules, as described in the zonal model (31), provide favourable conditions for cross-polymerization of these molecules. These coupling reactions imply that particles of MnO₂ may be buried under thick layers of stable molecules under conditions that do not favour the complete dissolution of the mineral. These organo-mineral interactions warrant further investigation if interested in the reactivity of these mineral in natural systems.

3) Microbial Mn oxidation as a pathway for Mn(III) generation

A few studies have highlighted the link between MnO₂ precipitation and the C content of a system [see **Chapter 4** and (182)]. Coupled to the recent recognition of the presence of Mn(III) in natural systems, this observation raises the following question: could there be a rapid cryptic cycling of Mn between Mn(II) and Mn(III) that precedes MnO₂ precipitation in C rich system, with MnO₂ precipitating only when C is sufficiently depleted? This redox cycle would be similar to the Mn redox cycle maintained by the white-rot fungi for lignin degradation (76), with the accumulation of solid-phase Mn observed on dead hyphae, when stabilising ligands are no longer provided for Mn(III) stabilization. Studies should thus investigate the conditions (pH, C-content) under which the Mn(II) oxidizing enzymes are active, and assess whether the Mn(II) oxidizing activity is necessarily correlated with MnO₂ precipitation. This hypothetical cycling of Mn(II) and Mn(III) prior to the precipitation of MnO₂ questions the relative role of Mn(III) and MnO₂ as the oxidants of choice in rapidly redox cycling systems.

4) Co-existence of MnO₂ with living microorganisms

In biogenic MnO₂ suspensions, the oxide particles co-exist with living biomass. This co-existence seems paradoxical, in light of the types of the damage to biomolecules that MnO₂ can induce (for eg: hydrolysis of peptide bond and therefore irreversible damage to proteins, oxidative degradation, see **Sections 3.1** and **3.3**). How do microorganisms protect themselves against these damages? Organo-mineral interactions may help to modulate the reactivity of the mineral particles and aid the survival of cells in close contact with MnO₂.

5) Heterogeneity of soil Mn oxides

The vast majority of the studies investigating the reactivity of MnO₂ are laboratory-based, using suspensions of synthetic δ -MnO₂ (93, 172) or biogenic MnO₂ obtained from model Mn(II)-oxidizers (bacteria and fungi)(146, 149). However the reactivity of naturally-occurring, mixed-valent Mn oxides, which often contain various concentrations of impurities and/or co-occur with other mineral phases such as Fe oxides, is expected to differ from that of pure, well-characterised Mn oxide phases. Furthermore, the occurrence of Mn oxides in nodules or its co-occurrence with Fe in ferromanganese nodules and concretions may significantly affect the pathways of interaction with organic molecules. For example, the bury of some Mn oxide crystallites within the nodule may diminish its reactivity towards the soil solution relative to dispersed particles, and the co-existence with Fe oxides may enhance the chances of Mn of interacting with organic molecules. There is therefore a need to better understand how to integrate the heterogeneity of soil Mn oxides into existing knowledge based on well-characterised oxides.

6) Field measurements of Mn distribution

Ultimately, the impact Mn can have on its ecosystem is limited by its abundance. Field-based studies of Mn reactivity are scarce, with Mn literature largely dominated by laboratory-based studies. While these studies allow to grasp the complexity of Mn reactivity, there is a need to better understand the occurrence and distribution of Mn in the field.

REFERENCES

1. Horwath W. Carbon cycling: the dynamics and formation of organic matter. *Soil Microbiol. Ecol. Biochem.*, 2015; 4:339-82.
2. Sutton R, Sposito G. Molecular structure in soil humic substances: the new view. *Environ. Sci. Technol.*, 2005; 39(23):9009-15.
3. Eswaran H, Van Den Berg E, Reich P. Organic carbon in soils of the world. *Soil Sci. Soc. Am. J.*, 1993;57(1):192-4.
4. Sollins P, Homann P, Caldwell BA. Stabilization and destabilization of soil organic matter: mechanisms and controls. *Geoderma*. 1996;74(1-2):65-105.
5. Alexander M. Biodegradation: problems of molecular recalcitrance and microbial fallibility. *Adv. Applied Microbiol.*, 7: Elsevier; 1965. p. 35-80.
6. Parton WJ, Ojima DS, Cole CV, Schimel DS. A general model for soil organic matter dynamics: sensitivity to litter chemistry, texture and management. *Quantitative modeling of soil forming processes*. 1994:147-67.
7. Kleber M. What is recalcitrant soil organic matter? *Environmental Chemistry*. 2010;7(4):320-32.
8. Schmidt MWI, Torn MS, Abiven S, Dittmar T, Guggenberger G, Janssens IA, et al. Persistence of soil organic matter as an ecosystem property. *Nature*. 2011;478(7367):49-56.

9. Lützow Mv, Kögel-Knabner I, Ekschmitt K, Matzner E, Guggenberger G, Marschner B, et al. Stabilization of organic matter in temperate soils: mechanisms and their relevance under different soil conditions—a review. *Europ. J. Soil Sci.*, 2006; 57(4):426-45.
10. Dungait JA, Hopkins DW, Gregory AS, Whitmore AP. Soil organic matter turnover is governed by accessibility not recalcitrance. *Global Change Biol.*, 2012;18(6):1781-96.
11. Mikutta R, Kleber M, Torn MS, Jahn R. Stabilization of soil organic matter: association with minerals or chemical recalcitrance? *Biogeochem.*, 2006;77(1):25-56.
12. Keil R, Mayer L. 12.12-Mineral matrices and organic matter. 2014.
13. Kleber M, Eusterhues K, Keiluweit M, Mikutta C, Mikutta R, Nico PS. Chapter One-Mineral–Organic Associations: Formation, Properties, and Relevance in Soil Environments., *Adv. Agron.*, 2015;130:1-140.
14. Kögel-Knabner I, and W. Amelung. Dynamics, Chemistry, and Preservation of Organic Matter in Soils., editor. *Treatise on Geochemistry. Second Edition ed*: Oxford: Elsevier; 2014. p. pp. 157-215.
15. Kögel-Knabner I, Kleber, M. Mineralogical, Physicochemical, and Microbiological Controls on Soil Organic Matter Stabilization and Turnover. *Handbook of Soil Science Resource Management and Environmental Impacts*. 2nd ed 2011.
16. Kögel-Knabner I, Guggenberger G, Kleber M, Kandeler E, Kalbitz K, Scheu S, et al. Organo-mineral associations in temperate soils: Integrating biology, mineralogy, and organic matter chemistry. *J. Plant Nut. Soil Sci.*, 2008;171(1):61-82.
17. Kleber M, Mikutta R, Torn M, Jahn R. Poorly crystalline mineral phases protect organic matter in acid subsoil horizons. *Europ. J. Soil Sci.*, 2005;56(6):717-25.
18. Keiluweit M, Nico PS, Kleber M, Fendorf S. Are oxygen limitations under recognized regulators of organic carbon turnover in upland soils? *Biogeochem.*, 1-15.
19. Tisdall JM, Oades JM. Organic matter and water-stable aggregates in soils. *Europ. J. Soil Sci.*, 1982;33(2):141-63.
20. Oades JM. Soil organic matter and structural stability: mechanisms and implications for management. *Biological Processes and Soil Fertility*: Springer; 1984. p. 319-37.
21. Six J, Bossuyt H, Degryze S, Denef K. A history of research on the link between (micro) aggregates, soil biota, and soil organic matter dynamics. *Soil and Tillage Research*. 2004;79(1):7-31.
22. Murphy EM, Zachara JM, Smith SC. Influence of mineral-bound humic substances on the sorption of hydrophobic organic compounds., *Environ. Sci. Technol.*, 1990;24(10):1507-16.
23. Chorover J, Amistadi MK. Reaction of forest floor organic matter at goethite, birnessite and smectite surfaces. *Geochim Cosmochim Ac.* 2001;65(1):95-109.
24. Eusterhues K, Rumpel C, Kögel-Knabner I. Organo-mineral associations in sandy acid forest soils: importance of specific surface area, iron oxides and micropores. *Europ. J. Soil Sci.*, 2005;56(6):753-63.
25. Mayer L. Extent of coverage of mineral surfaces by organic matter in marine sediments. *Geochim Cosmochim Ac.* 1999;63(2):207-15.
26. Mayer LM, Xing B. Organic matter–surface area relationships in acid soils. *Soil Sci. Soc. Am. J.*. 2001;65(1):250-8.
27. Ransom B, Kim D, Kastner M, Wainwright S. Organic matter preservation on continental slopes: importance of mineralogy and surface area. *Geochim Cosmochim Ac.* 1998;62(8):1329-45.
28. Mayer LM. Surface area control of organic carbon accumulation in continental shelf sediments. *Geochim Cosmochim Ac.* 1994;58(4):1271-84.
29. Guo M, Chorover J. Transport and fractionation of dissolved organic matter in soil columns. *Soil Sci.*, 2003; 168(2): 108-18.

30. Meier M, Namjesnik-Dejanovic K, Maurice PA, Chin Y-P, Aiken GR. Fractionation of aquatic natural organic matter upon sorption to goethite and kaolinite. *Chem Geol.* 1999;157(3):275-84.
31. Kleber M, Sollins P, Sutton R. A conceptual model of organo-mineral interactions in soils: self-assembly of organic molecular fragments into zonal structures on mineral surfaces. *Biogeochem.*, 2007;85(1):9-24.
32. Morgan JJ. Manganese in natural waters and earth's crust: Its availability to organisms. Metal ions in biological systems. 2000;37:1-34.
33. Post JE. Manganese oxide minerals: Crystal structures and economic and environmental significance. *Proc. Nat. Acad. Sci.*, 1999;96(7):3447-54.
34. Spiro TG, Bargar JR, Sposito G, Tebo BM. Bacteriogenic manganese oxides. *Accounts of chemical research.* 2009;43(1):2-9.
35. Villalobos M, Bargar J, Sposito G. Mechanisms of Pb (II) sorption on a biogenic manganese oxide. *Environ. Sci. Technol.*, 2005;39(2):569-76.
36. Manceau A, Lanson B, Drits VA. Structure of heavy metal sorbed birnessite. Part III: Results from powder and polarized extended X-ray absorption fine structure spectroscopy. *Geochim Cosmochim Ac.* 2002;66(15):2639-63.
37. Grangeon S, Manceau A, Guilhermet J, Gaillot A-C, Lanson M, Lanson B. Zn sorption modifies dynamically the layer and interlayer structure of vernadite. *Geochim Cosmochim Ac.* 2012;85:302-13.
38. Peña. Contaminant Metal Immobilization by Biogenic Manganese Oxide Nanoparticles: Implications for Natural Attenuation and Bioremediation (Dissertation). 2009.
39. Peña J, Kwon KD, Refson K, Bargar JR, Sposito G. Mechanisms of nickel sorption by a bacteriogenic birnessite. *Geochim Cosmochim Ac.* 2010;74(11):3076-89.
40. van Genuchten CM, Peña J. Sorption selectivity of birnessite particle edges: a d-PDF analysis of Cd(II) and Pb(II) sorption by δ -MnO₂ and ferrihydrite. *Environ. Sci. Process Impacts.*, 2016.
41. Ehrlich HL, Newman DK, Kappler A. Ehrlich's geomicrobiology: CRC press; 2015.
42. Shacklette HT, Boerngen JG. Element concentrations in soils and other surficial materials of the conterminous United States. 1984.
43. Bricker O. Some stability relations in system MnO₂-H₂O at 25 degrees and 1 atmosphere total pressure. *Am. Mineral.*, 1965;50(9):1296-.
44. Luther GW. *Inorganic Chemistry for Geochemistry and Environmental Sciences: Fundamentals and Applications*: John Wiley & Sons; 2016.
45. Sposito G. *The chemistry of soils*: Oxford university press; 2008.
46. Gorski CA, Edwards R, Sander M, Hofstetter TB, Stewart SM. Thermodynamic characterization of iron oxide-aqueous Fe²⁺ redox couples. *Environ. Sci. Technol.*, 2016;50(16):8538-47.
47. McKenzie R. The adsorption of lead and other heavy metals on oxides of manganese and iron. *Soil Research.* 1980;18(1):61-73.
48. Manceau A, Charlet L, Boisset M, Didier B, Spadini L. Sorption and speciation of heavy metals on hydrous Fe and Mn oxides. From microscopic to macroscopic. *App. Clay Sci.*, 1992;7(1-3):201-23.
49. Tani Y, Ohashi M, Miyata N, Seyama H, Iwahori K, Soma M. Sorption of Co (II), Ni (II), and Zn (II) on biogenic manganese oxides produced by a Mn-oxidizing fungus, strain KR21-2. *J. Environ Sci. Health., Part A.* 2004;39(10):2641-60.
50. Toner B, Manceau A, Webb SM, Sposito G. Zinc sorption to biogenic hexagonal-birnessite particles within a hydrated bacterial biofilm. *Geochim Cosmochim Ac.* 2006;70(1):27-43.
51. Zhu M, Ginder-Vogel M, Sparks DL. Ni (II) sorption on biogenic Mn-oxides with varying Mn octahedral layer structure. *Environ. Sci. Technol.*, 2010;44(12):4472-8.
52. Zhao W, Wang QQ, Liu F, Qiu GH, Tan WF, Feng XH. Pb²⁺ adsorption on birnessite affected by Zn²⁺ and Mn²⁺ pretreatments. *Journal of Soils and Sediments.* 2010;10(5):870-8.

53. Peña J, Bargar JR, Sposito G. Role of bacterial biomass in the sorption of Ni by biomass-birnessite assemblages. *Environ. Sci. Technol.*, 2011;45(17):7338-44.
54. Kwon KD, Refson K, Sposito G. Understanding the trends in transition metal sorption by vacancy sites in birnessite. *Geochim Cosmochim Ac.* 2013;101:222-32.
55. Droz B, Dumas N, Duckworth OW, Pena J. A comparison of the sorption reactivity of bacteriogenic and mycogenic Mn oxides nanoparticles. *Environ. Sci. Technol.*, 2015.
56. Simanova AA, Kwon KD, Bone SE, Bargar JR, Refson K, Sposito G, et al. Probing the sorption reactivity of the edge surfaces in birnessite nanoparticles using Nickel (II). *Geochim Cosmochim Ac.* 2015;164:191-204.
57. Villalobos M. The role of surface edge sites in metal(loid) sorption to poorly-crystalline birnessites. *Advances in the Environmental Biogeochemistry of Manganese Oxides: ACS Publications*; 2015. p. 65-87.
58. Remucal CK, Ginder-Vogel M. A critical review of the reactivity of manganese oxides with organic contaminants. *Environ. Sci. Process. Impacts*, 2014;16(6):1247-66.
59. Stone AT. The reduction and dissolution of Mn (III) and Mn (IV) oxides by organics. 1983.
60. Stone AT, Morgan JJ. Reduction and Dissolution of Manganese(III) and Manganese(IV) Oxides by Organics 1. Reaction with Hydroquinone. *Environ. Sci. Technol.*, 1984;18(6):450-6.
61. Stone AT, Morgan JJ. Reduction and dissolution of manganese (III) and manganese (IV) oxides by organics. Part 2. Survey of the reactivity of organics. *Environ Sci Technol.* 1984;18(8).
62. Stone AT. Microbial Metabolites and the Reductive Dissolution of Manganese Oxides - Oxalate and Pyruvate. *Geochim Cosmochim Ac.* 1987;51(4):919-25.
63. Stone AT. Reductive dissolution of manganese(III/IV) oxides by substituted phenols. *Environ. Sci. Technol.*, 1987;21(10):979-88.
64. Stone AT, Ulrich H-J. Kinetics and reaction stoichiometry in the reductive dissolution of Mn(IV) dioxide and Co(III) oxide by hydroquinone. *J. Coll. Interf. Sci.*, 1989;132(2):509-22.
65. Toner B, Sposito G. Reductive dissolution of biogenic manganese oxides in the presence of a hydrated biofilm. *Geomicrobiol J.* 2005;22(3-4):171-80.
66. Wang Y, Stone AT. The citric acid–Mn^{III},IVO₂(birnessite) reaction. Electron transfer, complex formation, and autocatalytic feedback. *Geochim Cosmochim Ac.* 2006;70(17):4463-76.
67. Wang Y, Stone AT. Reaction of Mn^{III},^{IV} (hydr)oxides with oxalic acid, glyoxylic acid, phosphonoformic acid, and structurally-related organic compounds. *Geochim Cosmochim Ac.* 2006;70(17):4477-90.
68. Sunda WG, Kieber DJ. Oxidation of humic substances by manganese oxides yields low-molecular-weight organic substrates, *Nature*, 1994.
69. Allard S, Gutierrez L, Fontaine C, Croué J-P, Gallard H. Organic matter interactions with natural manganese oxide and synthetic birnessite. *Sci. Tot. Environ.*, 2017;583:487-95.
70. Murray JW. The surface chemistry of hydrous manganese dioxide. *J. Coll. Interf. Sci.*, 1974;46(3):357-71.
71. Toner B, Fakra S, Villalobos M, Warwick T, Sposito G. Spatially resolved characterization of biogenic manganese oxide production within a bacterial biofilm. *App. Environ. Microbiol.*, 2005;71(3):1300-10.
72. Nelson YM, Lion LW, Shuler ML, Ghiorse WC. Lead binding to metal oxide and organic phases of natural aquatic biofilms. *Limnology and Oceanography*. 1999;44(7):1715-29.
73. Flemming H-C, Wingender J. The biofilm matrix. *Nature Reviews Microbiology*. 2010;8(9):623-33.
74. Berg B, Steffen K, McLaugherty C. Litter decomposition rate is dependent on litter Mn concentrations. *Biogeochem.*, 2007;82(1):29-39.
75. Davey MP, Berg B, Emmett BA, Rowland P. Decomposition of oak leaf litter is related to initial litter Mn concentrations. *Botany*. 2007;85(1):16-24.
76. Keiluweit M, Nico P, Harmon ME, Mao J, Pett-Ridge J, Kleber M. Long-term litter decomposition controlled by manganese redox cycling. *Proc. Nat. Acad. Sci.*, 2015;112(38):E5253-E60.

77. Hofrichter M. Review: lignin conversion by manganese peroxidase (MnP). *Enzyme and Microbial technology*. 2002;30(4):454-66.
78. Trouwborst RE, Clement BG, Tebo BM, Glazer BT, Luther GW. Soluble Mn (III) in suboxic zones. *Science*. 2006;313(5795):1955-7.
79. Madison AS, Tebo BM, Mucci A, Sundby B, Luther GW. Abundant porewater Mn (III) is a major component of the sedimentary redox system. *science*. 2013;341(6148):875-8.
80. Oldham VE, Owings SM, Jones MR, Tebo BM, Luther GW. Evidence for the presence of strong Mn (III)-binding ligands in the water column of the Chesapeake Bay. *Marine Chem.*, 2015;171:58-66.
81. Oldham VE, Mucci A, Tebo BM, Luther GW. Soluble Mn (III)-L complexes are abundant in oxygenated waters and stabilized by humic ligands. *Geochim Cosmochim Ac.* 2017;199:238-46.
82. Johnson KS. Manganese redox chemistry revisited. *Science*. 2006;313(5795):1896-7.
83. Kostka JE, Luther GW, Nealson KH. Chemical and biological reduction of Mn (III)-pyrophosphate complexes: potential importance of dissolved Mn (III) as an environmental oxidant. *Geochim Cosmochim Ac.* 1995;59(5):885-94.
84. Hansel CM, Ferdelman TG, Tebo BM. Cryptic cross-linkages among biogeochemical cycles: novel insights from reactive intermediates. *Elements*. 2015;11(6):409-14.
85. Berg JS, Michellod D, Pjevac P, Martinez-Perez C, Buckner CR, Hach PF, et al. Intensive cryptic microbial iron cycling in the low iron water column of the meromictic Lake Cadagno. *Environ. Microbiol.*, 2016;18(12):5288-302.
86. Kappler A, Bryce C. Cryptic biogeochemical cycles: unravelling hidden redox reactions. *Environ. Microbiol.*, 2017;19(3):842-6.
87. Tipping E. The adsorption of aquatic humic substances by iron oxides. *Geochim Cosmochim Ac.* 1981;45(2):191-9.
88. Tipping E, Heaton M. The adsorption of aquatic humic substances by two oxides of manganese. *Geochim Cosmochim Ac.* 1983;47(8):1393-7.
89. Estes E, Andeer P, Nordlund D, Wankel S, Hansel C. Biogenic manganese oxides as reservoirs of organic carbon and proteins in terrestrial and marine environments. *Geobiol.*, 2017;15(1):158-72.
90. Johnson K, Purvis G, Lopez-Capel E, Peacock C, Gray N, Wagner T, et al. Towards a mechanistic understanding of carbon stabilization in manganese oxides. *Nature Comm.*, 2015;6.
91. Lopez-Sangil L, Rovira P. Sequential chemical extractions of the mineral-associated soil organic matter: An integrated approach for the fractionation of organo-mineral complexes. *Soil Biol. Biochem.*, 2013;62:57-67.
92. Kaiser K, Guggenberger G. Mineral surfaces and soil organic matter. *Europ. J. Soil Sci.*, 2003;54(2):219-36.
93. Marafatto FF, B. Lanson and J. Peña. Crystal growth and aggregation in suspensions of δ -MnO₂ nanoparticles: Implications for surface reactivity. In press *Environ. Sci. Nano.*, 2017.
94. Tebo BM, Bargar JR, Clement BG, Dick GJ, Murray KJ, Parker D, et al. Biogenic manganese oxides: properties and mechanisms of formation. *Annu Rev Earth Planet Sci.* 2004;32:287-328.
95. Peña J, Bargar JR, Sposito G. Copper sorption by the edge surfaces of synthetic birnessite nanoparticles. *Chem Geol.* 2015;396:196-207.
96. Villalobos M, Lanson B, Manceau A, Toner B, Sposito G. Structural model for the biogenic Mn oxide produced by *Pseudomonas putida*. *Am. Mineral.*, 2006;91(4):489-502.
97. Grangeon S, Lanson B, Lanson M, Manceau A. Crystal structure of Ni-sorbed synthetic vernadite: a powder X-ray diffraction study. *Mineralogical Magazine*. 2008;72(6):1279-91.
98. Sollins P, Swanston C, Kleber M, Filley T, Kramer M, Crow S, et al. Organic C and N stabilization in a forest soil: evidence from sequential density fractionation. *Soil Biol. Biochem.*, 2006;38(11):3313-24.

99. Majcher EH, Chorover J, Bollag J-M, Huang P. Evolution of CO during birnessite-induced oxidation of C-Labeled catechol. *Soil Sci. Soc. Am. J.*, 2000;64(1):157-63.
100. Matocha CJ, Sparks DL, Amonette JE, Kukkadapu RK. Kinetics and mechanism of birnessite reduction by catechol. *Soil Sci. Soc. Am. J.*, 2001;65(1):58-66.
101. Ahn M-Y, Martínez CE, Archibald DD, Zimmerman AR, Bollag J-M, Dec J. Transformation of catechol in the presence of a laccase and birnessite. *Soil Biol. Biochem.*, 2006;38(5):1015-20.
102. Chien SC, Chen H, Wang M, Sessaiah K. Oxidative degradation and associated mineralization of catechol, hydroquinone and resorcinol catalyzed by birnessite. *Chemosphere*. 2009;74(8):1125-33.
103. Li C, Zhang B, Ertunc T, Schaeffer A, Ji R. Birnessite-induced binding of phenolic monomers to soil humic substances and nature of the bound residues. *Environ. Sci. Technol.*, 2012;46(16):8843-50.
104. Ukrainczyk L, McBride MB. Oxidation of phenol in acidic aqueous suspensions of manganese oxides. *Clays and Clay Minerals*. 1992;40(2):157-66.
105. Hättenschwiler S, Vitousek PM. The role of polyphenols in terrestrial ecosystem nutrient cycling. *Trends Ecol. Evol.*, 2000;15(6):238-43.
106. Hättenschwiler S, Hagerman A, Vitousek P. Polyphenols in litter from tropical montane forests across a wide range in soil fertility. *Biogeochemistry*. 2003;64(1):129.
107. Coulson C, Davies R, Lewis D. Polyphenols in plant, humus, and soil. *Europ. J. Soil Sci.*, 1960;11(1):30-44.
108. Constantinides M, Fownes J. Nitrogen mineralization from leaves and litter of tropical plants: relationship to nitrogen, lignin and soluble polyphenol concentrations. *Soil Biology and Biochemistry*. 1994;26(1):49-55.
109. Hardie A, Dynes J, Kozak L, Huang P. The role of glucose in abiotic humification pathways as catalyzed by birnessite. *Journal of Molecular Catalysis A: Chemical*. 2009;308(1):114-26.
110. Maillard L. Formation de matieres humiques par action de polypeptides sur sucres. *CR Acad Sci*. 1913;156:148-9.
111. Clayden J, Greeves N, Warren S, Wothers P. *Organic Chemistry*: Oxford University Press; 2001.
112. Jenkins S. *CRC Handbook of Chemistry and Physics*. Chemical Engineering. 2012;119(9):9-10.
113. Martins SI, Jongen WM, Van Boekel MA. A review of Maillard reaction in food and implications to kinetic modelling. *Trends Food Sci. Technol.*, 2000;11(9):364-73.
114. Jokic A, Frenkel A, Vairavamurthy M, Huang P. Birnessite catalysis of the Maillard reaction: Its significance in natural humification. *Geophysical Research Letters*. 2001;28(20):3899-902.
115. Jokic A, Wang M, Liu C, Frenkel A, Huang P. Integration of the polyphenol and Maillard reactions into a unified abiotic pathway for humification in nature: the role of δ -MnO₂. *Org Geochem*. 2004;35(6):747-62.
116. Jokic A, Frenkel A, Huang P. Effect of light on birnessite catalysis of the Maillard reaction and its implication in humification. *Canadian J Soil Sci.*, 2001;81(3):277-83.
117. Huang P, Hardie A. Formation mechanisms of humic substances in the environment. *Biophysico-Chemical Processes Involving Natural Nonliving Organic Matter in Environmental Systems* (Eds N Senesi, B Xing, PM Huang). 2009:41-109.
118. Hardie A, Dynes J, Kozak L, Huang P. Influence of polyphenols on the intergrated polyphenol-Maillard reaction: humification pathways as catalysed by birnessite. *Ann. Environ. Sci.*, 2007.
119. Hardie AG, Dynes JJ, Kozaka LM, Huang PM. Abiotic catalysis of the maillard and polyphenol-maillard humification pathways by soil clays from temperate and tropical environments. *Molecular Environmental Soil Science at the Interfaces in the Earth's Critical Zone*: Springer; 2010. p. 26-8.
120. Semenov V, Tulina A, Semenova N, Ivannikova L. Humification and nonhumification pathways of the organic matter stabilization in soil: A review. *Eurasian Soil Sci.*, 2013;46(4):355-68.
121. Luther III GW. Manganese (II) oxidation and Mn (IV) reduction in the environment—two one-electron transfer steps versus a single two-electron step. *Geomicrobiol J*. 2005;22(3-4):195-203.

122. Xyla AG, Sulzberger B, Luther III GW, Hering JG, Van Cappellen P, Stumm W. Reductive dissolution of manganese (III, IV)(hydr)oxides by oxalate: The effect of pH and light. *Langmuir*. 1992;8(1):95-103.
123. Zhang H, Chen W-R, Huang C-H. Kinetic modeling of oxidation of antibacterial agents by manganese oxide. *Environ. Sci. Technol.*, 2008;42(15):5548-54.
124. Stumm W. Reactivity at the mineral-water interface: dissolution and inhibition. *Colloids and Surfaces A: Physicochemical and Engineering Aspects*. 1997;120(1):143-66.
125. Grassian VH. *Environmental catalysis*: CRC press; 2005.
126. Wang Y, Stone AT. The citric acid–Mn^{III},^{IV}O₂ (birnessite) reaction. Electron transfer, complex formation, and autocatalytic feedback. *Geochim Cosmochim Ac*. 2006;70(17):4463-76.
127. Furlani G, Pagnanelli F, Toro L. Reductive acid leaching of manganese dioxide with glucose: identification of oxidation derivatives of glucose. *Hydrometallurgy*. 2006;81(3):234-40.
128. Maslak P, Asel SL. ESR investigation of carbon-carbon bond cleavage in radical cations. *Journal of the American Chemical Society*. 1988;110(24):8260-1.
129. Wariishi H, Valli K, Gold MH. Oxidative cleavage of a phenolic diarylpropane lignin model dimer by manganese peroxidase from *Phanerochaete chrysosporium*. *Biochemistry*. 1989;28(14):6017-23.
130. Ten Have R, Teunissen PJ. Oxidative mechanisms involved in lignin degradation by white-rot fungi. *Chemical reviews*. 2001;101(11):3397-414.
131. Tuor U, Wariishi H, Schoemaker HE, Gold MH. Oxidation of phenolic arylglycerol. beta.-aryl ether lignin model compounds by manganese peroxidase from *Phanerochaete chrysosporium*: oxidative cleavage of an. alpha.-carbonyl model compound. *Biochemistry*. 1992;31(21):4986-95.
132. Valli K, Brock BJ, Joshi DK, Gold M. Degradation of 2, 4-dinitrotoluene by the lignin-degrading fungus *Phanerochaete chrysosporium*. *Applied Environ. Microbiol.*, 1992;58(1):221-8.
133. Ziegenhagen D, Hofrichter M. Degradation of humic acids by manganese peroxidase from the white-rot fungus *Clitocybula dusenii*. *J. Basic Microbiol.*, 1998;38(4):289-99.
134. Van Aken B, Hofrichter M, Scheibner K, Hatakka AI, Naveau H, Agathos SN. Transformation and mineralization of 2, 4, 6-trinitrotoluene (TNT) by manganese peroxidase from the white-rot basidiomycete *Phlebia radiata*. *Biodegradation*. 1999;10(2):83-91.
135. Mitchell MB, Sheinker V, Mintz EA. Adsorption and decomposition of dimethyl methylphosphonate on metal oxides. *J. Phys. Chem. B.*, 1997;101(51):11192-203.
136. Hoffmann M, Stumm W. *Aquatic Chemical Kinetics: Reaction Rates of Processes in Natural Waters*. Wiley, New York; 1990.
137. Stone AT. Enhanced rates of monophenyl terephthalate hydrolysis in aluminum oxide suspensions. *J. Col. Interf. Sci.*, 1989; 127(2):429-41.
138. Gschwend PM. *Environmental organic chemistry*: John Wiley & Sons; 2016.
139. Baldwin DS, Beattie JK, Coleman LM, Jones DR. Hydrolysis of an organophosphate ester by manganese dioxide. *Environ. Sci. Technol.*, 2001;35(4):713-6.
140. Baldwin DS, Beattie JK, Jones DR. Hydrolysis of an organic phosphorus compound by iron-oxide impregnated filter papers. *Water Research*. 1996;30(5):1123-6.
141. Inman MP, Beattie JK, Jones DR, Baldwin DS. Abiotic hydrolysis of the detergent builder tripolyphosphate by hydrous manganese dioxide. *Water Research.*, 2001;35(8):1987-93.
142. Reardon PN, Chacon SS, Walter ED, Bowden ME, Washton NM, Kleber MW. Abiotic protein fragmentation by manganese oxide: implications for a mechanism to supply soil biota with oligopeptides. *Environ. Sci. Technol.*, 2016; 50.

143. Andersen A, Reardon PN, Chacon SS, Qafoku NP, Washton NM, Kleber M. Protein–Mineral Interactions: Molecular Dynamics Simulations Capture Importance of Variations in Mineral Surface Composition and Structure. *Langmuir*. 2016;32(24):6194-209.
144. Lovley DR, Phillips EJ. Novel mode of microbial energy metabolism: organic carbon oxidation coupled to dissimilatory reduction of iron or manganese. *Applied Environ. Microbiol.*, 1988;54(6):1472-80.
145. Myers C, Nealson KH. Bacterial manganese reduction and growth with manganese oxide as the sole electron acceptor. *Science*. 1988;240(4857):1319-21.
146. De Schampelaire L, Rabaey K, Boon N, Verstraete W, Boeckx P. Minireview: The potential of enhanced manganese redox cycling for sediment oxidation. *Geomicrobiol J.*, 2007;24(7-8):547-58.
147. Lovley DR, Holmes DE, Nevin KP. Dissimilatory Fe(III) and Mn(IV) reduction. *Adv. Microb. Physiol.*, 2004;49:219-86.
148. Thamdrup B. Bacterial manganese and iron reduction in aquatic sediments. *Advances in microbial ecology*: Springer; 2000. p. 41-84.
149. Tebo BM, Johnson HA, McCarthy JK, Templeton AS. Geomicrobiology of manganese (II) oxidation. *Trends in Microbiology*. 2005;13(9):421-8.
150. Tebo BM, Clement BG, Dick GJ. Biotransformations of manganese. *Manual Environ. Microbiol.*, 2007;3:1223-38.
151. Santelli CM, Webb SM, Dohnalkova AC, Hansel CM. Diversity of Mn oxides produced by Mn(II)-oxidizing fungi. *Geochim Cosmochim Ac.* 2011;75(10):2762-76.
152. Butterfield CN, Soldatova AV, Lee S-W, Spiro TG, Tebo BM. Mn (II, III) oxidation and MnO₂ mineralization by an expressed bacterial multicopper oxidase. *Proc. Nat. Acad. Sci.*, 2013;110(29):11731-5.
153. Soldatova AV, Romano CA, Tao L, Stich TA, Casey WH, Britt RD, et al. Mn (II) oxidation by the multicopper oxidase complex Mnx: A coordinated two-stage Mn (II)/(III) and Mn (III)/(IV) mechanism. *J. Am. Chem. Soc.*, 2017; 139(33): 11381-91.
154. Soldatova AV, Tao L, Romano CA, Stich TA, Casey WH, Britt RD, et al. Mn (II) oxidation by the multicopper oxidase complex Mnx: A binuclear activation mechanism. *J. Am. Chem. Soc.*, 2017;139(33):11369-80.
155. Geszvain K, Tebo BM. Identification of a two-component regulatory pathway essential for Mn (II) oxidation in *Pseudomonas putida* GB-1. *Applied Environ. Microbiol.*, 2010;76(4):1224-31.
156. Geszvain K, McCarthy JK, Tebo BM. Elimination of manganese (II, III) oxidation in *Pseudomonas putida* GB-1 by a double knockout of two putative multicopper oxidase genes. *Applied Environ. Microbiol.*, 2013;79(1):357-66.
157. Geszvain K, Smesrud L, Tebo BM. Identification of a third Mn (II) oxidase enzyme in *Pseudomonas putida* GB-1. *Applied Environ. Microbiol.*, 2016;82(13):3774-82.
158. Wright MH, Geszvain K, Oldham VE, Luther III GW, Tebo BM. Oxidative Formation and Removal of Complexed Mn (III) by *Pseudomonas* Species. *Front. Microbiol.*, 2018;9:560.
159. Hansel CM, Francis CA. Coupled photochemical and enzymatic Mn (II) oxidation pathways of a planktonic *Roseobacter*-like bacterium. *Applied Environ. Microbiol.*, 2006;72(5):3543-9.
160. Learman D, Voelker B, Vazquez-Rodriguez A, Hansel C. Formation of manganese oxides by bacterially generated superoxide. *Nature Geosci.*, 2011;4(2):95.
161. Andeer PF, Learman DR, McIlvin M, Dunn JA, Hansel CM. Extracellular haem peroxidases mediate Mn (II) oxidation in a marine *Roseobacter* bacterium via superoxide production. *Environ. Microbiol.*, 2015;17(10):3925-36.
162. Hansel CM, Zeiner CA, Santelli CM, Webb SM. Mn (II) oxidation by an ascomycete fungus is linked to superoxide production during asexual reproduction. *Proc. Nat. Acad. Sci.*, 2012;109(31):12621-5.
163. Geszvain K, Butterfield C, Davis RE, Madison AS, Lee S-W, Parker DL, et al. The molecular biogeochemistry of manganese (II) oxidation. Portland Press Limited; 2012.

164. Butterfield CN, Tebo BM. Substrate specificity and copper loading of the manganese-oxidizing multicopper oxidase Mnx from *Bacillus* sp. PL-12. *Metallomics*. 2017;9(2):183-91.
165. Webb SM, Dick GJ, Bargar JR, Tebo BM. Evidence for the presence of Mn(III) intermediates in the bacterial oxidation of Mn(II). *Proc. Nat. Acad. Sci.*, 2005;102(15):5558-63.
166. Schlosser D, Höfer C. Laccase-catalyzed oxidation of Mn²⁺ in the presence of natural Mn³⁺ chelators as a novel source of extracellular H₂O₂ production and its impact on manganese peroxidase. *Applied Environ. Microbiol.*, 2002; 68(7):3514-21.
167. Höfer C, Schlosser D. Novel enzymatic oxidation of Mn²⁺ to Mn³⁺ catalyzed by a fungal laccase. *FEBS letters*. 1999;451(2):186-90.
168. Learman D, Wankel S, Webb S, Martinez N, Madden A, Hansel C. Coupled biotic–abiotic Mn (II) oxidation pathway mediates the formation and structural evolution of biogenic Mn oxides. *Geochim Cosmochim Ac.* 2011;75(20):6048-63.
169. Templeton A, Knowles E. Microbial transformations of minerals and metals: recent advances in geomicrobiology derived from synchrotron-based X-ray spectroscopy and X-ray microscopy. *Annual Rev. Earth Planet. Sci.*, 2009;37:367-91.
170. Dixon J, White N. Soil mineralogy with environmental applications. In: Dixon JB, Schulze DG, *Soil Sci. Soc. Am.*, 2002.
171. Webb S, Tebo B, Bargar J. Structural characterization of biogenic Mn oxides produced in seawater by the marine *Bacillus* sp. strain SG-1. *Am. Mineral.*, 2005;90(8-9):1342-57.
172. Villalobos M, Toner B, Bargar J, Sposito G. Characterization of the manganese oxide produced by *Pseudomonas putida* strain MnB1. *Geochim. Cosmochim. Ac.*, 2003;67(14):2649-62.
173. Mandernack KW, Post J, Tebo BM. Manganese mineral formation by bacterial spores of the marine *Bacillus*, strain SG-1: Evidence for the direct oxidation of Mn (II) to Mn (IV). *Geochim Cosmochim Ac.* 1995;59(21):4393-408.
174. Bargar JR, Tebo BM, Bergmann U, Webb SM, Glatzel P, Chiu VQ, et al. Biotic and abiotic products of Mn (II) oxidation by spores of the marine *Bacillus* sp. strain SG-1. *Am. Mineral.* 2005;90(1):143-54.
175. Elzinga EJ. Reductive transformation of birnessite by aqueous Mn(II). *Environ. Sci. Technol.*, 2011;45(15):6366-72.
176. Lefkowitz JP, Rouff AA, Elzinga EJ. Influence of pH on the reductive transformation of birnessite by aqueous Mn (II). *Environ. Sci. Technol.*, 2013;47(18):10364-71.
177. Zhao H, Zhu M, Li W, Elzinga EJ, Villalobos M, Liu F, et al. Redox reactions between Mn (II) and hexagonal birnessite change its layer symmetry. *Environ. Sci. Technol.*, 2016;50(4):1750-8.
178. Manceau A, Tamura N, Celestre RS, MacDowell AA, Geoffroy N, Sposito G, et al. Molecular-scale speciation of Zn and Ni in soil ferromanganese nodules from loess soils of the Mississippi Basin. *Environ. Sci. Technol.*, 2003;37(1):75-80.
179. Gasparatos D, Tarenidis D, Haidouti C, Oikonomou G. Microscopic structure of soil Fe-Mn nodules: environmental implication. *Environmental Chemistry Letters*. 2005;2(4):175-8.
180. Rennert T, Händel M, Höschen C, Lugmeier J, Steffens M, Totsche K. A NanoSIMS study on the distribution of soil organic matter, iron and manganese in a nodule from a S tagnosol. *European journal of soil science*. 2014;65(5):684-92.
181. Lanson B, Drits VA, Gaillot A-C, Silvester E, Plançon A, Manceau A. Structure of heavy-metal sorbed birnessite: Part 1. Results from X-ray diffraction. *American Mineralogist*. 2002;87(11-12):1631-45.
182. Takahashi Y, Manceau A, Geoffroy N, Marcus MA, Usui A. Chemical and structural control of the partitioning of Co, Ce, and Pb in marine ferromanganese oxides. *Geochim Cosmochim Ac.* 2007;71(4):984-1008.
183. Keiluweit M, Bougoure JJ, Nico PS, Pett-Ridge J, Weber PK, Kleber M. Mineral protection of soil carbon counteracted by root exudates. *Nature Climate Change*. 2015.

184. Nico PS, Zasoski RJ. Importance of Mn (III) availability on the rate of Cr (III) oxidation on δ -MnO₂. *Environ. Sci. Technol.*, 2000;34(16):3363-7.
185. Nico PS, Zasoski RJ. Mn (III) center availability as a rate controlling factor in the oxidation of phenol and sulfide on δ -MnO₂. *Environ. Sci. Technol.*, 2001;35(16):3338-43.
186. Jokic A, Wang MC, Liu C, Frenkel AI, Huang PM. Integration of the polyphenol and Maillard reactions into a unified abiotic pathway for humification in nature: the role of delta-MnO₂. *Org Geochem.* 2004;35(6):747-62.
187. Brunetti G, Senesi N, Plaza C. Organic matter humification in olive oil mill wastewater by abiotic catalysis with manganese (IV) oxide. *Bioresource Technol.*, 2008;99(17):8528-31.
188. Chang R, Wang S, Liu Y, Chan Y, Hung J, Tzou Y, et al. Interactions of the products of oxidative polymerization of hydroquinone as catalyzed by birnessite with Fe (hydr) oxides—an implication of the reactive pathway for humic substance formation. *Rsc Advances.* 2016;6(25):20750-60.
189. Lehmann J, Kleber M. The contentious nature of soil organic matter. *Nature.* 2015;528(7580):60-8.
190. Burdon J. Are the traditional concepts of the structures of humic substances realistic? *Soil Science.* 2001;166(11):752-69.
191. Cheng C-H, Lehmann J, Thies JE, Burton SD, Engelhard MH. Oxidation of black carbon by biotic and abiotic processes. *Org Geochem.* 2006;37(11):1477-88.
192. Kelleher BP, Simpson AJ. Humic substances in soils: are they really chemically distinct? *Environ. Sci. Technol.*, 2006; 40(15):4605-11.
193. Rodríguez H, Fraga R. Phosphate solubilizing bacteria and their role in plant growth promotion. *Biotechnology advances.* 1999;17(4):319-39.
194. Gobat J-M, Aragno M, Matthey W. *Le sol vivant: bases de pédologie, biologie des sols*: PPUR Presses polytechniques; 2010.
195. Duchaufour P. *Introduction à la science du sol: sol, végétation, environnement.* 6e édition de l'Abrégé de pédologie. Dunod, Paris. 2001.
196. Hansel C. Small but mighty: how minor components drive major biogeochemical cycles. *Environ. Microbiol. Report.*, 2017;9(1):8-10.

Chapter 6

General conclusion

SUMMARY

Manganese oxides are secondary minerals ubiquitous in natural environments such as soils, water and sediments. These nanoparticles are extremely reactive, both acting as inorganic contaminant scavengers and as highly oxidizing species. In natural systems, because of the exceedingly slow abiotic oxidation of Mn(II) by O₂, MnO₂ is precipitated by microorganisms, which means the mineral particles often occurs admixed with intact cells and organic residues.

A common approach to study the reactivity of MnO₂ is to use synthetic δ -MnO₂, considered to be the closest analogue of freshly precipitated biogenic MnO₂ minerals. However, the co-existence of the mineral phase with the organic and biological components can significantly affect the solid's reactivity. Some studies have demonstrated that the biomass can contribute to the sorption capacity of the oxide by offering additional sorption sites, but may also passivate the mineral's reactive sites (1-6). Furthermore, biogenic MnO₂ are characterised by dynamic Mn(II) and Mn(III) content, due to a combination of comproportionation reaction with Mn(II), partial reduction of Mn(IV) by organics, and regeneration of Mn(IV) by Mn(II)-oxidizing

enzymes. The importance of Mn(III) centres, whether adsorbed in the interlayer or present within the layer of the mineral has become indisputable, as it can both lower the mineral's reactivity by capping vacancies (7-10), but also affects the redox reactivity of the mineral in ways that are not fully understood (7-13). The objective of this dissertation was therefore to study the reactivity of biogenic MnO₂, both its affinity towards metals and its interactions with organic molecules, taking into consideration contributions from the organic and biological matrices. We associated experimental work and a literature review to reflect on the reactivity of the bio-mineral assemblages in natural systems. We used wet chemical measurements, X-ray absorption spectroscopy techniques and biogenic MnO₂ suspensions precipitated by the laboratory-model Mn(II)-oxidizing bacteria *Pseudomonas putida* GB-1. To decouple the reactivity of the oxide to any biological contribution, we also used suspensions of δ -MnO₂.

In **Chapter 1**, we introduced the characteristics of MnO₂ nanoparticles, and highlighted the different mechanisms through which the association with metabolically active cells and organic residues can affect the reactivity of biogenic MnO₂.

In **Chapter 2**, we studied the sorption of Pb(II) and Zn(II), two common contaminants that are found on both sides of Mn on the affinity sequence for MnO₂, on biogenic MnO₂ at pH 5.5. We reported a significantly higher loading of Pb(II) relative to Zn(II). This difference was explained by the capacity of Pb(II), but not of Zn(II), to displace interlayer Mn(III) capping vacancies. For Zn(II), we instead observed a non-negligible partitioning to the biomass.

In **Chapter 3**, we studied the oxidative transformation of glucose and gluconate by δ -MnO₂ as a function pH (pH 4.5 – 6.5). We observed a greater reductive dissolution of MnO₂ and oxidation of the organic substrates at lower pH. For both substrates, we however measured little changes in the initial solution concentrations at all pH conditions and a pool of unreacted material was left in solution. This finding shows that the organic substrates were extensively oxidized by MnO₂, with more than 2 electrons transferred from a given molecule to the oxide. The solution pH was furthermore found to be more important than the nature of the organic substrate in governing the rate of reaction with the mineral.

In **Chapter 4**, we investigated how the metabolic activity of bacterial cells in biogenic MnO₂ suspensions can result in the reductive dissolution of the mineral. We demonstrated

that addition of glucose to stationary phase *P. putida* suspension resulted in the acidification of the extracellular solution. Both respiration and the secretion of organic acids can contribute to the observed acidification, but the latter was found to be the major source. In stationary-phase *P. putida* - MnO₂ suspensions, the acidification and the presence of reductants first resulted in significant reductive dissolution of the mineral. Regeneration of the mineral phase was then observed, seemingly as rates of Mn(II) oxidation overcame that of reductive dissolution of the mineral, due to more favourable pH conditions and reductant concentrations for the persistence of the oxide.

In **Chapter 5**, we reviewed the literature on the reactivity of MnO₂ with natural organic molecules, to assess the impact MnO₂ could have on the cycling of organic C in soils. We highlighted the current lack of consensus found in the literature. Some studies suggest that MnO₂ could contribute to the stabilization of organic C either through organo-mineral interactions or by catalysing polymerization reaction. Others suggest that MnO₂ could enhance the cycling of organic C either by enhancing the hydrolysis of ester bonds or through the oxidative degradation of organic moieties. Although laboratory-based experiments demonstrate that MnO₂ can be involved in these reactions, their relevance to natural systems remains unclear:

- 1) The lower abundance of Mn relative to Fe and Al, recognized as key mediators for the stabilization of organic C in soils, necessarily limits the extent of C sorption on MnO₂ phases. Furthermore, the long-term stabilization of organic molecules on MnO₂ is undermined by the susceptibility of the oxide to reductive dissolution.

- 2) If MnO₂ can catalyse a number of polymerization reactions, such as for example the Maillard reaction, the contribution this pathway could have on the soil C cycling is dubious. As soil scientists have moved away from the concept of humic substances, they have become sceptical of the importance of secondary polymerization reactions for the fate of SOM.

- 3) Although MnO₂ have been shown to enhance the hydrolysis of ester bonds, the relevance of the contribution to the C cycling in soils needs to be evaluated by considering the relative lability of these bonds and the various hydrolase enzymes secreted by microorganisms.

- 4) Manganese oxides can oxidatively degrade a wide range of organic molecules, because of the high redox potential of the Mn_{ox}/Mn_{red} couples. However, these oxidative

reactions become meaningful in the soil context only if an efficient mechanism for the regeneration of high-valent Mn species is present.

REACTIVITY OF BIOGENIC MnO_2 : CONTRIBUTION TO THE STATE OF THE ART

1. Additional sorption sites and passivation of reactive sites from organo-mineral interactions

Chapter 2 showed that partitioning on alternative binding sites on the biomass may be particularly important for metals such as Zn(II) that are unable to displace interlayer Mn(III) capping vacancies. Furthermore, the partitioning of Zn(II) to the biomass observed in the lowest loading sample, which is in contradiction with the study by Toner et al. (14) that reported a large preferential sorption the mineral at all loadings, questions the impact of organo-mineral interactions on the kinetic accessibility to interlayer vacancy sites on the oxide. Their study was conducted at higher pH (7.0, versus 5.5 in our experiment) and equilibrated for longer prior to filtration (48h, versus 24h in our experiment). We speculated that the slow diffusion of Zn(II) into the interlayer to reach vacancy sites at low Zn(II) concentrations may explain the greater partitioning of Zn(II) to the biomass observed in our study, but the impact of organo-mineral interactions on the diffusion of cations to interlayer sorption sites at different pH warrants further investigations.

2. Dynamic cycling of Mn: varying Mn(II, III) content

Chapter 2 showed that the interlayer Mn(III)-content of MnO_2 can lower the sorption capacity of the mineral, but only for metals such as Zn(II) that are unable to displace interlayer Mn(III). In light of the growing recognition of the impact of Mn(III) on the reactivity of the oxide, it is important to better apprehend pathways of Mn(III)-enrichment relative to reductive dissolution when MnO_2 reacts with organic molecules. In **Chapter 3**, we used changes in aqueous Mn(II) to estimate the number of electrons transferred from the organic to the mineral oxide. However this approach does not account for Mn(III) stored in the solid phase, which means that these measurements should be systematically complemented with solid-phase analysis of Mn oxidation state, as can be achieved by potentiometric titration or with pyrophosphate extractions of Mn(III) and subsequent quantification of Mn(III)-pyrophosphate complexes by UV-vis spectroscopy (7, 15).

3. Dynamic redox cycling of Mn: recycling of high valent Mn species

Chapter 4 highlighted the link between the Mn cycling and the carbon content available to neighbouring microorganisms. The results from this study demonstrated that MnO_2 solids were unstable when stationary phase bio-mineral assemblages were faced with an input of glucose. Translated to the context of bio-mineralization, these results suggest that the effective stability of any newly formed MnO_2 particles is compromised under conditions of high C turnover due to chemical conditions being favourable for reductive dissolution of the mineral.

Authors have noted that MnO_2 accumulation only takes place in stationary phase or under C starvation (17). When *P. putida* is grown in Leptothrix amended with 1 mM MnCl_2 , we observe a 13h lag period between the time at which bacterial suspensions reach stationary phase and the beginning of the observed MnO_2 precipitation (see **Figure 1**). The lag period between the start of stationary phase and the onset of MnO_2 accumulation might be ascribed to the time required to deplete the suspensions from the C-sources, with impact both on the C of reductant able to dissolve MnO_2 , but also on DO and pH conditions

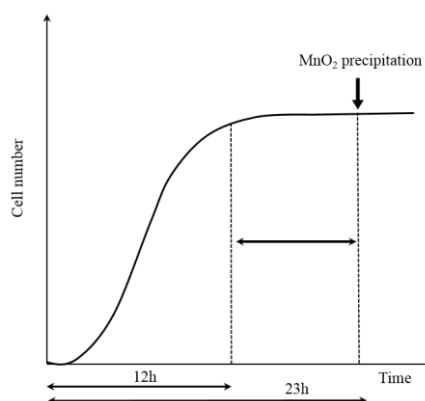


Figure 1 Schematic that represents the different stages of bacterial growth: 1) lag phase that lasts about 2h; 2) exponential phase that lasts about 11h and during which the optical density of the suspension exponentially increases; 3) stationary phase, which starts when the number of bacterial cells plateaus. The diagram also shows the delay between the onset of stationary phase and the start of MnO_2 accumulation.

This hypothesis is consistent with preliminary data¹ collected on freshly inoculated *P. putida* suspensions in Leptothrix growth media, which show that both O_2 concentrations and pH were perturbed during bacterial growth (see **Figure 2**). Both parameters were restored only 23h after inoculation, time at which we observed the start of the effective removal of Mn(II) from solution. These measurements therefore demonstrate a clear correlation between the time at which pH and O_2 went back to equilibrium condi-

¹ Experimental details are described in the Supplementary Information - **Chapter 6**

tions, and the start of the observed precipitation of MnO_2 . Furthermore, reducing the glucose concentration to 50 % and 0 % of the original *Leptothrix* glucose concentration brought forward the onset of MnO_2 precipitation (see **Figure 3**), again pointing to a link between glucose depletion and the start of MnO_2 precipitation.

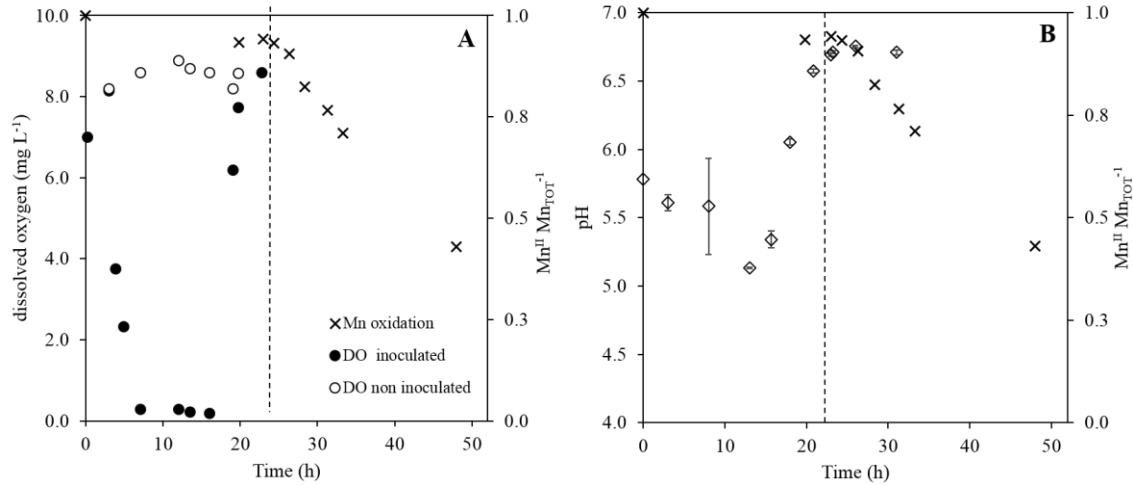


Figure 4 Changes in dissolved oxygen (A) and pH (B) as a function of time after *P. putida* was inoculated *Leptothrix* growth media amended with 1 mM MnCl_2 , plotted alongside measured changes in aqueous Mn(II).

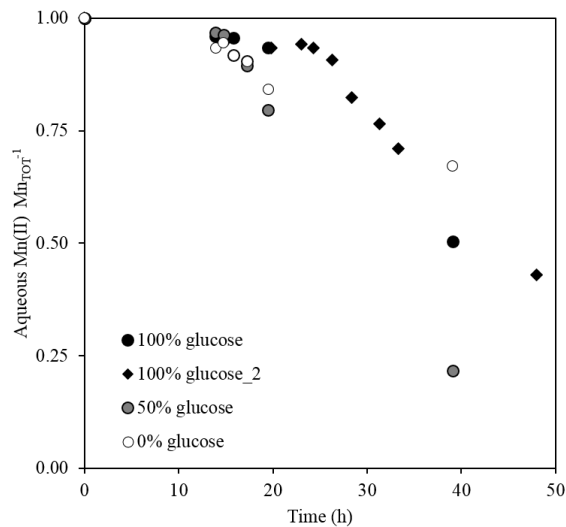


Figure 3 Onset of MnO_2 precipitation in the original *Leptothrix* (100 % glucose = 5.5 mM, 1 g L⁻¹) and the modified *Leptothrix* (0 % and 50 %). Two independent sets of measurements were combined for the 100 % glucose conditions (black symbols). Single sets of measurements for both the 50 % and 0 % condition.

The results from **Chapter 4**, supported by these preliminary measurements, question the relative importance of the geochemical and biological controls in governing biomineralization of MnO_2 . They suggest MnO_2 accumulation may only be observed when chemical conditions become favourable not only for enzymatic Mn(II)-oxidation but also MnO_2 persistence. This implies that particles of MnO_2 will only accumulate when the rate of bacterial Mn(II) oxidation offsets that of MnO_2 reductive dissolution. Under

high C carbon conditions, a cryptic recycling of Mn through concomitant regeneration and dissolution of the oxide is possible. The MnO₂ accumulation therefore does not inform on whether enzymatic Mn(II) oxidation is taking place.

Chapters 3 highlighted the electron imbalance between the electron accepting and donating capacity of molar equivalent concentrations of MnO₂ and small organic substrates. As discussed in **Chapter 5**, considering the relative concentrations of organic molecules in soils relative to the average Mn soil concentration, it becomes evident that for MnO₂ to have any meaningful impact on oxidative degradation of organic molecules, an efficient concomitant Mn(II)-oxidizing mechanism is required to continuously regenerate the oxidative capacity of high valent Mn species. A better understanding of the rates of the cycling between Mn(II), Mn(III) and Mn(IV) species in bio-mineral assemblages and under different chemical conditions (for eg: pH, C content) is necessary to understand how the C and Mn cycles are coupled in natural systems.

4, Dynamic response of metabolically active cells can affect solution conditions

Chapter 4 demonstrated that microbial metabolic activity following the addition of a bioavailable C can lead to extensive reductive dissolution of MnO₂. Exposure to fluctuating pH conditions can impact both the long-term sorption capacity of the oxide and its redox reactivity. Other types of perturbations, such as exposure to a toxicant, scarcity of nutrients, may result in similar microbial responses that modify local chemical conditions and affect co-occurring minerals. The effective reactivity of MnO₂ in natural systems thus need to be examined in close relation to co-occurring metabolically active microorganisms.

DIRECTIONS OF FUTURE RESEARCH

Understanding the Mn cycle to understand its role to the C cycle

As previously stressed, Mn oxides minerals are characterized by two major properties: their large affinity for inorganic contaminants and their high redox potentials. There is a clear imbalance in the literature between the understanding of the reactivity of MnO₂ towards contaminants and towards organic molecules. In recent years, more efforts have been put in investigating the interactions of MnO₂ with organics, but there remains a lack of consensus of the impact MnO₂ can have on the C cycling in soils. Studies report different types of interactions with organic molecules, ones that can stabilize organic C

and others that contribute to the oxidative degradation of organic C. However, the relevance of these reactions in natural systems, under changing physico-chemical conditions, in the presence of high concentrations of reductants and a wide range of microorganisms and associated enzymes remains to be assessed.

The high redox potential of high valent Mn species means that these species are likely to get involved in redox reactions in soils. However, the oxidation of organic C by MnO₂ can only be relevant to the overall C cycle if there is an efficient recycling of high valent Mn species. The cycling of Mn between Mn(II) and Mn(III) maintained by white-rot fungi, which recruit Mn(II), oxidize it and stabilize Mn(III) through complexation with ligands is an example of the efficient exploitation of the oxidative capacity of Mn (19-21). Research on MnO₂ reactivity needs to focus on determining to what extent and under which conditions does the cycling between Mn(II), Mn(III) and Mn(IV) occur in natural systems (22-24).

Coupled biotic and abiotic oxidation of organic molecules by MnO₂

The strong pH-dependence of the reductive dissolution of MnO₂ makes these minerals particularly susceptible to variations in local pH conditions. In particular, the co-occurrence of MnO₂ with metabolically active bacteria exposes the oxide to changes induced by metabolic activity, notably following the addition of an easily biodegradable C substrate. A parallel can therefore be drawn with the priming effect, which describes the observed short-term enhanced microbial mineralization of native soil C following the input of fresh carbon in soils (25, 26). The priming effect has been observed in a number of lab-based and field-studies and is recognised as a key framework for C cycling in soils (25, 27). The oxidation of native molecules is thought to be driven by the enhanced microbial activity that occurs when a large input of bioavailable substrates is provided to the microbial community.

Recently, Keiluweit et al. (28) offered an insight into the possible abiotic contribution to the priming effect. Their work suggests that addition of fresh C substrates may not only enhance microbial metabolism, but also destabilise mineral phases and associated organic matter. The remobilised organic matter thus becomes available for microbial mineralization, suggesting that the coupling of biotic and abiotic processes may contribute to the priming effect. In light of the results collected in this study, an additional mechanism that couples biotic and abiotic oxidation and that could contribute to enhanced SOM mineralization following the addition of fresh C substrate to soils soil is proposed.

Upon input of fresh C, metabolic transformation of the labile fraction is expected to drive local drops in pH. This localised acidification will facilitate the reductive dissolution of MnO_2 and enhance its Lewis acidity, therefore facilitating the abiotic oxidation of native C by MnO_2 . The perturbation of the extracellular chemical conditions resulting from the microbial response to the input of bioavailable carbon substrates may thus tip the assemblage from an equilibrium 'non-metabolic bio-mineral', to an actively cycling machinery for C transformation through coupled-biotic and abiotic oxidation. This mechanism may provide further insight on the coupling between the C and Mn cycles in soil, providing a concomitant Mn(II)-oxidizing community continuously regenerate the oxidative capacity of high valent Mn species.

Consideration on the level of complexity that we want to approach

Because of dynamic nature soils, the numbers of players co-involved in its functioning, and the range of spatial and temporal scales covered by the multitude of co-occurring processes, understanding the soil functioning requires multidisciplinary approaches spanning wide range of orders of magnitudes. For example, the contemporary consensus concerning the stability of natural soil organic matter is that it cannot be predicted solely based on the intrinsic chemical properties of its component molecules. Turn-over of organic carbon is instead better understood as a function of global parameters, which include the microbial and the mineralogical signature of a given ecosystem, as well as climatic factors and the connectivity between the different soil compartments (29, 30).

If the importance of considering the soil as a whole to understand its biogeochemistry appears evident, investigating such a system is far from straightforward. While qualitative observations allow to grasp processes at an ecosystem scale, obtaining quantitative information and mechanistic understanding of the biogeochemistry governing soil processes require to change scale and ponder molecular interfaces (31). This is however only possible if the systems studied are simplified, fixing certain parameters and allowing only a few to vary.

At the micro- to nano- scale, this thesis demonstrated that the reactivity of MnO_2 is significantly affected by co-occurring organic molecules and microbial cells. The reactivity of the mineral was shown to be very different from that of $\delta\text{-MnO}_2$, despite it being a structurally close analogue to the biogenic mineral, as some of the dynamic nature of MnO_2 , in terms of Mn(II), Mn(III) and Mn(IV) content, and sensitivity to external conditions are missed when the abiotic mineral is studied alone. However, this study also

demonstrated the complexity brought to the studied system by integrating just a few contributions from the organic and the biotic domains. The level of mechanistic details gathered from studies on bio-minerals does not compare to those obtained from studies that employ purely abiotic suspensions such as δ -MnO₂. For example, irradiating δ -MnO₂ in a pure water solution allowed to understand the mechanisms of photoreduction of δ -MnO₂, with the formation of transient Mn(III) and its stabilization in the interlayer (32). In biogenic MnO₂, this process would likely be hidden by co-occurring reactions, such as for example the light-excitation of organic moieties and injection of electrons into the oxide (33, 34). Similarly, if the relative contribution of edge sites and vacancy sites can be discussed for the sorption of a number of contaminants on δ -MnO₂ (7, 8, 35, 36), the presence of the biomass in biogenic MnO₂ means this distinction is difficult to make because of the difficulty in differentiating edge sites and biomass with EXAFS spectroscopy.

In any system, the prevailing mechanisms are those leading to an equilibrium at the local or global energy minimum. In a simplified system, in which the number of variables and the parameters at play are controlled, a thorough mechanistic understanding of an observed phenomenon can be gathered. However, the position of this energy minimum depends tremendously on any of the other variables when those are set free to vary, as well as on the actors that are left out in the simplified system. Any simplification made to an experimental system to allow a deeper mechanistic understanding of the underlying processes comes with an increased risk of losing relevance to the natural system, as any additional level of complexity can affect the position of the equilibrium. Understanding these natural systems therefore require multidisciplinary and multiscale approaches to understand the mechanisms that govern the soil functioning.

REFERENCES

1. Toner B, Manceau A, Marcus MA, Millet DB, Sposito G. Zinc sorption by a bacterial biofilm. *Environ. Sci. Technol.*, 2005; 39(21): 8288-94.
2. Toner B, Sposito G. Reductive dissolution of biogenic manganese oxides in the presence of a hydrated biofilm. *Geomicrobiol. J.*, 2005;22(3-4):171-80.
3. Villalobos M, Bargar J, Sposito G. Mechanisms of Pb (II) sorption on a biogenic manganese oxide. *Environ. Sci. Technol.*, 2005;39(2):569-76.

4. Peña. Contaminant Metal Immobilization by Biogenic Manganese Oxide Nanoparticles: Implications for Natural Attenuation and Bioremediation (Dissertation). 2009.
5. Peña J, Bargar JR, Sposito G. Role of bacterial biomass in the sorption of Ni by biomass-birnessite assemblages. *Environ. Sci. Technol.*, 2011;45(17):7338-44.
6. Droz B, Dumas N, Duckworth OW, Pena J. A comparison of the sorption reactivity of bacteriogenic and mycogenic Mn oxides nanoparticles. *Environ. Sci. Technol.*, 2015
7. Simanova AA, Kwon KD, Bone SE, Bargar JR, Refson K, Sposito G, et al. Probing the sorption reactivity of the edge surfaces in birnessite nanoparticles using Nickel (II). *Geochim. Cosmochim. Ac.*, 2015;164:191-204.
8. Simanova A, Peña J. Time-resolved investigation of cobalt oxidation by Mn(III)-rich δ -MnO₂ using quick X-Ray absorption spectroscopy. *Environ Sci Technol.* 2015;49(18):10867-76.
9. Wang Y, Benkaddour S, Marafatto F, Pena J. Diffusion-and pH-dependent reactivity of layer-type MnO₂: Reactions at particle edges versus vacancy sites. *Environ. Sci. Technol.*, 2018.
10. Hinkle MA, Dye KG, Catalano JG. Impact of Mn (II)-Manganese Oxide Reactions on Ni and Zn Speciation. *Environ. Sci. Technol.*, 2017.
11. Nico PS, Zamoski RJ. Importance of Mn (III) availability on the rate of Cr (III) oxidation on δ -MnO₂. *Environ. Sci. Technol.*, 2000;34(16):3363-7.
12. Nico PS, Zamoski RJ. Mn(III) center availability as a rate controlling factor in the oxidation of phenol and sulfide on δ -MnO₂. *Environ. Sci. Technol.*, 2001;35(16):3338-43.
13. Ukrainczyk L, McBride MB. Oxidation of phenol in acidic aqueous suspensions of manganese oxides. *Clays and Clay Minerals.* 1992;40(2):157-66.
14. Toner B, Manceau A, Webb SM, Sposito G. Zinc sorption to biogenic hexagonal-birnessite particles within a hydrated bacterial biofilm. *Geochim. Cosmochim. Ac.*, 2006;70(1)
15. Klewicki J, Morgan J. Dissolution of β -MnOOH particles by ligands: pyrophosphate, ethylenediaminetetraacetate, and citrate. *Geochim. Cosmochim. Ac.*, 1999;63(19):3017-24.
17. Geszvain K, McCarthy JK, Tebo BM. Elimination of manganese (II, III) oxidation in *Pseudomonas putida* GB-1 by a double knockout of two putative multicopper oxidase genes. *Appl. Environ. Microbiol.*, 2013;79(1):357-66.
18. Shacklette HT, Boerngen JG. Element concentrations in soils and other surficial materials of the conterminous United States. 1984.
19. Berg B, Steffen K, McClaugherty C. Litter decomposition rate is dependent on litter Mn concentrations. *Biogeochem.*, 2007;82(1):29-39.
20. Davey MP, Berg B, Emmett BA, Rowland P. Decomposition of oak leaf litter is related to initial litter Mn concentrations. *Botany.* 2007;85(1):16-24.
21. Keiluweit M, Nico P, Harmon ME, Mao J, Pett-Ridge J, Kleber M. Long-term litter decomposition controlled by manganese redox cycling. *Proc. Natl. Acad. Sci.*, 2015; 112(38): 5253-60.
22. Hansel CM, Ferdelman TG, Tebo BM. Cryptic cross-linkages among biogeochemical cycles: novel insights from reactive intermediates. *Elements.* 2015;11(6):409-14.
23. Berg JS, Michellod D, Pjevac P, Martinez-Perez C, Buckner CR, Hach PF, et al. Intensive cryptic microbial iron cycling in the low iron water column of the meromictic Lake Cadagno. *Environ. Microbiol.*, 2016;18(12):5288-302.
24. Kappler A, Bryce C. Cryptic biogeochemical cycles: unravelling hidden redox reactions. *Environ. Microbiol.*, 2017;19(3):842-6.

25. Kuzyakov Y, Friedel J, Stahr K. Review of mechanisms and quantification of priming effects. *Soil. Biol. Biochem.*, 2000;32(11):1485-98.
26. Kuzyakov Y, Blagodatskaya E, Blagodatsky S. Comments on the paper by Kemmitt et al.(2008)'Mineralization of native soil organic matter is not regulated by the size, activity or composition of the soil microbial biomass–A new perspective'[*Soil Biol. Biochem.*, 40, 61–73]'. *Soil. Biol. Biochem.*, 2009;41(2):435-9.
27. Blagodatskaya E, Kuzyakov Y. Mechanisms of real and apparent priming effects and their dependence on soil microbial biomass and community structure: critical review. *Biol. Fert. Soils.*, 2008;45(2):115-31.
28. Keiluweit M, Bougoure JJ, Nico PS, Pett-Ridge J, Weber PK, Kleber M. Mineral protection of soil carbon counteracted by root exudates. *Nature Clim. Change*, 2015.
29. Schmidt MWI, Torn MS, Abiven S, Dittmar T, Guggenberger G, Janssens IA, et al. Persistence of soil organic matter as an ecosystem property. *Nature*. 2011;478(7367):49-56.
30. Keiluweit M, Nico PS, Kleber M, Fendorf S. Are oxygen limitations under recognized regulators of organic carbon turnover in upland soils? *Biogeochem.*, 2015, 1-15.
31. Templeton A, Knowles E. Microbial transformations of minerals and metals: recent advances in geomicrobiology derived from synchrotron-based X-ray spectroscopy and X-ray microscopy. *Ann. Rev. Earth Planet Sci.*, 2009;37:367-91.
32. Marafatto FF, Strader ML, Gonzalez-Holguera J, Schwartzberg A, Gilbert B, Peña J. Rate and mechanism of the photoreduction of birnessite (MnO₂) nanosheets. *Proc. Natl. Acad. Sci.*, 2015; 112(15): 4600-5.
33. Katz JE, Gilbert B, Zhang X, Attenkofer K, Falcone RW, Waychunas GA. Observation of transient iron (II) formation in dye-sensitized iron oxide nanoparticles by time-resolved X-ray spectroscopy. *J. Phys. Chem. Lett.*, 2010;1(9):1372-6.
34. Gilbert B, Katz JE, Huse N, Zhang X, Frandsen C, Falcone RW, et al. Ultrafast electron and energy transfer in dye-sensitized iron oxide and oxyhydroxide nanoparticles. *Phys. Chem. Chem. Phys.*, 2013;15(40):17303-13.
35. Manceau A, Marcus MA, Grangeon S, Lanson M, Lanson B, Gaillot A-C, et al. Short-range and long-range order of phyllosulfate nanoparticles determined using high-energy X-ray scattering. *J. Appl. Crystallogr.*, 2013;46(1):193-209.
36. van Genuchten CM, Peña J. Sorption selectivity of birnessite particle edges: a d-PDF analysis of Cd(II) and Pb(II) sorption by δ -MnO₂ and ferrihydrite. *Environ. Sci. Process. Impact*, 2016

Chapter 7 Supplementary Information

Chapter 2

Pb, Zn and Mn sorption on biogenic MnO₂: contaminant loading and competitive access to vacancy sites

Table 2-S1 Samples investigated by EXAFS spectroscopy. Surface loading (q) and concentration of Mn(II) measured in solution (c_{Mn}) are reported for each sample. The pH_{time} refer to the pH measured following the addition of the metal solution to the biogenic MnO₂ suspensions (t_{0h} = time of addition). Suspensions (pH 6.16 ± 0.01 ; $c_{Mn, aq}$ approx. 2 μ M) were harvested at 120h \pm 5h.

Sample ID	pH_0h	pH_24h	q (mol i mol ⁻¹ Mn)	c_{MnO_2} (μ M)	c_{Mn}^{II} (μ M)	K_d
Zn_6%_pH5.0	5.72	5.56	0.06	1129.5	n.d	-
Zn_8%_pH5.0	5.62	5.45	0.08	1126.3	5.4	0.003
Zn_15%_pH5.0	5.44	5.27	0.12	1059.6	28.0	0.000
Pb_4%_pH5.5	5.57	5.58	0.04	1091.5	n.d ^a	-
Pb_24%_pH5.5	4.59	5.67*	0.24	1083.9	101.1	-
Pb_44%_pH5.5	4.37	5.10**	0.44	1074.4	125.4	0.006
ctrl_0%_pH5.5	-	-	-	1097.2	n.d	-

^a n.d = not detected

* pH_4h: 4.60 \rightarrow 5.40 (addition of NaOH)

** pH_4h: 4.34 \rightarrow 5.27 (addition of NaOH)

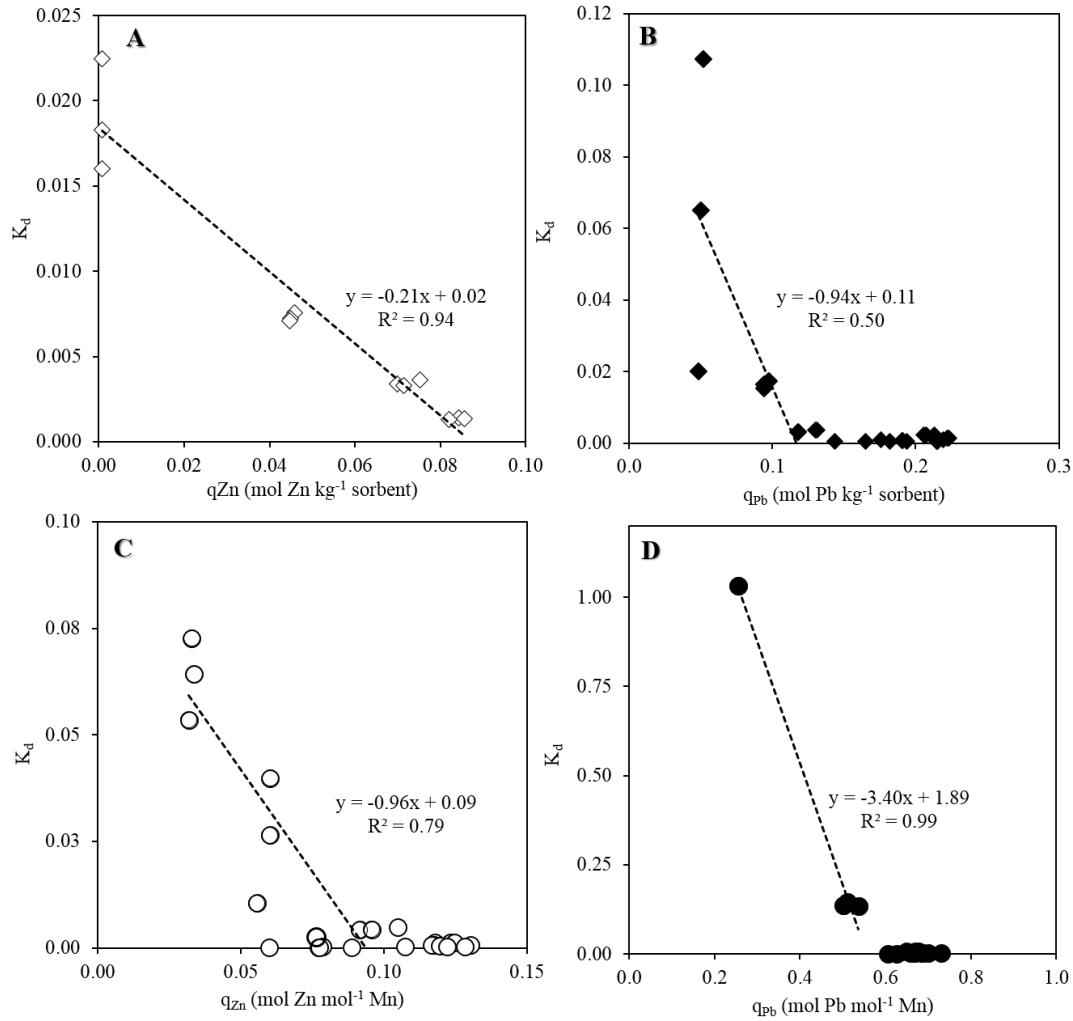


Figure 2-S2 Plots of the distribution coefficient K_d versus surface excess q_i for Zn(II) (open circles) and Pb(II) (filled circles) sorbed on biomass (A – B) and on biogenic MnO_2 (C-D). The initial data points for high affinity isotherms are not included because $c_i = 0 \mu M$.

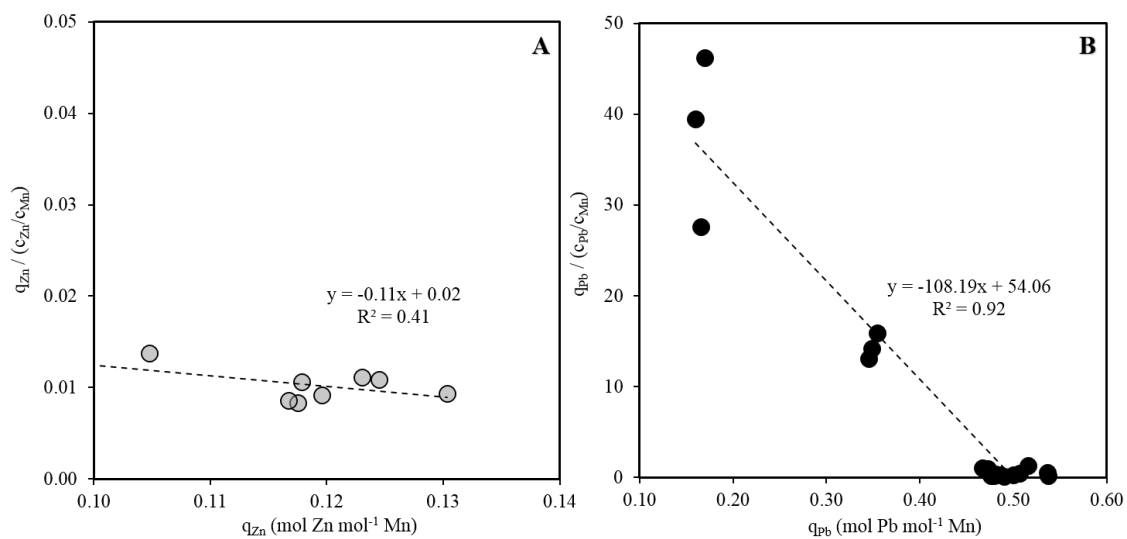


Figure 2-S3 Plots of $q_i/c_i/c_{Mn}$ versus q_i , for $i = \text{Zn(II)}$ and Pb(II) in A) and B) respectively. The dashed lines show the regression lines for q_i values $> 0.1 \text{ mol } i \text{ mol}^{-1} \text{ Mn}$.

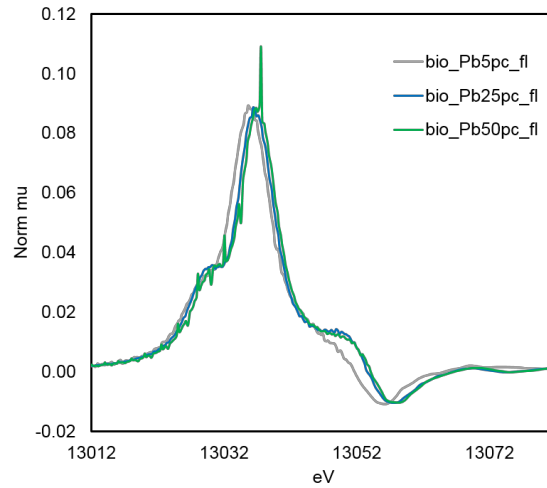


Figure 2-S4 First derivative of mu spectra for the Pb loaded biogenic MnO₂ samples

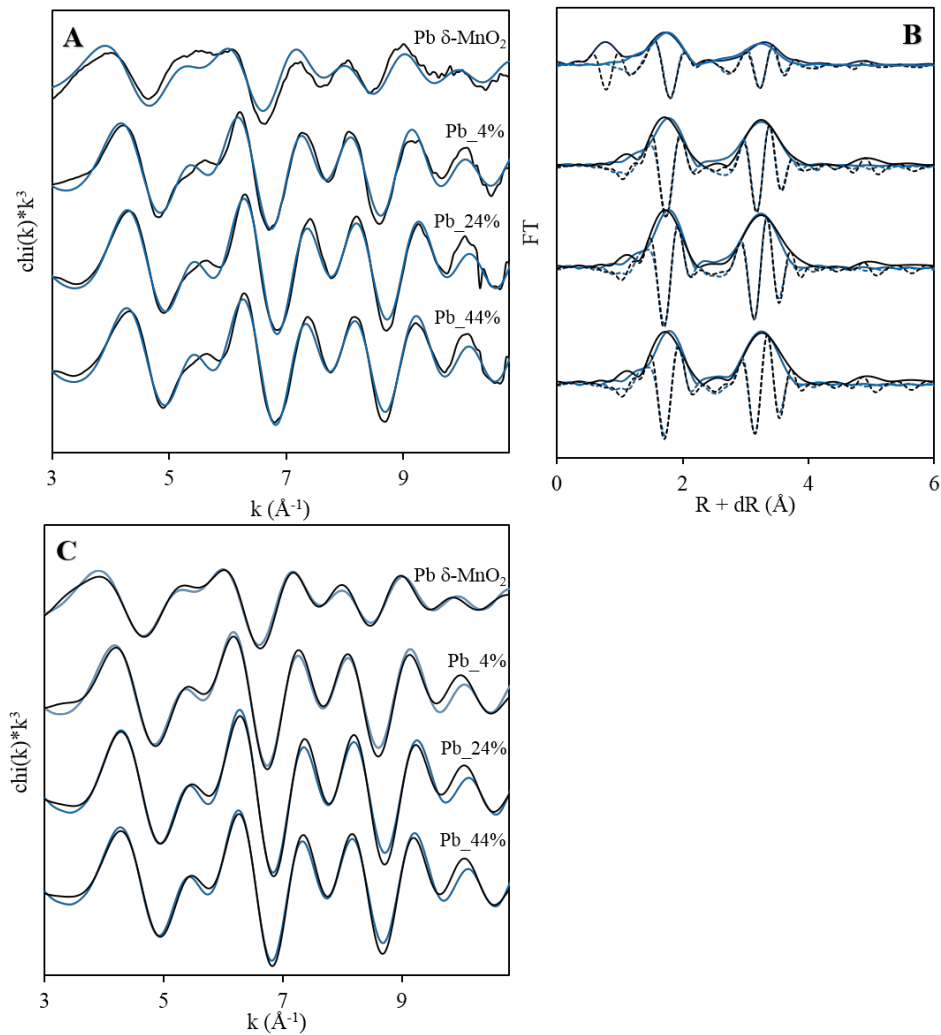


Figure 2-S5 EXAFS spectroscopic spectra (A) and their Fourier transforms (B) for Pb(II) loaded on biogenic MnO₂ and a reference spectrum of Pb(II) loaded on δ -MnO₂ [0.2 mol Pb mol⁻¹ MnO₂, pH 5.5], modelled by shell-by-shell fittings using a three-shells model. Figures (C) shows the Fourier-filtered chi spectra and the imaginary parts of the data and the fittings. The data is plotted as a black line, the fittings as the blue lines.

Table 2-S2 Fitting parameters for Pb(II) sorption on biogenic MnO₂, for samples with loadings (q_{sample}) of 0.04, 0.24 and 0.44 mol Pb mol⁻¹ Mn, obtained by shell-by-shell fitting of EXAFS spectra using a three-shells model. Fitting parameters for a reference spectrum of Pb sorbed on δ-MnO₂ provided by Villalobos et al. (2005) are plotted alongside the data. Fittings were run with a value for s₀² fixed to 0.843 and with the coordination number constrained as N_{INT} = 6 x f and N_{EXT} = 2 x (1-f).

Shell		Pb_δ-MnO ₂	Pb_4%	Pb_24%	Pb_44%
Pb-O	R (Å)	2.32 ± 0.02	2.29 ± 0.02	2.26 ± 0.02	2.28 ± 0.02
	N	2.49 ± 0.68	2.46 ± 0.72	2.37 ± 0.64	2.32 ± 0.66
	σ ² (Å)	0.012 ± 0.003	0.009 ± 0.003	0.007 ± 0.003	0.008 ± 0.003
Pb-Mn _{EXT}	R (Å)	3.44 ± 0.09	3.73 ± 0.02	3.25 ± 0.26	3.71 ± 0.02
	N	0.91	0.29	0.18	2.73
	σ ² (Å)	0.005 ± 0.007	0.010 ± 0.003	0.007 ± 0.029	0.010 ± 0.003
Pb-Mn _{INT}	R (Å)	3.72 ± 0.02	3.73 ± 0.02	3.70 ± 0.02	3.29 ± 0.09
	N	0.64	0.29	2.95	0.21
	σ ² (Å)	0.009 ± 0.005	0.011 ± 0.003	0.010 ± 0.003	0.002 ± 0.013
	E _o	-9.55 ± 2.47	-2.83 ± 2.20	-1.36 ± 2.06	-0.87 ± 2.10
	R	0.05	0.05	0.04	0.04
	χ ² _{red}	89.9	456.7	138.3	619.9

Chapter 3

Abiotic oxidation of glucose and gluconate by δ -MnO₂

1. Characterisation of glucose and gluconate ATR- FTIR spectroscopic spectra

Glucose and gluconate standards were prepared by dissolving glucose and Na-gluconate in ultrapure water. Subsequently, the pH dependence of the gluconate spectrum was assessed by gradually acidifying a gluconate solution (200 mM) with HCl (4 M to 50 mM) and measuring ATR-FTIR spectra of the resulting gluconate solutions at pH values ranging from 7.6 to 3.4. To verify the impact Mn(II) complexation could have on the position of the carboxylate vibrational band, we equilibrated an aqueous gluconate solution (pH 7.6, 50 mM) with a stoichiometric excess of Mn(II) (pH 7.6) and compared the resulting ATR-FTIR spectra from that of Na-gluconate. Finally, to estimate the sensitivity of method, calibration curves were prepared from the intensity of the vibrational peaks at 1035 cm⁻¹ and 1092 cm⁻¹ for glucose and gluconate respectively.

Characterization of end-membered solutions

The FTIR spectrum of glucose (250 mM, pH 7) is plotted in **Figure 3-S1A**, alongside a spectrum for the deprotonated form of gluconate (200 mM, pH 7.6 >> pK_a = 3.8). The two spectra show distinct absorption features in different regions of the IR electromagnetic spectrum. Glucose shows 5 multiple peaks in the region between 950 - 1200 cm⁻¹. These peaks correspond to C-O stretching vibrations (27). The spectrum also shows a region between 1320 and 1500 cm⁻¹ with vibrational contributions, that have been associated to bending vibrations of COH (27). The spectrum of gluconate shows 3 multiple peaks between 1000 - 1150 cm⁻¹, which are similarly assigned to different C-O stretching vibrations. The FTIR spectrum of gluconate also shows intense vibrational bands at 1585 cm⁻¹ and 1400 cm⁻¹ that are associated to the deprotonated carboxyl functional group (61, 62). Another peak centred at 1361 cm⁻¹ is observed, as well as a weak shoulder at 1240 cm⁻¹.

Because glucose and gluconate have relatively similar structures, the FTIR spectra have many overlapping regions. Glucose however shows a peak at 993 cm⁻¹, which is absent in gluconate, which may allow to track its presence in mixed solutions. In general, glucose can be distinguished from small organic acids by the absence of the vibrational bands associated to the carboxyl functional group around 1600 cm⁻¹. For gluconate, because of the pH dependence of the vibrational bands corresponding to the carboxyl functional

group, no peak between 1150 – 1750 cm^{-1} can be chosen to quantify gluconate in systems for which the pH is dynamic.

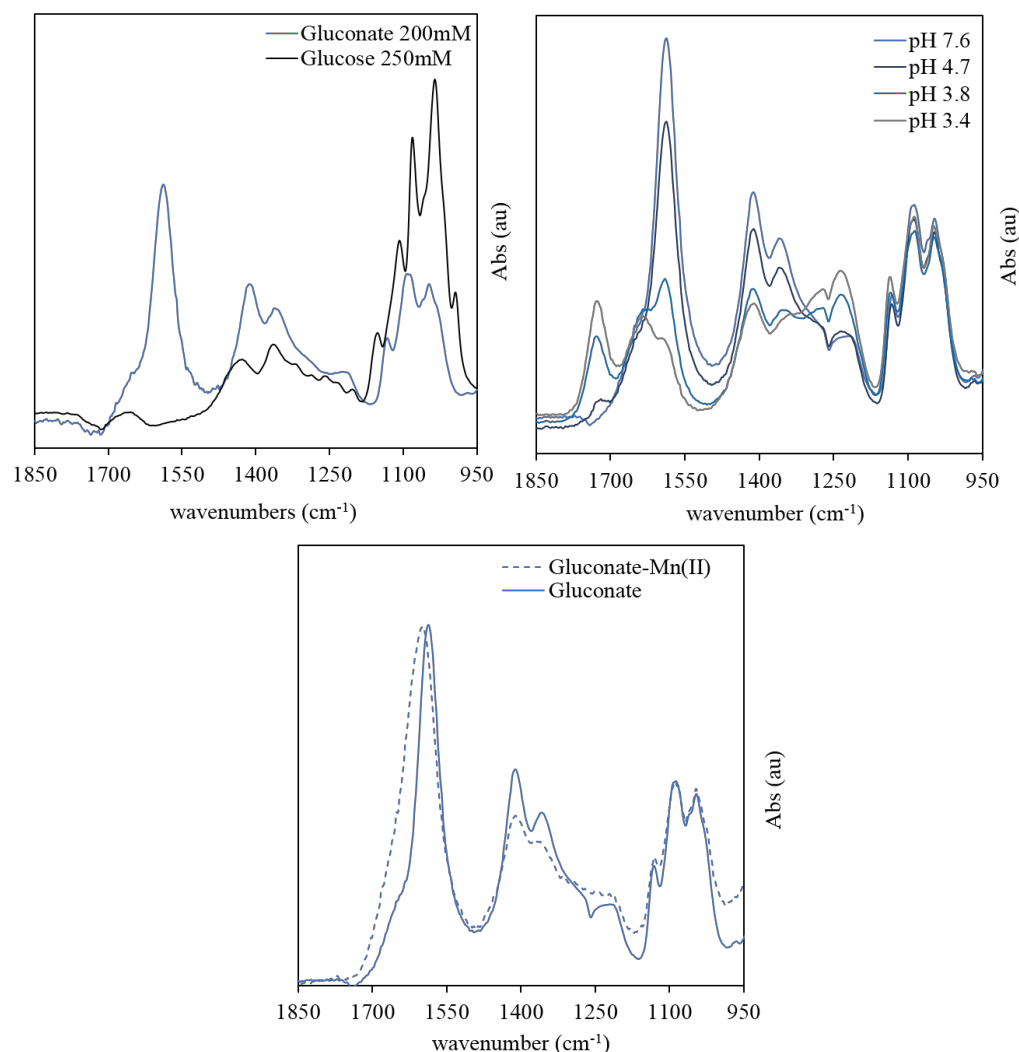


Figure 3-S1 Characterisation of end-membered glucose and gluconate solutions by ATR-FTIR. Panel A shows the influence of the oxidation of glucose to gluconate by showing ATR-FTIR spectra for glucose, 250mM and gluconate, 200 mM at pH 7.6. Panel B shows the effect of pH on the vibrational bands of gluconate, by showing spectra for gluconate solutions at different pH. Panel C shows the effect of the complexation of Mn(II) by gluconate, by comparing spectrum of Na-gluconate with spectrum for gluconate equilibrated with excess Mn(II).

pH dependence of gluconate spectra

The ATR-FTIR spectra of gluconate at pH 7.6, 4.7, 3.8 and 3.4 are shown in **Figure 3-S1B**. The spectra show a pH independent region between 950 - 1150 cm^{-1} , and a region of pH-dependent vibrations between 1150 and 1750 cm^{-1} that depends on the protonated state of the carboxylic functional group (63). At the highest pH condition (pH 7.6), the spectrum shows a large peak at 1585 cm^{-1} and another one at 1400 cm^{-1} . These peaks have been assigned to the asymmetric (ν_{as}) and symmetric (ν_{s}) stretching vibration of the

deprotonated carboxyl functional group (61, 62, 64). These two peaks decrease as the pH of the solution decreases. At pH 3.8 (where $\text{pH} = \text{pK}_A$), the spectrum shows a distinct peak at 1731 cm^{-1} , a peak at 1630 cm^{-1} and a peak at 1240 cm^{-1} . All three peaks are present or increase as the pH decreases down to pH 3.4. The peaks at 1731 cm^{-1} and the one at 1240 cm^{-1} have been assigned to the C = O and C - O stretching vibration of the protonated carboxyl functional group (61-63).

Mn(II)-gluconate complex formation

The position of the vibrational bands associated to deprotonated carboxylate is known to be sensitive to the coordination of metal cations as a result of delocalisation of the electrical charge (61, 64, 65). The ATR-FTIR spectra of an aqueous solution of sodium gluconate (pH 7.6, 50 mM) equilibrated with a stoichiometric excess of Mn(II) (pH 7.6) are shown in **Figure 3-S1C**. The relative position of the two bands ($\Delta\nu_{\text{COO}^-}$) has been associated to different mode of coordination (65). The ν_{as} band is shifted to 1600 cm^{-1} in the gluconate-Mn(II) solution, relative to 1587 cm^{-1} in the sodium-gluconate solution. The ν_{s} band is centred around 1413 cm^{-1} for the two solutions, yielding a $\Delta\nu_{\text{COO}^-_{\text{Mn(II)}}} = 187 \text{ cm}^{-1}$ relative to $\Delta\nu_{\text{COO}^-_{\text{Na(I)}}} = 174 \text{ cm}^{-1}$. Considering that $\Delta\nu_{\text{COO}^-_{\text{Mn(II)}}} > \Delta\nu_{\text{COO}^-_{\text{Na(I)}}}$, one could presume that the dominant coordinating mode is a monodentate (65), with little delocalisation of the negative charge. More relevant for this study, this comparison demonstrates that coordination to Mn(II) does not affect significantly the gluconate spectra. Apart from the small shift of the peak corresponding to the ν_{as} vibration ($\Delta\nu = 13 \text{ cm}^{-1}$), the position of no other peak was affected by the presence of an excess of Mn(II).

Quantitative detection of glucose and gluconate using ATR-FTIR

The ATR-FTIR spectra of glucose solutions of decreasing concentrations (from 10 to 250 mM) are plotted in **Figure 3-S2A**. The intensity of the absorption features decreased with decreasing concentrations. The characteristic features in the region of $950 - 1200 \text{ cm}^{-1}$ remain discernible in the 10 mM solution. Lower concentrations would probably be difficult to detect. A concentration of 10 mM is therefore taken as the limit of the sensitivity of the method for glucose detection. When corrected by a 20x concentration factor, we estimate that a glucose concentration of 0.5 mM in the experimental sample will be detected. The absorbance at 1035 cm^{-1} was plotted as a function of glucose concentration in **Figure 3-S2B**. The plot shows a good linear relation ($R^2 = 0.99$) with an

associated error < 10 % for concentration greater than 10 mM. At 10 mM the associated error was 27 %.

Figure 3-S2C shows the absorbance of gluconate spectra at 1092 cm^{-1} against the solution concentrations. Similarly to glucose, the plot shows a reasonable linear relation ($R^2 = 0.98$) with an associated error < 10% for concentrations greater than 10 mM. At 50 mM the spectrum shows the distinct vibrational signature assigned to gluconate. At 10 mM the gluconate signal is only barely discernible. A concentration of 20 mM is therefore taken as the limit of the sensitivity of the method for gluconate detection. When corrected by a 20x concentration factor, we estimate that a gluconate concentration of 1.0 mM in the experimental sample will be detected. The absorbance at 1092 cm^{-1} was plotted as a function of glucose concentration in **Figure 3-S2D**. The plot shows a good linear relation ($R^2 = 0.99$) with an associated error < 10 % for concentration greater than 10 mM. At 10 mM the associated error was 55 %.

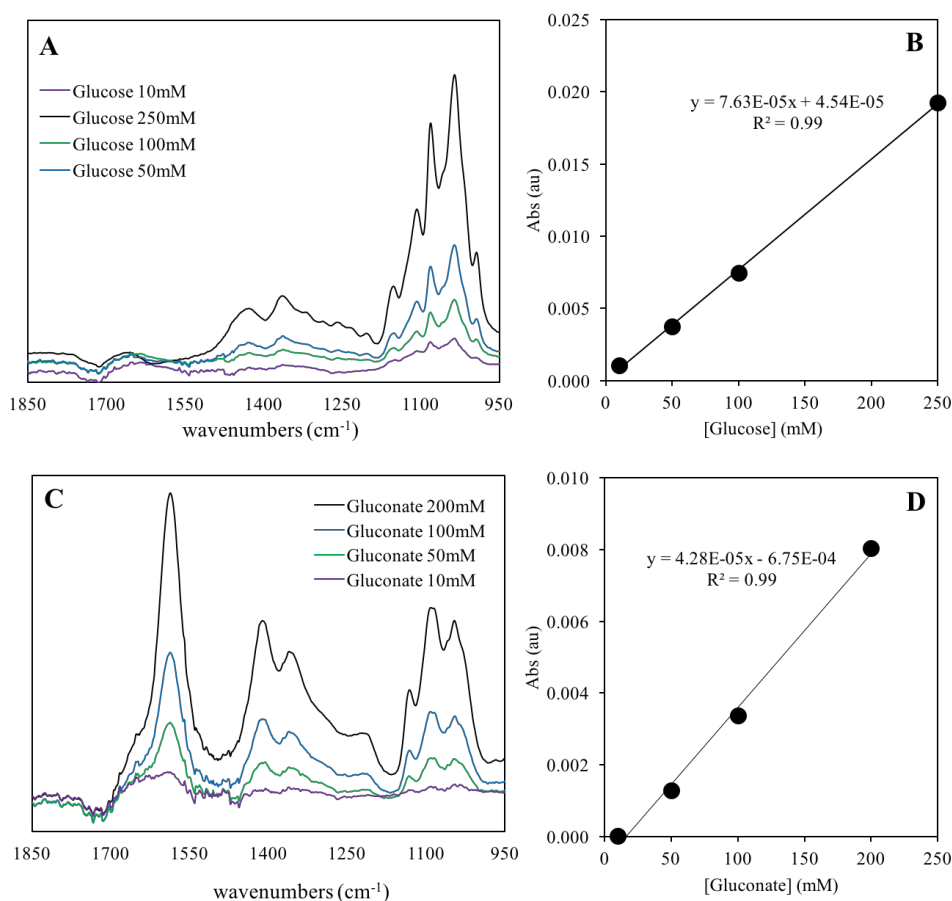


Figure 3-S2 Quantitative detection of glucose and gluconate by ATR-FTIR. Panel A) shows spectra for glucose solutions of concentrations of 250, 100, 50 and 10 mM. Panel B) shows the absorbance (au) at 1035 cm^{-1} as a function of glucose concentrations. Panel C shows spectra for gluconate solutions of concentrations of 200, 100, 50 and 10 mM. Panel D shows the absorbance (au) at 1092 cm^{-1} as a function of gluconate concentrations.

2. Redox stability of Mn species – E_h -pH diagram

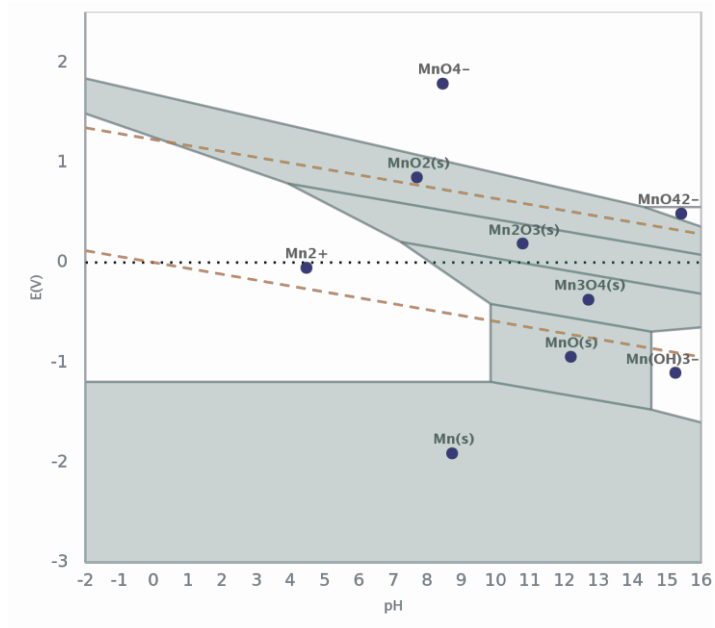


Figure 3-S3 E_h -pH diagram showing the thermodynamic stability of solid Mn, aqueous Mn and Mn oxide phases as a function of pH. The diagram was generated on The Materials Project website (www.materialsproject.org (1)) for a Mn concentration of 0.1 mM. The top orange dashed line shows the water oxidation condition and the bottom orange dashed line shows the water reduction condition.

Chapter 4

Extracellular response of *Pseudomonas putida* GB-1 to glucose addition and impact on the stability of biogenic MnO₂

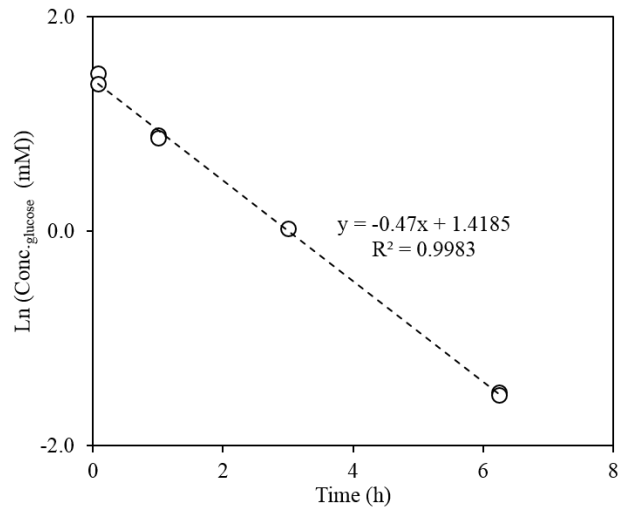


Figure 4-S1 Linearization of glucose consumption rate for biomass suspensions (kept in spent medium) spiked an aliquot of glucose (5.5 mM initial concentration).

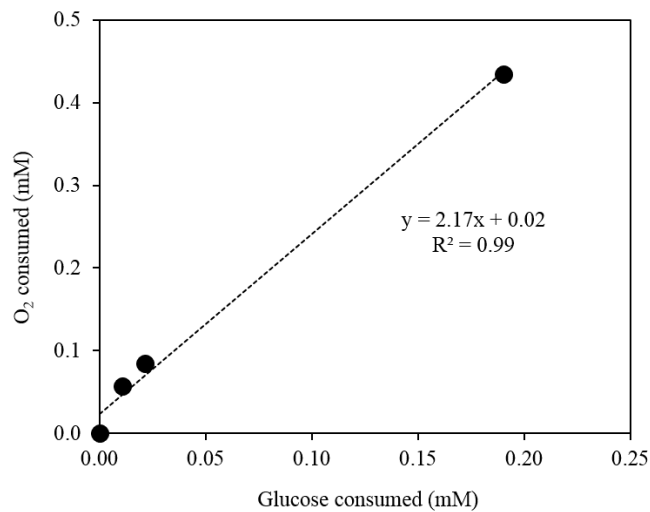


Figure 4-S2 O₂ consumed at a time t as a function of glucose consumed. The slope is used to determine the fraction f_x of glucose uptaken invested in respiration relative to that invested in biomass growth.

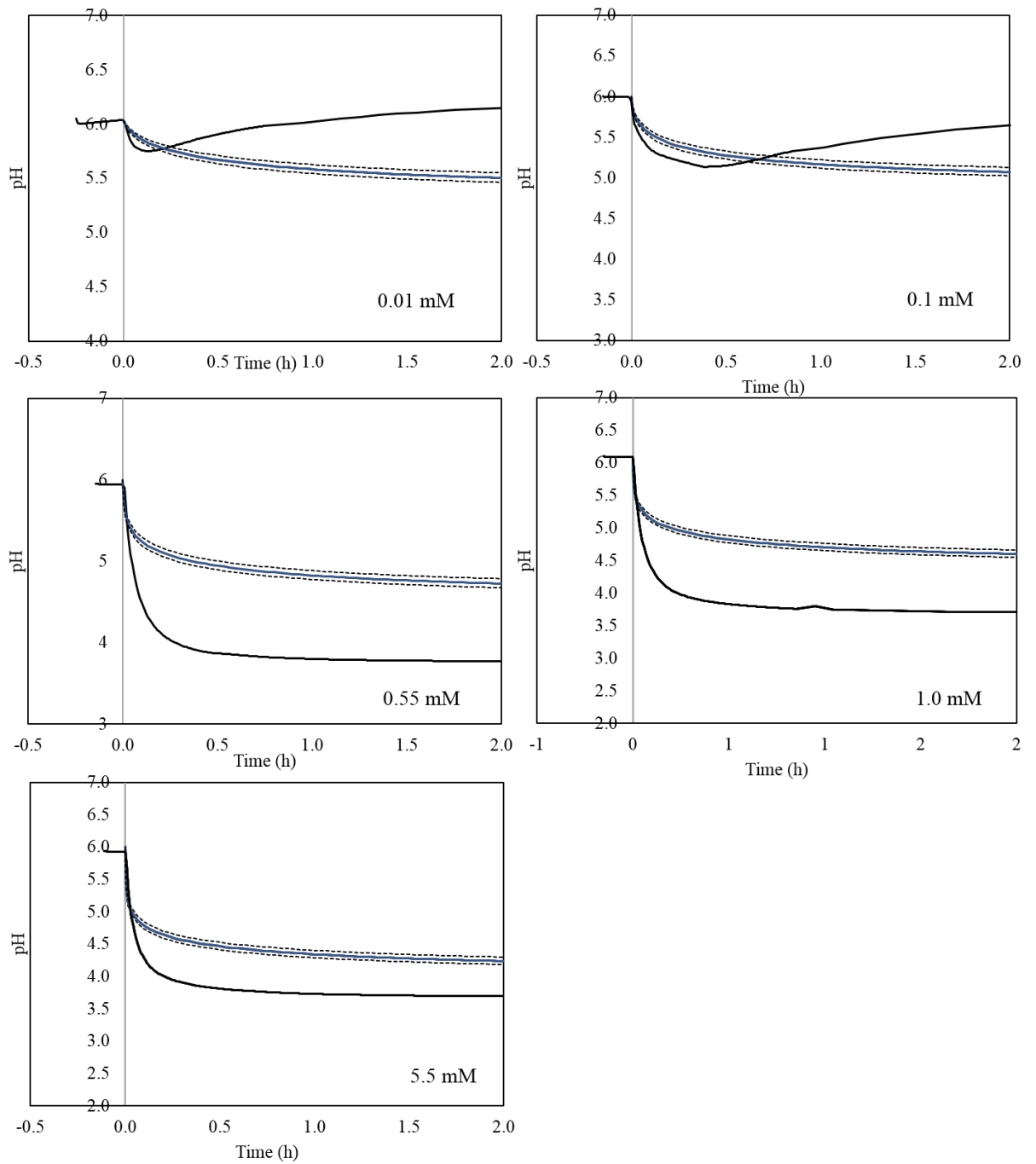


Figure 4-S3 Extracellular acidification of washed biomass suspensions during the first 2h following a pulse with a range of glucose concentrations (0.01, 0.1, 0.55, 1.0 and 5.5 mM initial concentrations). Individual panels show measured pH traces (solid black lines) and calculated traces (solid blue lines) based solely on H_2CO_3 accumulation. The dashed lines represent the values obtained when performing a sensitivity test on f_x (0.36 ± 0.10).

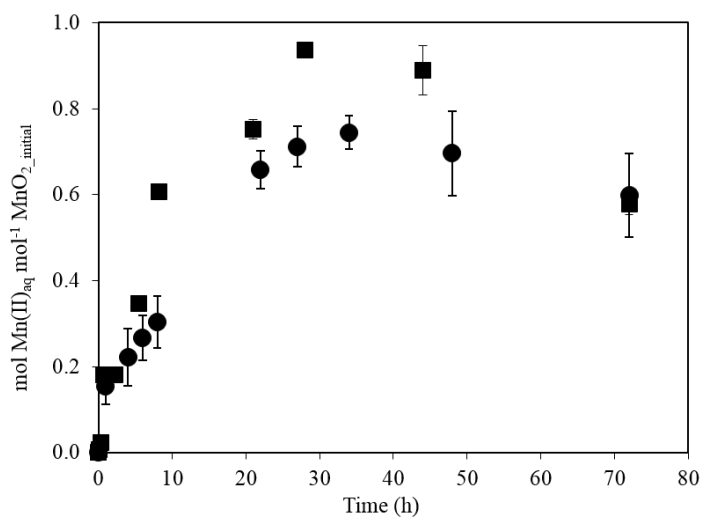


Figure 4-S4 Release of Mn(II) as a function of time when biogenic MnO₂ suspensions (kept in spent growth media) were spiked an aliquot of glucose (5.5 mM initial concentration). Two independent sets of measurements collected 6 months apart are presented here. Each set shows the average of triplicate measurements.

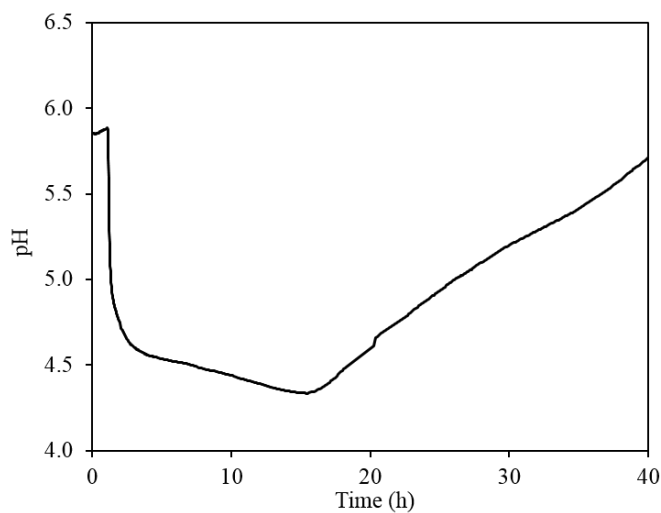


Figure 4-S5 Changes in pH measured in biogenic MnO₂ suspensions (kept in spent growth medium) spiked with glucose (5.5 mM initial concentration).

Table 4-S4 Summary of experimental details conducted in this chapter

Experiment	Experimental	Age when harvested	Washed?	Electrolyte	(+)/(-) Mn?	Vol. flask (mL)	Type of mixing	Number of replicates
Glucose consumption in biomass	Enzymatic assay GAGO (Sigma-Aldrich)	120 ± 12h	No	Spent medium	(-)	100 /250 mL Erlenmeyer	150 RPM (in incubator, dark 37°)	2 replicates, except for 3h sample (1x)
(Keto)-Glucuronate production	Enzymatic assay (Megazymes)	120 ± 12h	No	Spent medium	(-)	100 /250 mL Erlenmeyer	150 RPM (in incubator, dark 37°)	Glucuronate: 2-4 replicates, except 60s sample (x1) Ketogluconate: 2 replicates
Glucuronate consumption rate	Enzymatic assay (Megazymes)	120 ± 12h	No	Spent medium	(-)	100 /250 mL Erlenmeyer	150 RPM (in incubator, dark 37°)	2 replicates
Glucose-induced changes in O ₂	Galvanic O ₂ sensor	120h ± 24h	No	Spent medium	(-)	250 mL Erlenmeyer	0-7h: ~ 100 RPM (on table-top shaker, 25, dark 20-25°C) 7h- 24h: 150 RPM (in incubator, dark 37°)	1 measurement (28 sampling points)
Glucose-induced acidification	pH electrode (calibrated on 3 buffers) Measured automatically using pH stat (Titrino / Titrand, Metrohm)	120 ± 12h	Yes	Spent medium Electrolyte 2 Electrolyte 3	(-)	Grown in 250 mL Experiment in 100 mL beaker	Stir bar and magnetic stirring	1 measurement for each condition
Glucose-induced acidification as a function of glucose concentration	pH electrode (calibrated on 3 buffers) Measured automatically using pH stat (Titrino / Titrand, Metrohm)	120 ± 12h	Yes	Electrolyte 1	(-)	Grown in 250 mL Erlenmeyer. Experiment in 100 mL beaker	Stir bar and magnetic stirring	1 measurement for each condition
Electron-donating	pH electrode (calibrated on 3 buffers)	120 ± 12h	Yes	Electrolyte 1	(-)	Grown in 250 mL Erlenmeyer.	Stir bar and magnetic stirring	3 replicates

capacity of biomass	Measured automatically using pH stat (Titrino / Titrande, Metrohm)	Experiment in 100 mL beaker
Glucose-induced reductive dissolution of MnO ₂	- synthetic bio-mineral assemblage - biogenic MnO ₂	120 ± 12h Yes Electrolyte 1 (+) 100 mL Erlenmeyer 150 RPM incubator, dark 37° (in 2 replicates for each condition)

Chapter 6

Conclusion

Bacterial C-metabolism and impact on the precipitation of biogenic MnO₂

All solutions were prepared using ultrapure water ($> 18 \text{ m}\Omega \text{ cm}$) and ACS-grade reagents. The Mn(II)-oxidizing bacterium *Pseudomonas putida* GB-1 (*P. putida*) was used as a model organism. All bacterial suspensions were grown under sterile conditions. Once harvested, and unless stated otherwise, experiments were conducted in glass beakers or Erlenmeyer flasks at room temperature, kept open to the atmosphere and loosely covered with parafilm. Leptothrix medium was prepared by dissolving glucose (1.0 g L^{-1} , 5.5 mM), casamino acids (0.50 g L^{-1}), yeast extract (0.50 g L^{-1}) and HEPES acid (2.38 g L^{-1} , 10 mM) in ultrapure water and autoclaved at 120°C for 20 minutes. After cooling to room temperature and before inoculation, the medium was completed with filter-sterilised CaCl_2 (0.5 mM), MgSO_4 (0.83 mM), FeCl_3 ($3.7 \mu\text{M}$), CuSO_4 (40 nM), ZnSO_4 (152 nM), CoCl_2 (84 nM), Na_2MoO_4 (54 nM). Cultures were propagated in 125 mL or 50 mL of growth medium, contained in 250 mL or 100 mL Erlenmeyer flasks capped with foam or cellulose stoppers in a table-top shaking incubator in the dark (27°C , 150 RPM). Experimental suspensions were inoculated from stationary-phase suspensions ($30\text{h} \pm 12\text{h}$) grown in Leptothrix growth medium.

Variations in pH and DO

A separate series of 100 mL Erlenmeyer flasks capped with cellulose stoppers and filled with 50 mL of Leptothrix growth media amended with 1 mM MnCl_2 were inoculated with *P. putida*. Changes in pH were measured as a function of time after inoculation using a pH electrode (Orion Ross, ThermoScientific) calibrated against three buffers (4, 7, 10). Measurements were conducted in triplicate sets of flasks. Once measured, flasks were sacrificed to avoid effects of contamination effects from dipping the pH electrode in the suspensions. All flasks were kept in a table-top incubator (27°C , 150 RPM , in the dark) prior to being measured.

In a separate experiment, a series of 100 mL Erlenmeyer flasks capped with cellulose stoppers and filled with 50 mL of *Leptothrix* growth media amended with 1 mM MnCl_2 were inoculated with *P. putida*. *The dissolved oxygen concentrations were measured using a galvanic oxygen sensor (OxiCal, WTW)*. Once measured, flasks were sacrificed to avoid effects of contamination effects from dipping the oxygen sensor in the suspensions. Dissolved oxygen measurements were conducted against a control non-inoculated *Leptothrix* volume kept under the same conditions. All flasks were kept in a table-top incubator (27°C, 150 RPM, in the dark) prior to being measured.

Changes of the initial glucose concentration and impact on MnO_2 precipitation

In a separate experiment, 100 mL Erlenmeyer flasks capped with cellulose stoppers and filled with 50 mL of *Leptothrix* growth media amended with 1 mM MnCl_2 were inoculated with *P. putida*. Aliquots of the suspension were collected at different time-points and immediately filtered (0.20 μm pore size, polyethersulfone) for chemical analysis. Aqueous Mn(II) was measured by ICP-OES in diluted and acidified (50 μL HNO_3 66 % in 5 mL sample). Initial MnO_2 concentrations were determined by sampling 1 mL of the suspensions and acid digesting the solids using concentrated nitric acid (50 μL , 66 %) and excess oxalic acid (50 μL , 1 M), and diluting the resulting solution with ultrapure water. Manganese concentration were determined by ICP-OES (Perkin-Elmer Optima 8300) at three emission lines and using Sc as an internal standard.

Modified growth media based on the *Leptothrix* recipe (1-3) were prepared by dissolving casamino acids (0.50 g L^{-1}), yeast extract (0.50 g L^{-1}) and HEPES acid (2.38 g L^{-1} , 10 mM) in ultrapure water and varying the initial glucose concentration (0 % and 50 % glucose, where % glucose refers to percentage of the glucose in the original *Leptothrix* growth media (100 % glucose = 1 g L^{-1} , 5.5 mM). The modified media were autoclaved and completed with filter-sterilised CaCl_2 (0.5 mM), MgSO_4 (0.83 mM), FeCl_3 (3.7 μM), CuSO_4 (40 nM), ZnSO_4 (152 nM), CoCl_2 (84 nM), Na_2MoO_4 (54 nM) and 1 mM MnCl_2 . A series of 100 mL Erlenmeyer flasks were filled with 50 mL modified *Leptothrix* media solutions (0 % and 50 %). The solutions were inoculated from suspensions (30h \pm 12h) grown in the original *Leptothrix* growth medium. Inoculated solutions were placed in the table-top incubator (27°C, 150 RPM, in the dark). Aliquots of the suspension were collected at different time-points once the suspensions had reached stationary phase (> 14h). Aqueous Mn(II) concentrations were measured by ICP as described above.

Chapter 8 Appendix – Raw data

Chapter 2

Pb, Zn and Mn sorption on biogenic MnO₂: contaminant loading and competitive access to vacancy sites

Table 2-A1 Zn sorption isotherm on biomass. Concentration of biomass was 0.43 g L⁻¹ in suspensions. Ionic concentrations are reported in μM.

c_{Zn_TOT}	c_{Zn_AQ}	q_{Zn} (mol kg ⁻¹ sorbent)	Kd (q_{Zn} (mol kg ⁻¹)/ c_{Zn} (mol L ⁻¹))
0.33	0.04	0.001	0.01705
0.33	0.05	0.001	0.01490
0.35	0.04	0.001	0.02093
24.37	6.05	0.043	0.00705
24.20	6.22	0.042	0.00673
24.17	6.29	0.042	0.00661
48.70	20.71	0.065	0.00314
50.37	21.81	0.066	0.00304
50.73	20.65	0.070	0.00339
93.73	59.99	0.078	0.00131
97.07	62.79	0.080	0.00127
95.47	62.69	0.076	0.00122
184.20	154.27	0.070	0.00045
183.30	162.68	0.048	0.00029
183.13	157.47	0.060	0.00038
272.13	252.70	0.045	0.00018

276.77	252.35	0.057	0.00023
274.17	228.95	0.105	0.00046
359.77	339.78	0.072	0.00021
370.57	355.30	0.168	0.00047
427.43	426.50	0.002	0.00001
535.20	525.03	0.024	0.00005
547.07	493.80	0.124	0.00025
554.83	544.05	0.025	0.00005

Table 2-A2 Pb sorption isotherm on biomass. Concentration of biomass was 0.40 g L⁻¹ in suspensions. Ionic concentrations are reported in μM.

C _{Pb_TOT}	C _{Pb_AQ}	q _{Pb} (mol kg ⁻¹ sorbent)	Kd (q _{Pb} (mol kg ⁻¹)/ C _{Pb} (mol L ⁻¹))
0.00	0.00	0.000	-
0.00	0.00	0.000	-
0.00	0.00	0.000	-
20.80	0.77	0.050	0.06503
21.73	2.41	0.048	0.02004
21.13	0.48	0.052	0.10755
44.57	5.62	0.097	0.01733
43.40	5.75	0.094	0.01637
43.87	6.14	0.094	0.01536
85.17	38.00	0.118	0.00310
86.78	34.79	0.130	0.00374
89.57	37.19	0.131	0.00352
171.23	88.92	0.206	0.00231
176.37	91.13	0.213	0.00234
170.60	87.58	0.208	0.00237
250.70	161.87	0.222	0.00137
245.67	175.35	0.176	0.00100
265.60	176.42	0.223	0.00126
329.10	252.72	0.191	0.00076
337.47	261.40	0.190	0.00073
346.47	258.75	0.219	0.00085
414.57	357.08	0.144	0.00040
413.33	340.60	0.182	0.00053
419.37	353.35	0.165	0.00047
497.77	411.97	0.215	0.00052
535.03	448.98	0.215	0.00048
516.00	438.52	0.194	0.00044

Table 2-A3 Zn sorption isotherm on biogenic MnO₂. Concentration of biomass was 0.53 g L⁻¹ in suspensions. Ionic concentrations are reported in μM .

$C_{\text{Mn_TOT}}$	$C_{\text{Mn_AQ}}$	$C_{\text{Zn_TOT}}$	$C_{\text{Zn_AQ}}$	q_{Zn} (mol kg ⁻¹ sorbent)	q_{Zn} (mol mol ⁻¹ Mn)	K_{App}	K_{d}
782.66	0.00	2.62	0.15	0.005	0.003	-	0.02034
798.49	0.00	2.50	0.23	0.004	0.003	-	0.01259
783.73	0.00	2.50	0.21	0.004	0.003	-	0.01361
811.34	0.00	26.89	0.52	0.050	0.034	-	0.06426
814.20	0.00	26.54	0.60	0.049	0.032	-	0.05355
779.57	0.00	26.06	0.45	0.048	0.033	-	0.07264
764.81	0.21	48.20	2.27	0.087	0.060	0.00	0.02642
807.89	0.14	50.22	5.30	0.085	0.056	0.00	0.01050
797.06	0.00	49.50	1.51	0.091	0.060	0.00	0.03984
651.76	2.87	81.04	21.71	0.112	0.091	0.01	0.00421
831.93	2.89	101.03	21.75	0.150	0.096	0.01	0.00440
824.43	2.80	107.46	21.36	0.162	0.105	0.01	0.00491
815.27	8.57	193.85	94.60	0.187	0.123	0.01	0.00130
877.39	8.28	202.66	94.48	0.204	0.124	0.01	0.00132
868.46	8.45	194.80	93.47	0.191	0.118	0.01	0.00126
786.23	12.98	273.34	182.47	0.171	0.118	0.01	0.00064
760.53	11.97	264.18	166.63	0.184	0.130	0.01	0.00078
777.43	13.75	275.72	186.58	0.168	0.117	0.01	0.00063
814.32	21.13	370.33	275.46	0.179	0.120	0.01	0.00043
870.60	21.67	374.37	283.20	0.172	0.107	0.01	0.00038
834.19	21.73	347.96	284.09	0.120	0.079	0.01	0.00028
742.20	19.59	404.24	311.48	0.175	0.128	0.01	0.00041
813.72	24.53	463.51	402.68	0.115	0.077	0.00	0.00019
777.07	24.71	432.57	387.44	0.085	0.060	0.00	0.00015
843.59	29.11	565.61	466.27	0.187	0.122	0.01	0.00026
847.99	29.65	566.80	494.13	0.137	0.089	0.01	0.00018
811.58	29.11	552.16	491.57	0.114	0.077	0.00	0.00016

Table 2-A4 Pb sorption isotherm on biogenic MnO₂. Concentration of biomass was 0.44 g L⁻¹ in suspensions. Ionic concentrations are reported in μM.

C _{Mn_TOT}	C _{Mn_AQ}	C _{Pb_TOT}	C _{Pb_AQ}	q _{Pb} (mol kg ⁻¹ sorbent)	q _{Pb} (mol mol ⁻¹ Mn)	K _{app}	K _d
774.43	0.10	0.00	0.00	0.00	0.00	0.0	-
736.83	0.10	0.00	0.00	0.00	0.00	0.0	-
744.40	0.14	0.00	0.00	0.00	0.00	0.0	-
721.60	0.48	27.43	0.00	0.06	0.04	18.3	-
729.97	0.47	29.07	0.00	0.07	0.04	18.7	-
734.30	0.49	27.77	0.00	0.06	0.04	0.2	-
709.53	2.75	57.00	0.00	0.13	0.08	2.2	-
741.73	2.93	57.90	0.00	0.13	0.08	45.9	-
763.03	2.91	60.27	0.00	0.14	0.08	46.1	-
730.87	24.79	112.53	0.00	0.26	0.16	39.5	-
697.13	27.34	113.60	0.00	0.26	0.17	46.2	-
708.10	26.72	112.83	0.16	0.26	0.17	27.6	1.0335
744.27	110.05	227.20	2.45	0.51	0.35	15.9	0.1446
782.70	98.43	238.97	2.60	0.54	0.35	13.1	0.1329
736.80	105.13	222.93	2.58	0.50	0.35	14.2	0.1355
766.57	136.55	363.93	66.22	0.68	0.47	1.0	0.0071
751.63	140.43	365.93	71.38	0.67	0.48	1.3	0.0068
752.53	138.35	346.33	60.48	0.65	0.47	1.1	0.0077
722.00	143.58	460.97	167.00	0.67	0.51	0.4	0.0030
771.97	130.73	468.07	146.77	0.73	0.50	0.5	0.0034
754.83	144.88	459.70	166.18	0.67	0.48	0.4	0.0029
726.40	147.02	555.27	265.83	0.66	0.50	0.3	0.0019
770.17	147.88	576.13	273.90	0.69	0.49	0.3	0.0018
779.47	143.02	582.37	274.08	0.70	0.48	0.2	0.0018
701.83	139.87	684.43	408.72	0.63	0.49	0.2	0.0012
714.83	154.82	681.57	380.55	0.68	0.54	0.2	0.0014
696.13	141.37	667.90	401.90	0.60	0.48	0.2	0.0012

Table 2-A5 Control measurements for solid Pb precipitates when 10 – 650 μM PbNO_3 was added to a NaCl solution (10 mM).

Sample ID	Conc. (μM) in solution in filtrated sample	Conc. (μM) after total digestion of the solid phase	% difference
10_1	12.81	12.67	-1.08
10_2	9.84	9.82	-0.24
10_3	9.59	9.58	-0.07
50_1	50.14	50.68	1.07
50_2	48.31	49.35	2.11
50_3	47.64	48.82	2.43
100_1	95.26	95.70	0.46
100_2	93.89	95.19	1.37
100_3	96.61	96.85	0.24
250_1	237.48	239.57	0.87
250_2	234.78	233.48	-0.56
250_3	242.62	242.32	-0.13
450_1	421.97	433.20	2.59
450_2	418.97	429.02	2.34
450_3	422.49	427.26	1.12
650_1	645.78	657.40	1.77
650_2	617.97	615.26	-0.44
650_3	625.16	627.50	0.37

Chapter 3

Abiotic oxidation of glucose and gluconate by δ -MnO₂

Table 3-A1 Raw data from ICP-OES measurements of Mn concentrations during the reaction of glucose and δ -MnO₂ as a function of pH. Initial MnO₂ (t0h) was measured once or in duplicate for each set of measurement. When two values were available, MnO₂_t0h was taken as the average concentration (\pm SD).

Condition n	MnO ₂ at t0h (μ M)	Time (h)	Mn(II) _{aq} (μ M)	mol Mn(II) mol ⁻¹ MnO ₂ . t0h
pH 4.5	1129.7	0.0	44.6	0.04
	1059.4	0.3	38.9	0.04
	1094.6 \pm 49.7 μ M	0.6	83.1	0.08
		1.1	134.1	0.12
		1.6	189.4	0.17
		3.3	316.4	0.29
		6.6	489.0	0.45
		24.0	1297.3	-
1460.0	0.0	80.0	0.05	
	3.0	370.0	0.25	
	6.0	588.0	0.40	
	22.0	1014.0	0.69	
	23.8	1063.0	0.73	
	1104.8 1077.1 1090.9 \pm 19.6 μ M	0.0	18.3	0.02
0.2		34.8	0.03	
0.6		99.1	0.09	
2.3		237.1	0.22	
5.2		400.8	0.37	
8.6		521.9	0.48	
24.0		777.3	0.71	
pH 5.5	1235.7	0.0	7.6	0.01
	1188.1	0.2	9.2	0.01
	1211.9 \pm 33.7 μ M	0.6	18	0.01
		2.1	57.5	0.05
		5.0	95.9	0.08
		8.5	160.2	0.13
		24.0	337.5	0.28
pH 6.5	1591.0	0.0	0.0	0.00
		3.0	0.0	0.01
		9.0	2.8	0.00
		21.8	147.0	0.09
		24.0	180.0	0.11

Table 3-A2 Raw data from ICP-OES measurements of Mn concentrations during the reaction of gluconate and δ -MnO₂ as a function of pH. Initial MnO₂ (t_{0h}) was measured once for each set of duplicate samples for each pH conditions.

Condition	MnO ₂ at t _{0h} (μ M)	Time (h)	Mn(II) _{aq} (μ M)	mol Mn(II) mol ⁻¹ MnO ₂ . t _{0h}
pH 4.5	1191.6 1106.8	0.0	68.0	0.06
		0.0	35.1	0.03
		0.6	77.7	0.07
		0.6	107.6	0.10
		1.5	181.3	0.15
		1.5	199.7	0.18
		2.3	252.7	0.21
		2.3	247.5	0.22
		3.3	321.7	0.27
		3.3	308.4	0.28
		4.2	374.4	0.31
		4.2	374.8	0.34
		7.0	487.0	0.41
		7.0	508.9	0.46
		8.8	557.2	0.47
	8.8	566.8	0.51	
	22.3	878.4	0.74	
	22.3	855.4	0.77	
pH 5.5	1257.0 1154.3	0.0	3.1	0.00
		0.0	5.7	0.00
		1.0	33.4	0.03
		1.0	50.6	0.04
		3.0	113.8	0.09
		3.0	125.9	0.11
		6.0	193.0	0.15
		6.0	189.7	0.16
		8.0	131.6	0.10
		8.0	245.3	0.21
		24.0	241.1	0.19
		24.0	218.4	0.19
pH 6.5	1161.3 1088.9	0.0	28.3	0.02
		0.0	20.5	0.02
		1.1	9.5	0.01
		1.1	7.9	0.01
		2.7	37.3	0.03
		2.7	21.8	0.02
		5.0	58.1	0.05
		5.0	40.4	0.04
		7.0	78.0	0.07
		7.0	52.5	0.05
		24.0	136.7	0.12
		24.0	123.5	0.11

Table 3-A3 Raw data from the colorimetric assay for glucose concentration measured upon reaction of glucose with δ -MnO₂. The reported predicted concentration determined from the absorbance at 540 nm (Conc. Abs at 540 nm) are corrected for the dilution factor.

Sample ID	Reaction time (h)	Conc. Abs at 540 nm (mM)	Known conc. (mM)	Error*
Standard1	/	0.00	0.00	na
Standard2	/	0.12	0.11	5 %
Standard3	/	0.22	0.22	1 %
Standard4	/	0.33	0.33	1 %
Standard5**	/	0.40	0.44	10 %
check- 5.5mM_DF20	/	5.39	5.50	2 %
check- 5.5mM_DF20	/	5.42	5.50	1 %
check- 5.5mM_DF20	/	5.40	5.50	2 %
check- 5.5mM_DF20	/	5.55	5.50	1 %
check- 5.5mM_DF50	/	5.75	5.50	5 %
check- 5.5mM_DF50	/	5.96	5.50	8 %
check- 5.5mM_DF20	/	5.63	5.50	2 %
check- 5.5mM_DF20	/	5.61	5.50	2 %
Blank	/	0.01	0.00	/
Blank	/	0.00	0.00	/
Blank	/	0.00	0.00	/
Blank	/	0.03	0.00	/
Blank	/	0.02	0.00	/
Blank	/	0.03	0.00	/
R_pH4.5_t0h_DF20	0.0	5.4	/	/
R_pH4.5_t18'_DF20	0.3	5.5	/	/
R_pH4.5_t34'_DF20	0.6	5.5	/	/
R_pH4.5_t64'_DF20	1.1	5.5	/	/
R_pH4.5_t1h38_DF20	1.6	5.3	/	/
R_pH4.5_t2h30_DF20	2.5	5.4	/	/
R_pH4.5_t6h_DF20	6.0	5.2	/	/
R_pH4.5_t24h_DF20	24.0	4.9	/	/
R_pH4.5_t0h_DF20	0.0	5.2	/	/
R_pH4.5_t2h15_DF20	2.3	5.1	/	/
R_pH4.5_t8h_DF20	8.0	5.0	/	/
R_pH4.5_t24h_DF20	24.0	4.8	/	/
R_pH5.5_t0h_DF20	0.0	5.1	/	/
R_pH5.5_t24h_DF20	24.0	5.2	/	/
R_pH5.5_t0h_DF20	0.0	5.2	/	/
R_pH5.5_t12'_DF20	0.2	5.1	/	/
R_pH5.5_t2h15_DF20	2.3	5.1	/	/
R_pH5.5_t24h_DF20	24.0	5.3	/	/
R_pH6.5_t0h_DF20	0	5.2	/	/
R_pH6.5_t2h30_DF20	2.5	5.1	/	/
R_pH6.5_t5h30_DF20	5.5	4.9	/	/
R_pH6.5_t21h_DF20	21.0	5.2	/	/
R_pH6.5_t24h_DF20	24.0	5.2	/	/
R_pH6.5_t0h_DF20	0	5.7	/	/
R_pH6.5_t2h30_DF20	2.5	5.4	/	/
R_pH6.5_t5h30_DF20	5.5	5.5	/	/
R_pH6.5_t21h_DF20	21.0	5.9	/	/
R_pH6.5_t24h_DF20	24.0	5.5	/	/

* Error was calculated on known and predicted concentrations with all associated significant figures. Only two significant figures are reported for the concentration of the standards in the table.

** Standard 5 was left out of the calibration curve as its absorbance was outside the linear range.

Table 3-A4 Quantitative determination of glucose and gluconate from ATR-FTIR spectra of a range of solution concentrations. The % error is calculated from the predicted concentration from the calibration at 1035 and 1092 cm^{-1} for glucose and gluconate respectively, relative to the known concentrations of the standards.

Glucose			Gluconate		
<i>Known</i> <i>conc. (mM)</i>	<i>Conc. Abs at 1035 cm-1</i> <i>(mM)</i>	<i>Error</i>	<i>Known</i> <i>conc.</i> <i>(mM)</i>	<i>Conc. Abs at 1092 cm-1</i> <i>(mM)</i>	<i>Error</i>
10	12.7	27 %	10*	17.9	55 %
50	45.9	8 %	50	49.7	9 %
100	92.7	7 %	100	101.8	6 %
250	239.8	4 %	200	218.4	2 %

Chapter 4

Extracellular response of *Pseudomonas putida* GB-1 to glucose pulse and impact on the stability of biogenic MnO₂

Table 4-A1 Raw data from the enzymatic colorimetric assay (GAGO 20, Sigma Aldrich) for glucose concentration measurements. Blank samples and calibrations samples, measured from the absorbance at 540 nm. The absorbance of all samples was collected against a reagent blank.

Sample ID	Known conc. (g L ⁻¹)	Known conc. (mM)	Conc. Abs _{540 nm} (mM)	Error
Blank_1	0.00	0.00	0.01	/
Blank_2	0.00	0.00	0.00	/
Blank_3	0.00	0.00	0.00	/
Blank_4	0.00	0.00	0.03	/
Blank_5	0.00	0.00	0.02	/
Blank_6	0.00	0.00	0.03	/
Standard1	0.02	0.11	0.116	4 %
Standard2	0.04	0.22	0.225	1 %
Standard3	0.06	0.33	0.330	1 %
Standard4	0.08	0.44	0.401	10 %

Table 4-A2 Raw data from the enzymatic colorimetric assay (Gluconate/ d-Glucono- δ -lactone, Megazymes) for gluconate concentration measurements. Blank, calibrations and control samples, in which glucose (5.5 mM) is added to cell-free bacteria supernatant, in which the gluconate concentrations are measured from the absorbance at 340 nm.

Sample ID	Known conc. (mM)	Conc. Abs at 340 nm (mM)	Error
Blank_ultrapure water_1	0.000	0.004	/
Blank_ultrapure water_2	0.000	0.000	/
Blank_cell-free supernatant_1	0.000	0.000	/
Blank_cell-free supernatant_2	0.000	0.000	/
Standard1	0.083	0.086	3 %
Standard2	0.250	0.248	1 %
Standard3	0.500	0.501	0 %
Glucose_cell-free supernatant_1	/	0.00	/
Glucose_cell-free supernatant_2	/	0.00	/

Table 4-A3 Raw data from the colorimetric assay (GAGO, Sigma-Aldrich) for the measurement of glucose concentration as a function of time for biomass suspensions spiked with glucose (5.5 mM). The measured glucose concentrations, determined from the absorbances at 540 nm ($\text{Conc.}_{\text{Abs at 540 nm}}$), are corrected for any dilution factors. The initial concentration ($t = 0\text{h}$) was taken as the gravimetric glucose added. The absorbance of all samples was collected against a reagent blank. Mass of the biomass was estimated to be 0.40 g L^{-1} , based on the measurements reported in Chapter 1.

Sample ID	Time (h)	$\text{Conc.}_{\text{Abs at 540 nm}}$ (mM)
-	0.0	5.50
Glucose_5min_1	0.1	4.36
Glucose_5min_2	0.1	3.97
Glucose_1h_1	1.0	2.46
Glucose_1h_2	1.0	2.40
Glucose_3h	3.0	1.03
Glucose_6h15_1	6.3	0.22
Glucose_6h15_2	6.3	0.22

Table 4-A4 Raw data from the enzymatic colorimetric assay (Gluconate/ d-Glucono- δ -lactone, Megazymes) for gluconate concentration as a function of time for biomass suspensions spiked with glucose (5.5 mM). The measured glucose concentrations, determined from the absorbances at 340 nm ($\text{Conc.}_{\text{Abs at 340 nm}}$), are corrected for any dilution factors. In hydrolysed samples, the keto-gluconic acid is hydrolysed to gluconic acid. The measured $\text{Conc.}_{\text{Abs 340 nm}}$ (mM) is therefore the sum of the concentrations of gluconic and keto-gluconic acids. Mass of the biomass was estimated to be 0.40 g L^{-1} , based on the measurement reported in Chapter 1.

Sample_ID	Time (h)	$\text{Conc.}_{\text{Abs at 340 nm}}$ (mM)
Glucose_30s_1	0.01	0.356
Glucose_30s_2	0.01	0.421
Glucose_60s	0.02	0.425
Glucose_5min_1	0.08	0.711
Glucose_5min_2	0.08	0.717
Glucose_5min_3	0.08	0.762
Glucose_15min_1	0.25	1.059
Glucose_15min_2	0.25	1.017
Glucose_21min_1	0.35	0.861
Glucose_21min_2	0.35	0.898
Glucose_30min_1	0.50	0.910
Glucose_30min_2	0.50	0.873
Glucose_30min_1	0.50	1.034
Glucose_30min_2	0.50	0.984
Glucose_40min_1	0.67	0.638
Glucose_40min_2	0.67	0.450
Glucose_1h05	1.08	0.420
Glucose_1h05	1.08	0.387
Glucose_2h_1	2.00	0.033
Glucose_2h_2	2.00	0.020
Glucose_15min_hydrolysed	0.25	0.939
Glucose_15min_hydrolysed	0.25	1.001
Glucose_30min_hydrolysed	0.50	1.034
Glucose_30min_hydrolysed	0.50	0.984
Glucose_5h_hydrolysed	5.00	0.168
Glucose_5h_hydrolysed	5.00	0.155

Table 4-A5 Raw data from the enzymatic colorimetric assay (Gluconate/ d-Glucono- δ -lactone,

Megazymes) for gluconate concentration as a function of time for biomass suspensions spiked with gluconate (~ 4.5 mM). The measured gluconate concentrations, determined from the absorbances at 340 nm (Conc. Abs at 340 nm), are corrected for any dilution factors. Control samples were collected in cell-free solutions spiked with gluconate and are taken as the t0h concentration. Mass of the biomass was estimated to be 0.40 g L⁻¹, based on the measurement reported in Chapter 1.

Sample ID	Time (h)	Conc. Abs at 340 nm (mM)
Gluconate_control_1	0.00	4.366
Gluconate_control_2	0.00	4.613
Gluconate_2min_1	0.03	4.078
Gluconate_2min_2	0.03	4.284
Gluconate_7min_1	0.12	3.913
Gluconate_7min_2	0.12	4.313
Gluconate_15min_1	0.25	3.625
Gluconate_15min_2	0.25	3.542
Gluconate_30min_1	0.50	2.698
Gluconate_30min_2	0.50	2.224

Table 4-A6 Raw data for dissolved oxygen (DO) measurements in biomass suspensions spiked an aliquot of glucose (5.5 mM initial glucose concentration), measured with a galvanic dissolved oxygen sensor (OxiCal, WTW). The negative times (h) represent the baseline DO concentrations measured prior to the glucose spike. The t0h corresponds to the glucose spike.

Time (h)	DO (mg L ⁻¹)
-1.50	8.20
-1.45	8.25
-1.42	8.24
-1.37	8.20
-1.27	8.10
-1.21	8.03
-1.19	8.03
-1.17	8.07
-1.15	7.97
-1.02	8.05
-0.88	7.89
-0.67	7.84
-0.02	7.93
0.00	6.90
0.01	6.40
0.08	0.10
0.32	0.00
1.59	0.00
2.09	0.00
2.43	0.00
4.34	0.00
5.76	0.00
6.59	0.00
10.09	0.00
25.09	4.74
28.09	6.80
31.01	8.41
37.09	8.46

Table 4-A7 Raw data from ICP-OES measurements of Mn concentrations following the addition of 5.5mM glucose to a synthetic biomineral assemblage (biomass and δ -MnO₂). The initial MnO₂ concentration was $566.4 \pm 47.9 \mu\text{M}$.

Conditions	MnO ₂ _initial (μM)	Time (h)	Mn(II) (μM)	Mn ^{II} / MnO ₂ _initial
5.5 mM glucose Biomass δ -MnO ₂	566.4 ± 47.9	0.0	0.09	0.00
		0.0	0.1	0.00
		0.1	7.7	0.01
		0.1	7.8	0.01
		0.8	50.3	0.09
		0.8	47.3	0.08
		2.0	89.8	0.16
		2.0	93.9	0.17
		3.3	192.7	0.34
		3.3	127.0	0.22
		7.0	154.1	0.27
		7.0	282.1	0.50
		21.0	149.2	0.26
		21.0	210.5	0.37
		24.0	156.9	0.28
		24.0	148.7	0.26

Table 4-A8 Raw data from ICP-OES measurements of Mn concentrations following the addition of 5.5mM glucose to a biogenic MnO₂ suspension.

Conditions	MnO ₂ _initial (μM)	Time (h)	Mn(II) (μM)	Mn ^{II} / MnO ₂ _initial
0.01 mM glucose Biogenic MnO ₂	826.9 ± 44	0.0	0.0	0.00
		0.0	0.0	0.00
		0.5	2.4	0.00
		0.5	1.9	0.00
		1.5	5.9	0.01
		1.5	3.3	0.00
		3.0	4.3	0.01
		3.0	0.9	0.00
		5.0	0.7	0.00
		5.0	0.4	0.00
		21.0	2.6	0.00
		21.0	0.0	0.00
		24.0	16.1	0.02
		24.0	3.8	0.00
0.55 mM glucose Biogenic MnO ₂	783.4 ± 44.4	0.0	21.2	0.03
		0.0	23.0	0.03
		0.5	33.1	0.04
		0.5	44.6	0.05
		1.5	76.8	0.09
		1.5	76.2	0.09
		3.0	89.8	0.11
		3.0	83.7	0.10
		5.0	79.1	0.10
		5.0	77.2	0.09

		21.0	21.3	0.03
		21.0	21.8	0.03
		24.0	2.3	0.00
5.5 mM glucose	783.4 ± 44.4	0.0	0.1	0.00
Biogenic MnO ₂		0.0	0.1	0.00
		0.1	6.1	0.01
		0.1	6.2	0.01
		0.8	20.8	0.03
		0.8	18.6	0.02
		2.0	50.5	0.06
		2.0	46.2	0.06
		3.3	63.4	0.08
		3.3	64.2	0.08
		7.0	66.6	0.09
		7.0	125.2	0.16
		21.0	210.5	0.27
		21.0	192.3	0.25
		24.0	164.1	0.21
		24.0	147.1	0.19

Table 4-A9 Raw data from ICP-OES measurements of Mn concentrations. The electron-donating capacity of the biomass is measured by adding an aliquot of δ -MnO₂ and measuring the releasing of aqueous Mn as a function of pH when the bio-mineral suspension is kept at pH 4.5.

MnO ₂ _initial (μM)	Time (h)	Mn(II) (μM)	Mn ^{II} / MnO ₂ _initial
658.2	0.0	0.2	0.00
	0.0	0.4	0.00
	1.0	0.0	0.00
	2.8	0.4	0.00
	3.5	0.2	0.00
	19.5	81.4	0.12
	23.0	84.5	0.13
	23.0	153.8	0.23
651.1	1.0	0.7	0.00
	3.0	0.2	0.00
	5.0	0.2	0.00
	8.0	4.1	0.01
	22.5	9.4	0.01
	24.0	9.6	0.01
840.8	1.0	1.3	0.00
	3.0	0.2	0.00
	6.0	121.4	0.14
	9.0	40.2	0.05
	24.0	156.5	0.19

